



Swansea University
Prifysgol Abertawe



Swansea University E-Theses

Sodium salicylate effects on prostate cancer aggressiveness and development of prostate cancer spheroids for drug evaluation

Wang, Ruisong

How to cite:

Wang, Ruisong (2019) *Sodium salicylate effects on prostate cancer aggressiveness and development of prostate cancer spheroids for drug evaluation*. Doctoral thesis, Swansea University.

<http://cronfa.swan.ac.uk/Record/cronfa51919>

Use policy:

This item is brought to you by Swansea University. Any person downloading material is agreeing to abide by the terms of the repository licence: copies of full text items may be used or reproduced in any format or medium, without prior permission for personal research or study, educational or non-commercial purposes only. The copyright for any work remains with the original author unless otherwise specified. The full-text must not be sold in any format or medium without the formal permission of the copyright holder. Permission for multiple reproductions should be obtained from the original author.

Authors are personally responsible for adhering to copyright and publisher restrictions when uploading content to the repository.

Please link to the metadata record in the Swansea University repository, Cronfa (link given in the citation reference above.)

<http://www.swansea.ac.uk/library/researchsupport/ris-support/>

SODIUM SALICYLATE EFFECTS ON
PROSTATE CANCER AGGRESSIVENESS AND
DEVELOPMENT OF PROSTATE CANCER
SPHEROIDS FOR DRUG EVALUATION

RUISONG WANG

Submitted to the Swansea University in Fulfilment
of the Requirements for the Degree of Doctor of
Philosophy

SWANSEA UNIVERSITY

2019

SUMMARY

Prostate cancer (PCA) is one of the most common cancers in males' affecting the genitourinary system. Although early stage PCA can be effectively treated, therapeutic options for patients with aggressive PCA are more limited and have lesser efficacy. In recent years, aspirin has been found to be an effective chemo-preventative treatment for a range of cancers. However, its mechanism of its action is not fully understood yet. Aspirin has shown great promise in PCA and is currently being employed in clinical trials. Thus, defining aspirin's molecular impact on prostate cancer cells would provide valuable information to improve the clinical management of PCA patients. This thesis aimed to evaluate the consequence of aspirin exposure on cell cycle, proliferation and functional parameters of prostate cancer cells to determine aspirin's mechanistic role in supporting the treatment of prostate cancer patients. This thesis also established a 3D culture system to enhance our standard *in vitro* models applied in the evaluation of drug efficacy and toxicity.


The metabolite of aspirin, salicylate, was exposed to PC3 and DU145 prostate cancer cell, and PNT2, a normal prostate cell line. Cytotoxicity analysis based upon relative population doubling (RPD), Real-Time Quantitative Polymerase Chain Reaction (RT-qPCR) for gene expression profiling and INCell Analyzer 2000 analysis for cell morphological and DNA damage assessment, were used to evaluate the cellular impact of salicylate exposure. The role of the COX-2 signalling pathway in salicylate's mode of action was considered by repeating salicylate exposure experiments in the presence of the inhibitor celecoxib; while activation of the NF- κ B pathway was also studied. To better understand the consequence of salicylate exposure on a human tumour, PC3 cell-spheroids were fabricated on agarose-coated 96 well-plates and were characterised by the MTT assay (cell viability), confocal microscopy (to assess necrosis, oxygen availability and morphology), and RT-qPCR for COX-2 expression. Salicylate was subsequently exposed to these spheroids and consequence of this treatment was established by comparing the experimental outcomes to the endpoints evaluated in 2D PC3 cell exposures.

Salicylate was found to downregulate effects on growth and COX-2 gene expression; it induced morphological changes, DNA damage and cell mitochondria loss; delayed the cell cycle; and increased intracellular Ca²⁺ level. These effects were more prominent in the PCA cells than in PNT2 cells indicating that the cancer cells were more sensitive to salicylate toxicity than normal prostate cells. The role of salicylate in PCA was partially COX-2-dependent and NF- κ B-dependent. Although similar responses were noted when salicylate was exposed to PC3 cell spheroids, generally the level of response was lower than observed in the 2D PC3 cultures.

The data contained within this thesis demonstrates that aspirin induces anti-cancer effects on PCA cells partially via NF- κ B and COX-2 mediated pathways. The 3D culture system provided an exciting and more realistic model for drug evaluation. Aspirin, therefore, has significant potential value for the clinician management of PCA patients.

DECLARATION

This work has not previously been accepted in substance for any degree and is not being concurrently submitted in candidature for any degree.

Signed  (candidate)

Date8/7/2019.....

STATEMENT 1


This thesis is the result of my own investigations, except where otherwise stated. Where correction services have been used, the extent and nature of the correction is clearly marked in a footnote(s). Other sources are acknowledged by footnotes giving explicit references. A bibliography is appended.

Signed  (candidate)

Date8/7/2019.....

STATEMENT 2

I hereby give consent for my thesis, if accepted, to be available for photocopying and for inter-library loan, and for the title and summary to be made available to outside organisations.

Signed  (candidate)

Date8/7/2019.....

TABLE OF CONTENTS

SUMMARY.....	I
DECLARATION	II
TABLE OF CONTENTS	III
ACKNOWLEDGEMENTS	VIII
LIST OF FIGURES.....	IX
LIST OF TABLES.....	XIII
ABBREVIATIONS.....	XIV
CHAPTER 1 GENERAL INTRODUCTION	1
1.1 Prostate cancer.....	1
1.1.1 Introduction to PCA	1
1.1.2 PCA Incidence Rates.....	5
1.1.3 Detection and grading methods for prostate cancer	6
1.1.4 Progression from localised to metastatic cancer	10
1.2 Available treatments for cancer patients	12
1.2.1 Watchful waiting.....	12
1.2.2 Radical prostatectomy	12
1.2.3 Radiotherapy.....	13
1.2.4 Transurethral resection of the prostate (TURP)	14
1.2.5 Hormone therapy.....	15
1.3 Aspirin's Pharmacology	16
1.3.1 Aspirin and its benefits for cancer patients	18
1.4 Cyclooxygenase and Cyclooxygenase-2 effects on cancer.....	20
1.4.1 Functions of <i>COX-2</i> and its involvement in cancer.....	21
1.4.2 <i>COX-2</i> expression in prostate cancer	22
1.4.3 Relationships between aspirin and the molecular mechanisms underlying PCA development	23
1.5 NF- κ B pathway.....	25
1.5.1 The NF- κ B signalling pathways	27
1.5.2 Aspirin's influence on the NF- κ B pathway.....	29
1.6 Aims.....	31
CHAPTER 2 MATERIALS AND METHODS.....	32
2.1 Chemicals and equipment.....	32
2.2 Computer software.....	35
2.3 Recipes for general buffers and solutions	35

2.3.1	Tris-HCl	35
2.3.2	NaS stock solution.....	35
2.3.3	20x saline-sodium citrate (SSC) solution	36
2.3.4	70% formamide/2xSSC	36
2.3.5	Celecoxib stock solution	36
2.3.6	Buffers used in western blotting	36
2.4	Cell lines and their culture methods.....	37
2.5	Cytotoxicity assay based on relative population doubling (RPD)	38
2.6	RNA extraction	38
2.7	cDNA synthesis.....	39
2.8	RT-qPCR.....	39
2.9	Assessment of cell morphological changes	40
2.10	Invasion assay	40
2.11	Migration assay	42
2.12	Nuclear and cytoplasmic protein extraction	43
2.13	Protein quantification.....	44
2.14	Western blotting.....	44
2.14.1	Preparation of stacking and resolving gels.....	44
2.14.2	Gel running and transferring.....	45
2.14.3	Primary and secondary antibody incubation	46
2.14.4	Membrane stripping and re-probing	47
2.15	Micronucleus assay.....	47
2.16	Micronucleus assay with centromere stain.....	48
2.17	Statistical analysis	49
CHAPTER 3 SODIUM SALICYLATE TOXICITY ON PROSTATE CANCER CELLS		50
3.1	Introduction	50
3.1.1	Effects of aspirin on invasion and migration	50
3.1.2	Micronucleus assay	51
3.1.3	Aims.....	53
3.2	Materials and Methods.....	55
3.2.1	Materials	55
3.2.2	Cell culture	55
3.2.3	Cytotoxicity assay	55
3.2.4	COX-2 gene expression assay.....	56
3.2.5	INCell analysis for morphological changes.....	57
3.2.6	MN frequency	57
3.2.7	Aneugenicity and clastogenicity mode of action analysis	57
3.2.8	High content morphological alterations.....	57

3.2.9	Cell cycle analysis.....	59
3.2.10	Invasion assay and migration assay.....	59
3.2.11	RT-qPCR array.....	60
3.2.12	RT-PCR for gene expression analysis.....	61
3.2.13	Statistical analysis.....	62
3.3	Results.....	63
3.3.1	NaS impact on inducing cytotoxicity in prostate cells.....	63
3.3.2	Impact of NaS on <i>COX-2</i> gene expression.....	64
3.3.3	Induction of DNA damage in response to NaS exposure.....	66
3.3.4	Aneugenicity and clastogenicity of NaS.....	67
3.3.5	INCell Analysis for cell cycle profile and cell morphological features.....	69
3.3.6	Cytvia™ Health Kit for Calcium level and mitochondrial changes.....	74
3.3.7	NaS effects on metastasis.....	78
3.3.8	PC3 and DU145 gene expression profiles after NaS treatment.....	84
3.4	Discussion.....	89
CHAPTER 4 EXPLORATION OF SODIUM SALICYLATE'S MODE OF ACTION.....		101
4.1	Introduction.....	101
4.1.1	<i>COX-2</i> inhibitors.....	102
4.1.2	<i>COX-2</i> -independent pathways and aspirin.....	104
4.1.3	Aims.....	105
4.2	Materials and methods.....	106
4.2.1	Materials.....	106
4.2.2	Cell culture.....	106
4.2.3	Pre-treatment to eliminate <i>COX-2</i> expression.....	106
4.2.4	<i>COX-2</i> RNA levels profile following celecoxib treatment.....	107
4.2.5	Cytotoxicity assay (RPD).....	109
4.2.6	INCell analysis for intracellular Ca ²⁺ and mitochondrial mass.....	109
4.2.7	Cell cycle analysis.....	111
4.2.8	NaS effects on NF-κB pathway and downstream targets.....	111
4.2.9	Statistical analysis.....	114
4.3	Results.....	115
4.3.1	Purity check for contamination of cytoplasmic extracts in nuclear cell extracts.....	115
4.3.2	Role of NF-κB with nuclear p65 and cytoplasmic IκBα.....	117
4.3.3	Impact of NaS toxicity when <i>COX-2</i> expression is inhibited.....	129
4.4	Discussion.....	137
CHAPTER 5 DEVELOPMENT AND CHARACTERISATION OF PROSTATE CANCER 3D SPHEROIDS AND EVALUATION OF SODIUM SALICYLATE IMPACTS ON SPHEROIDS CELLS.....		148

5.1 Introduction	148
5.1.1 Advantages and limitations of 3D versus 2D <i>in vitro</i> cell culture	148
5.1.2 3D cell culture techniques	152
5.1.3 Aims.....	154
5.2 Method and materials	157
5.2.1 Chemicals and kits used.....	157
5.2.2 Cell culture	157
5.2.3 PC3 Spheroid fabrication and size determination.....	158
5.2.4 NaS dosing.....	158
5.2.5 RNA extraction, cDNA synthesis and RT-PCR	158
5.2.6 <i>COX-2</i> expression analysis.....	159
5.2.7 miRNA extraction.....	159
5.2.8 cDNA synthesis.....	160
5.2.9 miRNA RT-PCR.....	161
5.2.10 MTT assay.....	163
5.2.11 Cell culture for imaging purposes	164
5.2.12 Confocal microscopy	164
5.2.13 Western blots	166
5.2.14 Statistical analysis	166
5.3 Results	167
5.3.1 Evaluation of spheroid growth and viability over time	167
5.3.2 Cell survival analysis of PC3 cells grown as spheroids	172
5.3.3 Structural analysis of PC3 spheroids	174
5.3.4 Profile of <i>COX-2</i> gene expression in 3D PC3 spheroids over time	175
5.3.5 NaS effects on cell viability in 3D PC3 models as compared to 2D monolayer cultures ..	176
5.3.6 NaS effects on the NF- κ B pathway in 3D PC3 cultures.....	178
5.3.7 NaS effects on <i>COX-2</i> expression in 3D PC3 spheroids compared to 2D PC3 culture.....	181
5.4 Discussion	184
5.4.1 Rationale for selection of seeding density and dosing time point	185
5.4.2 Oxygen availability in spheroids	187
5.4.3 Response of PC3 spheroids to NaS	188
CHAPTER 6 GENERAL DISCUSSION.....	197
REFERENCES	215
APPENDIX 1- IN CELL ANALYSER 2000 ANALYSIS PIPELINE FOR MICRONUCLEUS IDENTIFICATION	249
APPENDIX 2-REPRESENTATIVE IMAGES OF DU145 NUCLEI FOLLOWING 24-H NAS TREATMENT.....	253
APPENDIX 3-PCR ARRAY RAW RESULTS FOR CHAPTER 3	255

APPENDIX 4-WESTEN BLOTS UNDERLYING DENSITOMETRY DATA IN CHAPTERS 4 AND 5.....	262
APPENDIX 5- CONFOCAL MICROSCOPY GENERATED Z-STACK IMAGES SUPPORTING DATA IN CHAPTER 5.....	272

ACKNOWLEDGEMENTS

I have extremely enjoyed my four years of PhD study at Swansea University, which is sadly coming to an end. In the theoretical study stage, every step of the topic selection, queries, experiments and write-ups were carefully guided and helped by my supervisors, Professor Shareen Doak and Professor Gareth Jenkins. I would like to take this opportunity to express my heartfelt thanks to these guides. I would like to thank Shareen and Gareth who have taught me so much professional knowledge. In the writing of the thesis, Shareen always gives me profound and meticulous guidance. It is this selfless help and enthusiasm from her which means that my graduation thesis can be successfully completed. Without their kind and patient help, I could not be in this position and submit this thesis. I will always be grateful for all the help with my experiments from Ms Marg Clatworthy, Ms Sally James, Dr Kulsoom Shah, and all students in our labs.

I would also like to thank my family. Over the years, I have always been really grateful to my parents, Mr Wang Yijiang and Ms Cui Xiubin, for their unconditional support. Although they are not always geographically around, whenever I encounter setbacks or small achievements, they are always there for me. For 29 years, my parents have provided a rich material platform to enable me to go to school, and encouragement to realise my dreams. Without the love from you, I would have nothing. I would especially like to thank my wife, Huang Lan, who has shared all my highs and lows of my PhD. My four years of PhD study, tough but happy, would be completely eclipsed without her.

At last, I also wanted to say thank you to Ms. Kirsten Clift and Dr Stephanie Burnell. Their help with proofreading and reviewing has made this thesis more readable.

LIST OF FIGURES

Figure 1.1. Front view of the main tissue zones of the prostate.	2
Figure 1.2. Prostate anatomy and its location.....	3
Figure 1.3. Hydrolysis of aspirin that typically occurs in the liver <i>in vivo</i>	17
Figure 1.4. Relationship between plasma salicylate levels and oral administration of aspirin.....	18
Figure 1.5. Canonical NF- κ B pathway.	28
Figure 1.6. Non-canonical NF- κ B pathway.....	29
Figure 1.7. Proposed pathway for NaS interfering with the NF- κ B pathway. .	30
Figure 2.1. Schematic side view of a 24-well plate with insert utilised for the invasion assay.....	41
Figure 2.2. Schematic side view of a 24-well plate with insert utilised for the migration assay. Red areas indicate cells suspension.	42
Figure 2.3. Cassette setup for the membrane transfer stage of western blotting.	46
Figure 3.1. Plate layout for Cytivia™ Health kit INCell Analyser 2000 morphological analysis.....	58
Figure 3.2. RPD analysis for the PC3, DU145 and PNT2 cells following exposure to NaS.....	64
Figure 3.3 Relative COX-2 gene baseline expression in three prostate cell lines (PC3, DU145 and PNT2 cells).....	65
Figure 3.4. COX-2 expression profile after 24-h exposure to NaS. After 24 h of dosing, the RNA was extracted from the three cell lines (PC3, DU145 and PNT2 cells).	66
Figure 3.5. MN frequency in PC3, DU145 and PNT2 cells following NaS exposure..	67
Figure 3.6. Percentage of kinetochore positive MN in binucleated DU145 cells treated with NaS (6, 8 or 10 mM).	68
Figure 3.7. Representative images of binucleated DU145 nuclei when stained with Human Chromosome Pan-Centromeric paints.	69
Figure 3.8. Representative PC3 cells population distribution within the distinct cell cycle phases of based on DAPI intensity, as measured by the INCell Analyser 2000.	70
Figure 3.9. Cell cycle profile for A, PC3, B, DU145 and C, PNT2 cell lines.....	71
Figure 3.10. Representative working interface of INCell Analyser Workstation for transferring image data to numerical data.	72

Figure 3.11. Nuclear area in PC3 cells, DU145 cells and PNT2 cells treated with NaS.	74
Figure 3.12. Example INCell images of PC3 cells treated with the positive controls ionomycin and FCCP.	75
Figure 3.13. Representative images of the changes in mitochondria count in PC3 cells.	76
Figure 3.14. Mitochondria counts in each cell line. FCCP was the positive control for mitochondria.	76
Figure 3.15. Representative images of the changes in intracellular Ca ²⁺ level in PC3 cells.	77
Figure 3.16. Ca ²⁺ level in PC3 cells DU145 cells and PNT2 cells treated with NaS.	78
Figure 3.17. The NaS effects on migratory capacity of PC3 cells imaged at 0 (when the inserts were removed), and 24 h following the removal of the insert.	80
Figure 3.18. The NaS effects on migratory capacity of DU145 cells imaged at 0 (when the inserts were removed), and 24 h following the removal of the insert.	81
Figure 3.19. The NaS effects on migratory capacity of PNT2 cells imaged at 0 (when the inserts were removed), and 24 h following the removal of the insert.	82
Figure 3.20. Changes in average size of the gap between two sections of cells in the migration assay in PC3, DU145 and PNT2 cells after NaS treatment.	83
Figure 3.21. Invasive capacity of PC3, DU145 and PNT2 cells following NaS treatment.	84
Figure 3.22. Gene expression profiles changes in PC3 and DU145 cells treated with 0 and 4 mM NaS, based on the analysis of 84 genes.	86
Figure 3.23. Further exploration of the gene expression profiles of <i>CXCR2</i> , <i>ILB1</i> and <i>NR4A3</i> in PC3 cells following NaS exposure.	87
Figure 3.24. Further exploration for profiles of <i>CD44</i> , <i>CTSL1</i> and <i>ITGB3</i> profiles in DU145 cells following the PCR array in DU145 cells.	88
Figure 4.1. Flow chart of <i>COX-2</i> gene expression profiling after celecoxib treatment.	107
Figure 4.2. Examples of the purity check for contamination of cytoplasmic extracts in nuclear extracts in: A and B) PC3 cell extracts; C and D) PNT2 and PC3 cell extracts.	116
Figure 4.3. Profile of IκBα and nuclear p65 protein levels after TNF-α	

treatment in PC3 cells over the time.....	118
Figure 4.4. Profile of nuclear p65 protein levels after TNF- α treatment in PNT2 cells over the time.....	120
Figure 4.5. Profile of I κ B α protein levels after TNF- α treatment in PNT2 cells over the time.....	122
Figure 4.6. Representative example of western blots membrane of NaS role in the activated NF- κ B pathway in PNT2 cells by TNF- α	124
Figure 4.7. NaS role in the activated NF- κ B pathway in PNT2 cells by TNF- α	125
Figure 4.8. Representative image of western blots for PC3 cells exposed to NaS to evaluate nuclear p65 and cytoplasmic I κ B α	127
Figure 4.9. NaS role in PC3 cells with constitutive activation of NF- κ B pathway. A) 0.5 h's exposure time. B) 2 h's exposure time.....	128
Figure 4.10. <i>COX-2</i> gene expression profile after celecoxib treatment in PC3 and PNT2 cells.....	130
Figure 4.11. Cytotoxic effects of NaS on PC3 and PNT2 cells when pre-treated with celecoxib for 72 h to deplete <i>COX-2</i> gene expression.....	132
Figure 4.12. Nuclear and cell area in A) PC3 and B) PNT2 cells pre-treated with celecoxib, followed by NaS exposure.....	133
Figure 4.13. Cell cycle analysis in A) PC3 and B) PNT2 with co-exposure of celecoxib and NaS.....	134
Figure 4.14. Intracellular Ca ²⁺ levels in PC3 and PNT2 cells following co-exposure of celecoxib and NaS.....	135
Figure 4.15. Mitochondrial number in PC3 and PNT2 cells following co-exposure to celecoxib and NaS.....	136
Figure 5.1. Variation in diameter of PC3 spheroids over a 7-day culture period.....	168
Figure 5.2. Cell viability of PC3 spheroids and 2D monolayer cell culture over time.....	170
Figure 5.3. Confocal imaging comparing live cells and dead cells between the first day of culture and the 12th day at differing starting seeding densities.....	171
Figure 5.4. Images of oxygen availability in PC3 spheroids over 7 days of culture.....	173
Figure 5.5. <i>miR-210</i> gene expression in PC3 spheroids over 7 days of culture.....	174
Figure 5.6. Morphological evaluation of PC3 spheroids.....	175
Figure 5.7. Profile of <i>COX-2</i> gene expression in 3D PC3 spheroids compared to	

PC3 cells in 2D culture.....	176
Figure 5.8. Cell viability of PC3 in 3D culture vs. 2D culture when cells and spheroids were treated with NaS.	177
Figure 5.9. α -tubulin expression in nuclear extracts of PC3 spheroids to detect contamination of cytoplasmic extracts.	178
Figure 5.10. Examples of a representative western blot of A) cytoplasmic <i>IκBα</i> expression, and B), Nuclear p65 in PC3 spheroids treated with NaS.	180
Figure 5.11. Nuclear p65 and cytoplasmic <i>IκBα</i> expression in PC3 spheroids treated with NaS.	181
Figure 5.12. Baseline analysis for <i>COX-2</i> gene expression levels in PC3 spheroids, PC3 cells in 2D and PNT2 cells in 2D.	182
Figure 5.13. Effect of NaS exposure on <i>COX-2</i> gene expression levels in PC3 spheroids.	183
Figure 5.14. Schematic representation of NF- κ B suppression due to NaS treatment.....	192
Figure 6.1. NaS affects <i>COX-2</i> gene expression profiles via the NF- κ B pathway.	209

LIST OF TABLES

Table 2.1. Materials used for the project.	32
Table 2.2. Software used in this thesis.	35
Table 2.3 Buffers used in western blotting.	36
Table 2.4. Recipe for 4% stacking gel and 12% resolving gel.	45
Table 3.1. Materials used in Chapter 3.	55
Table 3.2. Primer sequences used for gene expression analysis by RT-qPCR in Chapter 3.	56
Table 3.3 Filter usage for the four reagents in Cytiva™ cell health kit.	59
Table 3.4. Primers used for further exploration of gene profiles after aspirin treatment.	62
Table 3.5. Genes with the highest expression changes in PC3 and DU145 cells after NaS treatment.	85
Table 4.1. Materials used in Chapter 4.	106
Table 4.2. Primer sequences used for gene expression analysis by RT-qPCR.	108
Table 4.3. Antibodies and ladders used for western blotting.	112
Table 5.1. Comparison of key growth and functional characteristics of cells cultured using 3D versus 2D technologies.	150
Table 5.2. Advantages, disadvantages and examples of different 3D culture systems available.	155
Table 5.3 Chemicals and kits used in Chapter 5.	157
Table 5.4. Reverse transcription reaction components.	161
Table 5.5. Reaction setup for real-time PCR.	162
Table 5.6. Primers for mRNA RT-qPCR.	162

ABBREVIATIONS

%	Percentage
<	Less than
=	Equal to
>	Larger than
α	Alpha
μg	Microgram
μL	Microliter
μm	Micrometer
103Pd	103Palladium
125I	125Iodine
2D	Two dimensional
3D	Three dimensional
3D CRT	Three-dimensional conformal radiation therapy
AC	Acinar adenocarcinomas
ADT	Androgen deprivation therapy
AEE	Aspirin eugenol ester
AJCC	American Joint Committee on Cancer
APS	Ammonium persulfate
AR	Androgen receptor
ATPase	Adenosine triphosphate monophosphates
Bcl-2	B-cell lymphoma 2
bFGF	Basic fibroblast growth factor
BM	Basement membrane
BMI	Body mass index
BPH	Benign prostatic hyperplasia
BSA	Bovine serum albumin
°C	Degree Celsius scale
CA	Carbonic anhydrase
CAB	Complete androgen block
CDKs	Cyclin-dependent kinases
CIAP2	Baculoviral IAP repeat-containing protein3
COX	Cyclooxygenases
COX-2	Cyclooxygenase-2

CPA	Cyproterone acetate
CRPC	Castration-resistant prostate cancer
CTSL1	Cathepsin L1
CXCL	CXC motif chemokine ligand
CXCR2	C-X-C Motif Chemokine Receptor 2
CZ	Central zone
DC	Ductal carcinoma
DHT	Dihydrotestosterone
DMSO	Dimethyl sulfoxide
DNA	Deoxyribonucleic acid
DRE	Digital rectal examination
e.g.	For example
EAU	European Association of Urology
ECM	Extracellular matrix
Egr-1	Early growth response protein 1
EMSA	Electrophoretic mobility shift assay
EP1	Prostaglandin E2 receptor 1
ERK	Extracellular signal-regulated kinase
FBS	Foetal Bovine Serum
FCCP	Carbonyl cyanide 4-(trifluoromethoxy)phenylhydrazone
FDA	Food and Drug Administration
fPSA	free Prostate-specific antigen
g	Gram
Gy	Gray
h	Hour
HBx gene	hepatitis B virus X gene
HCC	Hepatocellular carcinoma
HCl	Hydrogen chloride
HHBS	Hanks and 20 mM HEPES buffer
HR	Hazard Ratio
HRcP	Hormone-resistant PCA
i.e.	That is
IKK	I κ Bs kinase
IL-1	Interleukin-1
IL1β	Interleukin 1 beta
IL-6	Interleukin 6

IL-8	Interleukin 8
IMRT	Intensity modulated radiation therapy
iNOS	Nitric oxide synthase
ISUP	International society of urological pathology
ITGB3	Integrin beta-3 (β 3)
IκBα	Nuclear factor of kappa light polypeptide gene enhancer in B-cells inhibitor, alpha
kg	Kilogram
LH	Luteinising hormone
LHRH	Luteinising hormone releasing hormone
LHRHa	LHRH agonist
mCRPC	metastatic castration-resistant PCA
MDSC	Myeloid derived suppressor cells
mg	Milligram
min	Minute
miRNA	microRNA
mM	Millimole
MMP-2	Metalloproteinase 2
MMP-9	Metalloproteinase 9
MN	Micronucleus
MoA	Mode of action
MTT	3-(4,5-Dimethylthiazol-2-yl)-2,5-diphenyltetrazolium bromide
NaCl	Sodium chloride
NaS	Sodium salicylate
NASA	The National Aeronautics and Space Administration
NB	<i>Nota bene</i>
NF-κB	Nuclear factor kappa-light-chain-enhancer of activated B cells
NR4A3	Neuron-derived orphan receptor 1
NS-398	N-[2-(Cyclohexyloxy)-4-nitrophenyl]methanesulfonamide
NSAID	Non-steroidal anti-inflammatory drug
OA	Osteoarthritis
OS	Overall survival time
PBS	Phosphate buffered saline
PCA	Prostate cancer
PKD1	Phosphoinositide-dependent kinase 1
PFA	Paraformaldehyde
PGE2	Prostaglandin E2

PGI2	Prostacyclin
PI	Propidium iodide
PSA	Prostate-specific antigen
PZ	Peripheral zone
RA	Rheumatoid arthritis
RCCS	Rotary cell culture system
RNA	Ribonucleic acid
RPD	Relative population doubling
RPL-19	60S ribosomal protein L19
RT-qPCR	Real-Time Quantitative Polymerase Chain Reaction
Ru(ddd)	Tris(4,7-diphenyl-1,10-phenanthroline)ruthenium(II) dichloride complex
s	Second
SC-236	4-[5-(4-Chlorophenyl)-3-(trifluoromethyl)-1H-pyrazol-1-yl]-benzenesulfonamide
SCC	Small-cell carcinoma
SCF	Skp, Cullin, F-box containing complex
SDS	Sodium dodecyl sulphate
SQCC	Squamous cell carcinoma
SSC	Saline-sodium citrate
STAT3	Signal transduction and activation of the transcription 3
Survivin	Baculoviral inhibitor of apoptosis repeat-containing 5
TNF	Tumour necrosis factor
T/E	Trypsin/EDTA
TNM	Tumour, node and metastasis
TOMO	TomoTherapy
tPSA	total Prostate-specific antigen
TRUS	Transrectal ultrasound-guided
TURP	Transurethral resection of the prostate
TZ	Transition zone
UICC	International Union for Cancer Control
VEGF	Vascular endothelial growth factors
VMAT	Volumetric Modulated Arc Therapy
w/v	Weight/volume
XIAP	X-linked inhibitor of apoptosis protein
β	Beta
μM	Micromole
Δ	Delta

Chapter 1 General Introduction

1.1 Prostate cancer

Prostate cancer (PCA) is the most common malignancy reported among men in the world. It has the highest incidence and highest mortality rates compared to other types of cancer (Torre *et al.*, 2015). In the United Kingdom, the incidence rate of PCA ranks first in males and follows behind breast cancer rates when both genders are considered (NHS, 2015; CRUK, 2014a). There is a higher incidence of PCA in developed countries compared with developing countries (CRUK, 2014b). The incidence rate of PCA increases with age, like most cancer types, while men aged 50 and above suffer from a higher incidence of clinical PCA than that of young men (CRUK, 2014c).

1.1.1 Introduction to PCA

The prostate is an organ in the male mammalian reproductive system, consisting of glandular tissue and muscle tissue. The surface of the prostate is covered with fascia sheath, known as the prostate capsule, while the prostate venous plexus (consisting of the prostatic veins) lie between the capsule and the prostate. There are 4 different zones that exist within the prostate; they are the peripheral zone (PZ), central zone (CZ), fibromuscular zone and transition zone (TZ; Fig. 1.1). The prostate is an unusual organ in the human body as it has the capacity to act as both an exocrine and endocrine gland. As an exocrine gland, the prostate secret about 2 mL per day of prostatic fluid, which is the main component of semen. The primary function of the prostate is to store prostatic fluid, which is combined with sperm to produce semen. As an endocrine gland, the prostate secret hormones which are called "prostaglandins." There are anatomical, physiological and evolutionary differences of the prostate structure dependent on the species. For a healthy human male whose prostate size is slightly larger than a walnut, the prostate is located at the bottom of the pelvic cavity, under the bladder, on the urethra, at the back of the pubis, and in front of the rectum (Figure 1.2). The upper diameter of the prostate is about 4 cm, and the vertical diameter is about 3 cm.

Prostate zones

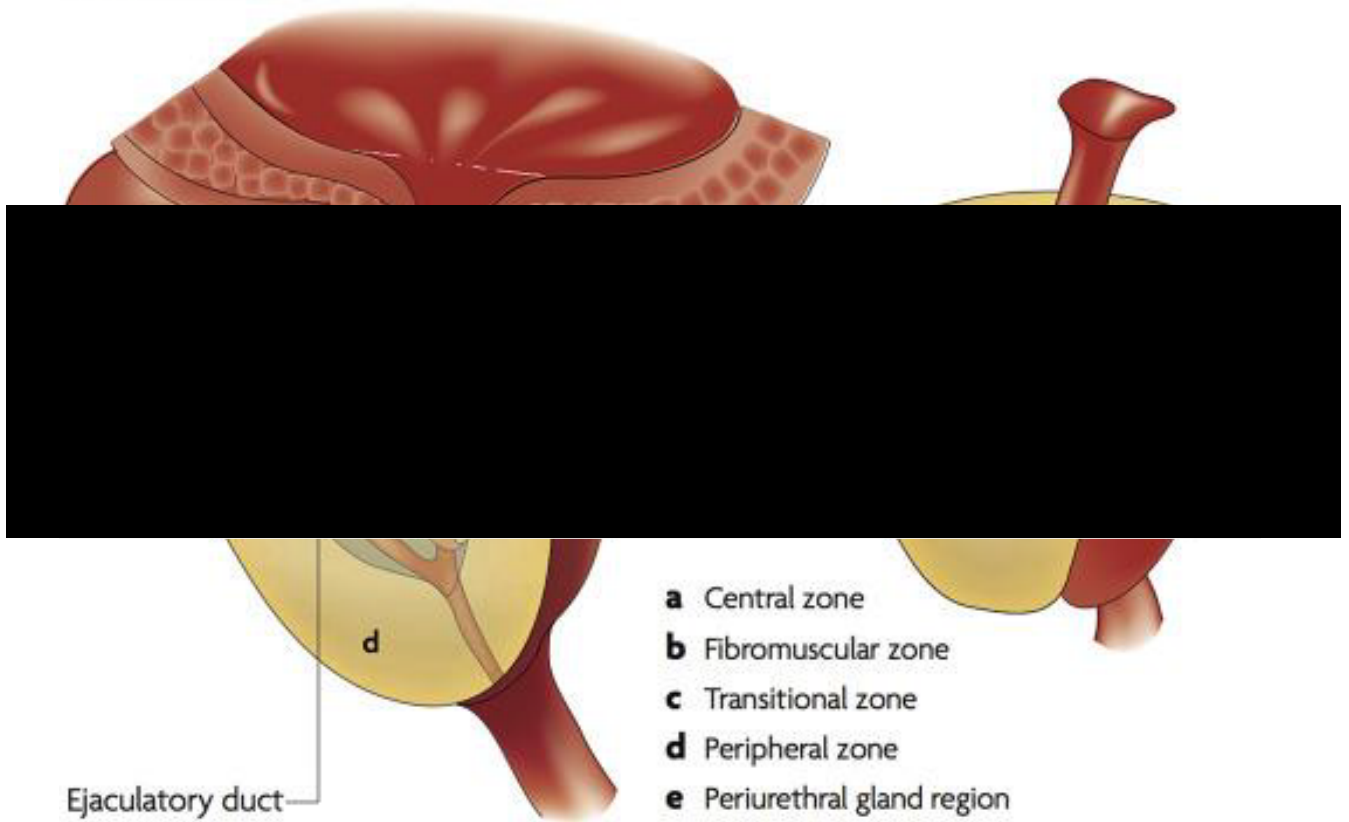
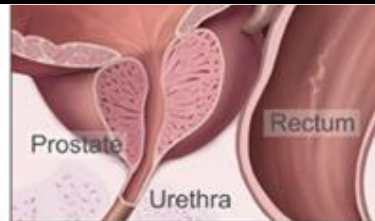
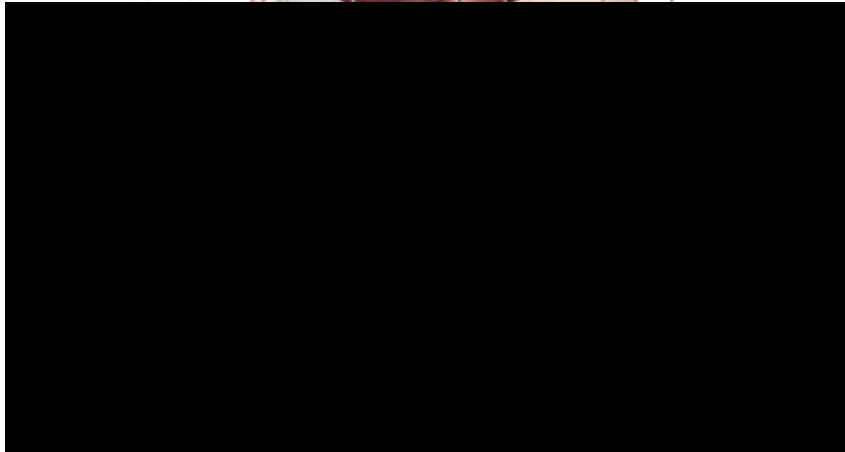
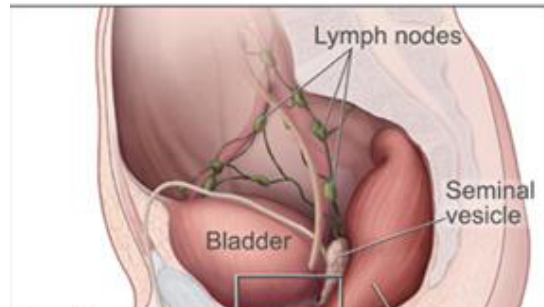


Figure 1.1. Front view of the main tissue zones of the prostate.

Source: Reeves et al., 2016.



This shows the inside of the prostate, urethra, rectum, and bladder.

Figure 1.2. Prostate anatomy and its location.

Source: <https://www.cancer.gov/publications/patient-education/prostate.pdf> on 22nd March 2017.

PCA is a malignant tumour appearing in the prostate. In addition to volume expansion and invasion of adjacent organs, cancerous cells may also metastasise to other parts of the body, especially the bones and lymph nodes. Prostate tumours predominantly develop in the PZ, with 75% of PCAs occurring in this zone (Shaikhibrahim *et al.*, 2012). At the dorsal and dorsolateral side of the prostate, only 20% of PCAs occur in the transitional zone (TZ) (Shaikhibrahim *et al.*, 2012; McNeal *et al.*, 1988; Guo *et al.*, 2009). It is currently unclear what molecular mechanisms dictate the zonal location of an individuals' prostate tumour; one theory suggests an embryological basis (Shaikhibrahim *et al.*, 2012).

PCA may cause discomfort, pain or aching in the testicles, difficulty in urinating, erectile dysfunction, lack of libido and blood in the urine. Acinar adenocarcinomas (AC) is the most common tumour type which clinicians encounter in daily diagnostic work (up to 95%) (Munoz *et al.*, 2007; Li and Wang, 2016). This tumour type is originally from the gland cells that line the prostate gland (Devita Jr *et al.*, 2015; Tobias *et al.*, 2014; CRUK, 2016; Li and Wang, 2016). There are several rare histologic variants coexisting, including ductal carcinoma (DC), squamous cell carcinoma (SQCC), small-cell carcinoma (SCC) (CRUK, 2016; Li and Wang, 2016; Huang and Chen, 2012). DC is the most common rare variant, accounting for 5% of total PCAs, and it develops from the primary periurethral prostatic ducts; on the contrary, AC arises from non-primary periurethral prostatic ducts (Baig *et al.*, 2015). Compared to AC, DC grows and metastasises more rapidly (DeVita *et al.*, 2012; Tobias and Hochhauser, 2014; CRUK, 2016). DC is rarely seen but is often found in association with an acinar component (Huang and Chen, 2012). Transitional cell cancer originates from the bladder and metastasises into organs nearby, such as the prostate. Therefore, it is rare to see transitional cell cancer arise in the prostate and when identified, it has likely spread from the urothelium (DeVita *et al.*, 2012; Tobias and Hochhauser, 2014; CRUK, 2016). As neuroendocrine cancer, the prostatic SCC was first defined more than 30 years ago. Since then, 0.5–2% of men with prostate cancer have been reported with this sub-type of PCA (DeVita *et al.*, 2012; Tobias and Hochhauser, 2014; CRUK, 2016). It is reported that this SCC arises from the same site as AC. SQCC of the prostate is a particularly unusual pathological and clinical entity, accounting for 0.5% to 1% of PCAs (MALIK *et al.*, 2011). Due to its rarity, the origin of SQCC has not been conclusively determined, and its cell of origin is also subject to debate. Older literature suggests the source of this rare malignancy is the prostatic urethral mucosa; however, in more recent articles, it has been suggested that SQCC arises from the transitional epithelium of periurethral ducts or the basal cells of prostatic acini (MALIK *et al.*, 2011; WERNERT *et al.*, 1990). These cancer cells have a similar growth rate and metastasis rate to AC (DeVita *et al.*, 2012; Tobias and Hochhauser, 2014; CRUK, 2016).

1.1.2 PCA Incidence Rates

Male Caucasian and African Americans have a higher incidence of PCA than xanthoderm populations in the world, especially within economically developed countries (Jemal *et al.*, 2011; Kimura, 2012). Within these sub-populations, there however is still variance in worldwide incidence rates, resulting from differences in screening practice, genetics and cultural background.

Firstly, genetic background has been confirmed as a risk factor, though the underlying mechanism of the cancer initiation remains mostly unknown (Colloca and Venturino, 2011). The risk of PCA is higher if family members have been diagnosed with the cancer compared to people without a family history of PCA (Pomerantz and Freedman, 2010; Lichtenstein *et al.*, 2000). Although there is a high risk in Caucasian populations, different countries have different incidence rates of PCA. According to Cancer Research UK statistics, in Australia and New Zealand, there were an estimated 101.86 cases of PCA per 100,000 men in 2012, and it is estimated that 26,130 cases were diagnosed in Oceania (CRUK, 2014d; Kimura, 2012). However, this incidence rate was 60% higher than that of Europe, where there were an estimated 64 cases of PCA per 100,000 male Europeans in 2012. Oceania had an incidence rate 4 times higher than Africans (23.19 cases of PCA per 100,000 men in 2012). In Asia, the incidence rate was much lower than any of the areas above, with an estimated 9.43 cases of PCA per 100,000 men in 2012. It is noteworthy that there is high variability in east Asian countries and southeast Asian countries, which is associated with their economic development (Kimura, 2012). Taiwan, Japan and South Korea have been financial leaders for a long time, and it has been found that the incidence rate of PCA in these countries (over 20 per 100,000) was higher than in other countries, such as China Mainland (9 per 100,000), Vietnam (5 per 100,000), and Philippines (less than 15 per 100,000). As the Philippines has had a higher GDP per capita for around 20 years than that of China, this may in part explain the slightly higher incidence (The World Bank, 2016).

It appears that the incidence rate of PCA can be explained via geographical and genetic

differences. Nevertheless, the differences cannot be fully explained. In the United States, which has a complex population with a high proportion of immigrants, there were an estimated 75.01 cases of PCA per 100,000 men in 2012. For Asian immigrants, their incidence rate of PCA was higher than Caucasian living in America as well as some European countries, which in turn is substantially higher than the incidence rates in their countries of origin (Arnold *et al.*, 2010). Thus, screening practice is thought to explain this because in China, Vietnam and other developing countries, even Japan, a screening practice (e.g. use of prostate-specific antigen (PSA) analysis), has not been incorporated into a systematic PCA screening programme. In Tianjin, a city of China, there is an international programme for PCA screening, and here the incidence rate is significantly increasing (Song *et al.*, 2008; Ito, 2014). Therefore, access to screening practice (such as PSA testing) substantially contributes to the global differences in the incidence rate of PCA. Nonetheless, despite immigrants having greater access to PSA screening compared to people in their birth country, their PCA incidence rate is still lower than that of African Americans and Europeans living in the same regions (Kimura, 2012). Some diet factors could be responsible for the elevated risk of PCA (Aune *et al.*, 2015; Lin *et al.*, 2015). For example, soy diets are popular in Asians while they are not often seen on the table of Caucasians and blacks and are thought to lower the risk of PCA by 25 – 30% (Yan and Spitznagel, 2009; Kurahashi *et al.*, 2007; Hwang *et al.*, 2009).

1.1.3 Detection and grading methods for prostate cancer

Based on a simple blood test, PSA has been widely used in the clinic and is currently the most sensitive tumour marker used in PCA detection and monitoring (Foekens *et al.*, 1999; Diamandis *et al.*, 1999). If the level of PSA is extremely high, then a digital rectal examination (DRE) is usually performed, with biopsy often recommended as a follow up. Prostate biopsy is the gold standard for the diagnosis of PCA. Hodge first proposed the 6-core transrectal ultrasound-guided prostate biopsy in 1989 (Hodge *et al.*, 1989). However, nowadays, a 12-core transrectal ultrasound-guided prostate biopsy has been found to improve the accuracy of the diagnosis (Abd *et al.*, 2011; Guo *et al.*, 2017).

1.1.3.1 Prostate specific antigen

PSA is a protein produced by prostate and ductal epithelial cells. The level of PSA can be measured with a blood sample from patients. In recent years, PSA screening has been increasingly applied for early screening of PCA. Under normal physiological conditions, prostate tissue can act as a natural barrier to high levels of PSA, limiting the level of serum PSA. Therefore, the level of PSA in the serum is not high in individuals that have no prostate-associated disease. However, when lesions exist, tissue architecture is abnormal and/or with rupture of prostate tissue, a large amount of PSA leaks into the serum, therefore increasing the level of PSA that can be detected in the blood. Based on this, testing serum levels of PSA has become an important method in prostate disease detection in clinical settings. Serum PSA levels have also become an important indicator for early observation and prognosis of PCA (Small and Roach, 2002; Polascik *et al.*, 1999; Nash and Melezinek, 2000).

From a general clinical viewpoint, serum PSA < 4 ng/mL is normal; however, PSA > 10 ng / mL indicates an increased risk of PCA (Atan and Güzel, 2013). This method is simple, and the price for screening is relatively cheap. This screening can eliminate the concern for most men as to whether they are suffering from PCA. Through PSA screening, PCA can be detected and treated in a timely manner, thereby reducing the incidence of metastatic disease and improving the survival rate of patients with PCA. At present, the "normal" threshold is reported as 0.0 to 4 ng/mL, but this value does varies with age (Lee and Oesterling, 1995; Goonewardene *et al.*, 2014). The prostate continues to grow with age and the continued proliferation of epithelial cells in the prostate affects both the volume of the gland and PSA levels; thus, the PSA range considered "normal" typically increases with age. In addition to age, there are other conditions not associated with cancer that can elevate PSA, such as the inflammatory condition, benign prostatic hyperplasia (BPH) (Kim *et al.*, 2016). The high PSA levels of the elderly may be also related to ischemia, embolism, subclinical inflammation, and physiological defences in the prostate gland (Khosravi *et al.*, 2016).

The scientific literature demonstrates that there is a direct correlation between the level of

PSA in serum and tumour progression (Lee and Oesterling, 1995; Goonewardene *et al.*, 2014; Wood *et al.*, 2016). Tumour stage can affect the level of PSA, which impacts the reliability to predict the degree of tumour progression. If a number of preoperative parameters, including the clinical stage (usually by DRE) and tumour classification (by biopsy) are combined, it can improve the PSA's predictivity (Lee and Oesterling, 1995; Goonewardene *et al.*, 2014; Wood *et al.*, 2016). In the actual clinical application of the PSA screening process, other parameters including volume of the prostate, free prostate specific antigen (fPSA) and total PSA (tPSA) will generally be used to improve the accuracy of PSA testing. By measuring the volume of the prostate, the ratio of the prostate volume to the serum PSA level can be obtained. Clinically, this ratio is often called PSA density. fPSA is not attached to proteins in a blood sample while bound PSA is attached to proteins in the blood. tPSA is equal to bound PSA and fPSA. In multivariate analysis, only PSA density and biopsy were considered to be the most relevant factors for PCA detection (Aslan *et al.*, 2005; Liu and Pan, 2014; Lin *et al.*, 2015).

PSA screening is however not infallible. In order to identify the normal baseline for males of different ages, a large amount of screening is still needed. Although PSA screening of asymptomatic men may prevent a person from dying of PCA, this is at the cost of screening a large number of healthy people. Secondly, during the screening process, each step causes a certain degree of harm to the body and mental burden. Moreover, as the sensitivity of PSA testing is not high, the false positive results (caused by age and non-cancer related disease) in particular may increase the patient's mental stress. It is also well known, that PSA is not always elevated in PCA in all patients, which means some patients with the disease can be missed or cannot be monitored appropriately upon diagnosis. A further problem is that although PSA screening enhances detection of PCA, in many of these patients the tumour will not affect the patient's quality of life as most often they are slow growing such that patients often die with the disease rather than dying because of their cancer. Thus, the cancer diagnosis can lead to over-treatment that in turn results in the patient suffering side-effects to the treatment that affect their quality of life. For example, radiotherapy and chemotherapy after radical resection can result in erectile dysfunction, urinary incontinence, and urethral complications (Korfage

et al., 2007). Thus, the cost-effectiveness of PSA screening is difficult to measure because of the lack of relevant data and the inability to calculate the economic, physical and mental costs of the patients (Korfage *et al.*, 2007).

In summary, PSA level is an important indicator for PCA screening, and early screening of PCA is of great significance to the early detection of PCA, having a positive effect on survival rates. However, as a biomarker, PSA it is not wholly ideal and further research to enhance the accuracy of PCA detection and subsequent monitoring is still warranted.

1.1.3.2 Transrectal ultrasound guided biopsies

Transrectal ultrasound-guided (TRUS) biopsies are the gold standard for the diagnosis of PCA (Kumari and Durga, 2014). The TRUS technique clearly shows the internal structure of the prostate, measures the size of the tumour and guides the biopsy. The advantages of TRUS are low costs, wide availability, and improved ability to visualize the prostate in real time (Kumari and Durga, 2014).

In 1989, Hodge *et al.* proposed a classic 6-core systematic prostate biopsy that has long been considered a standard for the diagnosis of PCA (Hodge *et al.*, 1989). However, it has been reported that the false negative rate with this puncture method was high due to insufficient puncture points covering the PZ where 80% of PCA originate (Eskicorapci *et al.*, 2004; Ceylan *et al.*, 2014). The detection rate of the tumour was therefore improved by increasing the number of biopsy cores taken (Eskicorapci *et al.*, 2005; Kanao *et al.*, 2014). At present, 8, 10, 11, 12, and 13 cores are now advised, dependent upon the patient's age, prostate volume and patient health among other clinical factors (Rifkin, 1998; Ukimura *et al.*, 2011; Thrasher, 2006). Older patients usually are associated with a shorter life expectancy, and so less cores are preferred to avoid complications. However, for young patients with longer life expectancy and when the PCA volume is small, by expanding the puncture area and increasing the number of cores, clinicians can obtain a more accurate diagnosis and classification of the tumour (Luciani *et al.*, 2006; Santoni *et al.*, 2016).

1.1.3.3 Gleason score

Grading PCA is important in prostate pathology to understand the severity of the disease and the degree of tumour progression, this is achieved by assigning a Gleason score based on the biopsy tissue morphology. Gleason score reflects the nine types of tissue growth of PCA. According to prognostic information, prostate tissue characteristics are divided into five patterns (Gleason, 1977). Low-score cancers (under Gleason 6) grow slowly and they are usually not metastatic. The moderate score is Gleason 7, while tumours scored from Gleason 8 to 10 grow more quickly and are more likely to metastasise (Gleason, 1977). Some PCA has only one kind of Gleason structure pattern, but most have more than one with the tumours having a primary pattern and secondary pattern. In order to more accurately reflect biological behaviour, Gleason proposed a scoring approach whereby if cancer has two kinds of structural pattern, Gleason score would be determined according to the main structure pattern (level) + secondary structure pattern (level). Since the 1990s, the National Comprehensive Cancer Network guidelines recommended treatment of PCA be based on Gleason score, PSA levels and tumour stage as they have been the most important indicators for disease progression. The Gleason grading system has been incorporated into the WHO classification of prostate cancer, and the American Joint Committee on Cancer /International Union for Cancer Control (AJCC/UICC) staging system. In 2014, a modified edition of the classification of prostate cancer was proposed by the 2014 International Society of Urological Pathology (ISUP) consensus, and then adopted by the 2016 WHO classification for tumours of the prostate (Epstein *et al.*, 2016).

1.1.4 Progression from localised to metastatic cancer

Accurate staging consensus for PCA prognosis and clinical management is essential, with the tumour, node and metastasis (TNM) staging system for PCA being an important means to evaluate progression from localised to metastatic cancer (Cheng *et al.*, 2012).

Staging of the tumour is based on a T1 – T3 score. PCA at T1 is localised (Edge and Compton, 2010). T1 stage cancer is defined as a tumour that is clinically inaccessible or cannot be examined by imaging in the 2010 TNM staging system (Edge and Compton, 2010). T1 stage

PCA is further divided into three categories defined by the proportion of cancer tissue in transurethral resection of the prostate (TURP) specimens, where prostatic tissue is removed by electrocautery or sharp dissection (Rajab *et al.*, 2011): T1a, found by TURP and where tumour tissue accounted for $\leq 5\%$ of excision tissue; T1b, found by TURP and tumour tissue accounted for $> 5\%$ of excision tissue; T1c, found due to PSA increases, followed by a puncture biopsy to locate the tumour. These thresholds determine the patient's treatment options.

T2 stage tumours are still confined to the prostate, but involve a greater volume within the gland and are divided into three categories (Edge and Compton, 2010; Huang *et al.*, 2015). T2a tumours are unilateral, involving less than half of only one side of the prostate; T2b tumours are also unilateral, but involve more than half of only one side of the prostate; and T2c tumours are bilateral (The National Comprehensive Cancer Network, 2010).

T3 stage tumours are those that have invaded tissue outside the prostate and may locate in seminal vesicles (Edge and Compton, 2010; Huang *et al.*, 2015). Extracorporeal invasion of cancer tissue beyond the prostate capsule is considered a poor prognostic factor. In studies with autopsy and radical prostatectomy, it was confirmed that PCA invasion was associated with tumour metastasis, seminal vesicle invasion and high Gleason score (Mcneal *et al.*, 1986; Gorin *et al.*, 2014; Porcaro *et al.*, 2016). Specimens are diagnosed as a T3a tumour if an invasion into the surrounding tissue fat is found in the biopsy or if there is spread to the neck of the bladder (Edge and Compton, 2010). Specimens are diagnosed as a T3b tumour if a puncture biopsy finds seminal vesicular invasion, where biochemical recurrence is typically 20% within 10 years (Edge and Compton, 2010). The final tumour stage associated with invasion is T4 where the tumour has spread to other organs near the prostate, including the rectum, anal sphincter and / or pelvic wall, instead of seminal vesicles (Edge and Compton, 2010; Huang *et al.*, 2015).

In addition to tumour staging, the TNM classification system provides staging for lymph node invasion and metastasis. Patients with tumour spread to local pelvic lymph node are categorised as N1; while those with no lymph node invasion are N0. If PCA spreads beyond

local lymph nodes, the degree of metastases is graded, whereby: M1a designates tumour spread beyond lymph nodes, M1b indicates spread to bone, and M1c represents tumours that have spread to other organs, such as lung, liver or brain.

1.2 Available treatments for cancer patients

Treatment of PCA includes surgical treatment, endocrine therapy, radiation therapy and chemotherapy. Clinicians plan the treatment according to the patient's specific circumstances, taking into consideration the patient's life expectancy, general health conditions, cancer score and staging (Stangelberger *et al.*, 2008; American Cancer Society, 2018; NHS, 2018).

1.2.1 Watchful waiting

Watchful waiting refers to the proactive monitoring of the patient's PCA (Bill-Axelsson *et al.*, 2005; Bill-Axelsson *et al.*, 2014). The theoretical basis of this method is that the incidence of PCA is positively correlated with age. Due to the inert growth of PCA, the incidence is much higher than the mortality rate (Bill-Axelsson *et al.*, 2014), and because of the development of PSA tests, many early PCAs are detected. Many scientists and clinicians believe that treatment for most patients where there are no clinical signs of aggressive disease has no significance to the patients, particularly when the risks and side-effects associated with radical surgery and other active treatment are considered (Bill-Axelsson *et al.*, 2005; Bill-Axelsson *et al.*, 2014). The current evaluation of outcome following active treatment versus watchful waiting continues, and we expect more evidence-based medical research to guide clinical decision-making. However, for most low-risk PCA patients with a life expectancy of less than 10 years and in generally good health, watchful waiting therapy is an option to avoid over-treatment.

1.2.2 Radical prostatectomy

Radical prostatectomy is one of the most effective ways to cure localised PCA (Bill-Axelsson *et al.*, 2005; Sun *et al.*, 2014). Surgical indications consider the risk factors of the tumour, life expectancy and overall patient health status (Bill-Axelsson *et al.*, 2005; Xylinas *et al.*, 2013; Sun *et al.*, 2014). Low-risk and medium-risk patients with localised PCA are recommended for

radical surgery, instead of short-term neoadjuvant endocrine therapy. High-risk patients with localised PCA can be treated with radical surgery, and postoperative adjuvant therapy can be given. Very high-risk PCA patients must be strictly screened for radical surgery and are often not offered this as an option if there is evidence of spread beyond the prostate capsule. Additionally, only patients who have over 10 years of life expectancy, with good physical condition and no severe cardiopulmonary diseases, would be considered a suitable candidate for radical prostatectomy as a treatment option (Bill-Axelsson *et al.*, 2005; Xylinas *et al.*, 2013; Sun *et al.*, 2014).

1.2.3 Radiotherapy

Radiation therapy for localised PCA is one of the primary treatments of PCA in older patients (Gu *et al.*, 2018). Radiation therapy is widely used in the localised low-risk, medium risk and high risk to pelvic lymph node metastasis groups, but is even considered for patients with distant metastasis of PCA (Hinev *et al.*, 2012; Böhmer *et al.*, 2016; Prostate Cancer UK, 2018).

Radiotherapy for PCA includes external radiotherapy (conventional irradiation, three-dimensional conformal radiotherapy, and intensity modulated radiotherapy) and brachytherapy (interstitial placement) (Tree and Khoo, 2009). Radiation therapy is suitable for the treatment of various stages of the tumour. In particular, in recent years, development of three-dimensional conformal radiation therapy (3D CRT), and intensity modulated radiation therapy (IMRT) technology makes the dose to localised tumour further improved, while systemic toxicity risk to the gastrointestinal and urinary tract are significantly reduced (Zelefsky *et al.*, 2008; Jani *et al.*, 2007).

As the prostate is located between the bladder and the rectum, conventional radiation techniques inevitably include most of the bladder and rectum in the field of radiation, so the dose to the target area is limited. With the application of 3D CRT and IMRT in clinical practice, the improvement of dose to local tumour becomes possible. For patients with low-risk PCA, simple radical radiotherapy can achieve a survival rate of more than 60% (Roach III *et al.*, 2008). However, for patients with high-risk cancer, radiotherapy alone may not be enough to cure

the tumour. Several randomised studies have demonstrated that endocrine therapy combined with radiotherapy can significantly improve the survival of these patients (Roach III *et al.*, 2008; Jones *et al.*, 2011; Bolla *et al.*, 2009).

Brachytherapy is radiotherapy where radioactive substances are placed into the prostate tissue. At present, the commonly used radionuclides are ^{125}I and ^{103}Pd . Particle beam therapy can be used as a single therapy for patients with low-risk PCA. For patients with moderate risk, particle placement therapy can be combined with external irradiation (45 Gy), with or without neoadjuvant endocrine therapy. However, the incidences of complications are also increased. It is generally believed that high-risk localised advanced patients are not suitable for particle beam radiotherapy, but in recent years, some centres have demonstrated a combination of external irradiation and a high-dose-rate of brachytherapy can be safely applied for medium risk or high-risk PCA patients (Fang *et al.*, 2008; Pieters *et al.*, 2008; Soumarová *et al.*, 2007).

1.2.4 Transurethral resection of the prostate (TURP)

TURP is the primary method of removing a urethral obstruction in the prostate and is the main treatment for patients with BPH. After decades of clinical practice as a treatment of BPH, TURP has been recognised as the gold standard for PCA treatment (Pathak *et al.*, 2017). Patients with advanced clinical stages of PCA have limited treatment options including endocrine therapy, drug-based or surgical castration, total hormone block therapy, local irradiation and nuclear intraocular irradiation. These therapies can inhibit tumour cell growth, but advanced PCA patients are likely to have symptoms of urinary tract obstruction (Lieberman *et al.*, 2016). TURP can be used to alleviate this and improve the quality of life of patients in the short-term (Lee *et al.*, 2013; Lawrence *et al.*, 2015; Palmer *et al.*, 2017; Lieberman *et al.*, 2016). TURP alone is however considered a palliative treatment and does not prevent PCA progression.

1.2.5 Hormone therapy

Since Huggin *et al.* first reported that androgen therapy could block the progression of PCA, endocrine therapy has gradually become a vital palliative treatment for PCA (Huggins, 1978). However, due to adverse effects upon the quality of life of patients, including hot flushes, low libido, erectile dysfunction, male breast development, insulin resistance and cardiovascular disease, endocrine therapy is controversial. Additionally, endocrine therapy leading to castration-resistant PCA (CRPC) is still a clinical challenge, which limits its use.

Castration treatment aims to reduce the concentration of serum testosterone to castration level (5% to 10% of the baseline value before treatment) to inhibit the growth of PCA cells. Castration treatment mainly includes surgical castration and chemical castration (Heidenreich *et al.*, 2014). Surgical castration includes bilateral testicular resection and bilateral testicular parenchymal exfoliation to reduce the testosterone produced by the testes significantly. However, the psychological impact on patients is noticeable and the secretion of androgen from the adrenal gland can still promote the progression of PCA (Heidenreich *et al.*, 2014; Yuan *et al.*, 2014). Currently, it is used for the treatment of patients with bone metastatic spinal cord compression (Tazi *et al.*, 2003; Wänman *et al.*, 2017). For most patients, chemical castration treatment is preferred, where testosterone can be reduced to castration level by drugs without removal of testes. Clinical trials have demonstrated that the efficacy of chemical castration is equivalent to bilateral testicular resection and the effects are reversible when treatment is discontinued (Zlotta and Debruyne, 2005; Tombal and Berges, 2005; Gomella, 2009; Griffin, 2018).

Anti-androgen therapy is the use of anti-androgen drugs to block or reduce the role of androgen. Anti-androgen drugs can compete with dihydrotestosterone (DHT) or testosterone in prostate cells' androgen receptor, and then initiate apoptosis and inhibit the growth of androgen-dependent PCA. Most patients can have their symptoms controlled by endocrine therapy; however, after 18 to 24 months (median), almost all patients will develop CRPC (Merseburger *et al.*, 2015). At this stage, treatment options become highly limited, with

docetaxel- and abiraterone-based regimens being the preferred treatment for CRPC, expanding patients' survival time by a median of 4 months (Cheever and Higano, 2011).

1.3 Aspirin's Pharmacology

Aspirin is a non-steroidal anti-inflammatory drug (NSAID) which is used for antipyretic, analgesic, anti-inflammatory and anti-platelet aggregation purposes, and has been widely applied in clinical practice. It is also a common household drug and is used for the prevention of cardiovascular disease, such as thrombosis, coronary heart disease and stroke (Ong *et al.*, 2007).

The gastrointestinal (GI) tract is the main place where aspirin is absorbed and it is primarily hydrolysed in the liver to the acetate and salicylate ions as shown in Figure 1.3 (Alfonso *et al.*, 2014). Both of these products subsequently circulate in the plasma. The acetyl group of aspirin can acetylate several proteins including COX proteins through a trans acetylation reaction *in vitro* and *in vivo* (Rainsford *et al.*, 1983; Alfonso *et al.*, 2014). Several other biomolecules, such as haemoglobin, DNA, RNA, histones, transglutaminase as well as other plasma constituents including hormones and enzymes can also be acetylated by aspirin (Lai *et al.*, 2010; Alfonso *et al.*, 2014). It has been demonstrated using radiolabelled aspirin that the binding of the acetyl group of aspirin occurs with several proteins, such as glycoproteins and lipids of the stomach, kidney, liver and bone marrow when administered *in vivo* (Rainsford *et al.*, 1983). The salicylate product from aspirin causes DNA degradation which is related to apoptosis induction (Ishiyama *et al.*, 2004; Dhanoya and Burn, 2016). It is also suggested that salicylates partially depolarize mitochondria, disturbing the uptake of calcium ions, which in turn has a negative impact on cell proliferation (Núñez *et al.*, 2006; Dhanoya and Burn, 2016). This is supported by studies in which sodium salicylate is found to induce apoptosis in cancer cells and it has been suggested that this anti-cancer effect is reliant on the salicylic acid component of aspirin (Dhanoya and Burn, 2016). The anti-neoplastic effects are generally attributed to inhibition of prostaglandin G/H synthase and cyclooxygenase (such as COX-2 protein) from converting arachidonic acid to potentially tumour-inducing prostaglandins (Dhanoya and Burn,

2016). These recent studies therefore indicate the salicylate metabolite is of particular interest when exploring the mechanistic anti-cancer properties of aspirin.



Figure 1.3. Hydrolysis of aspirin that typically occurs in the liver *in vivo*.

Despite its clinical benefits, due to its side effects of bleeding risk and ulcers, aspirin is not currently approved for cancer prophylaxis (Alfonso *et al.*, 2014). Aspirin is administered over a wide dose range from 75 mg (antiplatelet and cardiovascular diseases) to 325–600 mg (analgesic), and even up to 1.2 g (anti-inflammatory) depending on the conditions of patients (Dovizio *et al.*, 2013; Alfonso *et al.*, 2014). With oral administration, low-dose (less than 75 mg) aspirin gives a peak plasma concentration of about 7 μM ; however, analgesic (about 300 mg) and anti-inflammatory (1,200 mg) doses can yield plasma concentrations ranging from 30 to 150 μM (Figure 1.4) (Dovizio *et al.*, 2013; Alfonso *et al.*, 2014). Low-dose aspirin is estimated to provide 20 μM plasma salicylate concentrations obtained from the hydrolysis, whereas for analgesic purposes, the plasma levels can be up to 1000 μM , while anti-inflammatory effects are achieved at concentrations ranging from 2,000 to 4,000 μM after oral administration (Dovizio *et al.*, 2013; Alfonso *et al.*, 2014). It has been found in many studies that long-term oral administration with doses ranging from 81 to 325 mg lead to a decrease in the incidence and mortality associated with colorectal cancer (Rothwell *et al.*, 2012; Dovizio *et al.*, 2013). However, this relationship needs to be explored further with other cancer types where data is far more limited.

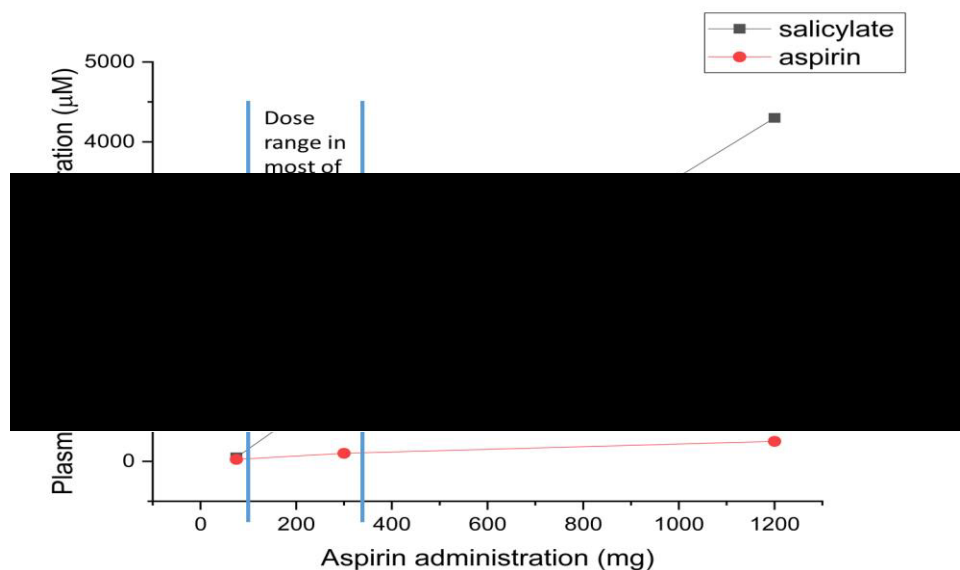


Figure 1.4. Relationship between plasma salicylate levels and oral administration of aspirin.

1.3.1 Aspirin and its benefits for cancer patients

Aspirin has demonstrated many clinical benefits for decades. In the 1970s, the effects of aspirin inhibiting platelet aggregation made its use wide-spread to prevent cardiovascular and cerebrovascular disease. It also demonstrates anti-diabetic, anti-heart disease, and anti-Alzheimer's disease properties (Ng *et al.*, 2015; Araujo *et al.*, 2016; Mc Menamin *et al.*, 2015). Aspirin is now recognized as the cornerstone of prevention of cardiovascular diseases. Long-term, rich clinical experience has also demonstrated the anti-inflammatory effects of aspirin. During this routine use however, it has been noted that aspirin appeared to reduce the morbidity and mortality of some cancers (Elwood *et al.*, 2016). Thus, the relationship between aspirin and cancer prevention has been the focus of increasing research interest.

Epidemiological studies have demonstrated that aspirin can reduce the incidence of colorectal cancer, oesophageal cancer, colon cancer and lung cancer, showing that aspirin has promising anti-tumour properties (Langley *et al.*, 2011; Mc Menamin *et al.*, 2015; Hao *et al.*, 2018; Li *et al.*, 2018). Experimental results show that aspirin can inhibit tumour cell growth and proliferation, induce tumour cell apoptosis, and inhibit tumour angiogenesis, invasion and

metastasis through multiple signal transduction pathways.

Animal experiments and epidemiological studies have confirmed that aspirin is effective in some common cancers and can prevent vascular disease (Rothwell *et al.*, 2012). For example, a study by Professor Rothwell, at Oxford University, provides strong evidence for aspirin's anti-cancer effect. The study included five large randomised controlled trials involving 17,285 subjects. For cardiovascular patients in the UK, aspirin (> 75 mg) was administered daily in the trial group to record the incidence of cancer in all new and concurrent patients, followed by an observation of the effect of aspirin on tumour metastasis. Cancer patients were classified according to tumour histology and clinical features. Among them, 987 patients were diagnosed with solid tumours at an average of 6.5 years (standard deviation of 2.0) during follow-up. Compared with the control group, aspirin reduced the risk of the distant metastasis rate for adenocarcinomas (Hazard Ratio, HR) to 0.64 (95% CI value of 0.48-0.84, $p=0.001$). However, it was ineffective for advanced cancers ($p=0.64$). The study also found that aspirin is effective for any age and gender group (Rothwell *et al.*, 2012). It was concluded that compared with the control group, taking aspirin daily could reduce the mortality of cancer patients. This study shows that aspirin contributes to the treatment of certain cancers, providing evidence of its efficacy in drug intervention, in particular by inhibiting tumour metastasis (Rothwell *et al.*, 2012). Aspirin is also a preventive measure for gastroenteric tumours, and it can inhibit proliferation of tumour cells (Chan *et al.*, 2005). Research has demonstrated that in colorectal cancer patients who had taken 325 mg aspirin per day for 31 months, only 17% had cancer recurrence, compared with 27% in the control group (Imperiale, 2013; Rosenberg *et al.*, 2009; Chan *et al.*, 2005). Whilst, in another study, after three-years of observation, it was found that when colorectal cancer patients took 81 mg aspirin daily, the recurrence rate was 19% lower than that of the control group who took a placebo. A population-based case-control study explored the relationship between aspirin and the risk of prostate cancer. The study analysed data from 1,001 prostate cancer patients and 942 older people between January 1st, 2002 and December 31st, 2005, and found that the risk of prostate cancer was 21% lower in patients taking aspirin than in those who did not (95% CI: 0.65 to 0.96) (Salinas *et al.*, 2010). It has no

preventive effect on endometrial cancer, and melanoma, but may reduce the risk of breast cancer, lung cancer, pancreatic cancer, and prostate cancer (Zhang *et al.*, 2015c; Bilani *et al.*, 2017).

Reports on the efficacy of aspirin in prostate cancer treatment do however vary in the literature (Baron *et al.*, 2003). The different administration dose and time, and the stage of PCA may be underlying reasons for some of the inconsistencies (Bosetti *et al.*, 2014; Elwood *et al.*, 2018). For example, a study involving 34,132 men of 50 to 76 years of age who participated in vitamin and lifestyle studies, reported that there was no relationship between NSAIDs including low-dose aspirin and conventional aspirin with the reduced risk of prostate cancer (Brasky *et al.*, 2010). However, in this study, Brasky *et al.* (2010) only used PSA as their indicator for prostate cancer, which is not an ideal approach given the limitations of PSA discussed above (Section 1.1.3.1).

The discovery of the aspirin anti-cancer effect has a practical significance to the prevention and treatment of cancer, which has aroused widespread interest, but there are some concerns as it may lead to a risk of gastrointestinal bleeding and so should only be used under the guidance of a clinician. At the moment there is limited understanding of the mechanisms by which aspirin functions as an anti-cancer agent and this is an area that requires further research.

1.4 Cyclooxygenase and Cyclooxygenase-2 effects on cancer

Cyclooxygenase (COX) is an important rate-limiting enzyme in the biosynthesis of prostaglandins by arachidonic acid and it participates in a variety of pathophysiological processes (Nørregaard *et al.*, 2015). Currently, three subtypes of COX have been found, namely, COX-1, COX-2 and COX-3 proteins. COX-1 proteins maintains normal physiological functions of the human body, such as gastrointestinal mucosal protection and renal blood flow regulation (Pathak *et al.*, 2014). It is involved in prostaglandin (PG) production as well as physiological processes. COX-3 protein is considered a variant of COX-1 protein, expressed mainly in the cerebral cortex and heart (Kraus *et al.*, 2013). However, COX-2 protein is an inducible enzyme

that is not expressed or expressed to a very low level in most cells (Nørregaard *et al.*, 2015). NSAIDs including aspirin, especially selective *COX-2* gene inhibitors, mainly regulate *COX-2* gene expression to affect growth of the cancer cells (Sobolewski *et al.*, 2010).

1.4.1 Functions of *COX-2* and its involvement in cancer

The *COX-2* gene is a "rapid response gene". It is a polypeptide consisting of 10 exons and 9 introns, which includes two activation protein-2 (AP-2) sites, 2 activation sites of nuclear factor kappa-light-chain enhancer of activated B cells (NF- κ B), TATA box sequence, CCAA enhancer binding protein site (C/EBP), cAMP responsive element (CRE), and Etw-1 transcription factor sites (Joan, 2003; Shi *et al.*, 2015). The *COX-2* gene is not expressed in most tissues or cells types, but is inducible and is often expressed in macrophages, synoviocytes, fibroblasts, osteoblasts, tumour cells, and activated endothelial cells (Araki *et al.*, 2003). The *COX-2* protein is a key enzyme in catalysing arachidonic acid synthesis of prostaglandin (PG). *COX-2* is an adaptive enzyme, located mainly in the nuclear membrane; the *COX-2* gene is also expressed in the central nervous system, and is associated with nerve responses to fever and pain (Martin *et al.*, 2007).

COX-2 gene plays an important role in the development of tumours, and its up-regulation is related to tumour cell proliferation, transformation, promotion of angiogenesis, invasion and metastasis (Shao *et al.*, 2012; Zhan *et al.*, 2013). Shirakawa *et al.* (2004) reported that there was a high expression of *COX-2* in benign lesions and malignant tumours such as PCA and breast cancer. They suggested that the *COX-2* gene may be involved in cancer occurrence and development (Shirakawa *et al.*, 2004). *COX-2* at the site of inflammation can catalyse the production of PGs associated with pro-inflammatory responses, it therefore plays an important role in inflammatory processes (Wang and DuBois, 2010). Factors that induce *COX-2* expression are oncogenes, hypoxia, ultraviolet light, interleukin-1, *etc.*, while antioxidants, dexamethasone and the tumour suppressor protein p53, can inhibit its expression (Fosslien and Science, 2000; Laube *et al.*, 2016). It is now generally considered that *COX-2* may be involved in tumour growth because it can suppress apoptosis and also promote cell proliferation (Sobolewski *et al.*, 2010). It is also associated with inhibition of immune function

and promoting angiogenesis (Liu *et al.*, 2015a).

Many studies show that chronic inflammation with tissues exhibiting abnormal expression of *COX-2* as a manifestation is closely related to the occurrence and development of a variety of tumours (Vendramini-Costa and Carvalho, 2012). This is evidenced by the fact that when cells are stimulated by pro-inflammatory cytokines, the *COX-2* gene is upregulated and is involved in continued inflammation and the formation and development of tumours (Gandhi *et al.*, 2017). Evidence from genetic and clinical studies suggest that increased gene expression of *COX-2* is one of the key steps of carcinogenesis (Kim *et al.*, 2011; Vendramini-Costa and Carvalho, 2012). Recent studies have demonstrated that the *COX-2* gene is highly expressed in many human malignancies and pre-cancerous lesions, such as colorectal cancer, lymphoma, malignant melanoma and breast cancer (Coussens and Werb, 2002; Mazhar *et al.*, 2006; Bundred and Barnes, 2005; Ferrandez *et al.*, 2003; Kim *et al.*, 2011; Pang *et al.*, 2016).

1.4.2 *COX-2* expression in prostate cancer

Overexpression of *COX-2* has also been reported in prostate cancer where it is closely related to progression and prognosis of PCA, and generally higher expression is associated with metastatic PCA (Kraus *et al.*, 2013). Yoshimura *et al.* evaluated *COX-2* expression levels in 28 cases of PCA tissue, 8 cases of normal prostate tissue and 8 cases of BPH tissue (Yoshimura *et al.* 2000). The results showed that relative to the normal prostate and BPH cases, the expression of *COX-2* in cancer tissue samples was significantly increased, suggesting that *COX-2* overexpression is closely related to the occurrence of PCA (Yoshimura *et al.*, 2000). In order to directly demonstrate the biological function of *COX-2* on the prostate, Fujita *et al.* (2002) transfected the human exogenous *COX-2* gene into LNCaP cells where the expression of endogenous *COX-2* was low. They found that the group transfected with the exogenous *COX-2* gene proliferated faster than the group with the low endogenous *COX-2* expression, indicating that *COX-2* can promote prostate cancer cell proliferation (Fujita *et al.*, 2002).

The biological function of *COX-2* protein is closely related to its products, the PG. Ruan and So (2014) transfected human embryonic kidney (HEK293) cells with *COX-2* protein and

Prostaglandin E2 (PGE2) to induce overexpression of the protein and co-cultured these cells with PCA cells. This study demonstrated that compared with the normal HEK293 cells, the proliferation of PCA cells cultured with transfected-HEK293 cells was more rapid suggesting the increase of *COX-2* and *PGE2* gene in the tumour microenvironment could promote PCA cell proliferation (Ruan and So, 2014). *COX-2* is also thought to inhibit apoptosis following a study evaluating tissues from 57 PCA patients where the *COX-2* gene was overexpressed (Kim *et al.*, 2011).

High expression of *COX-2* can upregulate the synthesis of PG (especially PGE2) with cancer-promoting activity (Sobolewski *et al.*, 2010). PGE2 protein can promote tumour growth by promoting the proliferation of tumour cells, promoting angiogenesis, and inhibiting the body's immune surveillance (Nakanishi and Rosenberg, 2013). In addition, PGE2 protein stimulates the paracrine and autocrine prostaglandin receptors, thereby inhibiting the occurrence of apoptosis in a variety of tissues (Jabbour *et al.*, 2002; Lalier *et al.*, 2011). It is believed that *COX-2* inhibitors can exert their anti-tumour effects by inhibiting the activity of *COX-2* and reducing the synthesis of PGE2 (Tsubouchi *et al.*, 2000). The acetylation of *COX-2* proteins is one way to inhibit its activity. The serine Ser530 active site of *COX-2* is acetylated by aspirin, thus irreversibly aspirin inhibits *COX-2* proteins' activity. Consequently, arachidonic acid is sterically prevented from contacting with the activated tyrosine Tyr385, subsequently blocking the synthesis of prostaglandins (Blobaum and Marnett, 2007; Kamble *et al.*, 2015; Lucido *et al.*, 2016). Hence, this evidence suggests that *COX-2* expression could be a promising target for the prevention and treatment of PCA (Algra and Rothwell, 2012; Gupta *et al.*, 2013; Shan *et al.*, 2013).

1.4.3 Relationships between aspirin and the molecular mechanisms underlying PCA development

Due to the multi-potent nature of aspirin, its mode of action in preventing the progression of PCA has not been clearly elucidated, although both *COX-2* dependent and independent pathways may be of importance.

1.4.3.1 COX-2-dependent pathway

It has been found that aspirin irreversibly acetylates and inactivates the cyclooxygenase protein (Vane, 1971; Roth *et al.*, 1975). Via the COX-2-dependent pathway, COX-2 gene expression can be downregulated and then PG synthesis is blocked or the COX-2 proteins' activity is reduced by aspirin's acetylation. Acetylation, is a significant post-translational modification that has a significant impact on the function of a wide range of proteins in humans (Choudhary *et al.*, 2009). Zhao *et al.* (2010) have found 41,000 proteins are naturally acetylated in human liver cells and they believe this nature of acetylation is universal. Acetylation is involved in activating, inactivating or destabilising metabolic enzymes thereby controlling enzyme activity (Xu *et al.*, 2014b). In cancer, acetylation is deregulated (Xu *et al.*, 2013). The capability of aspirin to chemically acetylate either proteins (COX-2) / biomolecules (RNA) has therefore enormous therapeutic significance (Alfonso *et al.*, 2014).

Given that aspirin is an NSAID, the mechanism of action of aspirin in preventing cancer may be related to a COX-2-dependent pathway. Hence, aspirin may inhibit the COX-2 pathway and block the proliferation of cancer cells, thereby preventing the cancer (Sostres *et al.*, 2014). However, little research has been done in this area with respect to PCA to date.

1.4.3.2 COX-2-independent pathways

Aspirin may also have an influence on COX-2-independent pathways leading to an anti-cancer effect. Aspirin can irreversibly acetylate a wide range of proteins. For example, Alfonso *et al.* (2014) found that aspirin can dose-dependently acetylate p53, up-regulating Bax induced tumour cell apoptosis. At the same time, aspirin can down-regulate the p21Cip1 protein (Alfonso *et al.*, 2009; Alfonso *et al.*, 2014). Marimuthu *et al.* (2011) found that aspirin can acetylate a large number of intracellular proteins in the colon cancer cells HCT-116. Moreover, aspirin arrests cells in G₁/G₀ phase; Luciani *et al.* (2007) found that aspirin can cause G₁ arrest and apoptosis in cells deficient in COX-2, through activation of the checkpoint kinase Ataxia-telangiectasia-mutated kinase (ATM). Aspirin's pro-apoptotic response is thought to occur through its ability to activate caspase and Bcl-2. Caspase is a cysteine-containing aspartate

proteolytic enzyme, which is a group of proteases that includes 13 members (caspase-1 to 13). Caspase usually exists as an inactive zymogen but activated caspase can rapidly induce apoptosis in diseased cells. Yan *et al.* (2013) applied aspirin to the breast cancer cell MDA-MB-453 and found that it can directly up-regulate caspase-3 by degrading transcription factor AP-2 alpha to induce tumour cell apoptosis. The Bcl-2 family of proteins is an endomembrane-associated protein that regulates programmed cell death (Youle and Strasser, 2008). Aspirin is known to down-regulate the expression of the anti-apoptotic protein Bcl-2 and promotes the expression of the pro-apoptotic protein Bax (Choi *et al.*, 2013).

Aspirin has also been found to affect angiogenesis. The progression of malignant tumours depends on the supply of oxygen and nutrients by blood vessels, which is a necessary process for tumour growth and metastasis. Borthwick *et al.* (2006) found that the combination of the COX-2 selective inhibitor celecoxib and the COX-1 selective inhibitor SC560 in the selected dose range did not affect angiogenesis. In contrast, aspirin, as a non-selective inhibitor of COX, demonstrated an inhibitory effect on angiogenesis, suggesting that aspirin's effect on angiogenesis is COX-independent (Borthwick *et al.*, 2006).

1.5 NF- κ B pathway

In 1986, NF- κ B was first identified as a nuclear factor consisting of a light chain gene (5c-GGGACTTTCC-3c) from an enhancer element of IgJ, the immunoglobulin. However, at that time it was believed that NF- κ B was specifically expressed in mature B cells (Oeckinghaus and Ghosh, 2009). Subsequent studies found that NF- κ B was expressed in most tissues and cells, but its activity differed in varying cells types and under different environmental conditions. Now it is understood that the Rel/NF- κ B family members are divided into two groups: one group includes NF- κ B 1 (p50 and its precursor p105) and NF- κ B 2 (p52 and its precursor p100); and the other group includes Rel (c-Rel), RelA (p65, or NF- κ B3) and RelB proteins, as well as the drosophila proteins, dorsal and Dif. The two groups differ in their capability to activate transcription. In humans, p50 / RelA (p50 / p65) were the first to be recognised, and the only one necessary for survival, which is commonly referred to as NF- κ B. There is a great affinity

between the dimer and the corresponding NF- κ B sites in DNA; located at the RelA's C terminal. The transcriptional activation domains can interact directly with basal transcription apparatus, and thus NF- κ B plays a transcriptional regulatory function (Sun, 2011).

As a group of important transcription factors, NF- κ B plays an impressive central role in fundamental cell functioning and a significant role in disease when the pathway does not signal appropriately. NF- κ B is formed by a group of polypeptides of the Rel/NF- κ B family, which is a group of transcription factors. NF- κ B plays a vital role in immunity, and inflammation. Its imbalance is directly related to many autoimmune diseases. Rheumatoid arthritis, asthma and chronic enteritis are just some of the diseases very closely related to inappropriate activation of the NF- κ B pathway (Tak and Firestein, 2001).

In addition, the NF- κ B pathway has also long been implicated in tumorigenesis, including PCA (Ghosh *et al.*, 1998; Rayet and Gelinas, 1999). The direct and indirect effects of this transcription factor complex on tumorigenesis and progression have been demonstrated in several animal models for hepatocellular carcinoma, gastric cancer and lung cancer (Xia *et al.*, 2014). In most tumours, NF- κ B signalling promotes processes such as proliferation, angiogenesis, invasion, metastasis, chemoresistance, and radioresistance (Pozdeyev *et al.*, 2015). However, studies have shown that in some cases, NF- κ B can induce apoptosis and positively regulate pro-apoptotic genes. Therefore, depending on the microenvironment, NF- κ B may have varying roles in different tissues. NF- κ B has been found to play an important role in the formation of new blood vessels (angiogenesis) in tumours by the production of cytokines such as TNF, interleukin-1 (IL-1) and interleukin-6 (IL-6). These cytokines stimulate the expression of *VEGF* gene, which is a major regulator of angiogenesis (Pahl, 1999; Maloney and Gao, 2015; Tanaka *et al.*, 2014). NF- κ B can also induce expression of additional angiogenesis regulators such as *CXCL1*, *CXCL8* and *IL8*. In addition, NF- κ B promotes the expression of adhesion molecules such as ICAM-1 and E-selectin as well as proteins involved in tumour cell invasion (metalloproteinases, MMPs). NF- κ B has been found to promote epithelial-mesenchymal transition (EMT), which is an event closely related to invasion and metastasis in many types of tumours (Pires *et al.*, 2017). Finally, the inflammatory

microenvironment, which is primarily activated by NF- κ B, also contributes to carcinogenesis through cytokine production and signal processing that promotes tumour growth (Karin, 2006; Lickteig *et al.*, 2007).

1.5.1 The NF- κ B signalling pathways

NF- κ B is activated by various signals via degradation of I κ Bs, and then the active NF- κ B binds DNA within the nucleus. Firstly, two conserved serine residues in I κ Bs are phosphorylated, catalysed by I κ B kinase (IKK). IKK is composed of a regulatory subunit, IKK- γ (also called NEMO) and two catalytic sub-units: IKK α and IKK β . Then I κ B is polyubiquitinated and degraded by Skp, Cullin, F-box containing (SCF) complex. The activated NF- κ B translocates to the nucleus, due to unmasking of a nuclear localisation sequence (NLS), where it binds to its associated DNA target site to induce transcription of specific genes. A variety of pathogens, including components of lipopolysaccharide, pro-inflammatory cytokines such as tumour necrosis factor (TNF), IL-1 and mitogen, can activate NF- κ B in this way (Liu *et al.*, 2017). This signalling pathway inducing NF- κ B activation and depending on the degradation of I κ Bs, is called the classical signalling pathway. Other pathways can also be involved in NF- κ B activation, which include dissociation of I κ B induced by phosphorylation and pathways based on protein kinase-2. After the release of I κ B, NF- κ B can be modified (e.g. the modification of the sub-unit to influence the effectiveness of their transcriptional activation). Activation of NF- κ B can induce I κ B α expression rapidly. Newly synthesised I κ B α enters the nucleus, and then translocates with NF- κ B out of the nucleus. Finally, NF- κ B returns to its resting state. This is the canonical pathway, where NF- κ B release is caused by I κ B α degradation as shown in Figure 1.5 (Palmer *et al.*, 2017).

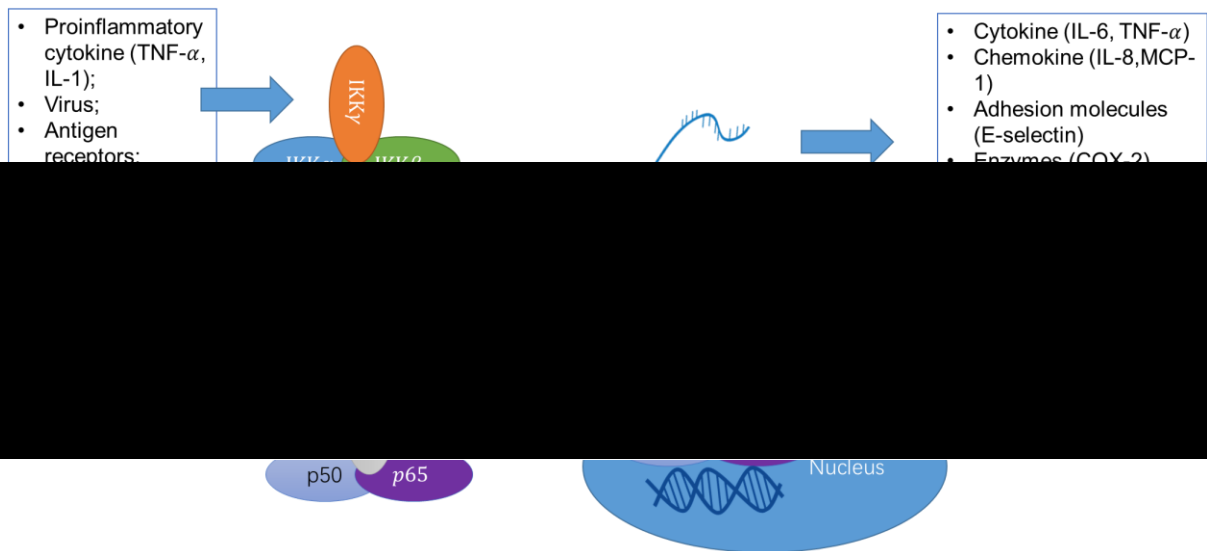


Figure 1.5. Canonical NF- κ B pathway. When it is inactive, RelA (p65) binds to I κ B, which remains in the cytoplasm and does not exhibit transcriptional activity. When the inflammatory factor and other stimuli are introduced, the upstream kinase of I κ B, I κ B kinase (IKK) is activated by phosphorylation. IKK degrades I κ B. p65 has a nuclear positioning signal. Without the shackles of I κ B, p50 will bind RelA (p65) and translocate into the nucleus. RelA (p65) recognises and binds to specific target DNA sequences to regulate the transcription of the target gene. Binding sequence of RelA (p65) on the promoter: 5'-GGG (A/G)(C/A/T)T(C/T) 3'. Source: Campbell, *et al.* 2004; Sun, 2011.

In contrast, the non-canonical pathway is activated by the RelB/p52 NF- κ B complex as demonstrated in Figure 1.6 (Sun, 2011). The I κ B family consists of p105 and p100, which are precursors. In addition to p50 and p52 sequences, these precursors also include the ankyrin region. The precursors p105 and p100 inhibit the activity of NF- κ B that they are associated with. The whole progression from the precursor to p50 and p52 is not fully understood, but this process requires protease activities during translation and post-translational processing. Signal-induced phosphorylation and processing of p52 from p100 does not require the classic IKK- γ -dependent pathway. IKK- and induction of NF- κ B-inducing kinase is essential, but IKK- β and IKK- γ are not required. Thus, this pathway is also known as the non-classical, alternative or new NF- κ B activation pathway (Campbell *et al.*, 2004).

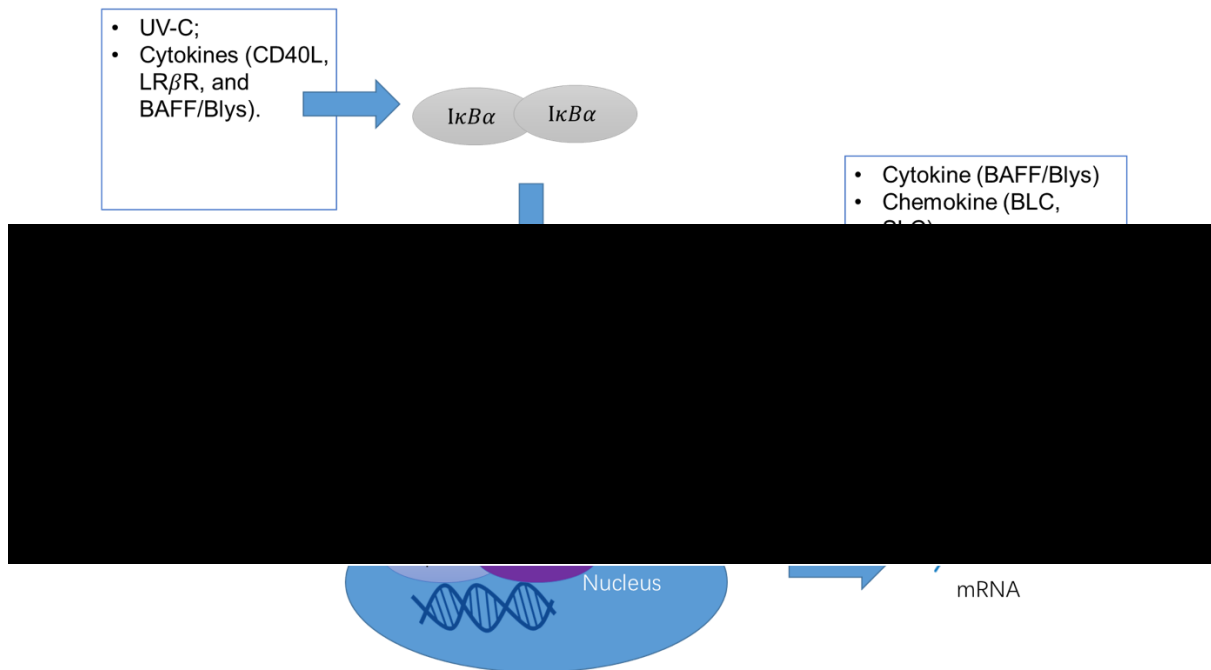


Figure 1.6. Non-canonical NF-κB pathway. After activation, NF-κB2 precursor protein p100 is phosphorylated and subsequently processed to form a mature sub-unit, p52, by proteasome. p52 dimerises with RelB and enters the nucleus. Source: Campbell, *et al.* 2004 ; Sun, 2011.

1.5.2 Aspirin's influence on the NF-κB pathway

The whole family of NF-κB transcription factors play crucial roles in immunity, inflammation, development and tumorigenesis. Therefore, the study of the behaviour and regulation of NF-κB has been increasingly attracting attention. Liao *et al.* (2015) conducted a series of experiments in which they found that aspirin can block the activity of NF-κB. Three cell lines, U2OS, ZOS and MG63 osteosarcoma cells, were transfected with a NF-κB luciferase plasmid. The activity of the luciferase was decreased by 50% after the cells were treated with aspirin for 24 h. The p65 protein was used as the indicator of NF-κB transcriptional activity and was decreased as detected by Western blotting when NF-κB was inhibited by aspirin treatments. This study therefore demonstrated that aspirin reduced the activity of p65, which has subsequently been confirmed by findings of other similar investigations (Sun, 2011; Palmer *et al.*, 2017). Thus, the proposed mechanism by which aspirin influences the NF-κB pathway is

illustrated in Figure 1.7.

Using a western blotting approach, B-cell lymphoma 2 (Bcl-2), Baculoviral IAP repeat-containing protein3 (CIAP2), baculoviral inhibitor of apoptosis repeat-containing 5 (Survivin), Livin and X-linked inhibitor of apoptosis protein (XIAP), which are downstream targets of NF- κ B, were all found to have their expression levels reduced by aspirin in a dose- and time-dependent manner in U2OS and ZOS cell lines (Liao *et al.*, 2015). NF- κ B is a ubiquitous and inducible cell transcription factor and a key regulator in the production of COX-2, thus, COX-2 gene expression can be also suppressed via this pathway (Shi *et al.*, 2015). These studies demonstrate the potential for aspirin to influence the NF- κ B signalling pathway, but this interplay in prostate carcinogenesis is not yet understood.

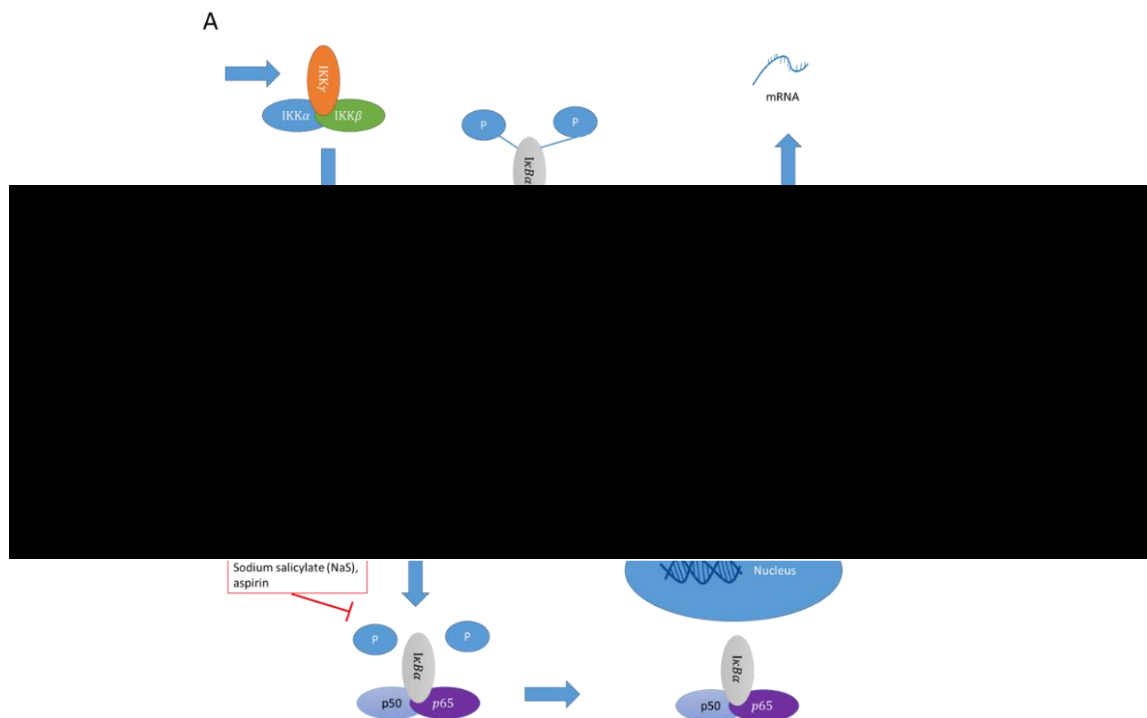


Figure 1.7. Proposed pathway for NaS interfering with the NF- κ B pathway. Aspirin and sodium salicylate (NaS) block I κ B α phosphorylation and degradation. The (A), NF- κ B pathway can be active when I κ B α is phosphorylated by IKK. Then the dimer p50-p65 will be released and translocated in the nucleus. However, with presence of NaS or aspirin (B), the phosphorylation of I κ B α is blocked, thus, the dimer cannot enter the nucleus.

1.6 Aims

The aim of this thesis was to investigate the effects of aspirin on PCA in order to develop further understanding on its underlying mechanism of action and thus its utility for PCA treatment. In the human body, biotransformation of aspirin yields salicylate; as the present study was an *in vitro* investigation, the aspirin metabolite NaS was selected. To achieve the aims of this study, the following objectives were addressed:

- Investigation of NaS toxicity – Chapter 3

Research in this chapter investigated NaS effects on growth, *COX-2* gene expression, migration and invasion of PCA cells. In addition, morphological changes, calcium levels and mitochondrial health were investigated.

- Exploration of NaS mode of action (MoA) – Chapter 4

This next results Chapter focused on exploring down-stream targets potentially associated with aspirin's MoA and evaluating the impacts of *COX-2* inhibitors on growth and morphology. In addition, NaS' role in impacting NF- κ B cell-signalling pathways were assessed.

- Development and characterisation of three-dimensional (3D) prostate cancer models for NaS evaluation – Chapter 5

Finally, a 3D prostate cancer model was established and characterised, including the model's growth features and *COX-2* gene expression profiles. This model was subsequently used as an advanced and more realistic tool to explore NaS' impact on toxicity, growth, *COX-2* expression and NF- κ B cell-signalling pathways as compared to standard monolayer (2D) culture systems.

Chapter 2 Materials and Methods

2.1 Chemicals and equipment

The materials used in this project are listed in 2.1.

Table 2.1. Materials used for the project.

Materials	Manufacturer	Catalogue Number
0.05% Trypsin/EDTA (T/E)	GIBCO, Paisley, UK	1839027
0.22 μ M pore size filter	Millex-GP, IRL	R7AA60906
0.2mL PCR tube, Flat cap	STARLAB, US	15073
1 x 1 mm haemocytometer	Hawksley	BS 748
1.1 x 50 mm Needle	BD Microlance 3	160518
15 μ -slide angiogenesis plate	ibidi, DE	8156
1-Butanol	Sigma-Aldrich, UK	B7906-500ML
3-[4,5-dimethylthiazol-2-yl]-2,5-diphenyltetrazolium bromide; thiazolyl blue (MTT)	Sigma-Aldrich, UK	M2128-100MG
30% acrylamide	Severn BIO-TECH, UK	20-2600-10
37% Hydrogen chloride (HCl)	Sigma-Aldrich, UK	435570
50 mL centrifugation tube	Greiner Bio-one, UK	
96-well plate	Thermo Fisher Scientific, UK	167008
96-well plate, low-profile	BIO-RAD, UK	MLL9601
Academy Microscope Slides	Smithscientific, UK	N/A-141
Agarose	Sigma-Aldrich, UK	A9539-10G
Alexa Fluor® 488 Phalloidin	Thermo Fisher Scientific, UK	A12379
Ammonium persulfate (APS)	Lancaster Synthesis, UK	10049089
BIOFUGE Fresco	Heraeus, UK	75005521
Bovine serum albumin (BSA)	Sigma-Aldrich, UK	A7906-100G
Clarity™ and Clarity Max™ Western ECL Blotting Substrates	Bio-Rad, UK	1705060S
Colcemid	Sigma-Aldrich, UK	0000000102 95892001
Confocal camera and its software	Zeiss, LSM 880	LSM710

Culture-Inserts 2 Well in μ -Dish 35 mm (wound healing assay)	ibidi, DE	81176
Cytospin 4	Thermo Shandon	A78300003
DEME without phenol red	GIBCO, Paisley, UK	180726
Dimethyl sulfoxide (DMSO)	GIBCO, US	
DU145 cells	ATCC, US	2215512
Fast SYBR Green Kit	QIAGEN, DE	204054
Filter tips 10 μ L	STARLAB, US	S1121-3810
Filter tips 1000 μ L	STARLAB, US	S1122-1830
Filter tips 200 μ L	STARLAB, US	S1120-8810
Foetal Bovine Serum (FBS)	GIBCO, US	42G79501c
Formamide	Sigma-Aldrich, UK	1181432000 1
Glutamine	GIBCO, US	25030-024
Glycine	Melford, UK	C22753
Hoechst 33342	Sigma-Aldrich, UK	38733
INCell analyser 2000	GE Healthcare Life Sciences	INCell analyser 2000
Isis Fluorescence Imaging System	Metafer 4 software, MetaSystems	
Laemmli buffer, non-smelling	Sigma-Aldrich, UK	14533-100MG
LumaScope 500 camera	Labtech International Limited	LumaScope 500
Mars Air Flow hood	Scanlaf	
Methanol	Fisher Chemical, UK	1717717
Microseal 'B' seal Seals (plate film)	BIO-RAD, UK	MSB1001
ND-1000 Spectrophotometer	LABTECH International, UK	ND-1000
NE-PER™ Nuclear and Cytoplasmic Extraction Reagents	Thermo Fisher Scientific, UK	78833
Non - essential amino acid	Thermo Fisher Scientific, UK	11140050
Paraformaldehyde (PFA)	Polyscience, US	18814-20
Phosphate buffered saline (PBS)	Corning, UK	29816005
PC3 cells	ECACC, UK	90112714
Pen / Strep	GIBCO, US	15140-122
PNT2 cells	ECACC, UK	95012613
POLARstar Omega plate reader	BMG Labtech Ltd., UK	N/A
Polish slide	BIO-RAD, UK	

Propidium iodide (PI)	Sigma-Aldrich, UK	P4170
Protein Assay Reagent	BIO-RAD, UK	
PVDF membrane	BIO-RAD, UK	162-0177
QCM ECMatrix Cell Invasion Assay, 24-well (8 µm), colorimetric	CHEMICON, UK	ECM551
Ready-to-use Human Chromosome Pan-Centromeric paints	Cambio, UK	1695-F-01
Reverse transcription Kit	QIAGEN, DE	205311
RNase-Free DNase Set (50)	QIAGEN, DE	79254
RNease Mini Kit (50)	QIAGEN, DE	154018589
RPMI 1640 medium	GIBCO, UK	1839799
Shandon Cytofunnel®, single funnel with white filter and cap	VWR, UK	SHAN5991040
Sodium chloride (NaCl)	Sigma-Aldrich, UK	SZBF3340V
Sodium Citrate	Sigma-Aldrich, UK	C8532-100G
Sodium dodecyl sulphate (SDS)	Invitrogen, US	91403743
Sodium salicylate (NaS)	Sigma-Aldrich, UK	BCBJ2699V
Stripping buffer	Thermo Fisher Scientific, UK	46430
T100 Thermo cycler	BIO-RAD, UK	T100
T25 flask	Greiner Bio-one, UK	690160
T75 flask	Greiner Bio-one, UK	658170
TEMED	Sigma-Aldrich, UK	T9281-25ML
Thermal cycler	BIO-RAD, UK	CFX Connect
TRIS	Melford, UK	G25803
Tris(4,7-diphenyl-1,10-phenanthroline)ru [ru(dpp)]	Santa Cruz, US	SC-213125
Triton-X100	Sigma-Aldrich, UK	X100-100ML
TWEEN® 20	Sigma-Aldrich, UK	MKBS1669V
VECTASHIELD Antifade Mounting Medium with DAPI	Vector Laboratories, Peterborough,UK	H-1200
Virkon	LabShop, UK	330001

2.2 Computer software

The software used in this thesis are listed in the table below (Table 2.2).

Table 2.2. Software used in this thesis.

Software	Version
INCell Analyser Workstation	3.7.1
BioRad CFX Manager	3.0
Mars Data analysis	1.20.R2
Metafer 4 (MSearch)	3.9.8
Microsoft Excel	2016
Microsoft Word	2016
Quantity One 1-D Analysis Software	4.62
SPSS	22.00
ZEN	Blue edition

2.3 Recipes for general buffers and solutions

2.3.1 Tris-HCl

A total of 121.1 g of Tris was dissolved in 700 mL of H₂O. Then HCl was used to adjust the pH to 7.6 and water was added until the volume reached 1 L. After aliquoting into five bottles, the solution was sterilised by autoclaving.

2.3.2 NaS stock solution

NaS, was made up to a 1 mol/L (M) stock solution, by dissolving 1.6 g NaS and 10 mL Tris-HCl. The stock solution was filtered with a 0.22 μ M pore size filter before dosing cultured cells with the compound.

2.3.3 20x saline-sodium citrate (SSC) solution

A total of 175.2 g NaCl (3 M) and 87.33 g (300 mmol/mL or mM) Trisodium citrate dihydrate were dissolved in of H₂O. This was adjusted with HCl to pH 7. Then the same volume of H₂O was added to dilute the SSC solution to 10x SSC. 100 mL of 10x SSC was diluted in 390 mL H₂O and the final volume should be adjusted to 500 mL. This is the 2x SSC.

2.3.4 70% formamide/2xSSC

A total of 49 mL of formamide was mixed with 7 mL of 20X SSC, and the total volume was adjusted to 70 mL with water.

2.3.5 Celecoxib stock solution

A total of 3.8137 mg celecoxib (Sigma, UK) was dissolved in 10 mL DMSO to form a stock solution at 1 mM.

2.3.6 Buffers used in western blotting

The buffers used in western blotting are listed in Table 2.3.

Table 2.3 Buffers used in western blotting.

	Solution	Recipe
Stock buffer	1 M Tris (pH 6.8)	30.3 g Tris in 250 mL distilled water and HCl used to adjust to pH 6.8
	1.5 M Tris (pH 8.8)	45.4 g Tris in 250 mL distilled water and HCl used to adjust to pH 8.8
	10% (w/v) APS	1 g APS in 10 mL distilled water
	10% (w/v) SDS	50 g SDS in 500 mL distilled water
	LaemmLi buffer	Ordered from Sigma-Aldrich, UK
	TBS (Tris-buffered saline) 10x	24.2 g Tris, 80.1 g NaCl in 1 L distilled water adjusted to pH 7.6 with HCl
	Tris / Glycine / SDS (TGS) 10x	30.3 g Tris, 144.1 g Glycine and 100 mL 10% (w/v) SDS in 1 L distilled water
Working buffer (stored at 4 °C)	Wash buffer	1 mL TWEEN® 20 and 100 mL TBS 10x in 1 L distilled water
	BSA Block buffer (10%)	25 g BSA in 250 mL wash buffer
	Running buffer	100 mL TGS 10x in 1 L distilled water
	Transfer buffer	100 mL TGS 10x and 200 mL methanol in 1 L distilled water

2.4 Cell lines and their culture methods

PC3, PNT2 and DU145 cell lines were cultured in RPMI 1640 medium supplemented with 10% FBS, 1% Pen Strep and 1% Glutamine, and incubated at 37 °C and 5% CO₂ for 2-3 days. PC3 cells are epithelial PCA cells derived from a metastatic site (bone), DU145 cells are epithelial PCA cells derived from a metastatic site (brain) and PNT2 cells are a normal prostate epithelium immortalized with Simian Virus 40.

All steps regarding cell culture were performed in a sterile Mars Air Flow hood (Scanlaf). All the materials used were sprayed with 70% ethanol prior to cell culture. Media was warmed in a water bath for at least 20 min prior to use.

Each vial of each cell line was taken from the liquid nitrogen and thawed in water bath. When the vial of cells was defrosted, the cells were transferred into a T25 flask for 24 hour (h) and moved to a T75 the next day containing 12 mL growth media at 37 °C and 5% CO₂ for 2-3 days. When 80% confluence was reached, culture medium was removed and discard into a pot containing approx. 3% Virkon. Next, the cell layer was rinsed with 3mL 0.25% (w/v) Trypsin/EDTA (T/E) for a 5-10 min in order to remove all traces of serum. Following this, 3.0 mL T/E was added to the flask. Within 5 to 15 min, the cells had detached, and this could be seen under a microscope. Then, 6 mL of culture medium was added into flask by gentle pipetting. The whole solution was transferred into a 50 mL centrifugation tube and centrifuged at 8000 g for 5 min. The supernatant was discarded, and 12 mL of growth medium was added into the tube to suspend the cells. Finally, 6 mL of the cell suspension was transferred into each of two T75 flasks containing 6 mL of growth medium and cultured at 37 °C and 5% CO₂. Every two days, the medium was renewed; the flask was taken from the incubator and the media discarded. PBS was used to wash the cells layer twice and 12 mL of fresh warm medium was added into the flask.

For harvesting cells, the cell layer was washed with PBS twice and T/E once. After incubation with 3 mL of T/E for 5 to 10 min, 6 mL of medium was added to the flask. The suspension was then spun down at 8000 g for 5 min. The cell pellet was re-suspended in the desired volume

of medium for the next experiment. For freezing cells down, the cell pellet was re-suspended in DMSO-FBS (1:10). The cell suspension was transferred into a cryovial and kept at -80 °C for 24 to 48 h. Finally, the vial was transferred to liquid nitrogen.

2.5 Cytotoxicity assay based on relative population doubling (RPD)

PC3, DU145 and PNT2 cells were seeded at 1×10^5 cells / cm^3 respectively and cultured for 24 h in the incubator. There were 6 flasks for each cell line which were dosed with 0 mM (Tris HCL negative control group), 2 mM, 4 mM, 6 mM 8 mM and 10 mM NaS for 24 h. On the third day, the NaS was washed off with PBS and replaced with fresh media; the cells were then allowed to recover for 24 h. On the fourth day, the cell concentration was determined by a 1 x 1 mm haemocytometer. Their population doubling (PD) and RPD values were then calculated by the following formulas (Equation 2.1 and Equation 2.2). Each experiment was carried out in triplicate.

$$PD = \log_2 \frac{\text{dosed cells concentration.}}{\text{initial cells concentration.}}$$

Equation 2.1.

$$RPD = \frac{PD_{\text{dose group}}}{PD_{\text{control}}} \times 100$$

Equation 2.2.

2.6 RNA extraction

PC3, PNT2 and DU145 cells were cultured for 24h before dosing with NaS. After 6 and 24 h of incubation with NaS, RNA was extracted from the cells using the Qiagen RNeasy Mini Kit according to the manufacturer instructions. The extracted RNA was quantified using a Nanodrop (ND-1000 Spectrophotometer). RNA quality was assessed by the A260:A280 ratio (which had to be between 1.8 and 2.0), where A260 is the peak absorbance of DNA/RNA and A280 is the peak absorbance of proteins or phenolic substances. Additionally, the A260:A230

ratio was evaluated, indicating salts and polysaccharide contamination (had to be greater than 1.8) in accordance with the instructions from the manufacturer. RNA was kept at -80 °C prior to use for reverse transcription. When the concentration of RNA was obtained, the following equation (Equation 2.3) was used to determine the volume to be used when producing cDNA.

$$V (\mu\text{L}) = \frac{1000 \text{ ng}}{c(\text{ng}/\mu\text{L})}$$

Equation 2.3. Equation for the volume of RNA required to produce cDNA. Where V is the volume of RNA used for the cDNA reaction and c is the concentration of the RNA sample quantified by NanoDrop.

2.7 cDNA synthesis

The QuantiTech Reverse Transcription Kit was used to reverse transcribe the RNA into cDNA according to the manufacturer's instructions. Briefly, 2 µL gDNA wipe-out buffer (7x), 1 µg Template RNA and a variable volume of RNase-free water (total volume was 14µL) were applied to a 0.2 mL PCR tube (flat cap). This solution was placed in a Thermal cycler for a 2-minute incubation at 42 °C. For each sample, 6 µL of master mix (1 µL QRT, 4 µL QRT Buffer (5x) and 1 µL RT Primer mix) was added to the tube to obtain a 20 µL solution. After mixing and spinning, the solution was placed in the Thermal cycler at 42 °C for 15 min and 95 °C for 3 min.

2.8 RT-qPCR

The Quantitative Real Time Polymerase Chain Reaction (RT-qPCR) was performed by placing 12.5 µL SYBR green, 0.25 µL of the forward and 0.25 µL reverse primer, 10 µL of distilled H₂O, and 2 µL cDNA samples (or cDNA dilution series or 2 µL distilled H₂O as the negative control) into 96-well PCR plates. The plates were then run on the BioRad CFX Manager to support the specific primers selected for analysis. This was carried out in triplicate for each sample analysed. RT-qPCR was run on a CFX Connect™ Real-Time PCR Detection System.

The real-time cycler was programmed as follows: the sample was initially incubated at 95 °C for 5 min to activate HotStarTaq DNA Polymerase, followed by 40 cycles of 10s-denaturation at 95 °C, combined step of annealing and extension were conducted at 60 °C for 30s and finally, a melt curve analysis was performed from 50 to 95 °C at the ramp rate of 0.5 °C/s.

2.9 Assessment of cell morphological changes

When 80% confluence was reached, PNT2, PC3 and DU145 cell lines were seeded at 0.8×10^5 cells / cm³ in 24-well plates for 24h at 37 °C and 5% CO₂ in a humid environment. After 24h, the cells were treated with 0, 2, 4, 6, 8 and 10 mM NaS and 60 µM colcemid (the positive control) for 24 h. Following the treatment, cells were given 24 h for recovery. When the recovery was finished, after three PBS washes, the cells were checked under the microscope for distribution in the wells. If the cells were distributed evenly with little overlap or over-growth, the cells were then fixed with 4% Paraformaldehyde (PFA) at room temperature for 15 min and the PFA was washed off three times with PBS. Then 0.1% Triton X-100 was applied to the cells in PBS for 5 minutes at room temperature. Cells were stained with 6.6 nM Alexa Fluor® 488 Phalloidin for cell body outline (1 µL into 1000 µL PBS) for 25 min and then 10 µg/mL Hoechst (nuclei stain) was added to the wells for 5 min. Their images were taken on an INCell Analyser 2000 (GE Healthcare Life Sciences, UK). Once they were obtained, the images were transferred to numeric data with INCell Analyser Workstation (GE healthcare Life Sciences, UK). All samples were analysed in triplicate.

2.10 Invasion assay

The invasion assay was performed using the QCM ECMatrix Cell Invasion Assay, based on a 24-well plate format. When PNT2, DU145 and PC3 cells reached 80% confluence in T75 flasks, they were treated with 0, 2, 4, 6, 8, 10 mM NaS in chemoattractant-free media (RPMI media containing 1% glutamine and 1% Pen / Strep without FBS) for 24 h. Then, they were harvested with T/E. For optimal results, the plates and reagents were equilibrated to room temperature (25 °C) before initiation of the assay. A total of 300 µL of pre-warmed chemoattractant-free

media was applied to the interior of the inserts to rehydrate the collagen layer for 15-30 minutes at room temperature. Next, 250 μL of media was removed carefully. 1.0×10^6 cells/mL cells were suspended in chemoattractant-free media. Following this, 250 μL of cell suspension was added to the upper chamber and 500 μL of growth media or serum free media (negative control) was added to the lower chamber. Please refer to the diagrammatic sketch (Figure 2.1). The plates were then incubated for 48 h at 37°C in a 5% CO_2 incubator. Following this, the cell suspension and media were removed from the topside of the insert and the invasion chamber was inserted into a clean well containing 400 μL of Cell Stain provided in the QCM ECMatrix Cell Invasion Assay kit. The chambers were stained for 20 minutes at room temperature. The chambers were rinsed in a beaker of water several times. A cotton-tipped swab was used to gently remove non-invading cells/collagen layer from the interior of the insert. This was done twice with two clean swabs. The insert was left to air dry for 24 h. On the next day, the stained inserts were placed into a clean well containing 200 μL of extraction buffer for 15 minutes at room temperature. Then, 100 μL of the dye mixture was transferred to a 96-well plate. The optical density was measured at 560 nm with POLARStar Omega plate reader (BMG Labtech Ltd., UK) and the data was analysed with Mars Data analysis. All experiments were carried out in triplicate.

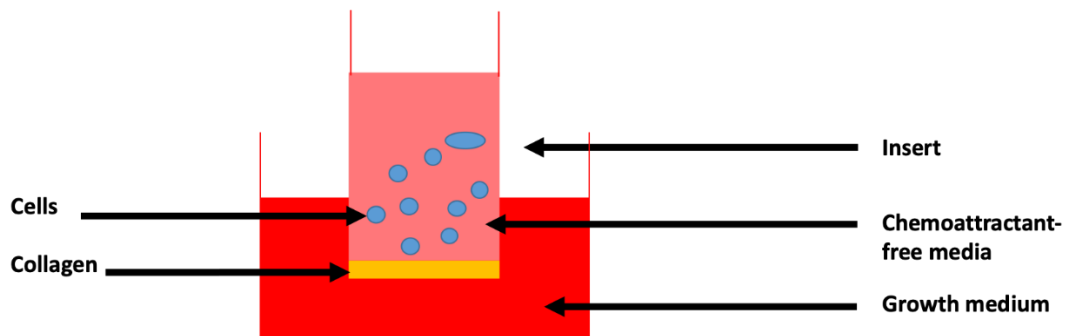


Figure 2.1. Schematic side view of a 24-well plate with insert utilised for the invasion assay. Red indicates growth media and pink indicates chemoattractant-free media. When cells were cultured in chemoattractant-free media, they are attracted by growth media containing FBS (the chemoattractant). Thus, their ability to migrate through the collagen matrix represents the cells' invasive capacity.

2.11 Migration assay

Cell culture inserts (ibidi) were utilised for investigating aspirin's effects on migration of PCA cells. When PNT2, DU145 and PC3 cells reached 80% confluence in T75 flasks, they were harvested with Trypsin-EDTA. The culture-inserts were placed into each well of a 24-well plate prior to seeding cells into the wells at 1×10^5 cells / cm^3 (70 μL). A total of 120 μL culture media was applied to the outside insert. After 24 h of culture, cells were treated with the same NaS dose range described in Section 2.4. Following 24 h of exposure, the inserts were removed and the cells allowed to migrate for 24 h. Then, the gap between two cell sections was measured by Zen blue light edition (Carl Zeiss) and the images were taken with LumaScope 600 camera. This was carried out 3 times for each sample analysed. The diagrammatic sketch can be found in the following Figure 2.2.

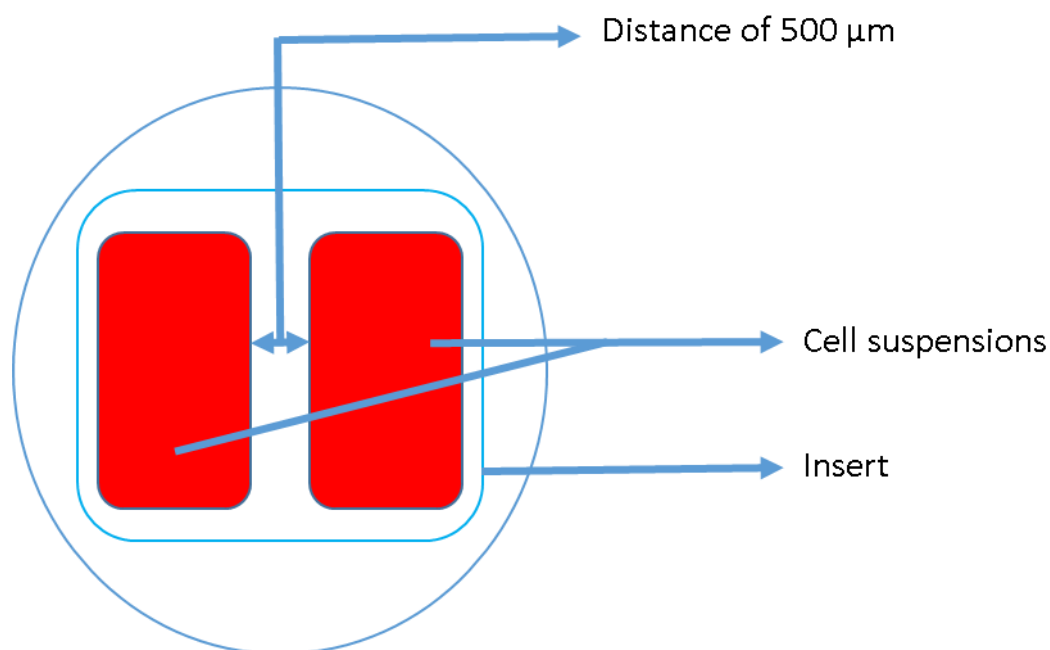


Figure 2.2. Schematic side view of a 24-well plate with insert utilised for the migration assay. Red areas indicate cells suspension. Their ability to migrate to cover the distance within 24 h indicating the cells' migration capacity.

2.12 Nuclear and cytoplasmic protein extraction

PNT2 cells and PC3 cells were seeded at 1×10^5 cells / cm³ in T75 flasks until they reached 80% confluence. PNT2 and PC3 cells were treated with TNF- α at 25 ng / mL or 50 ng / mL for 0.5, 2, 6 and 24 h (positive control). Using a cell counter, 2×10^6 cells were collected. Nuclear and cytoplasmic proteins from PNT2 and PC3 cells were extracted with NE-PER™ Nuclear and Cytoplasmic Extraction Reagents (Thermo Scientific, UK) as instructed by the manufacturer. Cells were harvested with T/E and spun down at $500 \times g$ for 5 min. Then the pellets were washed with PBS and transferred to 1.5 mL tubes. They were centrifuged at $500 \times g$ for 3 minutes. The supernatant was removed, and the pellets were left to dry. Following this, 200 μ L ice-cold CER I, which came from the NE-PER™ Nuclear and Cytoplasmic Extraction Reagents, was applied to the pellets. The cells were vortexed on the highest setting for 15 seconds to fully resuspend the cell pellet and then the tube was incubated on ice for 10 min. After this, 11 μ L ice-cold CER II, provided with the NE-PER™ Nuclear and Cytoplasmic Extraction kit, was added to the tube. After vortexing for 5 seconds on the highest setting, the tube was incubated on ice for 1 min. Following 5 seconds vortex on the highest setting, the tube was centrifuged for 5 min at maximum speed in a micro centrifuge ($\sim 16,000 \times g$) at 4 °C. When the centrifugation was finished, the supernatant (which was the cytoplasmic extract) was transferred to a clean pre-chilled 1.5 mL tube immediately and placed on ice for quantification.

The remaining insoluble material was resuspended with 100 μ L NER, a reagent in the NE-PER™ Nuclear and Cytoplasmic Extraction kit, and vortexed for 15 s on the highest setting. Then, the tube was placed on ice for 10 min. This process was repeated three more times. Next, the tube was centrifuged at maximum speed ($\sim 16,000 \times g$) for 10 min. Finally, the supernatant (which was the nuclear extract) was transferred to a clean pre-chilled 1.5 mL tube immediately and placed on ice for quantification.

2.13 Protein quantification

The protein extracts were quantified with the RC DC™ Protein Assay from Bio-Rad containing reagent A, B and S. A total of 20 µL reagent S was applied to 1 mL reagent A to prepare reagent A'. There were five dilutions of protein standard containing 0.4, 0.8, 1.2, 1.6, and 2 mg / mL Pierce™ Bovine Serum Albumin Standard Ampules. A total of 5 µL samples and standards were added into each well of a 96-well plate. This was done in triplicate. Then, 25 µL Reagent A' was added into each well, followed by 200 µL Reagent B. The plate was agitated gently for 1 min. After 15 min, absorbances were read at 750 nm with POLARStar Omega plate reader (BMG LABTECH International, UK). A standard curve was generated by the plate read software (Omega, Mars Data Analysis) ($r^2 \geq 0.99$). The determined concentration of the protein extracts was the average of the triplicates. Both cytoplasmic and nuclear proteins were kept at -80 °C when the quantification was finished prior to use. Based on the extracted protein concentration, 40 µg samples were prepared to load on the gel and this was calculated according the equation $\frac{40 \mu\text{g}}{\text{concentration of the sample } \mu\text{g}/\mu\text{L}}$

2.14 Western blotting

2.14.1 Preparation of stacking and resolving gels

The gels used for sodium dodecyl sulphate polyacrylamide gel electrophoresis (SDS-PAGE) were the 12% resolving and 4% stacking gels and were prepared for using the components listed in Table 2.4. For gel preparation, 1.5 mm glass and 15-well comb (for the nuclear p65 quantification) or 10-well comb (for the purity check for nuclear extracts) were used. Before preparation, glasses and other equipment, including stands and combs were wiped with 70% ethanol. Firstly, 8.5 mL of 12% resolving gel solution were applied between two glass panes. A total of 700 µL 1-butanol was added to the top of the solution. When the resolving gel solution had polymerised (30 min approximately), the 1-butanol was removed, and the 4% stacking gel solution was added to fill the remainder of the gap between the glass panes. After about 45 min, the gel was polymerised.

Table 2.4. Recipe for 4% stacking gel and 12% resolving gel.

	4% stacking gel for gels	12% resolving gel for 4 gels
30% acrylamide / mL	1.3	12
distilled water / mL	6	10
1.5 M Tris / mL	0	7.5
1 M Tris / mL	2.5	0
10% SDS / μ L	100	300
TEMED / μ L	10	30
10% APS / μ L	50	150

2.14.2 Gel running and transferring

Protein samples were thawed on ice, and then 40 μ g of each protein sample was mixed with the same volume of Laemmli buffer (Sigma-Aldrich, UK) and incubated at 95 $^{\circ}$ C for 5 min. After brief centrifugation, biotinylated ladder, dual colour ladder and protein samples for analysis were loaded onto gels directly from the left well to the right well. The gels were run for 15 min at 160 V, when bands reached the bottom of stacking gel and then for 125 min until the 10 kDa ladder reached the bottom of the gels. One PVDF membrane per gel was immersed in 100% methanol for 10 seconds. Then, per gel, a cassette was assembled including 2 fibre pads, 2 filter papers, a gel and 1 PVDF membrane, which were equilibrated for 10 min in pre-cooled transfer buffer at 4 $^{\circ}$ C. The order of the materials assembled is illustrated in the figure below (Figure 2.3). The cassette and an ice pack were placed in a tank filled with transfer buffer at 4 $^{\circ}$ C and the transfer conducted for 1 h at 400 mV.

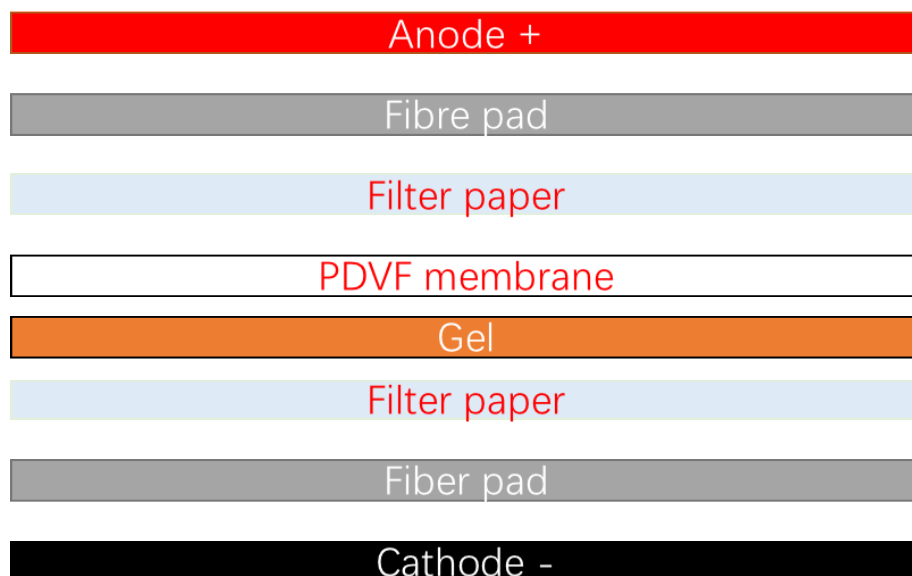


Figure 2.3. Cassette setup for the membrane transfer stage of western blotting.

2.14.3 Primary and secondary antibody incubation

After transfer, the membrane was cut into two pieces; the biotinylated ladder section (A) and the protein section (B), along the dual colour ladder. Membrane A was blocked for 24 h in 10% BSA followed with moderate agitation by overnight incubation with anti-biotin HRP linked antibody. Meanwhile, membrane B was blocked in 10% BSA overnight for approximately 16h for nuclear p65 (for other proteins, 1 h was the blocking time) at 4 °C with moderate agitation, which was the incubation with the primary antibodies. Following this incubation, the membrane was washed 5x10 minutes in wash buffer at room temperature with strong agitation. Following this, the secondary antibody at the appropriate concentration was added into 10 mL 10% BSA blocking buffer and incubated with membrane B; while 10 µL anti-biotin HRP-linked antibody was added into 10 mL 10% BSA blocking buffer incubated with membrane A. The appropriate concentration was defined in the corresponding results Chapters. This incubation lasted 1 h at room temperature with moderate agitation. After five 10 min rinses in wash buffer at room temperature with strong agitation, the membrane was

developed with ECL (Bio-Rad, UK) and visualised with under a Chemidoc (QuantityOne software of Bio-Rad), with analysis using the QuantityOne software (Bio-Rad). Western blots were carried out 3 times for each protein's analysis.

2.14.4 Membrane stripping and re-probing

To strip the bound antibodies from the membrane, the membranes were washed with wash buffer for 10 min and rehydrated with 100% methanol for 10 s. The membranes were then washed twice with stripping buffer (Thermo Fisher Scientific, UK) lasting 10 min per wash. The membranes were stripped only once.

2.15 Micronucleus assay

In order to explore the effect of aspirin on the induction of genotoxicity, a software analysis pipeline with CellProfiler was utilised. Images of treated cells were captured as described in Section 2.9 . The micronucleus (MN) detection pathway was utilised as a score for DNA damage (genotoxicity) induced in each sample evaluated, which was developed by Dr. Kathrine Chapman in the *In vitro* Toxicology Group at Swansea University (the pipeline is attached in the electronic version of the thesis, namely, Appendix 1). The pipeline identified nuclei from the DAPI image and the whole cell outlines from the FITC image. Then, a subtraction was used for the identified nuclei from the associated cell to pin-point the cytoplasm. In addition, a "Masking" was then used to block out the nuclei, avoiding the incorrect identification of MN within the nucleus. Finally, the frequency of MN within cells could be calculated. Within each replicate conducted, 2000 cells were analysed for the presence of MN. Each sample was conducted in triplicate, thus a total of 6000 cells were analysed for MN presence per dose.

2.16 Micronucleus assay with centromere stain

In order to investigate if DNA damage induced by aspirin was the result of an aneugenic or a clastogenic event, centromere staining was used. Firstly, cells were harvested to prepare the cells slides. When cells reached 80% confluence, cells were washed with PBS once, then incubated with 4 mL T/E for 5 min followed by the addition of 4 mL media to the flask. Cell pellets were collected by centrifugation and washed twice with PBS. Next, cells were re-suspended in 10 mL PBS. 100 μ L of the cell suspension was added into a single funnel with white filter and cap (Shandon Cytofunnel[®]) and centrifuged onto a polish slide (Academy Microscope Slides) at 10000 g for 5 min by Cytospin 4 (A78300003, Thermo Shandon). The cells on the slides were evaluated by light microscopy to ensure the cell preparations were not be too sparse or confluent. The slides were left to air dry. Finally, the slides were fixed with 90% ice-cold methanol for 10 min, left to air dry and were kept at -20°C.

Following slides preparation, the slides were stained with Ready-to-use Human Chromosome Pan-Centromeric paints. Both the sample slides and 30 μ g/mL 0.01 M HCl pepsin (pH 2.7-3) were pre-warmed to 37 °C in an incubator for 10 min. Five drops of pepsin was added to the cells and left at 37 °C for 50 seconds. The slides were placed in PBS for 5 min to arrest the pepsin treatment followed by a further 5 min in 50 mM MgCl₂/PBS solution (to protect cells and chromosomes from further erosion by the pepsin). The slides were dehydrated in 70%, 80%, and 95% ethanol for 2 min each. Chromosomes on the slide were denatured in 70% formamide/2 \times SSC for 2 min at 70 °C. Following this, the slides was immersed in ice-cold 70% ethanol and dehydrated through a series of ethanol washes: 70%, 90%, and then 100%. When the wash was finished, the slides were left for air dry at room temperature standing vertically. The ready-to-use human chromosome pan-centromeric paints were warmed to 37 °C for 5 min and mixed well. Five μ L of probe per slide was added to a micro centrifuge tube. The probe was denatured for 10 min at 85 °C and immediately placed on ice. Five μ L of probe was applied to slide, and the slide was hybridized for 16 h at 37 °C in a humidified chamber with coverslips. Then the coverslips were removed, and the slides wash for 5 min at 37 °C in x2 SSC. The slides were washed in 50% formamide/2 \times SSC at 37 °C, for 5 min and this was

repeated once more. The slides were finally counterstained with 30 μL (approximately 3 drops of 10 μl evenly spaced) VECTASHIELD Antifade Mounting Medium with DAPI. They were then viewed with an Isis Fluorescence Imaging System (Metafer 4 software, MetaSystems). According to the Organization for Economic Co-operation and Development (OCED) requirements for use of the *in vitro* MN assay, only the doses that did not cause more than 50% RPD reduction were tested. For the results, a centromeric signal indicated an aneugenic event had occurred, while lack of a signal in a MN indicated the DNA damage was the result of a clastogenic event. 100 cells with MN that were analysed for centromeric signals and the experiments were carried out in triplicates.

2.17 Statistical analysis

Statistical analysis was carried out with SPSS 22.0. Significance was analysed using a one-way ANOVA followed by a post-hoc. A level of $p < 0.05$ was considered significant. The specific methods for evaluating statistical significance of each experiment conducted, including the defined *post-hoc* tests selected, are reported in the corresponding results Chapters that follow. In all experiments, three biological replicates (based on the use of cells grown and handled on separate days) were used to derive statistical analysis.

Chapter 3 Sodium Salicylate Toxicity on Prostate Cancer Cells

3.1 Introduction

The use of aspirin clinically continues to be expanded owing to new discoveries of its pharmacological effects. As described in detail in Chapter 1, Section 1.3, aspirin has demonstrated promising anti-tumour effects in *in vivo* and *in vitro* experiments at the molecular level and also in epidemiological studies. In recent years, the anti-cancer effect of aspirin has received widespread attention, especially for the prevention or suppression of PCA (Alfonso *et al.*, 2014). Aspirin is a NSAID whose pharmacological action is to inhibit the activity of cyclooxygenase and to reduce prostaglandin synthesis (Vane, 2014; Patrignani *et al.*, 2015). Thus, aspirin's impact on expression profiles of the *cyclooxygenases* (COX) gene family is considered a potentially important factor underlying its MoA, as discussed in Chapter 1, Section 1.4.3. However, currently the mechanisms underlying aspirin's anti-cancer activities in PCA are currently not well understood and the role of the COX-2 signalling pathway require further investigation.

3.1.1 Effects of aspirin on invasion and migration

Tumour metastasis is the leading cause of cancer death with about 90% of cancer patients dying from tumour metastasis (Chaffer and Weinberg, 2011). Therefore, anti-cancer research aimed at better understanding tumour metastasis is a strategy that can potentially prolong the survival time of patients and improve their quality of life. Research on tumour metastasis has grown rapidly in the past two decades. However, despite there being a large amount of data supporting a range of possible mechanisms, it is still difficult to translate the research to clinically widespread therapeutic practice (Martin *et al.*, 2013). The fundamental problem lies in the complexity of the tumour metastasis process. Metastasis is a process where, under the influence of multiple factors with multiple genes involved, the tumour cells detach from the primary lesion and migrate to the distal organ through the blood circulation system and form new foci. This process is dynamic and continuous and can be divided into the following stages:

firstly, the cancer cells detach from the primary site and invade the extracellular matrix (ECM) (Bonnans *et al.*, 2014). These cancer cells break through the ECM and the basement membrane (BM), entering into the blood vessels or lymphatic system with the assistance of various degradation enzymes secreted by the cells. The surviving cancer cells are then transported further through the blood circulation system (Mundy, 2002; Martin *et al.*, 2013; Bonnans *et al.*, 2014). Before reaching the target organ, the cancer cells use platelet aggregation to form clumps, providing the cells with protection in the fluidic circulatory environment (Hudson *et al.*, 2013; Suva *et al.*, 2011). Through secretion of relevant enzymes, the cells are able to break through the BM and invade the secondary sites. Under suitable conditions, the physiological process of angiogenesis, where new blood vessels are formed from the existing vessels, is induced; this improved blood supply enables the cancer cells to continue to proliferate and develop a secondary tumour. Tumour metastasis is therefore a multi-organ, multi-factor, long-term and complex biological event. Hence, therapies that usually only target a single element of this complex pathway suffer limitations in the clinical management of such aggressive tumours (Martin *et al.*, 2013).

Aspirin has demonstrated some influence in controlling tumour metastasis. The latest findings from Professors Rothwell Group at Oxford University provide strong evidence for its anti-cancer effects, particularly the reduction of distant metastasis, as summarised in Chapter 1, Section 1.3.1 (Rothwell *et al.*, 2012). This therefore represents an exciting benefit for the use of aspirin clinically for patients with aggressive and invasive cancers. However, research into the underlying MoA is limited and further work is needed in this area before this form of treatment could be more seriously considered in the clinical management of cancer patients.

3.1.2 Micronucleus assay

When evaluating both the safety and the MoA of new drugs, it is important to consider the potential DNA damaging effects (genotoxicity) that may be induced following exposure. Genotoxicity refers to the fact that exposure to an exogenous agent may directly or indirectly damage DNA in cells, potentially leading to mutagenic and carcinogenic effects (Phillips and

Arlt, 2009). Many chemotherapy drugs act through a genotoxic MoA by damaging DNA and preventing cell division. Although this is a beneficial way of killing cancer cells, these anticancer therapies can be associated with severe side-effects due to their induction of genotoxicity in normal cells. Thus, there needs to be a balance between the positive (cancer killing) and negative (side-effects associated with damage to normal cells) exposure consequences when evaluating the both the efficacy and safety of a new drug.

No single method exists for the detection of all forms of DNA damage and thus several genotoxicity tests exist. For example, the Ames test and HPRT forward mutation tests can be used to quantify point mutations in bacterial and mammalian cells respectively. While the micronucleus (MN) assay is widely used in the genotoxicity evaluation of drugs, cosmetics, consumer products, *etc.*, to sensitively quantify gross chromosomal damage (Zapata *et al.*, 2016; Fowler *et al.*, 2016). As a rapid, simple and economical method of genotoxicity detection, the MN assay has become a routine measure for genotoxicity detection in safety and hazard assessment (Corvi and Madia, 2017).

There are two main mechanisms for the formation of a micronucleus; one is chromosome breakage (clastogenicity), and the other is the disturbance of mitotic processes resulting in the loss / gain of whole chromosomes (aneugenicity; Samanta and Dey, 2012). Once this damage has arisen, if it is not repaired prior to cell division, then during the segregation of replicated chromosomes the spindle will fail to attach the acentric chromosome fragments (due to the lack of a centromere) or the whole chromosomes will not be divided into the daughter nuclei accurately (due to damage of proteins key to the chromosome segregation process). These full chromosomes or chromosome fragments excluded from the main daughter nucleus will subsequently be wrapped by a membrane resulting in the formation of a MN. They are similar to conventional nuclei in terms of their structure, but micronuclei are substantially smaller, in the range of 1/16 to 1/3 of the main nuclear size (Fenech *et al.*, 2003; Fenech *et al.*, 2011). The staining of micronuclei using nuclear dyes (e.g. such as DAPI) is consistent with that of the main nucleus, and thus they can be readily observed under an optical or fluorescent microscope (depending upon the nuclear stain applied). The presence

of micronuclei and their frequency, is therefore a measure of fixed chromosomal damage that has arisen following exposure to a test agent (Chapman *et al.*, 2015). The MN assay is currently used for the regulatory safety assessment of chemicals, following the OECD Test Guideline 487 “*In vitro* Mammalian Cell Micronucleus Test”. A key aspect for genotoxicity testing, is that DNA damage should only be measured within appropriate toxicity ranges, which is defined as doses associated with $55 \pm 5\%$ toxicity when calculated based on RPD. Thus, both cytotoxicity and genotoxicity need to be measured in parallel. Given the limited understanding of aspirin’s MoA, it is important to understand its genotoxic potential and if this is associated with the observed anti-cancer effects in clinical studies. This mechanistic aspect was therefore explored within this chapter using the MN assay to evaluate both the genotoxic and cytotoxic potential of the aspirin metabolite, NaS.

3.1.3 Aims

This Chapter was aimed at evaluating NaS’ potential toxicity, genotoxicity and anti-cancer effects on PCA cells and normal prostate cells. To achieve this aim, this chapter had the following key objectives:

- Establish the toxicity and effects on growth characteristics when NaS (aspirin’s active metabolite) was exposed to PCA cancer cells. In this study, we initially evaluated the cytotoxicity of NaS in the PCA cell lines PC3 and DU145 using the RPD method. In addition, apoptosis, nuclear size distribution, intracellular Ca^{2+} , and mitochondria number per cell were characterised following NaS exposure in PCA cells.
- Determine if exposure to NaS had an impact on the COX-2 expression profile of PCA cells based on RT-PCR analysis.
- Evaluate the genotoxic potential of NaS on PCA cells utilising the micronucleus assay, which measures the induction of gross chromosomal damage.
- Characterise the impact of NaS exposure on the migration and invasion capacity of PC3 and DU145 PCA cells. Additionally, an RT-PCR array approach was utilised to further

evaluate the transcriptional profile changes and therefore the signalling pathways involved following NaS treatment.

3.2 Materials and Methods

3.2.1 Materials

Table 3.1 lists the consumable materials applied in Chapter 3.

Table 3.1. Materials used in Chapter 3.

Materials	Manufacturer	Catalogue Number
Carbendazim	Sigma-Aldrich, UK	378674-100G
Carbonyl cyanide 4-(trifluoromethoxy)phenylhydrazone (FCCP)	Sigma-Aldrich, UK	C2920-10MG
Cytiva™ Cell Health Assay for High Content Analysis	GE Health care, UK	29024468
Cytochalasin B	Sigma-Aldrich, UK	C6762-1MG
Ionomycin	Sigma-Aldrich, UK	I3909-1ML
RT ² Profiler™ PCR Array Human Tumour Metastasis	Qiagen, GE	PAHS-028Z
RT ² First Strand Kit (12)	Qiagen, GE	330401
RT2 SYBR® Green qPCR Mastermixes (12)	Qiagen, GE	330502

3.2.2 Cell culture

Two PCA cell lines, PC3 and DU145, and a normal prostate cell line, PNT2, were used for this study. The cell culture techniques are as described in Chapter 2, Section 2.4.

3.2.3 Cytotoxicity assay

RPD was utilised to evaluate cytotoxicity; please refer to Chapter 2, Section 2.5 for the methodological details. The dose range used in Chapter 3 was 0, 2, 4, 6, 8 and 10 mM NaS. Although in clinical use, as cited in Chapter 1, Section 1.5, 1.2 g aspirin yield about 2 to 4 mM NaS *in vivo*, it is necessary to explore the effects at the higher doses to get a better understanding of the full dose-response of this compound with regards to its potential anti-

cancer effects. The concentrations of NaS selected in this study were therefore a physiologically relevant dose.

3.2.4 *COX-2* gene expression assay

Total RNA extraction, and cDNA synthesis were conducted following the protocol described in Chapter 2.6 and 2.7. The PCR running programme for *COX-2* and the housekeeping gene *B₂M* and *β-actin* were stated as follows and their sequences are found in Table 3.2:

The initial denaturation was 95 °C for 3 min. Next the following PCR cycle programme was applied 40 times: 95 °C for 30 s and then decreased to 60 °C for 30 s. After 40 cycles, the melt curve was measured by gradually increasing the temperature from 65 to 95 °C with a 0.5 °C increment and each incremental temperature was hold for 10 s. The melt curve was analysed to ensure it had only one peak corresponding to the test gene under evaluation.

Table 3.2. Primer sequences used for gene expression analysis by RT-qPCR in Chapter 3.

Primers	Sequence (5'→3')	Manufacturer	Use
<i>COX-2</i>	Forward: ACCCACTGAAAAAGATGA	Sigma - Aldrich	Gene of interest
	Reverse: ATCTCAAACCTCCATGATG	Sigma - Aldrich	
<i>B₂M</i>	Forward: CCTGAATTGCTATGTGTCTGGG	Sigma - Aldrich	Housekeeping gene
	Reverse: TGATGCTGCTTACATGTCTCGA	Sigma - Aldrich	
<i>β-actin</i>	Forward: GATGGCCACGGCTGCTTC	Sigma - Aldrich	Housekeeping gene
	Reverse: TGCCTCAGGGCAGCGGAA	Sigma - Aldrich	

The PCR primers that were used were all optimised for gene expression analysis in prostate cells by Dr Patrick Olaniyi during previous research projects in our laboratory.

3.2.5 INCell analysis for morphological changes

When PNT2, PC3 and DU145 cells reached 80% confluence, cells were seeded at 1×10^5 cells / cm³ for 24h and were then treated with 0, 2, 4, 6, 8, 10 mM NaS for 24 h. Then, INCell analysis was carried out in triplicate as described in Chapter 2, Section 2.9. DAPI and FITC filters were applied to visualise the signals. A 40x objective was used to take images of the samples on an INCell Analyzer 2000 (GE Healthcare) and images were acquired for 144 fields of view.

3.2.6 MN frequency

The MN frequency of PNT2, PC3 and DU145 cells, seeded at 1×10^5 cells / cm³, treated with 0-10 mM NaS with a 24-h exposure time were determined using the protocol described in Chapter 2, Section 2.15.

3.2.7 Aneugenicity and clastogenicity mode of action analysis

DU145 cells were seeded at 1×10^5 cells / cm³ and treated with the required NaS doses for 24 h. Carbendazim at 1 μ g/mL for 24 h was the positive control. Following exposure, all samples were treated with 1 μ g/mL Cytochalasin B to generate binuclear cells for 24 h. Next, cells were washed twice with PBS. Finally, cells were harvested and resuspended in PBS. The protocol for the centromere staining can be found in Chapter 2, Section 2.16. In Chapter 3, DU145 with a dose of 6, 8, and 10 mM NaS, which RPD values were not reduced by $(50 \pm 5) \%$, were tested with the micronucleus assay with centromere stain.

3.2.8 High content morphological alterations

PNT2, PC3 and DU145 cells were cultured in a 96 well plates to 80% confluence using the plate set-up format as demonstrated in Figure 3.1. They were then treated with 0, 2, 4, 6, 8, and 10 mM NaS for 24 h. Green, light blue, and dark blue wells, as illustrated in the Figure 3.1 schematic were not treated with NaS as they were the positive controls: 20 μ M Ionomycin for 20 min, 10 μ M Carbonyl cyanide 4-(trifluoromethoxy)phenylhydrazone (FCCP) for 20 min,

and 0.025% Triton X-100 for 20 min. Any empty wells in the plate were filled with PBS to minimise evaporation.

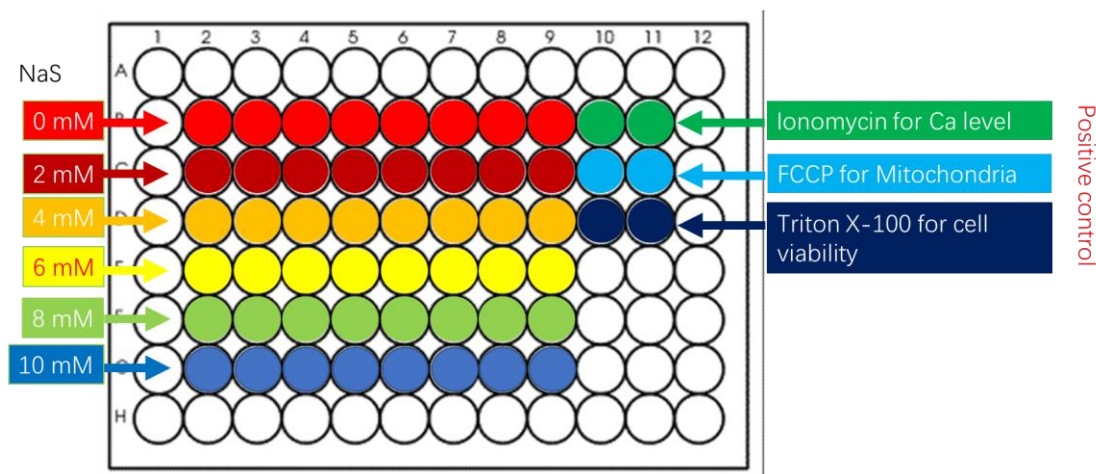


Figure 3.1. Plate layout for Cytivia™ Health kit INCell Analyser 2000 morphological analysis. White wells were filled with PBS to keep moisture in the plate. Other coloured wells were seeded with PNT2, PC3 or DU145 cells with each cell line in a separate individual plate.

There are four reagents in this Cytivia™ Health kit. Reagent A was membrane permeant nuclear stain reporting cell count, nuclear morphology and DNA content. Reagent B was membrane impermeant nuclear stain, which reported viability. Mitochondrial health was measured by Reagent C and intracellular Ca^{2+} level was measured with Reagent D (green, FITC). Reagent C and D as well as growth media were warmed in a water bath at 37 °C and Reagent A and B were warmed at room temperature. The four reagents were then centrifuged briefly. For a 96-well plate, 6 mL medium and 25 μ L of each reagent were mixed well in a 25 mL tube. A total of 50 μ L of the mix was dispensed into each well. The plate was incubated at 37 °C and 5% CO_2 for 1 h.

For image capture, the filter used for the four reagents can be found in Table 3.3. The INCell Analyser 2000 was set to maintain cell growth conditions (37 °C and 5% CO_2). Negative

control cells were used to adjust exposure time and focus. For Reagent A and C, 30-50% saturation was seen, and Reagent D's exposure was adjusted to 5-15% saturation. A 40x objective with 16 fields of view was used to capture images.

Table 3.3 Filter usage for the four reagents in Cytiva™ cell health kit.

Reagent	Filter for image output
A	DAPI
B	dsRED
C	dsRED
D	FITC

3.2.9 Cell cycle analysis

When images were acquired by the INCell Analyser, DNA content from the DAPI signal was used to facilitate cell cycle analysis. The nuclear intensity was measured by the INCell Analyser Workstation, which facilitated the evaluation of the proportion of cells in each phase of the cell cycle (G_1 , S and G_2/M) based on DNA content. Readings from triplicate samples within the same plate (*i.e.* technical replicates) were averaged; however, biological triplicates were performed with each replicate sample located on a separate plate. Thus, the data across the three plates were averaged and the variation across these plates was used to determine the SD.

3.2.10 Invasion assay and migration assay

PNT2, PC3 and DU145 cells were cultured to 80% confluence. The invasion assay and migration assays were then conducted following the instruction of the manufacturers, as described in Chapter 2, Section 2.10 and 2.11 respectively.

3.2.11 RT-qPCR array

RT-qPCR array was run on a CFX Connect™ Real-Time PCR Detection System. The RT-qPCR array employed in this chapter was the RT² Profiler™ PCR Array Human Tumour Metastasis (Qiagen, DE). Total RNA was extracted following the protocol described in Chapter 2, Section 2.6. The concentration and purity of RNA were determined with a Nanodrop™ (ND-1000 Spectrophotometer). The following conditions must be met prior to cDNA synthesis:

- $A_{260}:A_{230} > 1.7$;
- $A_{260}:A_{280}$ ratio should be between 1.8 and 2.0;

cDNA synthesis and RT-qPCR amplification were then carried out as follows:

RNA (0.5 μg) was used for cDNA synthesis. The RNA (stored at $-80\text{ }^{\circ}\text{C}$), and all reagents in the RT² First Strand Kit (Buffer GE, 5 \times Buffer BC3, Control P2, RE3 Reverse Transcriptase Mix and RNase-free water) were thawed on ice and once thawed were briefly centrifuged before usage.

The genomic DNA elimination mix was then prepared. This mix contains 2 μL Buffer GE, RNA sample containing 0.5 μg (μL , $\frac{0.5\ \mu\text{g}}{\text{concentration of RNA } \mu\text{g/mL}}$) and RNase-free water (μL , 8–volume of RNA sample). Then, the mix was incubated for 5 min at $42\text{ }^{\circ}\text{C}$ and placed on ice for 2 min.

When genomic DNA was eliminated, the following reverse-transcription mix was prepared: 4 μL 5 \times Buffer BC3, 1 μL Control P2, 2 μL RE3 Reverse Transcriptase Mix and 3 μL RNase-free water.

A total of 10 μL Reverse-transcription mix was combined gently with 10 μL genomic DNA elimination mix. The 20 μL reagents were incubated for 15 min at $42\text{ }^{\circ}\text{C}$ and the reaction was immediately stopped by incubation for 5 min at $95\text{ }^{\circ}\text{C}$. Then, 91 μL RNase-free water

was added to each reaction tube and mixed gently. Finally, synthesis of cDNA was complete. The cDNA was placed on ice prior to immediate use or was stored at -20°C.

cDNA, 2×SYBR Green mix, RNase-free water from RNA RT² SYBR® Green qPCR Master-mixes were thawed on ice and briefly centrifuged. Next, PCR components were prepared, containing 1350 μL 2×SYBR Green mix, 102 μL cDNA (the remaining 9 μL cDNA was kept in the freezer (-20°C)), and 1248 μL RNase-free water. A total of 25 μL mix was aliquoted into the wells of each plate.

Then, the plate was tightly sealed with Optical Thin-Wall 8-Cap strips (provided by the kit). The bubbles in the plate were removed by centrifugation at 1000 g for 1 min. The plate was placed on ice while the running programme was setting up. The real-time cyclers were programmed as follows: the sample was initially incubated at 95 °C for 5 min to activate HotStarTaq DNA Polymerase, followed by 40 cycles of 15 s-denaturation at 95 °C, combined step of annealing and extension were conducted at 60 °C for 1 min and finally, a melt curve analysis was performed from 50 to 95 °C at the ramp rate of 1 °C/s.

Finally, the data was analysed via the Web-based PCR array Data Analysis Software, which can be accessed at <http://saweb2.sabiosciences.com/pcr/arrayanalysis.php>.

3.2.12 RT-PCR for gene expression analysis

Total RNA, cDNA synthesis and PCR amplification followed the protocols described in Chapter 2, Section 2.6, 2.7 and 2.8. The primers were ordered from Sigma-Aldrich, which were pre-designed SYBR green primers. Their sequence information can be found in Table 3.4. Finally, data were analysed using $2^{-\Delta\Delta Ct}$ method performed by the CFX Manager software coming with CFX Connect™ Real-Time PCR Detection System.

Table 3.4. Primers used for further exploration of gene profiles after aspirin treatment.

Primers	Sequence/ 5'→3'		Annealing temperature / °C
<i>CD44</i>	Forward	TTATCAGGAGACCAAGACAC	60
	Reverse	ATCAGCCATTCTGGAATTTG	
<i>Cathepsin L1 (CTSL1)</i>	Forward	AGGCATTTATTTTGAGCCAG	60
	Reverse	AATTCCACAATGGTTTCTCC	
<i>Integrin Subunit Beta 3 (ITGB3)</i>	Forward	CCATCGAGTTCCCAGTG	60
	Reverse	AATTCTTCGAATCATCTGGC	
<i>Nuclear receptor subfamily 4 group A member 3 (NR4A3)</i>	Forward	CAAAGCACTTTTGGACAATG	60
	Reverse	TTAAGACACATCCTACCCTG	
<i>C-X-C Motif Chemokine Receptor 2 (CXCR2)</i>	Forward	TTCATCGTCAAGGTTGTTTC	60
	Reverse	AAACTTAAATCCTGACTGGG	
<i>Interleukin 1 beta (IL1β)</i>	Forward	CTAAACAGATGAAGTGCTCC	60
	Reverse	GGTCATTCTCCTGGAAGG	

3.2.13 Statistical analysis

All statistical analysis was conducted with SPSS 22.0 for windows (IBM, U.S). A *p*-value of less than 0.05 was considered significant. Shapiro-Wilk tests used with a $p \geq .05$ indicate normal distribution. Homogeneity of the variance was determined by One-way ANOVA. For the INCell analysis experiments, the data was tested with a One-way ANOVA plus *post hoc* Dunnett's T3 test to evaluate significance when the data were normally distributed. If the data was not normally distributed, the Kruskal Wallis test was used. For gene expression analysis, T-test (two-tail) was used. For the rest of the assays in this Chapter, if the data fitted a normal distribution with heterogenous variance, the Dunnett's T3 Test was used; whilst, if the data fitted a normal distribution with homogeneous variance, the LSD test was performed.

3.3 Results

In this chapter, the impact of aspirin exposure on a range of toxicity and anti-cancer related endpoints was tested in several prostate cell types to understand its potential therapeutic benefits in the treatment of PCA. The endpoints evaluated included cell growth, cytotoxicity, proliferation, morphological cell changes, DNA damage induction, *COX-2* gene expression profiles, cell migration and invasion.

3.3.1 NaS impact on inducing cytotoxicity in prostate cells

In order to investigate the cytotoxic effects of aspirin on PCA cells, RPD measurements were made on PC3, DU145 and PNT2 cells after exposure to a dose range of NaS (aspirin's active metabolite). As illustrated in Figure 3.2, all three cell lines demonstrated a dose-dependent reduction in cell viability with increasing NaS dose. NaS had the greatest effect on PC3 cells, and the least effect on DU145. It could be clearly seen that when compared with a dose of 0 mM (the control group), there was a significant reduction in cell viability from 2-10 mM dose for all cell lines. However, it is important to note that in all three cell lines, the cytotoxic effects appeared to plateau at the top three doses (6, 8 and 10 mM).

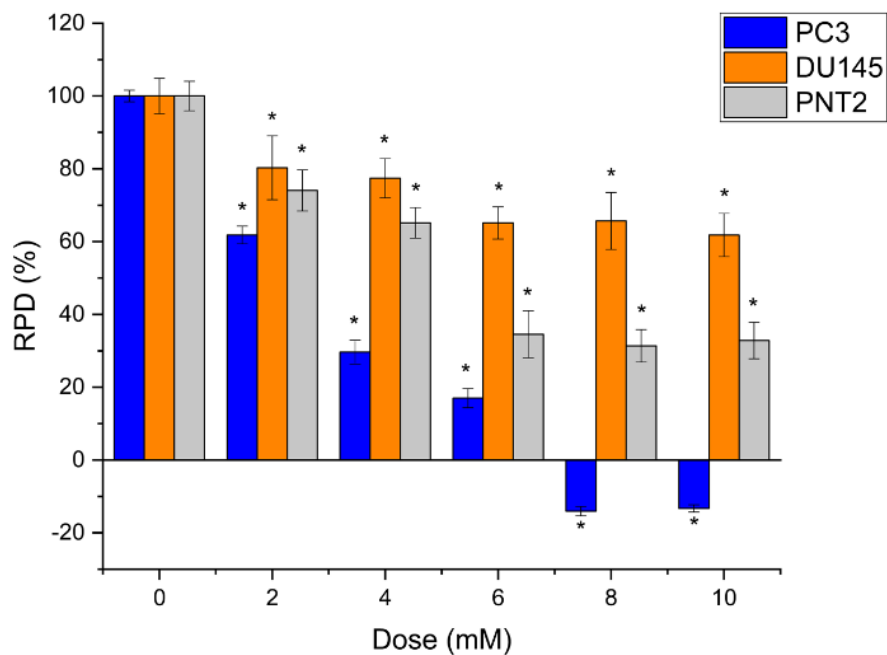


Figure 3.2. RPD analysis for the PC3, DU145 and PNT2 cells following exposure to NaS. All cell lines demonstrate cytotoxicity as the dose increases. Note: the '*' indicate significance compared to the control where $p < 0.05$, as determined by a one-way ANOVA with the *post hoc* Dunnett T3 test ($n=3$). Error bars indicate \pm SD (standard deviation).

3.3.2 Impact of NaS on *COX-2* gene expression

In the first instance, baseline *COX-2* gene expression analysis (*COX-2* gene expression without treatment) was evaluated. *COX-2* expression was higher in the two cancer cell lines than in the normal prostate cells ($p < 0.05$). PC3 cells had the highest baseline *COX-2* expression (Figure 3.3), which was 41-fold higher than in PNT2 ($p=0.003$). *COX-2* gene expression levels in DU145 cells were 4-fold higher than that of PNT2 cells ($p=0.011$).

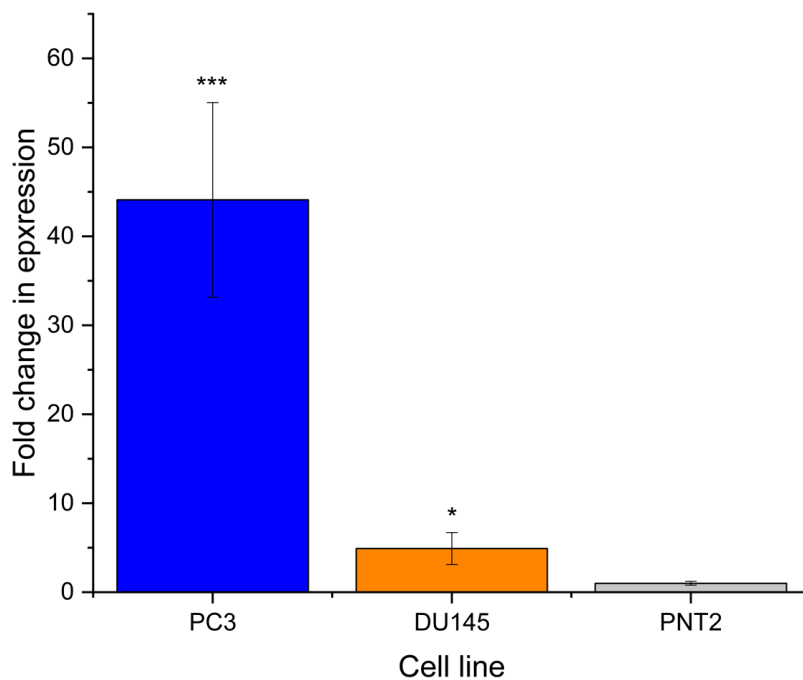


Figure 3.3 Relative COX-2 gene baseline expression in three prostate cell lines (PC3, DU145 and PNT2 cells). After 24 h of culture, the RNA was extracted from the three cell lines. PNT2 cells is the control group. *, and *** indicate significance compared to PNT2 cells (set as 1) where $p < 0.05$ and $p < 0.001$ respectively, as determined by a one-way ANOVA with the *post hoc* Dunnett T3 test ($n=3$). Error bar indicates the SD.

NaS was exposed to PNT2, PC3 and DU145 cells for 6 h at concentrations of 0mM (100 μ L Tris HCL, the negative control group), 2mM, 4mM, 6mM, 8mM, and 10mM. COX-2 expression was then measured by RT-PCR. For PNT-2 and DU145 cells, COX-2 expression remained unchanged over the dose-range of NaS applied. In contrast, PC3 cells did demonstrate a slight dose-dependent decrease in COX-2 expression, but this did not reach significance. NaS was then exposed to PNT2, PC3 and DU145 cells for an extended 24-h period. The bar chart (Figure 3.4) illustrates the COX-2 expression after the 24-h exposure period. COX-2 expression in PNT2 cells remained unchanged over the NaS dose rate applied. In contrast, for PC3 and DU145 cells, as the NaS dose concentration increased, there was a significant reduction in COX-2 expression. The expression of COX-2 was reduced by 35% in PC3 cells at 10mM, while DU145 cells exhibited a 25% reduction of COX-2 expression at the same dose.

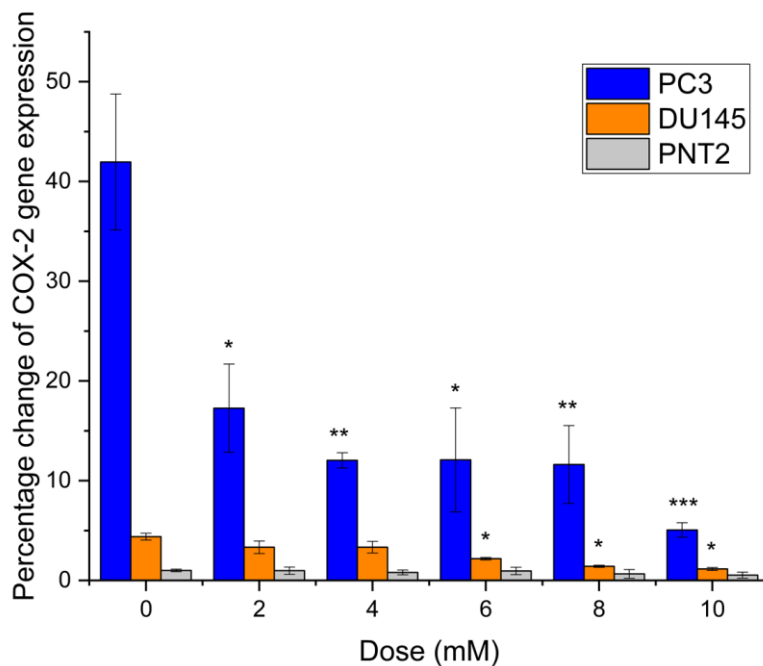


Figure 3.4. *COX-2* expression profile after 24-h exposure to NaS. After 24 h of dosing, the RNA was extracted from the three cell lines (PC3, DU145 and PNT2 cells). Only *COX-2* expression in PNT2 without treatment was set as “1”, with all data demonstrating the relative percentage change in *COX-2* gene expression normalised to this base-line. *, ** and *** indicate significance compared to the control where $p < 0.05$, $p < 0.01$ and $p < 0.001$ respectively, as determined by a one-way ANOVA with the *post hoc* Dunnett T3 test ($n=3$). Error bars indicate the SD.

In summary, *COX-2* expression was significantly reduced in the PCA PC3 and DU145 cells in a dose-dependent manner following a 24 h NaS treatment. In contrast, the *COX-2* levels remained unchanged in the normal prostate PNT2 cells following the same NaS exposure regimen indicating a clear difference in response to aspirin between cancer versus normal cells.

3.3.3 Induction of DNA damage in response to NaS exposure

The induction of MN was utilised as a measure of DNA damage generated as a result of exposure to NaS. The frequency of MN in prostate cells exposed to NaS were quantified with a Cell Profiler pipeline based on analysis of cell images generated on the INCell Analyser 2000 (provided and developed in-house by DR. K.E. Chapman). MN frequency was found to increase gradually from 2 mM to 10 mM NaS after a 24h exposure in PC3 and DU145 cells

(Figure 3.5). At higher doses, (6, 8, and 10 mM), the MN frequency of PC3 and DU145 cells were significantly increased compared to the negative control groups. This demonstrated that NaS is able to induce substantial DNA damage at the higher doses in these PCA cells. In contrast, the PNT2 cells did not demonstrate increases in DNA damage until the top 10 mM dose ($p=0.002$) indicating they are considerably less sensitive than PC3 and DU145 cells to NaS exposure in terms of chromosomal damage induction by NaS.

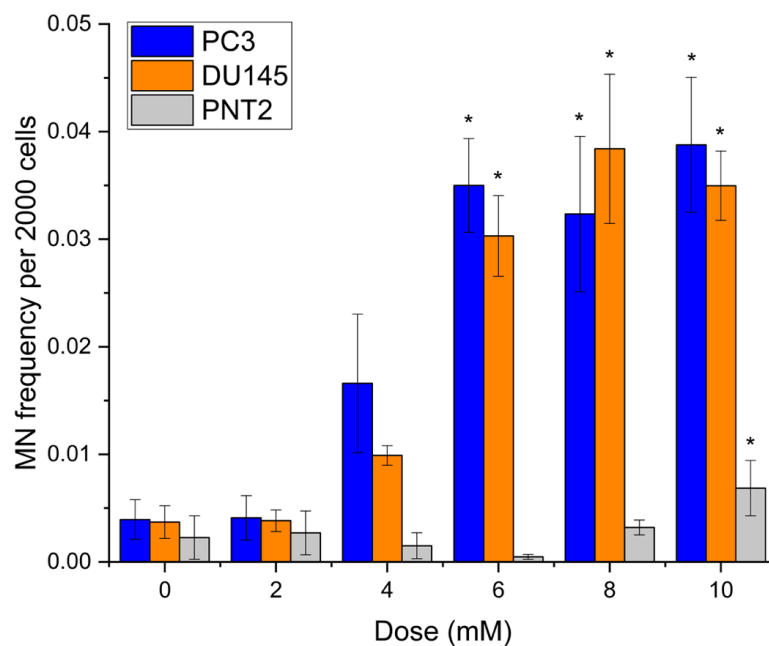


Figure 3.5. MN frequency in PC3, DU145 and PNT2 cells following NaS exposure. 2000 cells per cell line per replicate were evaluated for the presence of MN with each experiment conducted in triplicate. * indicate significance compared to the control where $p < 0.05$ as determined by a one-way ANOVA with the *post hoc* Dunnett T3 test ($n=3$). Error bars indicate the SD.

3.3.4 Aneugenicity and clastogenicity of NaS

The micronucleus assay measures the presence of two types of chromosomal damage, clastogenicity and aneugenicity. Clastogenicity indicates a chromosome breakage event where the MN only contains a chromosome fragment. In contrast, aneugenicity represents loss / gain of whole chromosomes, thus the resultant MN contains the whole chromosome

lost during cell division. To determine whether NaS induced clastogenic or aneugenic events, kinetochore staining was utilised in DU145 cells exposed to NaS, with the data illustrated in Figure 3.6 and example images in Figure 3.7. The positive control carbendazim is a compound that induces numerical chromosome aberrations and thus it induced a $68.67 \pm 5.51\%$ aneugenicity. For the NaS treatment from 6 to 10 mM dose, a dose dependent increase in aneugenicity was observed and the aneugenicity reached significance at level of 0.05 when DU145 cells were treated with 10 mM NaS. It was interesting to note that the aneugenic response noted in DU145 and induced by NaS was greater than that of the positive control compound and thus the DNA damage induced was clearly resulting in chromosome distribution errors during cell division. For the results in Figure 3.6, although the results with 6, 8 and 10 mM have overlap error bars, only significance found with the top dose.

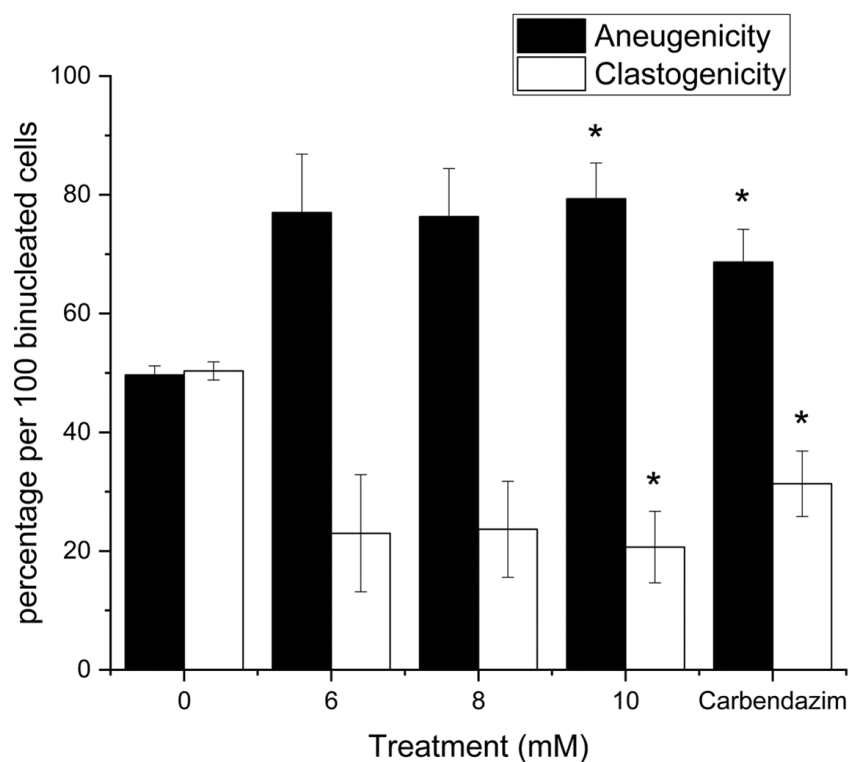


Figure 3.6. Percentage of kinetochore positive MN in binucleated DU145 cells treated with NaS (6, 8 or 10 mM). This was carried out three times with 100 binucleated cells scored per dose in total. Positive control was 24 h of 1 $\mu\text{g}/\text{mL}$ carbendazim treatment. * indicate significance compared to the control where $p < 0.05$ as determined by a one-way ANOVA with the *post hoc* Dunnett T3 ($n=3$). Error bars indicate the SD.

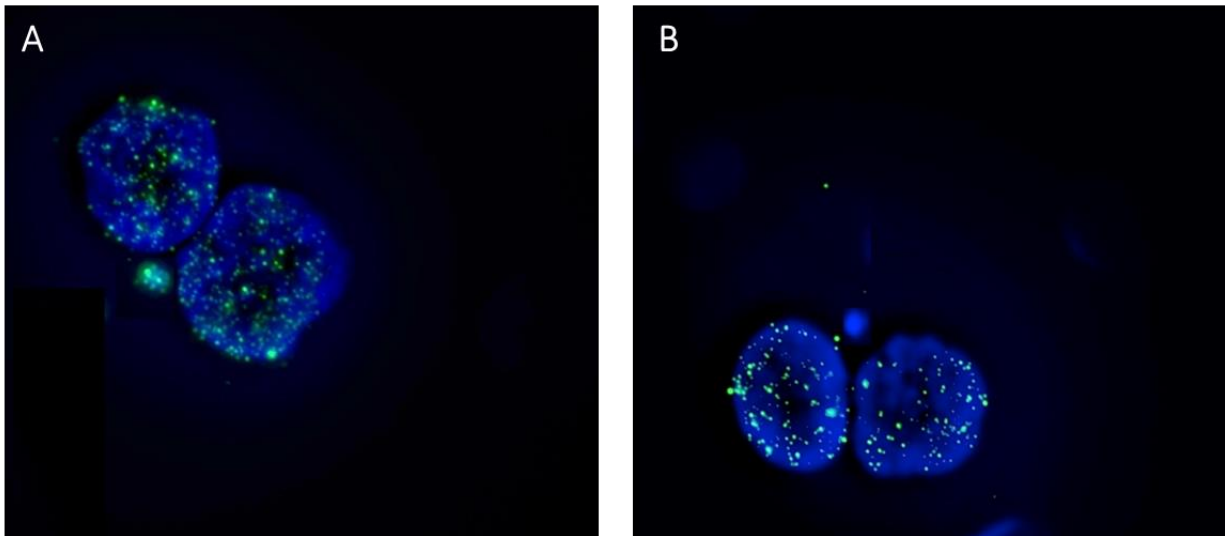


Figure 3.7. Representative images of binucleated DU145 nuclei when stained with Human Chromosome Pan-Centromeric paints. A, kinetochore-positive MN; B, kinetochore-negative MN. DAPI, blue, indicating the nuclei; FITC-green, indicating the centromeres.

3.3.5 INCell Analysis for cell cycle profile and cell morphological features

3.3.5.1 Cell cycle profile

Cell cycle profile analysis was obtained on the INCell Analyser 2000 based on DNA content as measured by DAPI intensity. Figure 3.8 is an example of the cell cycle profile of untreated PC3 cells. Most PC3 cells remained at the G_0/G_1 phase, where cells were identified with uniform and low DNA content values (the first peak). G_2/M cells had DNA content about twice that of G_0/G_1 cells (the second peak). The S phase cells with intermediate DNA content were in the middle of the two peaks. For the thresholds for the phase distinction, DAPI intensity between 135 and 170 was seen at G_0/G_1 , and the intensity with an arbitrary unit between 290 and 325 corresponded to the G_2/M phase. The intensity values in between these phases was where cells remained at the S phase. These three thresholds settings were used for all samples treated with NaS and the negative controls.

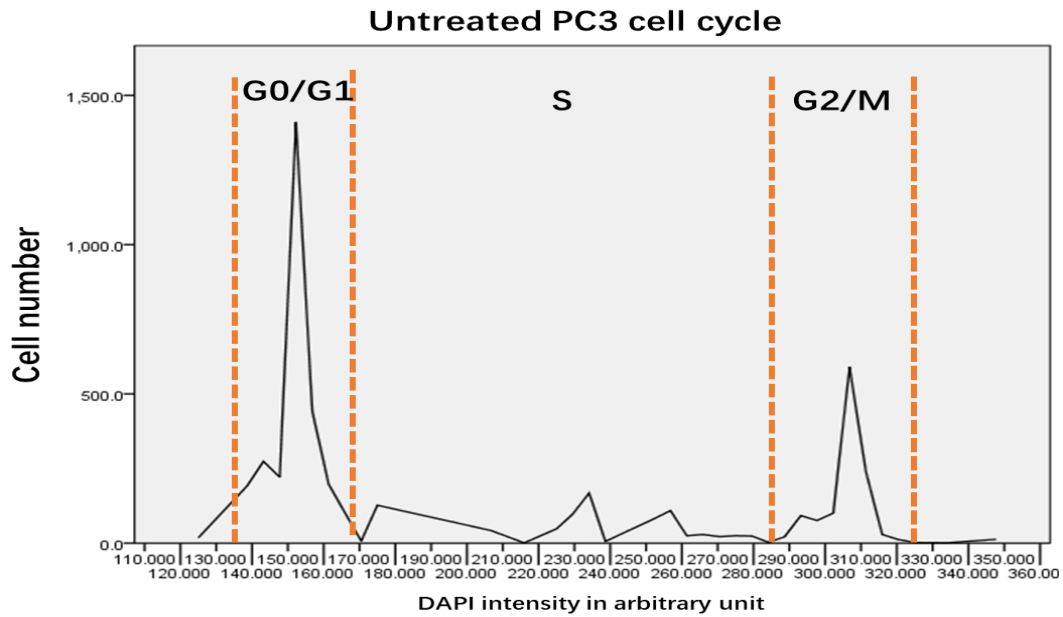


Figure 3.8. Representative PC3 cells population distribution within the distinct cell cycle phases of based on DAPI intensity, as measured by the INCell Analyzer 2000.

The numerical data for the cell cycle fluorescence profile of the PNT2, PC3 and DU145 cell lines with 24-h-exposure of NaS doses of 2, 4, 6, 8, and 10 mM is demonstrated in the Figure 3.9. For the positive control, cell cycle arrest occurred at the S phase following exposure to colcemid in all three cell lines. In contrast, with NaS exposure to PC3 cells, as the dose increased, there were more cells in the G₀/G₁ phase. There were 44.70% of untreated cells which remained at this G₀/G₁ phase; however, the number rose to 76.50% at 10 mM NaS in PC3 cells, indicating that cells were undergoing cell cycle arrest at this phase. From 6 mM the changes became significant. DU145 cells demonstrated a similar sensitivity in cell cycle phase progression following exposure to NaS. At the 6 mM NaS dose, the percentage of DU145 cells significantly remaining in the G₀/G₁ phase was increased by approximately 10% and about 18% cells were in the G₂/M phase following exposure. Interestingly, with the normal PNT2 cell line, the exposure to NaS did not impact the cell cycle profile, indicating that NaS only disturbed the cell cycle profile in the cancer cell lines.

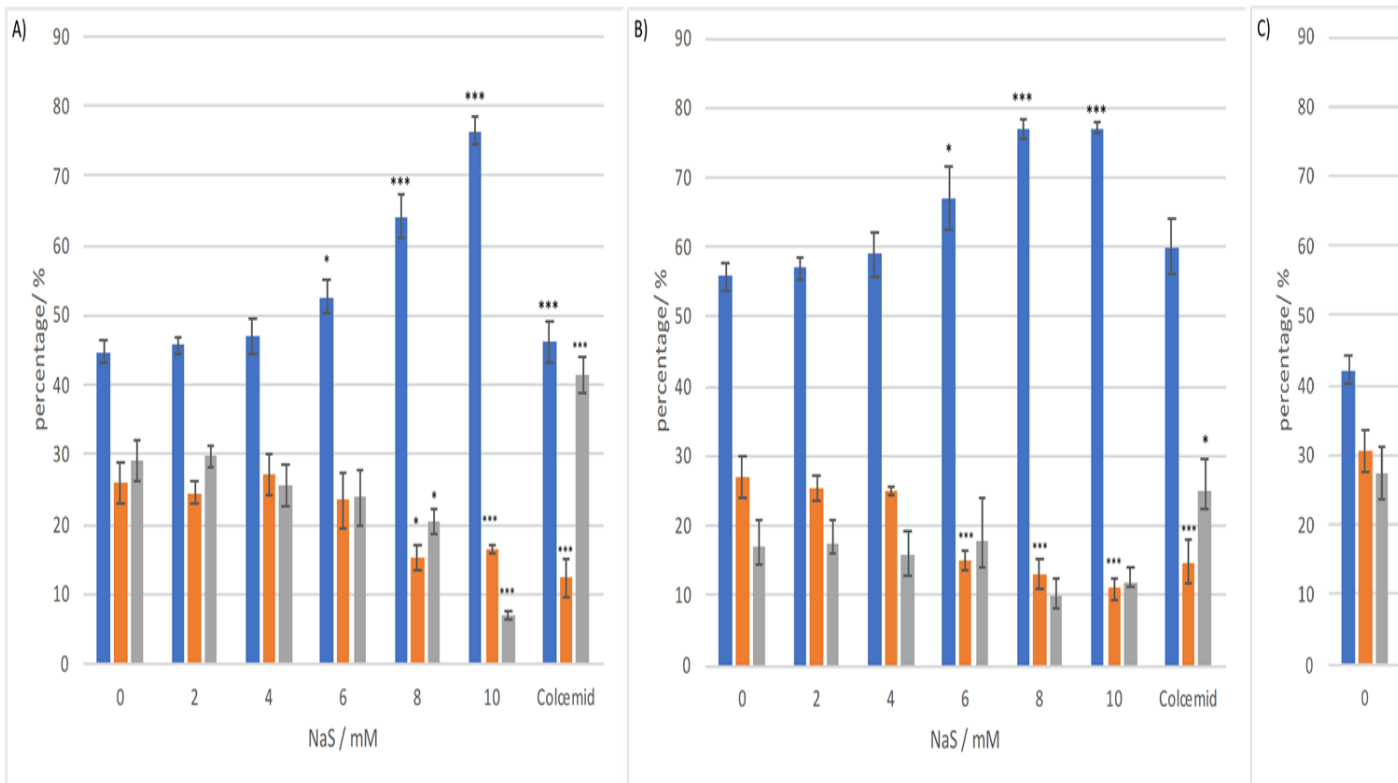


Figure 3.9. Cell cycle profile for A, PC3, B, DU145 and C, PNT2 cell lines. Cell cycle analysis was performed using Hoechst intensity (in images generated for samples treated with NaS for 24 h. Positive control: 60 nM colcemid; negative control: Tris-HCl. * and *** in where $p < 0.05$ and $p < 0.001$ respectively, as determined by a one-way ANOVA with the *post hoc* Dunnett T3 ($n=3$). Error bars indicate

3.3.5.2 Morphological changes

Figure 3.10 is a representative working process to illustrate how the image was transferred to numeric data.

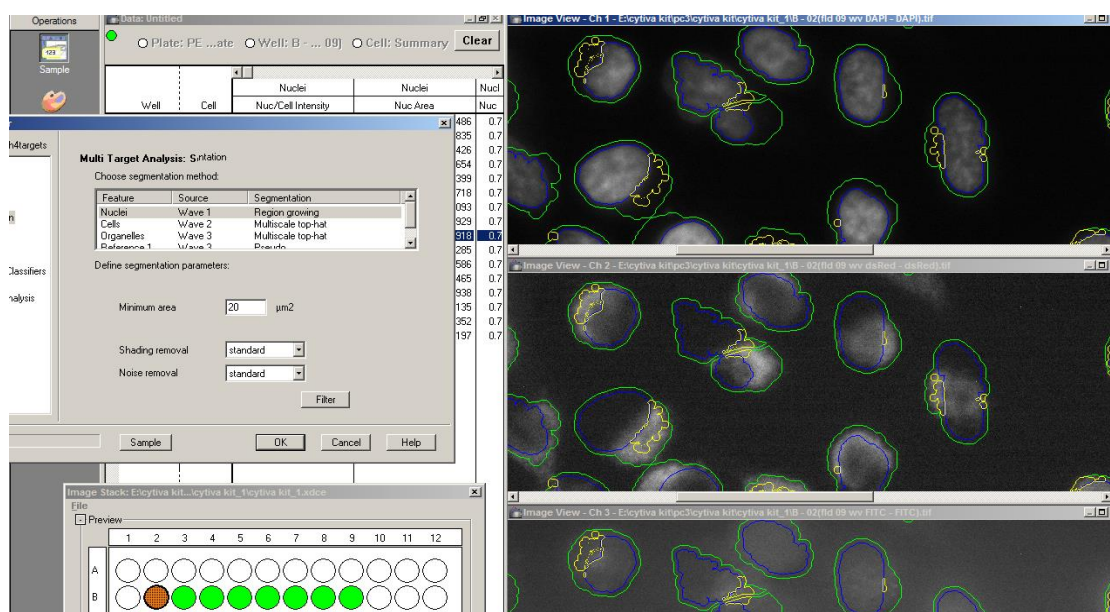


Figure 3.10. Representative working interface of INCell Analyser Workstation for transferring image data to numerical data. Right half: software outlining organelles (yellow), nuclei (blue) and cell body (green). Left half: segmentation setting up. For the segmentation, Wave 1, DAPI for nuclei with “Region growing” segmentation method (mini area: 20 μm); Wave 2 (mini area: 30 μm), FITC for cells with “Multiscale top-hat” segmentation method; Wave 3, dsRed for Ca^{2+} and mitochondria with “Multiscale top-hat” segmentation method (mini area: 5 μm). Shading removal and noise removal were both set up at “standard.”

The morphological changes to prostate cells following NaS exposure were analysed with an INCell analyser 2000. Firstly, nuclear area was analysed and was found to alter when all three cell lines except for PNT2 were exposed to NaS. For PC3 cells, nuclear area was not reduced

significantly until the cells were treated with 10 mM NaS ($p=0.025$) as show in Figure 3.11. In DU145 cells, 2 mM NaS did not result in a reduction of nuclear area, however, from 4 to 10 mM NaS, the nuclear area decreased as the dose increased ($p<0.01$) as demonstrated in Figure 3.11. However, at the highest dose of 10 mM, the nuclear area declined by only approximately 10% in PC3 cells, while in DU145 cells the reduction was far more striking at 50%. Therefore, although NaS reduced the nuclear area of both cancer cell lines, there was a difference in sensitivity between the cell lines with DU145 cells being more sensitive to NaS than PC3 cells. On the contrary, with the normal cell line, PNT2, the nuclear area was not changed at all over the dose range applied (Figure 3.11). It should be noted that the positive control only exhibited a marginally significant change in nuclear area in PNT2 cells, with large error bars in both the negative and positive controls. It is speculated that the positive control might need a longer exposure time in the normal PNT2 cells than necessary for the PC3 and DU145 cancer cells; the latter of which are more genetically unstable and therefore may be more sensitive to colcemid.

Other morphological indicators, including, cell and nuclear form (roundness), and cell area were also investigated. However, there were no significant changes found in any of these parameters with the three cell lines following NaS exposure.

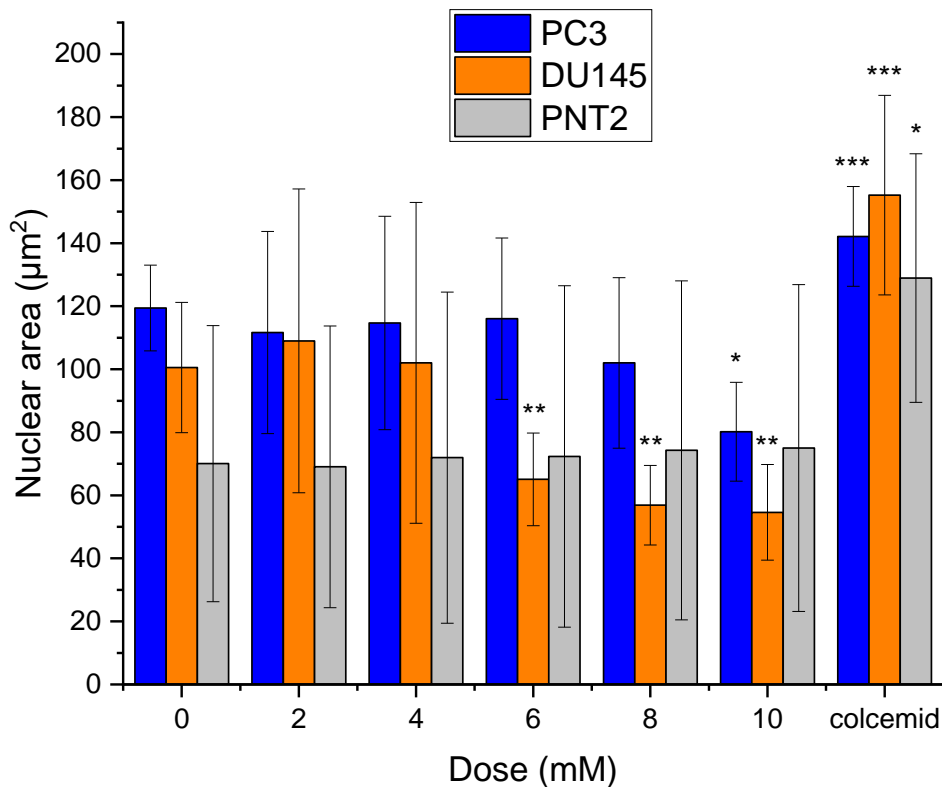


Figure 3.11. Nuclear area in PC3 cells, DU145 cells and PNT2 cells treated with NaS. Graph represents the mean value from DAPI signals. *, **, and *** indicate significance at levels of $p < 0.05$, $p < 0.01$ and $p < 0.001$ respectively, as determined by the Kruskal Wallis test relative to the control ($n=3$). Error bars indicate the SD.

3.3.6 Cytvia™ Health Kit for Calcium level and mitochondrial changes

In order to measure intracellular Ca^{2+} level and reduction in mitochondria count, which are related to apoptosis in cells, the Cytvia™ Health Kit was used. Figure 3.12 shows the examples of INCell images generated when cells were treated with the positive controls. FCCP is a chemical leading to the depolarisation of mitochondria, which resulted in a loss of mitochondrial staining as measured by Reagent C (dsRed, orange). The second positive control was ionomycin; this is a Ca^{2+} ionophore that significantly increases the intracellular Ca^{2+} level and was measured with Reagent D (green, FITC). In the ionomycin-treated cells, the

green (FITC) intensity and the number of green dots clearly increased as compared to the negative controls.

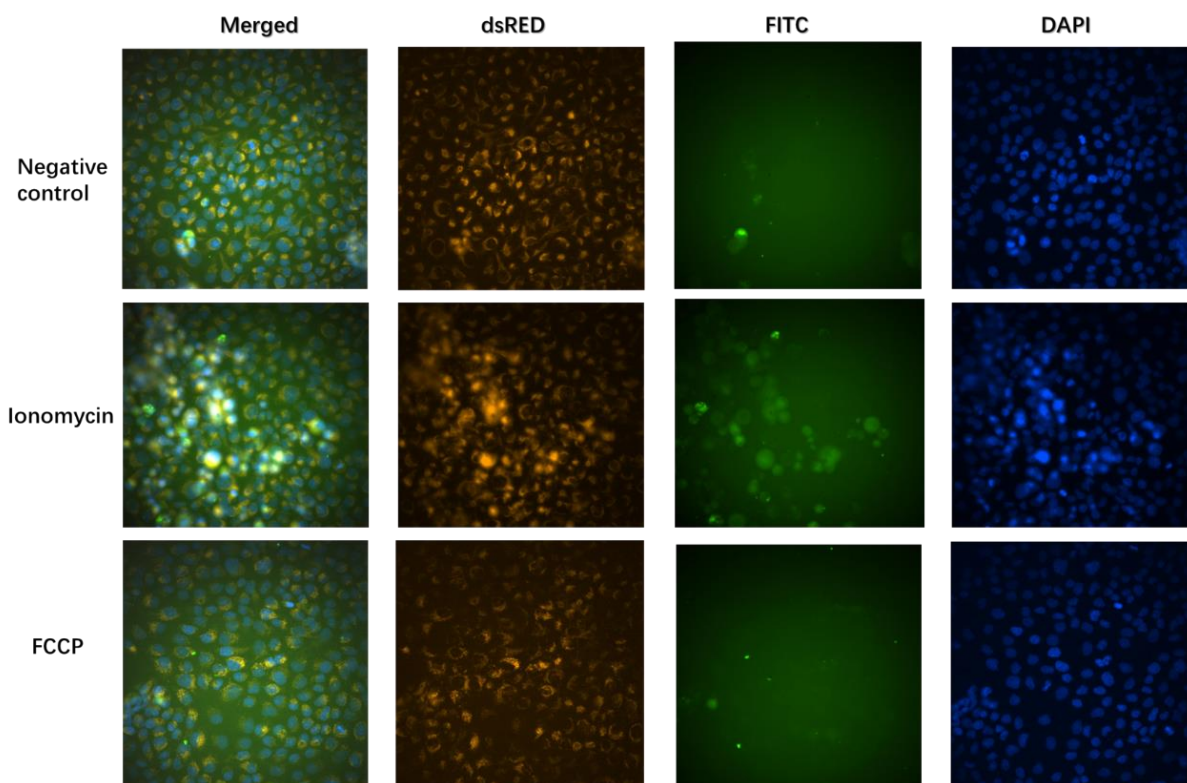


Figure 3.12. Example INCell images of PC3 cells treated with the positive controls ionomycin and FCCP. The first column to the far left is the merged images, with dsRed (orange, staining mitochondria), FITC (green, staining intracellular Ca^{2+}) and DAPI (blue, staining nuclei) individual channels from left to right.

When mitochondria counts were measured following exposure of PC3, DU145 and PNT2 cells to NaS, the number of mitochondria per cell significantly decreased in all three cell lines from 8 mM; representative images are illustrated in Figure 3.12, with the data from all cell lines presented in Figure 3.14. PNT2 cells were the most sensitive to the treatment, as 2 mM NaS was able to significantly reduce the organelles count. However, it should be noted that the error bars for the 2- and 4-mM doses largely overlapped with the PNT2 control. The higher doses of NaS (6-10 mM) reduced mitochondrial number more substantially and these does where highly significant. In contrast to PNT2, for the two cancer cell lines, the higher doses of 8 and 10 mM resulted in a significant reduction in mitochondria count per cell ($p < 0.05$).

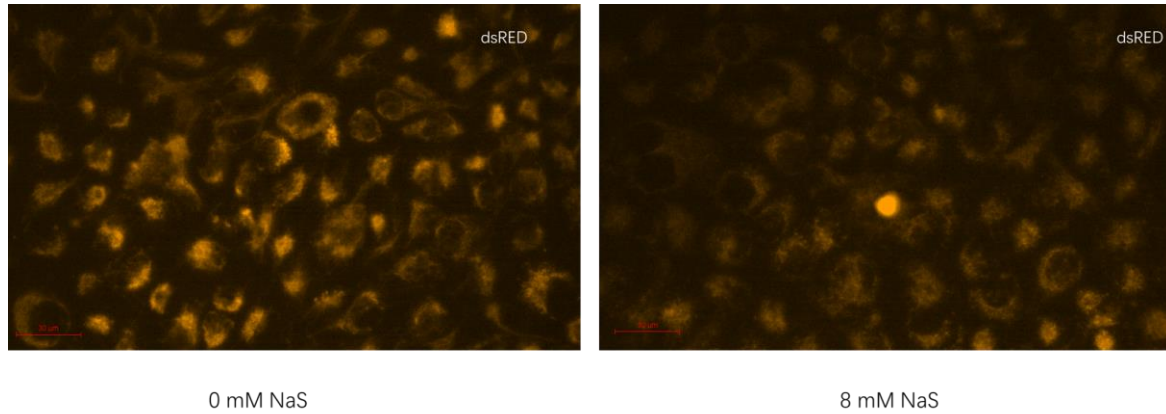


Figure 3.13. Representative images of the changes in mitochondria count in PC3 cells. The images illustrate the mitochondria count based on the signal intensity. 8 mM NaS reduced the intensity of the dsRed signal, indicating a decrease in mitochondria count. Intensity was determined by the INCell Analyser Workstation. Scale bar: 30 μm . Objective: 40x.

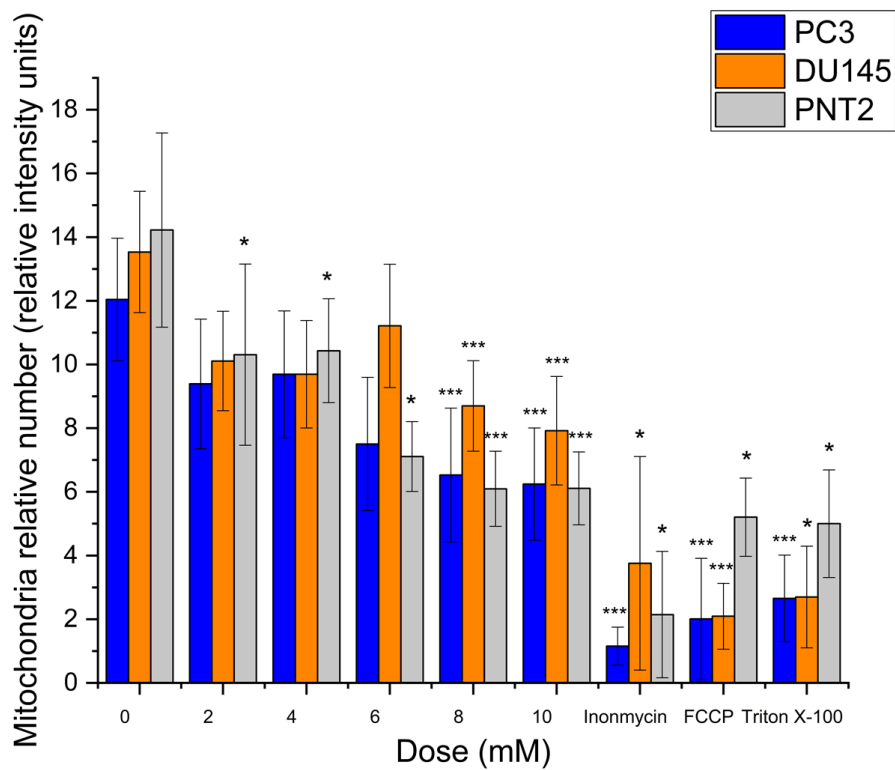


Figure 3.14. Mitochondria counts in each cell line. FCCP was the positive control for mitochondria. Triton x-100 was the positive control for cell viability (not relevant to this results). Ionomycin was the positive control for Ca^{2+} (not relevant to this results). * represents significance at level of $p < 0.05$ as determined by a one-way ANOVA and the *post hoc* Dunnett T3 ($n=3$). Error bars indicate SD coming from biological triplicates.

With Reagent D from the Cytvia™ Health Kit, the Ca²⁺ level in each cell line treated with NaS was evaluated (Representative images are presented in Figure 3.15) and the data is illustrated in Figure 3.16. As expected, the positive control Ionomycin, was able to increase intracellular Ca²⁺ level significantly ($p=0.042$). In contrast, the control FCCP did not affect Ca²⁺ levels and neither did Triton-X. Triton x-100 is suggested by the manufacturer as a positive control for the cell viability measurement aspects of the Cytvia™ Health Kit, because it permeabilises the cell membrane, which in turn results in cell death. The Triton-x 100 concentration applied has been carefully optimised by the manufacturer to selectively permeabilise the plasma membrane of a wide variety of cells without significantly affecting Ca²⁺-sequestering organelles. For the DU145 and PNT2 cells, Ca²⁺ levels were unchanged in response to NaS treatment; while there were significantly increased Ca²⁺ levels in PC3 cells only at the top 10 mM NaS dose. Thus, this suggests the PC3 cells were more sensitive to the induction of Ca²⁺ levels in response to NaS exposure than the DU145 and PNT2 cells.

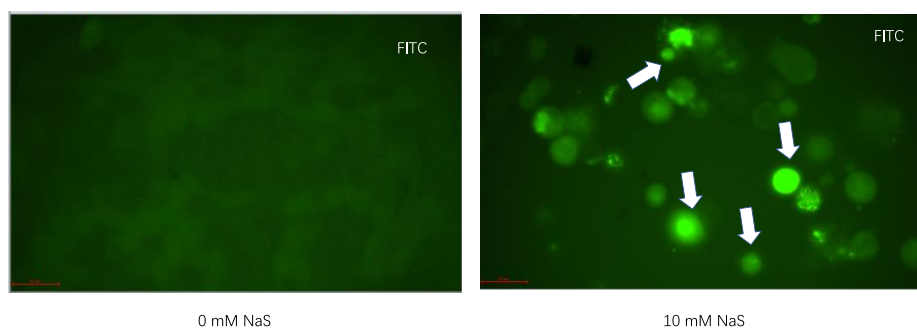


Figure 3.15. Representative images of the changes in intracellular Ca²⁺ level in PC3 cells. The two images show the intracellular Ca²⁺ level, where the level increases comparing to the negative control (0 mM NaS). Intensity was determined by INCell Analyser Workstation. Objective: 40x. Intensity was determined by INCell Analyser Workstation. Scale bar: 30 μ m. Objective: 40x.

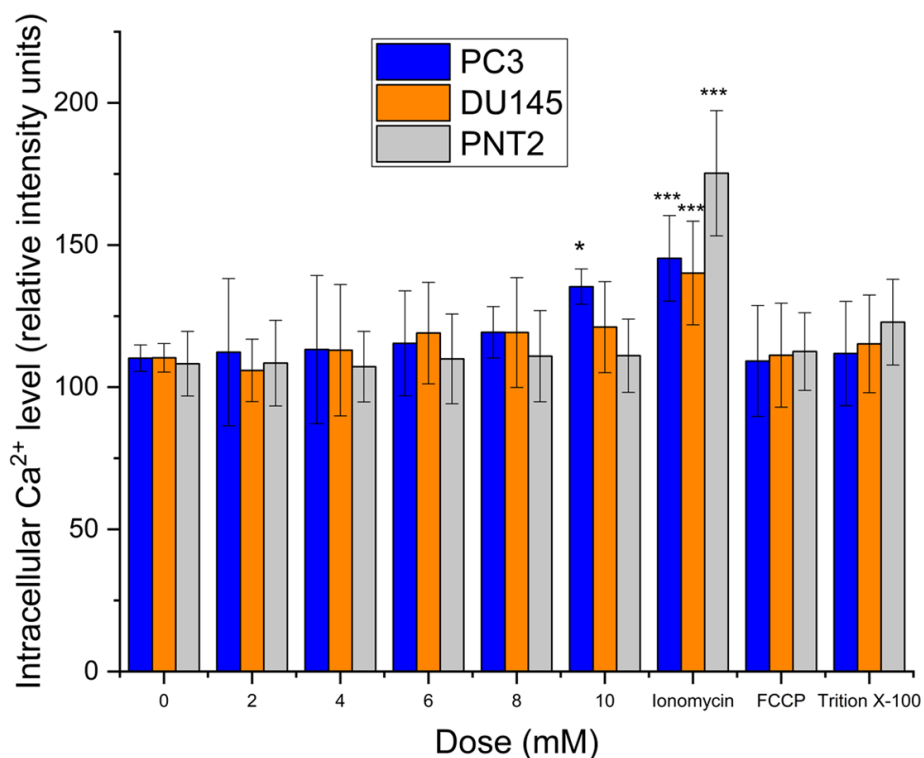


Figure 3.16. Ca^{2+} level in PC3 cells DU145 cells and PNT2 cells treated with NaS. Graphs represent the mean value from FITC signals. *, and *** represent significance at a level of $p < 0.05$, and $p < 0.001$ as determined by the Kruskal Wallis test relative to the control ($n=3$). Error bars indicate SD.

3.3.7 NaS effects on metastasis

3.3.7.1 Migration assay

Migration assays measure the ability and speed of cells to close a uniform gap created in a monolayer. The cells were seeded into two sections of an insert. After treatment the insert was removed, and the cells had 24-h recovery time to migrate. At the end of assay, the gap remaining between the cells was measured. The images in Figure 3.18-20 show images of the size of the remaining gaps at the end of the experiment, while the gap measurement data

generated is summarised in Figure 3.20. PNT2 cells were not able to migrate and close the gap between two sections over the 24h period when they were treated with NaS. The distance between two sections of PNT2 cells was not changed significantly ($p=0.707$) for these doses. Thus, aspirin did not affect the ability of PNT2 cells to migrate. They are generally a slow growing cell line that would take up to 48h to close the gap. However, what is notable is that the PNT2 cells appeared to be dying at the higher doses (6 – 10 mM) and were not as confluent as the control group after 24 h of migration and growth (Figure 3.19).

For the DU145 and PC3 PCA cells, following a 24 h of recovery time, complete gap closure was achieved with the untreated cells, but NaS exposure clearly resulted in a dose dependent reduction in migration. A dose of 2 mM NaS affected the migratory ability of both cell lines slightly (no statistical difference found, $p>0.05$). Although they were able to largely close the gap, it was not 100%. As the NaS concentration increased, PC3 cells were unable to close the gap and at the highest doses, the gaps sizes were roughly 500 μm for the PC3 cell line (Figure 3.17). A similar trend was found with DU145 cells, albeit to a lesser extent than the PC3 cells. In conclusion, aspirin was able to reduce migration of the PC3 and DU145 cell lines.

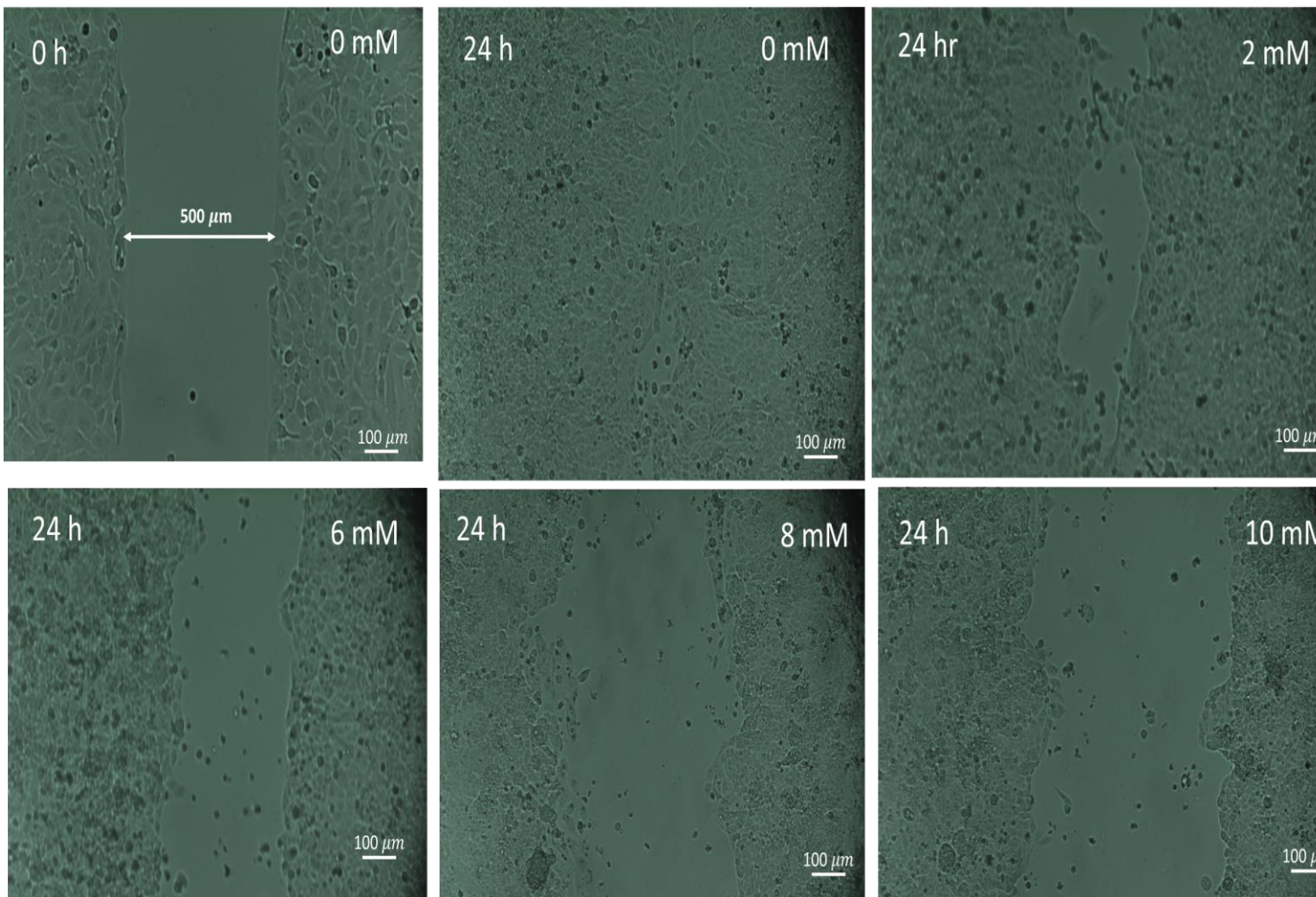


Figure 3.17. The NaS effects on migratory capacity of PC3 cells imaged at 0 (when the inserts were removed), and 24h following the removal of a full NaS dose-range before the insert was removed. The remaining distance between the cells was then measured with ZEN software (blue

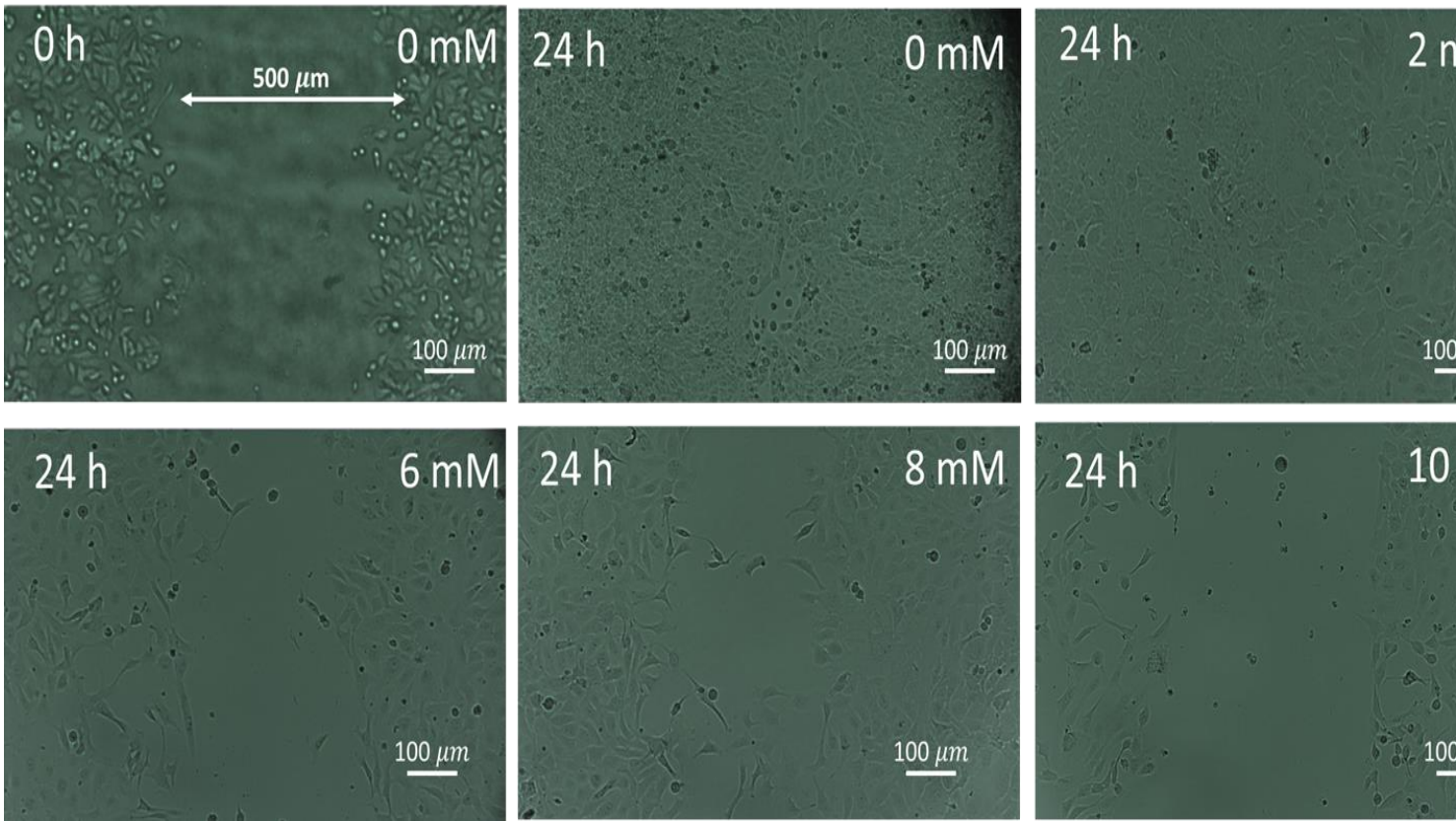


Figure 3.18. The NaS effects on migratory capacity of DU145 cells imaged at 0 (when the inserts were removed), and 24h following the removal of the full NaS dose-range before the insert was removed. The distance remaining between the cells was then measured with ZEN software (Zeiss).

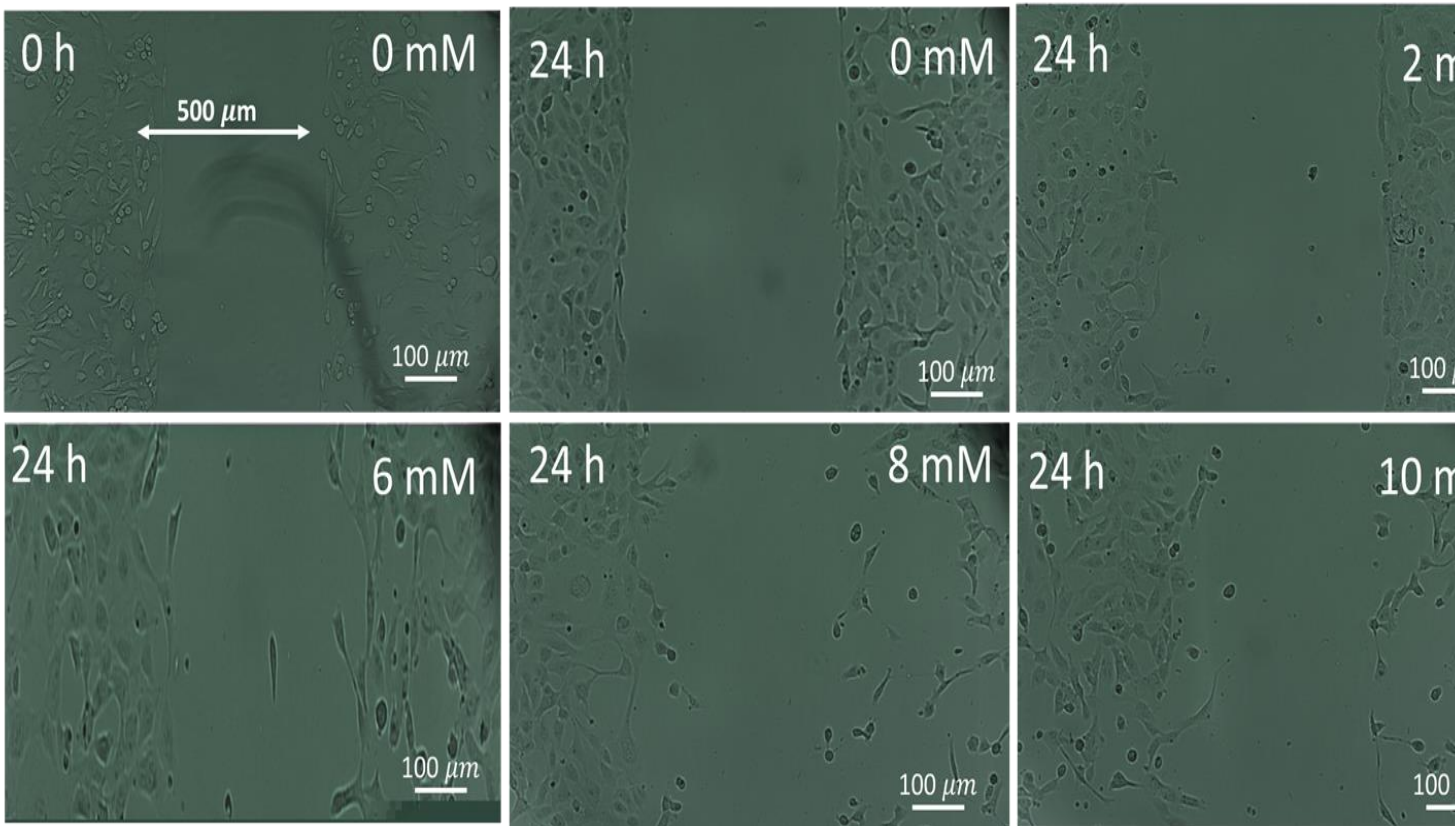


Figure 3.19. The NaS effects on migratory capacity of PNT2 cells imaged at 0 (when the inserts were removed), and 24h following the removal of the full NaS dose-range before the insert was removed. The distance remaining distance between the cells was then measured with ZEN software.

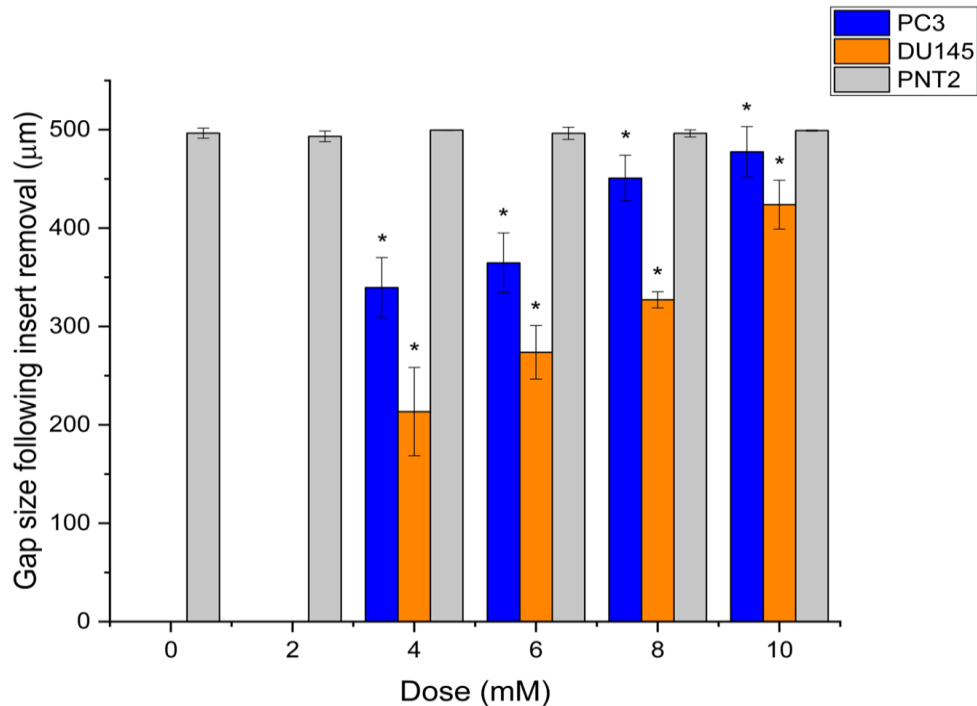


Figure 3.20. Changes in average size of the gap between two sections of cells in the migration assay in PC3, DU145 and PNT2 cells after NaS treatment. * represents significance at a level of $p < 0.05$ as determined by a one-way ANOVA and the *post hoc* Dunnett T3 ($n=3$). As PC3, and DU145 cells were able to close the gap when they were treated with 0 and 2 mM, there was no gap existed.

3.3.7.2 Invasion assay

The capacity for cancer cells to invade is another key feature of metastasis. Therefore, the QCM ECMatrix Cell Invasion Assay was used to measure the invasion ability when PCA and normal prostate cells were treated with NaS. As expected, the normal prostate cells, PNT2, were not capable of invasion, whilst the cancer cell lines readily invaded through a matrix. However, following NaS exposure, the invasive ability of PC3 and DU145 cells was significantly reduced in a concentration dependent manner (Figure 3.21). In the negative control group, PC3 and DU145 cells had a similar invasive capacity ($p=0.06$, 1.660 with SD 0.056 vs. 1.510 with SD 0.083 respectively). However, as the concentration of NaS increased to 10 mM, the invasive capacity of the PC3 cells were substantially lower than the DU145 cells, suggesting a greater sensitivity to the NaS treatment (Figure 3.21).

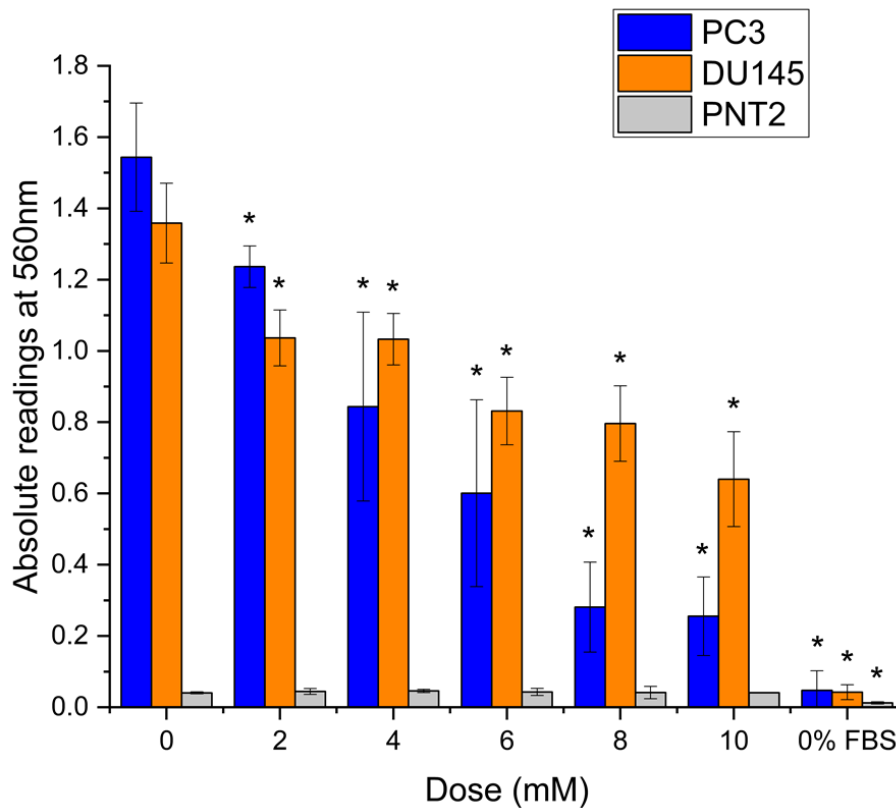


Figure 3.21. Invasive capacity of PC3, DU145 and PNT2 cells following NaS treatment. 0% FBS was included as a control as cells are unable to invade when there is no FBS in the lower chamber to draw them through except for the control PNT2 cells, which small number of cells passed through the membrane. *, indicate significance compared to the control where $p < 0.05$, as determined by a one-way ANOVA and the *post hoc* Dunnett T3 (n=3).

3.3.8 PC3 and DU145 gene expression profiles after NaS treatment

To profile gene expression changes in relation to signalling pathways involved in driving metastasis after NaS treatment, a PCR array evaluating 84 genes was performed. The results are illustrated in Figure 3.22 where the most prominently altered genes that lie outside of the 1.5-fold change in expression limits are highlighted. In PC3 cells three genes were substantially upregulated, including *IL-1 β* ; while the *CXCR2* and *NR4A3* genes were downregulated following NaS treatment. In DU145 cells, no genes were downregulated, but *CTSL1*, *ITGB3*,

and *RPLP0* genes were upregulated in the array following exposure to NaS (raw data located in Appendix 2).

When only the genes that had the highest level of up- / down-regulation were considered, in DU145 cells the top three genes that were substantially upregulated due to 4 mM NaS treatment were *CTSL1*, *ITGB3*, and *RPLP0*. Although *RPLP0* was the third most highly expressed gene, it was not selected for further analysis as it is a housekeeping gene and so is unlikely to have a mechanistic role in aspirin's effect on the cancer cells. As *RPLP0* was not classified as a gene of interest, the third most highly expressed gene considered was *CD44* with fold-change of 4.73. In PC3 cells, the top three most strikingly altered genes after 4 mM NaS exposure were *CXCR2* and *NR4A3* (reduced by -2.92 and -3.32-fold respectively), and *IL-1 β* , which was increased by a 5.33-fold-change in expression levels. The genes selected for further detailed qPCR analysis in both cell lines are summarised in Table 3.5

Table 3.5. Genes with the highest expression changes in PC3 and DU145 cells after NaS treatment.

Gene	Fold change	Cell line
<i>CTSL1</i>	6.54	DU145
<i>ITGB3</i>	5.24	DU145
<i>RPLP0</i>	4.84	DU145
<i>CD44</i>	4.73	DU145
<i>CXCR2</i>	-2.92	PC3
<i>NR4A3</i>	-3.32	PC3
<i>IL-1β</i>	5.33	PC3

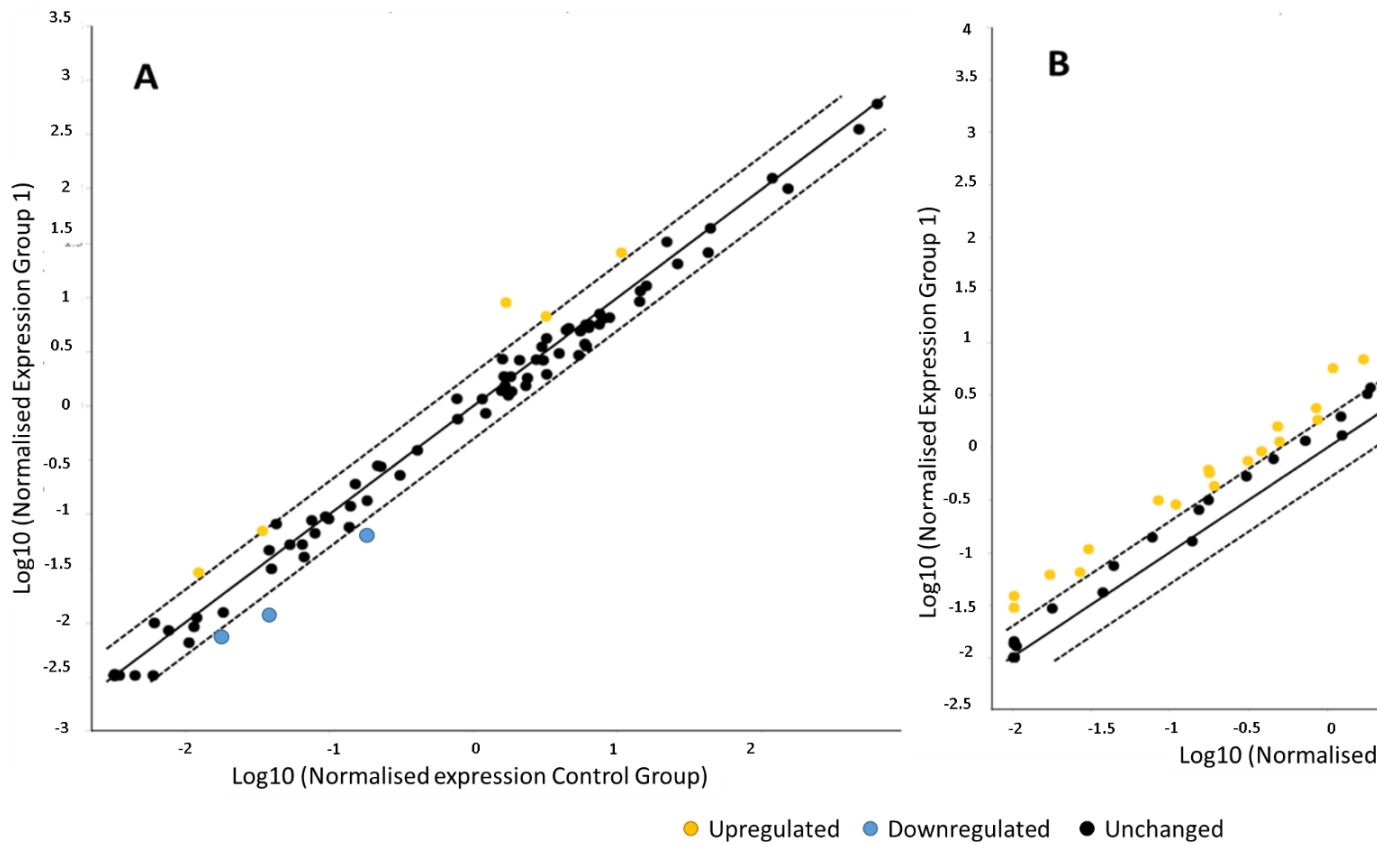


Figure 3.22. Gene expression profiles changes in PC3 and DU145 cells treated with 0 and 4 mM NaS, based on the analysis of 84 genes. The y-axis represents Log10(Normalised Expression Group 1) and the x-axis represents Log10(Normalised expression Control Group). The solid line represents unchanged gene expression levels, and the dashed lines represent a 1.5-fold change, which is the software designated threshold for prominent up- or down-regulation. Yellow dots indicate upregulated genes, blue dots indicate downregulated genes, and black dots represent genes whose expression did not fall outside the +/- 1.5-fold change in expression level in relation to the treatment.

For the DU145 and PC3 cell lines, the top three genes with the most highly altered expression levels were selected for more detailed analysis by RT-qPCR to confirm the PCR array results. In PC3 cells as illustrated in Figure 3.23, compared to the control, the *CXCR2* gene expression was reduced significantly by 3-fold ($p=0.027$) and *NR4A3* gene expression was 1-fold lower than the control ($p=0.156$), which complemented the array-based data. However, for the *IL-1 β* gene, there was a 7-fold significant reduction in expression in PC3 cells after 4 mM NaS treatment ($p=0.001$). *IL-1 β* was upregulated 5-fold after treatment in the PCR Array (Figure 3.23), which is completely different to the RT-qPCR results. The reason for this difference could be that the PCR array was only a single experiment, while the RT-qPCR experiment was conducted in triplicate (with one replicate, results are not as reliable as when an experiment in triplicate is conducted).

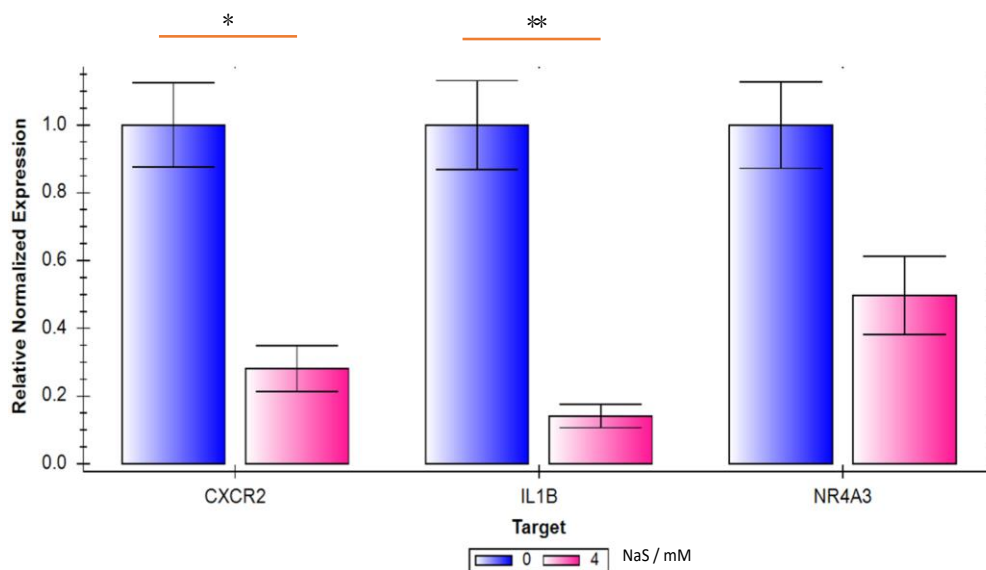


Figure 3.23. Further exploration of the gene expression profiles of *CXCR2*, *IL-1 β* and *NR4A3* in PC3 cells following NaS exposure. Blue bars are the control group, where the cells were untreated and the pink bars are the cells treated with 4 mM NaS. *, and ** indicate significance compared to the control where $p < 0.05$ and $p < 0.01$ respectively, as determined by a one-way ANOVA and the *post hoc* LSD ($n=3$).

In Figure 3.24, *CD44*, *CTSL1* and *ITGB3* gene expressions were measured with RT-qPCR in DU145 cells. There was 1.3-fold-change in *CTSL1* expression, 1.4-fold-change in *CD44* gene expression and 1.2-fold-change in *ITGB3* expression following NaS exposure. These transcriptional changes were however not statistically significant with the exception of the *CD44* gene expression change ($p=0.036$). Usually, a 1.5-fold-change in gene expression is considered biologically significant (Laaksonen *et al.*, 2006; Knudsen and Witkiewicz, 2016). However, since there was only 1.4-fold-change in *CD44* expression as compared to the control group, this was not a prominent gene expression alteration despite its statistical significance.

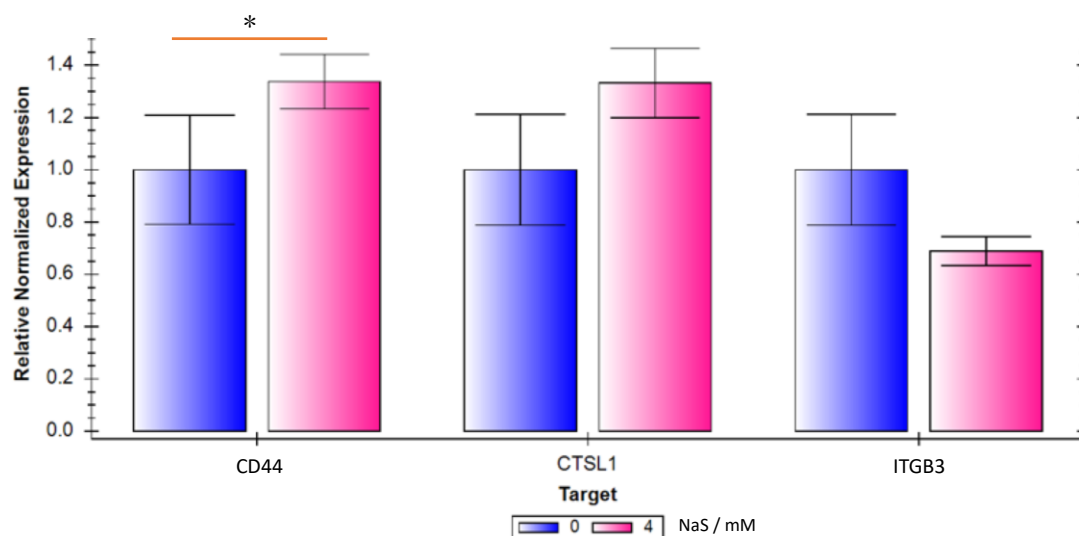


Figure 3.24. Further exploration for profiles of *CD44*, *CTSL1* and *ITGB3* profiles in DU145 cells following the PCR array in DU145 cells. Blue bars are the control group, where the cells were treated with 0 mM and the pink bars are the cells treated with 4 mM NaS. *, indicate significance compared to the control where $p < 0.05$ determined by a one-way ANOVA and the *post hoc* LSD (n=3).

3.4 Discussion

This chapter was aimed at understanding the effects of NaS on key characteristics associated with the aggressive behaviour of PCA cells. This involved analysing a variety of endpoints including cytotoxicity, *COX-2* gene expression changes, morphological assessments, intracellular Ca^{2+} levels, mitochondrial count, migration capacity and cell invasion ability. Finally, a PCR array was utilised to identify key genes that may be involved in governing the response of the cells to NaS treatment.

We firstly used the RPD method to study the effect of NaS on cytotoxicity induced in the PC3, DU145 and PNT2 cells. The results showed that low concentrations of NaS (2 and 4 mM) in PCA cells PC3 and DU145 and PNT2, can induce cytotoxicity. For the high doses of NaS (6, 8 and 10 mM) in the experiment, the trend of reduction in RPD values tended to be similar and plateaued at these high concentrations, indicating that PCA cells were not sensitive to high concentrations of NaS (over 6 mM). These results were consistent with the study of He *et al.* (2017), which found that 0.5 mM NaS treated PC3 resulted in a 13.4% viability loss. The authors believe that there are multiple pathways underlying the inhibitory effects of NaS on the growth of the PCA cells, but signal transduction and activation of the transcription 3 (STAT3)/NF- κ B pathways could be a potential mechanism (He *et al.*, 2017). STAT3 signalling is related to metastasis and proliferation of cancer cells (Sun *et al.*, 2012). NF- κ B activation regulates proliferation via multiple signalling pathways (De Simone *et al.*, 2015). The activation of NF- κ B, as well as STAT3, can be suppressed by aspirin, and consequently, proliferation is inhibited. It was notable that NaS was also toxic to PNT2. This does bear some concern as PNT2 are not a cancerous cell line and thus NaS (and potentially aspirin) could have a non-specific toxic effect on prostate cells. However, PNT2 is an immortalised cell line, so the cells may not respond in an identical manner to healthy human cells *in vivo*.

Following the RPD experiments, *COX-2* gene expression was quantified in each cell line. PC3 cells had the highest *COX-2* expression in the three cell lines and it was lowest in PNT2. Following NaS treatment, *COX-2* gene expression was reduced in both PC3 and DU145 cells from 2 mM, with a plateau at 8 mM. In contrast, *COX-2* expression in PNT2 cells remained unaffected by the NaS treatment.

Given the RPD results and the *COX-2* expression changes following the treatment, it is possible that there was a link between *COX-2* expression and drug sensitivity and there was the same saturation dose (6 mM) with PC3 and DU145; hence, *COX-2* could be an immediate factor in the NaS effects on the PCA cells. High expression of *COX-2* can inhibit apoptosis of cancer cells, increase the expression of anti-apoptotic protein B-cell lymphoma 2 (Bcl-2) and stimulate cell proliferation (Sobolewski *et al.*, 2010; Shi *et al.*, 2015). The role of NaS, aspirin's metabolite, and other NSAIDs in preventing tumours is attributed to *COX-2*, a key enzyme that inhibits the synthesis of prostaglandins. NaS not only alleviates the progress of inflammation, but also inhibits tumour growth and angiogenesis (Kyriakopoulos *et al.*, 2017; Dai *et al.*, 2017). *COX-2* is involved in various mechanisms for tumour progression, and it has been reported that NaS down-regulates the expression of *COX-2* and exerts anti-tumour effects by inhibiting the action of *COX-2* itself or inhibiting the synthesis of PGE2 (Poorani *et al.*, 2016). The specific mechanism may be: inhibition of tumour cell DNA synthesis and proliferation; promotion of immune surveillance, antibody production; inhibition of Bcl-2 expression and promotion of apoptosis; inhibition of tumour angiogenesis; inhibition of tumour cell invasion and metastasis (Escarcega *et al.*, 2007; Rice *et al.*, 2013). Overexpression of the *COX-2* gene can significantly increase the protein synthesis of prostacyclin (PGI₂) and PGE₂. PGE₂ has an important negative regulatory effect on immune function, especially on T lymphocyte subsets, NK cell activity, LAK cell activity, TNF and IL-2 activity. Thus, tumour cells are free from immune surveillance (Dikshit *et al.*, 2006). Many tumour cells have abnormal expression of *COX-2*,

which is related to the progression of cancer, tumour growth, autophagy and angiogenesis. High expression of *COX-2* can inhibit apoptosis, increase the expression of anti-apoptotic protein Bcl-2 and stimulate cell proliferation; *COX-2* overexpression can activate MMP, increase antigenic factors and promote tumour growth and invasion (Sokołowski *et al.*, 2012). From the evidence above, it is highly likely that *COX-2* plays a role in aspirin's/NaS ability to induce cytotoxicity, but the pathway of importance is unlikely to be limited to a *COX-2*-dependent pathway alone.

It is notable that PNT2 cells exhibited toxicity in response to NaS exposure, despite having very low expression levels of *COX-2*. Additionally, *COX-2* gene expression was not affected by the NaS exposure in PNT2 cells, whereas with PC3 and DU145 cells a significant reduction in *COX-2* expression was observed following NaS treatment. This data suggests that in PNT2 cells, NaS may be exerting its toxic effect via an independent-*COX-2* pathway. This difference may be due to the fact that PC3 and DU145 cells are cancerous cell lines, which exhibit high genetic instability, which is in direct contrast to PNT2 which is a normal prostate cell line. Further work is required in the future, to better understand the mechanism by which NaS results in toxicity to the normal PNT2 cells. This would involve evaluating alternative signalling pathways, such as pathways involving the Bcl-2 family proteins or Caspase family proteins (Sobolewski *et al.*, 2010; Norouzi *et al.*, 2016). Additionally, further work evaluating the apoptotic signalling pathways, for example, through the evaluation of Caspase-12 and Caspase-7 on the endoplasmic reticulum and the Bid and Bax proteins (that controlling the permeability of mitochondria), may provide insight into the mechanistic pathways of importance in PNT2 cells.

With the morphological analysis, it was found that the nuclear area was reduced when PC3 cells were exposed to NaS for 24 h. NaS was also able to significantly increase the DNA damage frequency (as measured by the MN assay) in PCA cells only leading to aneugenicity (chromosome loss). These two results were closely linked. NaS was able to increase the MN

frequency at the 6, 8- and 10-mM dose of NaS while nuclear area was reduced at these doses. Here, the chromosome loss could be one of the reasons for the reduced nuclear area in the cells. Additionally, reduced nuclear area is associated with apoptosis. For example, Helmy and Azim (2012) reported that Hep2 squamous cell carcinoma cells had a highly significant decrease in nuclear area when the cells were apoptotic (Helmy and Abdel Azim, 2012). It has been suggested that nuclear area can be seen as a measure of cell apoptosis and is also a sensitive measure to evaluate apoptotic effects of anti-cancer drugs (Helmy and Abdel Azim, 2012; DeCoster, 2007; Anilkumar *et al.*, 2017; Afifi *et al.*, 2012).

According to the scientific literature, apoptosis induced in cancer cells by NaS is mainly through a prolonged cell cycle (Chan *et al.*, 2007; Hossain *et al.*, 2012; Bilani *et al.*, 2017). It has been suggested that NaS induces cancer cell cycle arrest at the G_0/G_1 stage (Gao and Williams, 2012). Indeed, PC3 and DU145 cells were significantly impeded at the G_0/G_1 phase of the cell cycle at 6, 8, and 10 mM NaS, which is the early stage of DNA synthesis. With the same doses, RPD values for each cell line were reduced, too. Thus, it can be assumed that the prolonged stall at the G_0/G_1 phase would have had an impact on reducing the proliferative capacity of the cancer cells resulting in reduced population doubling. These findings are meaningful for cancer treatment as the administration of NaS to PCA patients would potentially result in reduced proliferation of the cancer cells and apoptosis associated with high levels of aneuploidy. It appears that aspirin therefore has both toxic and genotoxic effects on PCA cells.

Combining these findings, NaS mechanism of inhibiting growth is mainly manifested in inhibiting the process of mitosis in the PCA cell nucleus. In turn, it affects the cell cycle distribution. Eventually it achieves the biological effects of inducing apoptosis in PCA cells. The results showed that NaS treatment impede PC3 and DU145 cells in the G_0/G_1 phase, which is consistent with many other results. For example, mammary gland tumours cells were

inhibited in the G₀/G₁ phase when treated with NaS and Zong *et al.* (2016) reported that NaS caused cell cycle arrest of SGC-7901 cells (the gastric adenocarcinoma cell line) in the G₀/G₁ phase too (Zong *et al.*, 2016). However, the effects of aspirin on the cell cycle are variable between different cell types. For example, aspirin induced cell-cycle arrest in the G₂/M when the SW480 colon cancer cells were assessed (Gao and Williams, 2012).

A cytotoxicity assay, such as the RPD and MTT assay, can only identify whether the cultured cells are viable or not (Afifi *et al.*, 2012). However, with INCell analysis, a greater breadth of analysis is permitted, to provide further data indicating the mechanisms underlying the induction of apoptosis, by measuring increased intracellular Ca²⁺ level, a loss of mitochondria and even MN formation (DNA damage). In this study, this form of multiplex analysis proved highly beneficial. When NaS was applied to PNT2, PC3 and DU145 cells for 24 h, the intracellular Ca²⁺ was significantly increased, and the number of mitochondria per cell decreased significantly. When cells are undergoing apoptosis, the intracellular Ca²⁺ level increases, and mitochondria number will be reduced, thus both events are associated with cell death. This is consistent with the results of Clements *et al.* (2015). It has been demonstrated previously that when cell viability is decreased due to doxorubicin treatment, cytoplasmic Ca²⁺ concentration was elevated but mitochondrial measures, including count, area and mass were reduced (Clements *et al.*, 2015). Furthermore, Slaninová *et al.* (2012) used laser confocal microscopy to monitor the effects of melittin lasioglossin III (induces apoptosis) on Hep G2 hepatocellular carcinoma cells, and the results showed that when lasioglossin III continuously enters the cells, mitochondrial function is gradually destroyed as the intracellular Ca²⁺ level increased (Slaninová *et al.*, 2012).

The mechanism underlying these morphological changes could be that, on the one hand, NaS might destroy the tumour cell membrane and thus, the intracellular Ca²⁺ may be increased, resulting in disordered ion exchange and Ca²⁺ influx. On the other hand, due to a large amount

of calcium influx, mitochondria as an intracellular calcium pump, selectively absorbs excess cytoplasmic calcium in order to maintain intracellular calcium balance. With the increase of calcium in the mitochondria, the occurrence of calcium overload leads to the destruction of mitochondrial membrane structure. Thus, the number of mitochondria per cell reduces. The intracellular calcium overload and irreversible destruction of mitochondrial and cell membrane form a positive feedback type vicious cycle, and ultimately induce apoptosis (Celsi *et al.*, 2009; Nordin, 2013; Kalogeris *et al.*, 2012). Future analysis of Bcl-2, Apoptosis-inducing factor and Caspase-12 would add additional data to better understand the apoptotic signalling pathways underlying this response. Furthermore, the repetition of some of the experiments within Chapter 3 in the presence of Ca²⁺ channel blockers would yield data indicating the importance of this process in driving NaS toxic responses.

Tumour development is a complex process, where multi-stage, multi-factor, multi-gene interactions are involved in movement and migration, adhesion, angiogenesis, immune escape and many other aspects driving increased aggressive invasion (Geiger and Peeper, 2009; Suva *et al.*, 2011; Jiang *et al.*, 2015; Martin *et al.*, 2013). Research shows that abnormal movement of tumour cells itself is an important factor affecting tumour invasion and metastasis (Maishi and Hida, 2017). Therefore, the regulation and underlying mechanisms of tumour cell migration has become an important focus in the study of invasion and metastasis of PCA cells. In this chapter, a wound healing assay was used to determine if NaS exposure had an impact on tumour cells' migration ability. An insert separated cells into two sections and the gap between the two sections mimicked the distance that cancer cells migrate. Experimental results showed that NaS at the cellular level could substantially weaken the migration capacity of PC3 and DU145 cells. However, it was found that in the control group, the gap was not closed, hence the NaS had no effect other than causing toxicity in PNT2 cells.

In addition to migration, another key characteristic of aggressive cancer cells are their capacity to invade through tissue structures. It is known that malignant tumour cells exhibit activation of MMP-9 which then degrades the membrane structures of ECM and BM, facilitating tumour cell penetration of this barrier (Mehner *et al.*, 2014; Xu *et al.*, 2010). We used an *in vitro* invasion experiment to simulate this process. A membrane was coated in a chamber, mimicking the structure of the BM *in vivo* to conduct a comprehensive evaluation of NaS on tumour cell invasion capabilities. The experimental results showed that NaS dose-dependently inhibits tumour cell invasion. In the scientific literature aspirin has been found to inhibit cell migration and invasion in melanoma, colorectal cancer and PCA, which correlates with the results in this chapter (Tsai *et al.*, 2009; Liao *et al.*, 2015; Shi *et al.*, 2017). Aspirin and the selective COX-2 inhibitor NS-398 can lower the ability of HepG2 cells invasion, which is induced by Hepatocyte growth factor through ERK1/2 pathway (Abiru *et al.*, 2002; Lu *et al.*, 2013). Another study found that COX-2 inhibitors might play an anti-liver cancer effect through a non-COX pathway, namely PPAR α and PPAR γ (Jaradat *et al.*, 2001). *In vivo* and *in vitro* studies show that selective COX-2 inhibitors (such as JTE-522) can affect many aspects of the cell cycle of liver cancer cells (Nagahara *et al.*, 2007). JTE-522 induces liver cancer cell cycle arrest in the G₁/G₀ phase, to achieve the purpose of inhibiting the proliferation (Nagahara *et al.*, 2007).

Aspirin is a traditional, and one of the most commonly used, NSAIDs. In recent years, epidemiology and clinical studies have demonstrated that aspirin can induce tumour cell apoptosis, inhibit tumour invasion and metastasis and exert anti-tumour effect (Shi *et al.*, 2017; Liao *et al.*, 2015). The exact anti-cancer mechanism is not yet clear. The traditional view is that aspirin plays an anti-cancer effect mainly through the inhibition of the COX genes. However, in recent years, non-COX-dependent mechanisms have drawn much attention. The cell model used in the migration and invasion assays in this chapter was PC3 and its expression level of COX-2 is higher than normal prostate cells. Therefore, in PC3 cells, aspirin is most likely

to exert anti-invasion and migration characteristics through the *COX-2* pathway. Interestingly the *COX-2* expression level in DU145 was not as high as in PC3 cells, which correlates with the fact that generally, DU145 was not as sensitive to NaS as PC3 cells in all the experiments conducted. However, to truly evaluate the mechanistic importance of *COX-2*, we would need to repeat the experiments conducted in this chapter in PC3 cells that no longer exhibited *COX-2* expression. Thus, an important avenue of future work would involve utilising siRNA or CRISPR/Cas-9 technology to firstly knock out *COX-2* expression and then repeat the NaS exposure experiments in this chapter. Alternatively, *COX-2* inhibitors, such as celecoxib could be used. Thus, if *COX-2* was indeed responsible then the same level of cytotoxicity and reduced migration / invasion would not be seen.

It is possible that aspirin may also act through an alternative, non-*COX-2* pathway. The protein of MMP-2 is one of the potential molecular mechanisms. NSAIDs can directly inhibit the expression of MMP-2 by interfering with the extracellular signal-regulated kinase (ERK)/ Spl signalling pathway and can hinder the conversion of precursor MMP-2 to active MMP-2 by inducing the expression of the RECK gene (Liu *et al.*, 2012). Studies have also reported that aspirin inhibits the *in vitro* primary culture of prostate and colon cancer cells by down-regulating the activity of MMP-2 and MMP-9 (Wynne and Djakiew, 2010; Bilani *et al.*, 2017). In addition, invasion capacity was reduced by 44% in B16FO colon cells which has a strong metastatic activity, by inhibiting MMP-2 activity in a C57BL / 6J animal model (Tsai *et al.*, 2009). Therefore, aspirin may inhibit the migration and invasion of PCA cells by down-regulating MMP-2 and/or MMP-9 activity and *COX-2*. Future work is required to explore this hypothesis further and demonstrate whether or not aspirin affects MMP-2 expression and / or MMP-9 activity in the culture media. This can be done with assays measuring specific MMP proteins utilising the Amersham Biotrak™ assays.

As DU145 and PC3 cells could potentially respond to NaS treatment differently, a RT-qPCR array was applied to screen the expression profile of genes that may be altered in response to NaS exposure in order to identify mechanistic pathways of importance. The genes highlighted

by the array were then evaluated in further detail (with multiple replicates) by RT-qPCR. *IL-1 β* and *CXCR2* were the genes found to have significant transcriptional profile changes in PC3 cells. Their expression was reduced by 6-fold and 3-fold respectively following the 24-h NaS exposure.

IL-1 β can cause inflammation, and also induce *COX-2*, inducible nitric oxide synthase (iNOS), IL-6 and expression of other inflammatory factors, which further activate stromal cells and immune cells to produce more *IL-1 β* involved in inflammatory reactions (Ren and Torres, 2009; Park *et al.*, 2017). *IL-1 β* can cause DNA methylation changes and plays an important role in the development of many tumours; it promotes angiogenesis and the expression of *VEGF*, *IL-8*, *COX-2*, for example (Schweighofer *et al.*, 2009; Voronov *et al.*, 2014). Angiogenesis is a key step in tumour growth, invasion and metastasis. This process involves the remodelling of extracellular matrix, the proliferation and translocation of endothelial cells, and the formation of capillary lumens (Schweighofer *et al.*, 2009; Voronov *et al.*, 2014). Poeck *et al.* (2010) suggested that the activation of NF- κ B could in turn lead to the expression of pro-*IL-1 β* , which forms a biologically active IL-1 β protein after caspase-1 splicing (Poeck *et al.*, 2011). Given the data in Chapter 3, NaS treatment was found to reduce the ability of migration and invasion in PC3 cells, it is possible that this was a consequence of down-regulated *IL-1 β* . This is of particular importance *in vivo* as when the expression of *IL-1 β* is reduced, *VEGF* gene expression is subsequently reduced. As a result, angiogenesis, which is a key step in metastasis, is suppressed, which in turn inhibits migration and invasion (Voronov *et al.*, 2014).

IL-1 β is also of interest with respect to inflammation. A firm link exists between chronic inflammation and carcinogenesis; thus, the relationship between inflammation and cancer has become a hot topic of research (Balkwill and Mantovani, 2001; Rakoff-Nahoum, 2006; Tan *et al.*, 2018). Chronic inflammation plays a role in the initiation, proliferation, and progression of tumour development. The focus of current research has shifted from the study

of the properties of infiltrating immune cells to the main role of cytokines and their soluble mediators in tumour initiation (Shrihari, 2017; Bremnes *et al.*, 2011). *IL-1 β* , as a core factor in inflammatory mediator, is an important factor affecting the occurrence and development of PCA, but the mechanism is still not fully understood. Therefore, an in-depth study of *IL-1 β* can provide new ideas for revealing the pathogenesis of PCA, coupled to the role that aspirin may play in disturbing its function.

CXC receptor 2 (*CXCR2*) belongs to the G protein-coupled receptor family, and its ligands are CXCL1 (CXC motif chemokine ligand 1), CXCL2, CXCL3, CXCL5, CXCL6, CXCL7, CXCL8 (Steele *et al.*, 2016). So far, the *CXCR2* family promotes the development of colon cancer, squamous cell carcinoma (Jamieson *et al.*, 2012). *CXCR2* has the ability to concentrate other chemokines. It can participate in functions such as capillary formation and inflammatory infiltration (Ratajczak and Kim, 2012). *CXCR2* plays an important role in the process of tumour angiogenesis. The high expression of *CXCR2* can accelerate the capillary formation in tumour tissues. *CXCR2* regulates the metastasis of myeloid derived suppressor cells (MDSC) in pancreatic ductal adenocarcinoma and promotes breast cancer cell metastasis and invasion, and EMT (Sharma *et al.*, 2016; Yu *et al.*, 2017; Hsu *et al.*, 2013; Steele *et al.*, 2016). It plays an important role in the construction of the tumour microenvironment. At the same time, it has proangiogenic effects in breast tumours and pancreatic cancer (Lau *et al.*, 2015).

The *CXCR2* ligand, CXCL5, affects the prognosis and tumour development and metastasis of cancer patients by interacting with *CXCR2*. Begley *et al.* (2008) found that CXCL5 activates both MAPK and PI3K signalling pathways in prostate epithelial cells, thereby promoting epithelial cell proliferation and invasion; CXCL5 also promotes transcription of *EGR1* gene. *EGR1* encodes a C2H2-type zinc finger protein that promotes tumour growth and angiogenesis, revealing that the *CXCL5/CXCR2* axis may play an important role in PCA. *CXCR2* in PCA has not been fully studied yet. However, Kawamura *et al.* (Kawamura *et al.*, 2012)

measured CXCL5 in serum samples from 250 colorectal cancer patients compared with 30 normal controls and found that the concentration of serum CXCL5 in patients with colorectal cancer was significantly higher than that in normal subjects. At the same time, combined with its clinical pathological results and survival survey, it was found that the high serum concentration of CXCL5 was correlated with gender and liver metastasis. CXCL5 is likely to be a new marker for colorectal cancer, and its signal axis with *CXCR2* may be involved in the development and progression of colorectal cancer. Xu *et al.* (2013a) found that overexpression of *CXCR2* promoted proliferation, metastasis, invasion, anti-apoptosis, and tumour formation of breast cancer cells, and assists tumour metastasis by increasing *COX-2* expression and reducing AKT expression.

At present, how to effectively inhibit tumour angiogenesis is one focus of current targeted therapy, and the process of selectively inhibiting angiogenesis can effectively improve the prognosis of patients. Chao *et al.* (2016) inhibited the accumulation of neutrophils in pancreatic ductal adenocarcinoma by ablating *CXCR2* and found that it can reduce tumour growth dependent on T cells and inhibit the proliferation, invasion and metastasis of pancreatic tumours. Antagonists targeting tumour cells with *CXCR2* receptor can provide new therapeutic targets for inhibiting the progression of pancreatic cancer. Sharma *et al.* (2016) observed that the expression of *CXCR2* in drug-resistant murine mammary adenocarcinoma cell line Cl66 cells was down-regulated, but the expression of its ligand was increased. Further studies showed that the expression of stemness markers and interstitial cell markers in relation to drug-resistance increased. This suggests a certain correlation between the two, and targeted therapy of *CXCR2* signalling pathway may play a role in the treatment of drug-resistant cancer (Sharma *et al.*, 2016). Further work is required to more comprehensively understand the *CXCR2* genes' role following aspirin or NaS treatment. It would therefore be interesting to use siRNA or CRISPR technology to knock down this gene in PCA cancer cells

and then repeat the migration assay, invasion assay and toxicity measurements following NaS treatment to determine if an enhanced anti-cancer effect is noted.

In summary, in this chapter we explored NaS effects on the PCA cells, PC3 and DU145. It was found that RPD (associated with both cytotoxicity and cytostasis) was induced following treatment with NaS, with PC3 cells demonstrating greater sensitivity to the NaS than DU145 cells. Cell cycle analysis confirmed that PC3 and DU145 cells were arrested in G₀/G₁ stage of the cell cycle, which correlated with the RPD results, leading to a delayed proliferation of cells. With the morphological assessment, nuclear area was reduced due to NaS treatment, which could have been due to the increased DNA damage (chromosome loss) that was observed. When baseline *COX-2* analysis was performed, PC3's expression was highest amongst three cell lines followed by DU145. Interestingly, *COX-2* expression was decreased when PC3 and DU145 were exposed to NaS. With the wound healing and migration assays, both the migratory and invasion capability of PC3 cells and DU145 cells were reduced following NaS exposure, with PC3 cells demonstrating the most substantial response to the drug. Although the *COX-2* pathway is likely to be involved in mediating the effects of NaS on cancer cell growth, cell cycle progression, migration and invasion, the gene expression analysis conducted demonstrated that there were likely to be other pathways implicated including those that involve *IL-1β*. In conclusion, NaS clearly imparts strong anti-cancer effects that are likely to be beneficial clinically for PCA patients.

Chapter 4 Exploration of Sodium Salicylate's Mode of Action

4.1 Introduction

Cancer development involves the dysregulation of many signalling pathways and their component genes; one example of which is the *COX-2* signalling pathway (as described in detail in Chapter 1, Section 1.4). *COX-2* is involved in the occurrence and development of tumours through a variety of mechanisms. PGE₂, an enzymatic product of *COX-2*, stimulates cell proliferation, inhibits apoptosis, and activates the cAMP pathway to induce tumour angiogenesis (Sreeramkumar *et al.*, 2011; Zhang and Daaka, 2011). Thus, tumour invasion and metastasis are promoted through the *COX-2/PGE2* signalling pathway. In prostate cells, high expression of *COX-2* has been reported, where it is thought to promote the formation of a precancerous microenvironment at the site of chronic inflammation (Stark *et al.*, 2015; Aoki and Narumiya, 2017). A precancerous microenvironment has biological properties similar to that of the tumour microenvironment and can under conditions of chronic inflammation, result in tumour development (Kuwano *et al.*, 2004; Machida and Takemasa, 2010; Dörsam, 2017). In the past, the anti-cancer activity of *COX-2* inhibitors was believed to be dependent on the blockade of the *COX-2* pathway and the anti-cancer effect was achieved by reducing the production of *COX-2* products. With the progress of research, many *COX-2* independent pathways in which *COX-2* inhibitors could play roles have been discovered. Targets of these include calcium ATPase, protein kinase and its upstream phosphoinositide-dependent kinase 1 (PDK1), various cyclin-dependent kinases (CDKs) of the CDK/cyclin complex, carbonic anhydrase (CA), and ornithine dehydrogenase. Through these many pathways, *COX-2* inhibitors also have the effect of inhibiting cell cycle progression, inducing apoptosis, and inhibiting angiogenesis and migration (Zhang *et al.*, 2009). Therefore, *COX-2* inhibitors have

great potential for cancer treatment. Aspirin, as a well described *COX-2* inhibitor, can inhibit the growth of PCA cell lines as demonstrated through the impact of NaS exposure earlier in this thesis (Chapter 3), but the mechanism of action underlying this response remains unclear.

4.1.1 *COX-2* inhibitors

COX-2 inhibitors are NSAIDs. They can be divided into non-selective, selective and highly selective *COX-2* inhibitors. The mechanism of all highly selective *COX-2* inhibitors are similar, but their chemical structure, pharmacokinetic and pharmacodynamics are different (Patrignani and Patrono, 2015; McCormack, 2011). As non-selective *COX-2* inhibitors can cause inhibition of *COX-1*, leading to severe gastrointestinal reactions such as kidney damage, platelet dysfunction and other adverse reactions, selective *COX-2* inhibitors have a better clinical prospects (Patrignani and Patrono, 2015).

4.1.1.1 Celecoxib and cancer

The NSAID celecoxib is a highly selective *COX-2* inhibitor, which is approved by the FDA for the treatment of osteoarthritis (OA), rheumatoid arthritis (RA) and ankylosing spondylitis (McCormack, 2011). Studies have demonstrated that celecoxib can be effective against epithelial tissue cancers including gastric, colorectal, prostate, lung, pancreatic, breast, and head and neck cancers, and squamous cell carcinoma of the skin (Ghosh *et al.*, 2010; Hashemipour *et al.*, 2016; Chiang *et al.*, 2017). This drug is also particularly promising as its long-term use does not induce gastrointestinal bleeding through peptic ulcers or kidney damage, which is associated with traditional non-steroidal drugs that also inhibit *COX-1*. However, White *et al.* (2002) have found side effects in their CLASS study (the Celecoxib Long-term Arthritis Safety Study) where, when compared with traditional NSAIDs, the incidence of myocardial infarction was 0.2% in the group with celecoxib treatment, while the control group

was 0.11% ($p>0.05$). The incidence of atrial fibrillation was also higher than that of the control group. Some experts believe that selectivity is one of the risk factors leading to cardiovascular adverse events, but this is unlikely to be the only reason. In fact, all cardiovascular events occurred when the administration dose of celecoxib was higher than the approved dose (Nissen *et al.*, 2016). It was then suggested that 200 mg was the daily upper-limit for most patients, which may provide a potential safety and therapeutic benefit for patients (Nissen *et al.*, 2016). Thus, although celecoxib as a clinical application for malignancies is desirable, the safety issues caused cannot be ignored and need to be overcome, including strict control of the dosage and administration time.

Celecoxib inhibits RNA and protein expression of VEGF in pancreatic cancer cells, where it has been found to inhibit pancreatic cancer growth and proliferation in a dose-dependent manner (Wei *et al.*, 2004; Kumar *et al.*, 2013; Sahin *et al.*, 2014). Additionally, when Xie *et al.* (2009) treated hepatoma cells after they were transfected with hepatitis B virus X gene (*HBx* gene), they found that compared with the control group, celecoxib induced apoptosis of hepatoma cells with over-expression of *HBx*. In gastric cancer studies, the *COX-2* levels in gastric cancer patients who had been taking celecoxib for a certain period of time were significantly decreased and the level of tumour cell apoptosis was elevated, compared to the control group (Zhou *et al.*, 2007). Recently, 80 patients who had been undergoing laparoscopic radical gastrectomy were divided into 2 groups. One group received celecoxib and standard FOLFOX4 chemotherapy, and the other group received standard FOLFOX4 chemotherapy alone. After 6 courses of the treatment, the serum levels of *COX-2* and VEGF in the combined treatment group were significantly lower than those in the standard chemotherapeutic group (Han *et al.*, 2014). This suggests that celecoxib may reduce tumour angiogenesis, so celecoxib in advanced gastric cancer may be an important adjuvant in standard chemotherapy (Han *et al.*, 2014).

Despite its potential benefits, use of *COX-2* inhibitors clinically for cancer treatment is still not

possible due to several unanswered questions, such as, do combination of drugs and therapies with COX-2 inhibitors exhibit synergistic effects; which indicators can be used to determine efficacy of COX-2 inhibitors; what is the efficacy and safety of such treatments in varying cancer types? To answer these questions, further basic research to increase our understanding of the mechanistic anti-tumour effects of the COX-2 signalling pathway and its associated inhibitors is therefore required.

4.1.2 COX-2-independent pathways and aspirin

Aspirin has a preventive effect on prostate tumours and inhibits tumour proliferation in humans (Ishikawa *et al.*, 2014; Wodarz *et al.*, 2017; Haile *et al.*, 2005). At present, many studies suggest that aspirin also exerts its anti-tumour effects by inhibiting the NF- κ B signalling pathway (Kopp and Ghosh, 1994; Mitrugno *et al.*, 2016; Cheng *et al.*, 2017; Huo *et al.*, 2017). NF- κ B is a nuclear transcription factor widely expressed in many cell types (as described in detail in Chapter 1, Section 1.5). It is involved in gene regulation of various physiological and pathological processes such as inflammation, cell proliferation, cell cycle regulation and apoptosis. When stimulated by various activating factors such as TNF, NF- κ B is activated by dissociation of inhibitory I κ B molecules, resulting in the most common dimer p50-p65 entering the nucleus, which subsequently drives gene expression of target genes (Kutuk and Basaga, 2004; Cell Signalling, 2015). Given the potential importance of the NF- κ B pathway in underpinning aspirin's anti-cancer effects, further investigation on the impact of NaS exposure in relation to nuclear NF- κ B p65 and I κ B α , is necessary to better understand the underlying anti-tumour mechanism(s) of aspirin in prostate cancer cells.

4.1.3 Aims

The data in Chapter 3 indicated that the mechanisms underlying NaS anti-cancer effects on PCA cells may be related to *COX-2* expression. This chapter aimed to investigate the potential mode of action (MoA) of aspirin following exposure of prostate cell lines to the metabolite NaS. The study objectives were:

- To explore NaS effects on the NF- κ B pathway with western blots measuring protein levels of nuclear p65 and cytoplasmic I κ B α in PC3 and PNT2 cells.
- To demonstrate whether NaS affects growth, morphology and the cell cycle of PC3 and PNT2 cells via the mediator, *COX-2*. PNT2 cells and PC3 cells were pre-treated with the *COX-2* inhibitor celecoxib to reduce *COX-2* gene expression and then exposed to NaS prior to endpoint analysis. It was hypothesised that once the *COX-2* expression was blocked, if NaS toxic effects on PCA cells were substantially reduced then NaS effects on PCA cells were *COX-2*-dependent.

4.2 Materials and methods

4.2.1 Materials

Materials used in this chapter are listed in the table below (Table 4.1).

Table 4.1. Materials used in Chapter 4.

Name	Reference number	Manufacturer
Celecoxib	PZ0008-5MG	Sigma-aldrich, UK
Corning® 96 Well Black Polystyrene Microplate	CLS3603-48EA	Purchase from Sigma-aldrich, UK
Fluo-8 Calcium Flux Assay Kit - No Wash	ab112129	Abcam
Hank's Balanced Salt Solution	45001-152	Corning
1 M HEPES buffer solution	83264-100ML-F	Sigma-aldrich, UK
Mitochondrial Staining Kit - Orange (Ex405nm) – Cytosinker	ab138897	Abcam

4.2.2 Cell culture

PNT2 and PC3 cells were cultured following the methods described in Section 2.4.

4.2.3 Pre-treatment to eliminate *COX-2* expression

Celecoxib was used as the selective *COX-2* inhibitor. When the confluence of PC3 and PNT2 cells reached 60–70% in the flasks, the cells were treated with 6 μ M celecoxib for 72 h to remove *COX-2* expression as suggested by Wang *et al.* (2012).

4.2.4 COX-2 RNA levels profile following celecoxib treatment

For the *COX-2* profiling, the following experiments were designed (Figure 4.1). A total of 3x T75 flasks of PC3 and 3x T75 flasks of PNT2 cells were prepared. When PC3 and PNT2 cells reached 85% confluence in one T75 flask, total RNA was collected. The remaining cells from the other 2 flasks for each cell line were reseeded into T25 flasks at a density of 1×10^5 cell / mL. Hence, there were 5x T25 flasks for each cell line, each of which was exposed to 6 μ M celecoxib. The total RNA of each cell line was extracted after 24, 48 and 72 h of celecoxib treatment. The remaining two flasks were washed with 5 mL PBS three times to remove celecoxib at 72 h. RNA from the PC3 and PNT2 cells was then extracted 24 h and 48 h after washing. Total RNA was extracted as per the instruction of the manufacturer and quantified with the Nanodrop according to the details in Section 2.6. cDNA synthesis and RT-qPCR were conducted according to the methods in Section 2.7 and 2.8 respectively.

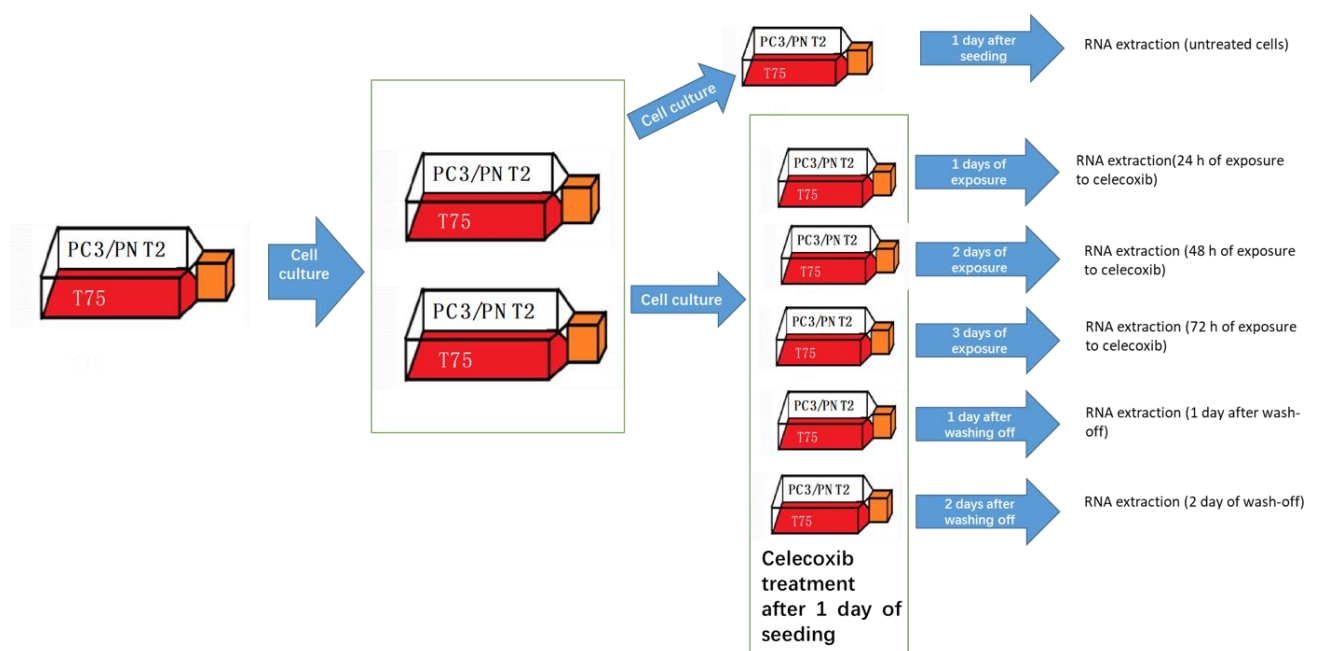


Figure 4.1. Flow chart of *COX-2* gene expression profiling after celecoxib treatment.

The primers used were *COX-2* and two housekeeping genes, *RPL-19* and *β-actin* primers. The sequence of *RPL-19* primers, which had been optimised for the SYBR green RT-qPCR system by the manufacturer, Sigma - Aldrich, can be found in the table below (Table 4.2). The PCR primers, *COX-2* and *β-actin* that were used were both optimised for gene expression analysis in prostate cells during previous research projects in our laboratory by Dr Patrick Olaniyi. It should be noted that *B₂M* was not used as the housekeeping gene in this chapter because it was not stable following treatment of celecoxib; thus *RPL-19* was selected as an alternative housekeeper which remained unaffected by the celecoxib treatment.

Table 4.2. Primer sequences used for gene expression analysis by RT-qPCR.

Primers	Sequence (5'→3')	Manufacturer	Use
<i>COX-2</i>	Forward: ACCCACTGAAAAAGATGA	Sigma - Aldrich	Gene of interest
	Reverse: ATCTTCAAACCTCCATGATG		
<i>RPL-19</i>	Forward: CAGAAGATACCGTGAATCTAAG	Sigma - Aldrich	Housekeeping gene
	Reverse: TGTTTTTGAACACATTCCCC		
<i>β-actin</i>	Forward: GATGGCCACGGCTGCTTC	Sigma - Aldrich	Housekeeping gene
	Reverse: TGCCTCAGGGCAGCGGAA		

The running programme was set as follows: The initial denaturation was incubation at 95 °C for 3 min and followed by 40 cycles of 95 °C for 30 s and 60 °C for 30 s (for annealing and extension). After 40 cycles, the melt curve was detected by ramping from 65 to 95 °C with a 0.5 °C increment per second. A melt curve with only one peak per primer set was considered acceptable.

4.2.5 Cytotoxicity assay (RPD)

After pre-treatment with celecoxib as described in Section 4.2.3, PNT2 and PC3 cells were washed three times with 5 mL PBS. After 72 h of exposure to celecoxib, PC3 and PNT2 cells were washed and these celecoxib-treated cells were then counted with a 1 x 1 mm haemocytometer and again seeded at 1×10^5 cells / cm³ (Concentration A). After 24 h of culture, the celecoxib-treated cells were exposed to 0, 2, 4, 6, 8 and 10 mM NaS for 24 h followed by a 24-h recovery period respectively and their concentration was counted with a 1 x 1 mm haemocytometer (Concentration B). A cytotoxicity assay (RPD), comparing Concentration A and B, was carried out with the washed cells in triplicate as described in Section 2.5.

4.2.6 INCell analysis for intracellular Ca²⁺ and mitochondrial mass

PC3 cells were cultured in Corning® 96 well black polystyrene microplates and seeded overnight at a density of 0.5×10^5 cells / cm³. Then, they were pre-treated with celecoxib as stated in Section 4.2.3. When the treatment was finished, PBS was used to wash off the celecoxib. The PC3 cells were subsequently treated with 0, 2, 4, 6, 8 and 10 mM NaS for 24 h followed by a 24-h recovery period.

For intracellular Ca²⁺ and mitochondrial health assessments, there were two separate plates prepared. On one plate, in order to assess the Ca²⁺ level in the cells; Fluo-8 Calcium Flux Assay Kit - No Wash (ab112129) from Abcam was utilised. A treatment of 20 µM ionomycin for 20 min was the positive control. For the preparation of the Ca²⁺ level kit, all the kit components were thawed at room temperature before use. A total of 20 µL of DMSO was added into Fluo-8 (Component A, contained in the kit) and mixed well to form Solution B.2. HHBS (Component C, contained in the kit) was then added into 1 mL of 10X Pluronic® F127 Plus (Component B,

contained in the kit), and mixed well to prepare Solution B.3. A total of 20 μL of Fluo-8 stock solution (Solution B.2) was added into 10 mL of 1X assay buffer (Solution B.3) and mixed well. This working solution (Solution B.4) was stable for at least 2 h at room temperature. A total of 100 μL /well (96-well plate) Fluo-8 dye-loading solution (Solution B.4) was added into the cell plate. The dye-loading plate was then placed in a 5% CO_2 37 $^\circ\text{C}$ cell incubator for 30 minutes. Next, Hoechst 33342 stain was used as a nuclear label at a concentration of 10 $\mu\text{g}/\text{mL}$. The plate was incubated at room temperature for another 30 minutes. Finally, the images were acquired with DAPI (nuclear) and FITC (intracellular Ca^{2+}) filters on an INCell Analyser 2000 (GE Healthcare, UK).

To prepare Hanks and 20 mM HEPES buffer (HHBS), 2.04 mL HEPES buffer was added into 100 mL Hank's Balanced Salt Solution. After the NaS treatment, the Mitochondrial Staining Kit - Orange (Ex405nm) - Cytopainter (ab138897) was used to measure the mitochondrial health in the treated cells. A total of 10 μM FCCP for 20 min was the positive control. Hoechst 33342 stain was also used as a nuclear label at a concentration of 10 $\mu\text{g}/\text{mL}$. All the components were brought to room temperature. The dye working solution was prepared by diluting 20 μL of MitoViolet Indicator (Component A contained in the kit) into 10 mL of Live Cell Staining Buffer (Component B contained in the kit), which was Solution A.2. When cells reached the desired confluence, 100 μL Solution A.2 and 50 μL of 10 $\mu\text{g}/\text{mL}$ Hoechst 33342 stain were added to the plate. The cells were incubated in a 37 $^\circ\text{C}$, 5% CO_2 incubator for 1 h. The dye-loading solution was replaced with 150 μL HHBS. The filter used for image acquisition was dsRed.

For image capture, the INCell Analyser 2000 was set to maintain cell growth conditions (37 $^\circ\text{C}$ and 5% CO_2) and the measurements were completed within 1 h. Negative control cells were used to adjust exposure time and focus. For Reagent dsRed, 30-50% saturation was seen, and

FITC's exposure time was adjusted to 5-15% saturation. A 40x objective capturing 16 fields of view was used per sample analysed.

4.2.7 Cell cycle analysis

Images for the cell cycle analysis of celecoxib-treated PC3 cells was conducted according to Section 2.9 and the cell cycle analysis followed the protocol in Section 3.2.9.

4.2.8 NaS effects on NF- κ B pathway and downstream targets

To study NaS effects on the NF- κ B pathway and downstream targets, a model was designed. Firstly, for profiling the nuclear p65 protein, PNT2 were treated with TNF- α at 25 ng / mL or 50 ng / mL for 0.5, 2, 6 and 24 h and PC3 cells were treated with TNF- α for 0.5, 2, 4, and 6 h when nuclear p65 was studied. Then, for profile of cytoplasmic I κ B α , PNT2 were treated with TNF- α at 25 ng / mL or 50 ng / mL for 0, 5, 10, 15, 20 and 30 min respectively and PC3 cells were exposed to TNF- α for 0.5, 2, 4 and 6 h. Following the upregulation of nuclear p65 protein profile and the degradation profiles of cytoplasmic I κ B protein to examine the mechanism for the inhibitory effect of NaS on TNF α - induced NF- κ B activation in PNT2 cells. To study NaS effects on the NF- κ B pathway, PNT2 cells and PC3 cells were pre-treated with various concentrations of (0, 2, 4, 6, 8 and 10 mM) NaS for 0.5 or 2 h. Only PNT2 cells were subsequently treated with TNF- α (25 ng /mL) for 30 min to extract nuclear proteins as PC3 cells have constitutively activated NF- κ B. Finally, western blots were used to determine the profiles of nuclear p65 and cytoplasmic I κ B α protein over a specified time period and with co-exposure of NaS and TNF- α . Extraction and quantification of proteins followed the protocol in Section 2.12 and 2.13 The western blotting was performed following the protocol in Section 2.14 in triplicate, with each blot cut according to their size as stated in Section 2.14 prior to hybridisation with the necessary antibodies. All the blot images generated in this study have

been included in Appendix 4. Histone H3 and α -tubulin are the loading control to p65 and I κ B α respectively.

4.2.8.1 Antibodies

All antibodies used for western blotting were purchased from Cell Signalling and Abcam as detailed in Table 4.3.

Table 4.3. Antibodies and ladders used for western blotting.

Usage	Antibody	Origin	Manufacturer	Reference number	Working concentration	Predicted weight
Control	Histone H3	Rabbit	Abcam	ab1791	1:2000	17 kDa
Purity check	α -tubulin	Rabbit	Abcam	ab4074	1:3000	55 kDa
Primary antibody	NF- κ B p65 (D14E12) XP [®] Rabbit mAb	Rabbit	Cell Signalling	8242	1:1000	64 kDa
Primary antibody	I κ B α (44D4) Rabbit mAb	Rabbit	Cell Signalling	4812	1:2000	39 kDa
Secondary antibody	Goat anti-rabbit antibody	Goat	Abeam	Ab6721	1:3000	N/A
Secondary antibody	Anti-rabbit IgG, HRP-linked Antibody	Goat	Cell Signalling	7074S	1:2000	N/A
Biotinylated Ladder	Biotinylated Protein Ladder	N/A	Cell Signalling	7727	10 μ L was loaded onto gels	N/A
Biotinylated Ladder	Secondary anti-biotin	N/A	Cell Signalling	7727	1:1000	N/A
Ladder	Precision Plus Protein™ Dual Colour Standards	N/A	Bio-Rad	1610374	10 μ L was loaded onto gels	N/A

4.2.8.2 Incubation with antibodies and visualisation of membranes

After transfer, the membrane was cut into two pieces, the biotinylated ladder section (A) and the protein section (B), along the dual colour ladder. A and B were blocked with 10% BSA for 24 h at 4 °C. Then, 3.34 μ L primary antibody α -tubulin was added into 10 mL 10% BSA (1:3000) to incubate membrane B overnight at 4 °C with 32g agitation (16 h approximately) while A was still blocking with 10% BSA at the same time. Following this incubation and five washes in wash buffer for 10 min at room temperature with 32 g agitation, 3.34 μ L goat anti-rabbit antibody was added into 10 mL 10% BSA (1:3000) for incubation with membrane B, and 10 μ L anti-biotin HRP-linked antibody was added into 10 mL 10% BSA (1:1000) blocking buffer to be incubated with membrane A. This incubation lasted 1 h at room temperature with 1 g agitation. After five washes in wash buffer for 10 min at room temperature with 32 g agitation, the membrane was developed with ECL (Bio-Rad, UK). The membrane could then be visualised with QuantityOne software (Bio-Rad).

In a second step, to measure the level of Histone H3 expression (the housekeeping protein), membranes were washed with wash buffer for 10 min and rehydrated with 100% methanol for 10 s. The membranes were then washed again two times with stripping buffer lasting 10 min. Then, 5 μ L primary antibody Histone H3 was added into 10 mL 10% BSA (1:2000) to incubate with membrane B overnight at 4 °C with 1 g agitation (16 h approximately) while Membrane A was still blocking with 10% BSA at the same time. Following this incubation, the membrane was washed five times in wash buffer and each wash lasted 10 min at room temperature with 32 g agitation. Next, 3.34 μ L goat anti-rabbit secondary antibody (1:3000) was added into 10 mL 10% BSA blocking buffer to be incubated with membrane B, and 10 μ L anti-biotin HRP-linked antibody was added into 10 mL 10% BSA blocking buffer for incubation with membrane A. This incubation lasted 1 h at room temperature with 1 g agitation. After five further 10min rinses in wash buffer 10 min at room temperature with 32 g agitation, the

membrane was developed with ECL (Bio-Rad, UK). The membrane could then be visualised with QuantityOne software (Bio-Rad).

Afterwards, the membranes were washed with wash buffer for 10 min and rehydrated with 100% methanol for 10 s. After 2 times washing with stripping buffer lasting 10 min, membranes A and B were washed three times in wash buffer. Each wash lasted 10 min. Next, membranes A and B were blocked in blocking buffer (10% BSA) for 24 h at 4 °C with 1 g agitation. To study the protein nuclear p65 or I κ B α protein, the methodology was conducted according to the instructions from Cell Signalling. A total of 10 μ L anti-p65 / I κ B α antibody was diluted in 10 mL blocking buffer (1:1000 dilution) for overnight incubation while membrane A was blocked with 10% BSA at 4 °C with 1 g agitation. Following the overnight incubation, five 10 min washes in wash buffer were performed at room temperature with 32g agitation. Next, 3.34 μ L anti-rabbit IgG, HRP-linked antibody was added into 10 mL 10% BSA blocking buffer (1:3000) for incubation with membrane B, and 10 μ L anti-biotin HRP-linked antibody was added into 10 mL 10% BSA blocking buffer and incubated with membrane A. This incubation lasted 1 h at room temperature with 1 g agitation. After five washes in wash buffer for 10 min each at room temperature with 32 g agitation, the membrane was developed with ECL (Bio-Rad, UK). The membrane could then be visualised with QuantityOne software (Bio-Rad).

4.2.9 Statistical analysis

Statistical analysis was carried out with SPSS 22.0 for Windows. All the data was normally distributed at .05. A one-way ANOVA was used to determine the significance coupled to the LSD *post-hoc* test for homogeneous variance ($p>0.05$) or the Dunnett's T3 *post-hoc* test if variance was not homogeneous ($p<0.05$).

4.3 Results

4.3.1 Purity check for contamination of cytoplasmic extracts in nuclear cell extracts

Prior to measuring the levels of nuclear p65, the extracts underwent a purity check for all the samples used in this chapter to assure there was no contamination of cytoplasmic extracts. Figure 4.2 illustrates an example of the purity check for contamination of cytoplasmic extracts in nuclear extracts in both the PNT2 and PC3 cell lines. α -Tubulin is a protein that is only expressed in the cytoplasm. In this figure, the cytoplasmic extracts were seen as a positive control, where α -tubulin was highly expressed, while there was no expression of the α -tubulin protein in nuclear extract samples. Histone H3 was included as the loading control in all the samples. This evaluation demonstrated that all nuclear samples extracted were of suitable quality for further analysis.

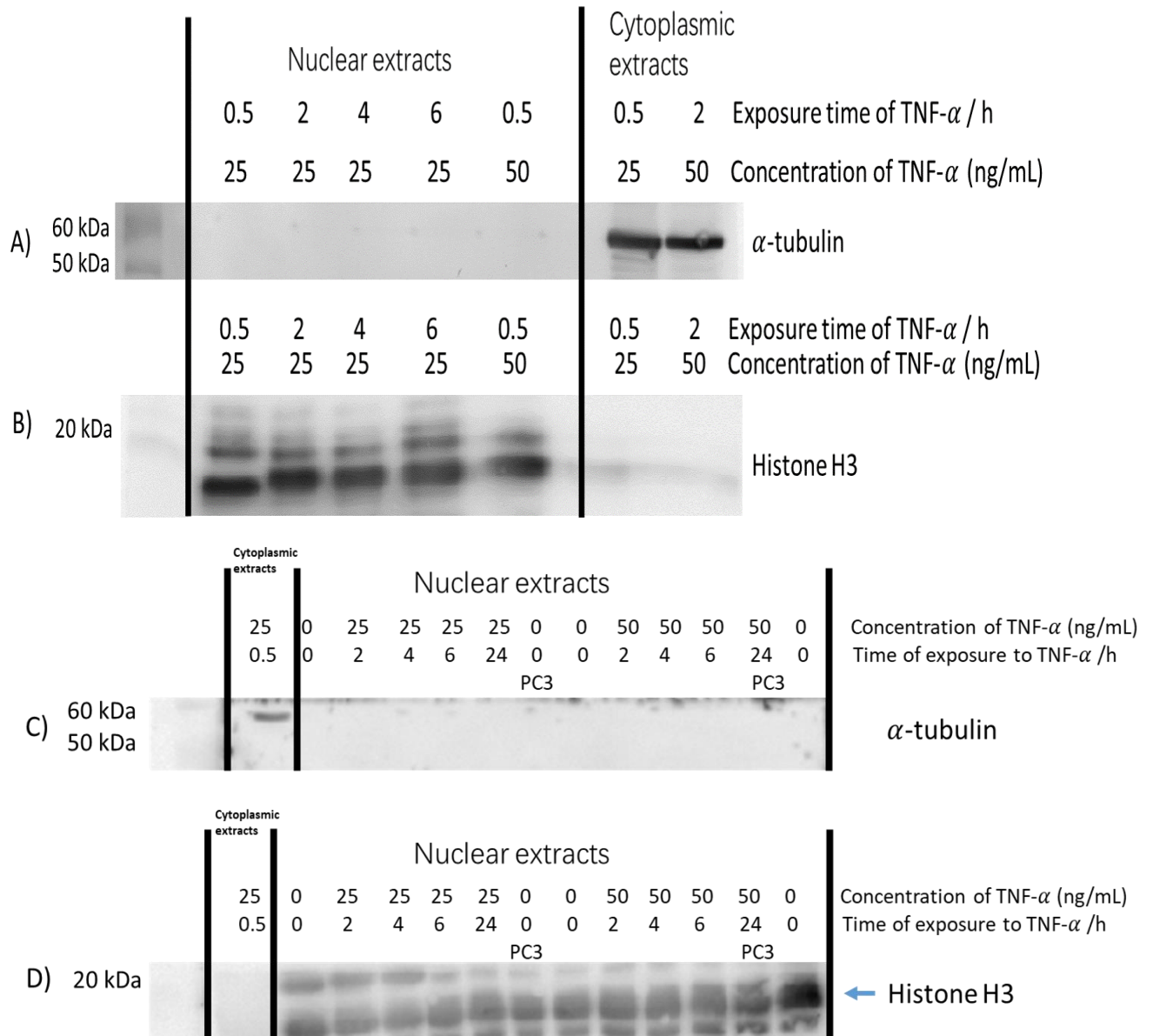


Figure 4.2. Examples of the purity check for contamination of cytoplasmic extracts in nuclear extracts in: A and B) PC3 cell extracts; C and D) PNT2 and PC3 cell extracts. The first lane is the cytoplasmic extracts from PNT2 cells. The 7th lane is the PC3 nuclear extracts and the rest of lanes are the PNT2 cells' nuclear extracts. Black lines around the gels in A-D distinct between different western blots cut to allow for staining as described in the Section 1.2.8. Histone H3 and α -tubulin are the loading control to p65 and I κ B α respectively.

4.3.2 Role of NF- κ B with nuclear p65 and cytoplasmic I κ B α

4.3.2.1 Profile of nuclear p65 and cytoplasmic I κ B α after TNF- α treatment over time in PC3 cells

PC3 cells were treated with TNF- α at 25 or 50 ng/mL for 0.5, 2, 4 and 6 h. Nuclear p65 and cytoplasmic I κ B α protein expressions were then analysed by western blots. From the data in Figure 4.3, there was no difference amongst treatment groups regarding nuclear p65 and cytoplasmic I κ B α . There was p65 found in the nuclei of cells without treatment, which means that the NF- κ B pathway had been activated in PC3 cells and TNF- α is not a stimulus to PC3 cells. Hence, it is not necessary to treat PC3 cells with TNF- α for further investigation of the NF- κ B pathway in PC3 cells.

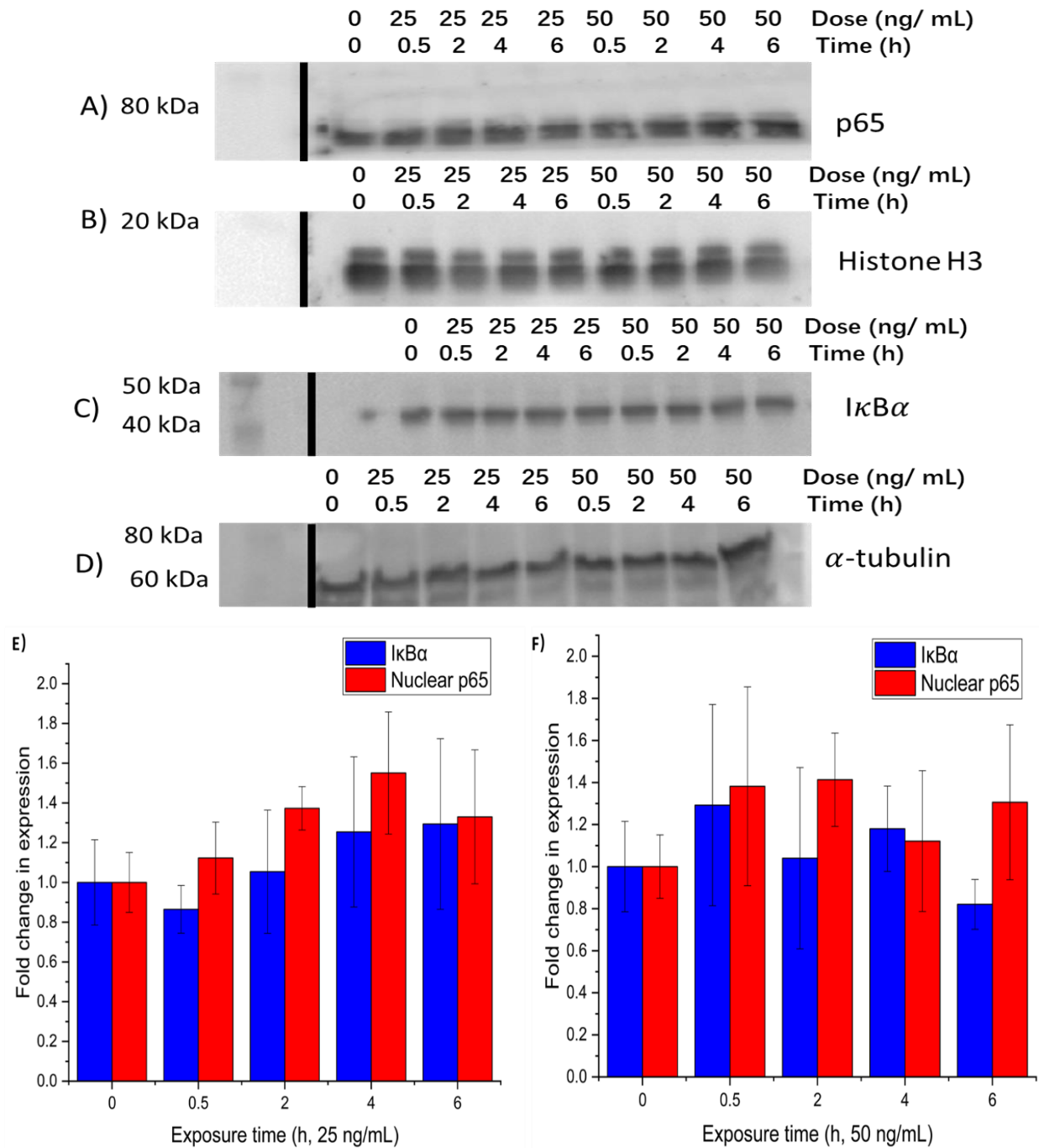


Figure 4.3. Profile of IκBα and nuclear p53 protein levels after TNF-α treatment in PC3 cells over the time. A-D) Representative example of western blot membrane and E and F) Densitometry data generated from the western blot membranes for IκBα and p53 respectively. 25 ng/mL and 50 ng/mL TNF-α were exposed to PC3 cells respectively. Error bars indicate the SD (n=3). Black lines around the gels in A-D distinct between different western blots cut to allow for staining as described in the Section 1.2.8. Histone H3 and α-tubulin are the loading control to p53 and IκBα respectively.

4.3.2.2 Profile of nuclear p65 and cytoplasmic I κ B α in PNT2 cells after TNF- α treatment over different time periods

TNF- α was similarly used to activate the NF- κ B pathway in PNT2 cells following the methods in Section 4.2.8. A representative profile of nuclear p65 in PNT2 cells after TNF- α treatment can be found in Figure 4.4A. For PNT2 cells, the NF- κ B pathway was activated by the treatment of TNF- α as there was increased p65 signal detected. When PNT2 cells were treated with 25 ng/mL TNF- α , the expression of p65 in the nucleus decreased when the exposure time was increased from 0.5 to 24 h. The reason for this is that p65 responds quickly to TNF- α , moves to the nucleus, but after time p65 was exported out of the nucleus, maybe by freshly made I κ B. The trend was similar when the dose was increased to 50 ng/mL.

The protein expression of nuclear p65 from the PNT2 cells treated with 25 ng/mL TNF- α at 0.5 h was significantly higher (4-fold-change, $p=0.001$) than untreated PNT2 cells. In addition, the p65 expression in the nucleus was also increased within 0.5 h due to 50 ng/mL TNF- α , but it was not significant. Therefore, the exposure of 25 ng/mL TNF- α for 0.5 h was selected to activate the pathway in PNT2 cells for the exploration of NaS effects on the NF- κ B pathway. As the NF- κ B pathway in PC3 cells is constitutively active, PC3 protein extract was included here as a positive control and indeed, without treatment of TNF- α , PC3 cells also exhibited p65 nuclear protein localisation (Figure 4.4 A).

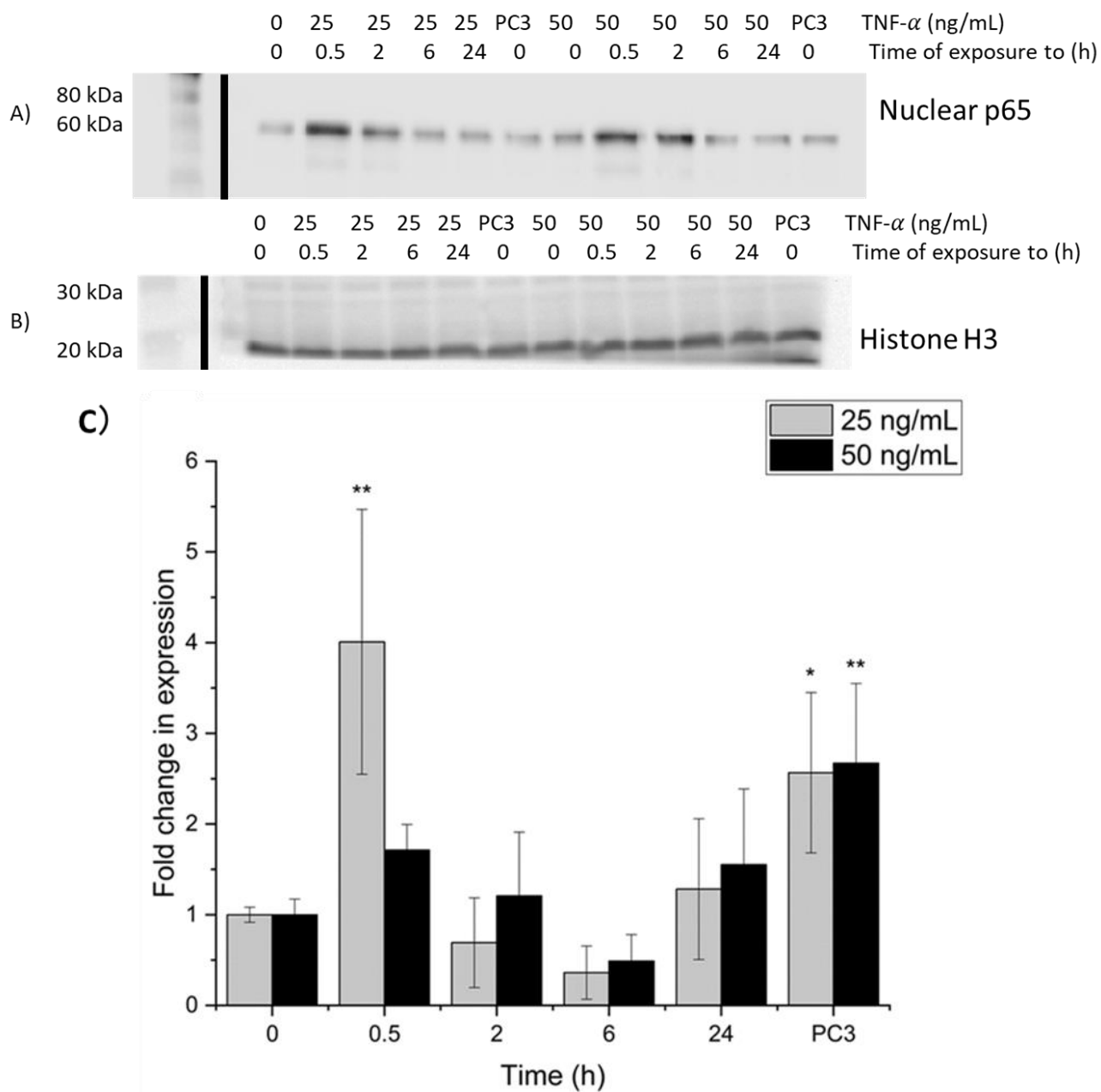


Figure 4.4. Profile of nuclear p65 protein levels after TNF- α treatment in PNT2 cells over the time. A and B) Representative example of western blot membrane and C) Densitometry data generated from the western blot membranes. PC3 indicates the extracts from PC3 cells without any treatment. The predicted weight of p65 is 65 kDa and Histone H3 is 17 kDa. *, and ** indicate significance compared to the control where $p < 0.05$, as determined by a one-way ANOVA with the *post hoc* Dunnett T3 ($n=3$). Error bars indicate the SD. Black lines around the gels in A-D distinct between different western blots cut to allow for staining as described in the Section 1.2.8. Histone H3 is the loading control to p65.

The protein expression profile of I κ B α after TNF- α treatment was evaluated by western blots over a 30 min exposure time (Figure 4.5A). The p65 expression in the nucleus peaked at 0.5 min of TNF- α treatment (both 25 and 50 ng/mL). As an upstream regulatory protein of p65, the timeframe for I κ B α protein degradation should be inversely correlated at a 30 min peak (Figure 4.5). I κ B α was expressed in PNT2 cells without treatment with TNF- α . For 25 or 50 ng/mL of TNF- α treatment, an increase of treatment time led to rapidly reduced expression of the I κ B α protein. Within 30 min of treatment, 50 ng/mL TNF- α was able to deplete almost all I κ B α expression; however, 25 ng/mL treatment could not do so within 30 min. Densitometry data support the membrane images (Figure 4.5B). In the 25 ng/mL treatment group, I κ B α was degraded in the first 5 min but this was not significant ($p>0.05$). However, degradation of I κ B α did become significant ($p<0.05$) at the 10-minute exposure time point with the 25 ng/mL dose, where a -2.5-fold change was observed compared to the control group. With a 50 ng/mL exposure to TNF- α treatment for 30 min, a -25-fold-change in I κ B α protein was found compared to the control group.

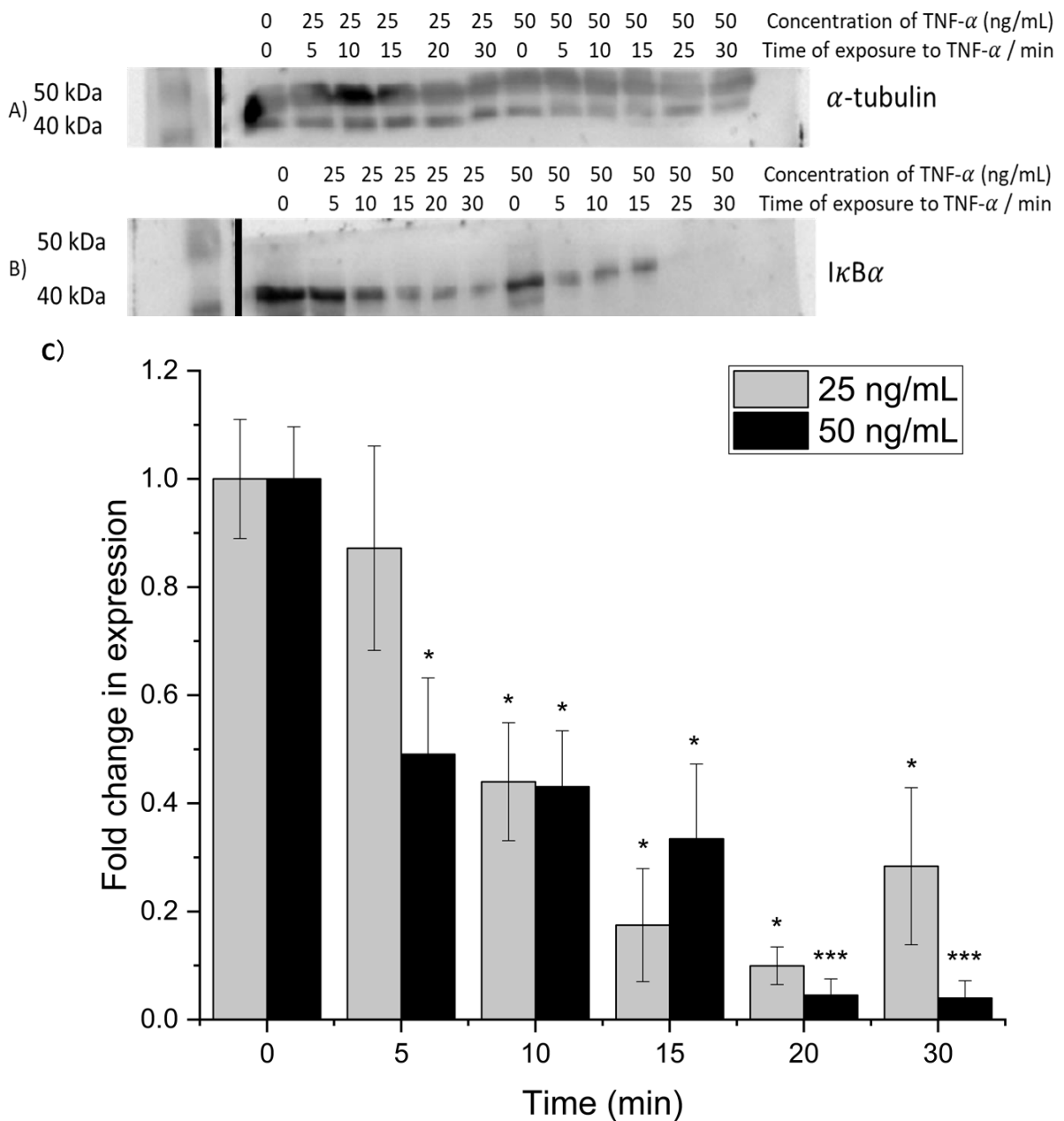


Figure 4.5. Profile of I κ B α protein levels after TNF- α treatment in PNT2 cells over the time. A and B) Representative example of western blot membrane and C) Densitometry data generated from the western blot membranes. The predicted weight of I κ B α is 39 kDa and α -tubulin is 55 kDa. * and *** indicate significance compared to the control where $p < 0.05$ and $p < 0.001$ respectively, as determined by a one-way ANOVA with the *post hoc*: Dunnett's T3 for 25 ng/mL and LSD for 50 ng/mL dose due to homogeneous variance ($n=3$). Error bars indicate the SD. Black lines around the gels in A-D distinct between different western blots cut to allow for staining as described in the Section 1.2.8. α -tubulin is the loading control to I κ B α .

4.3.2.3 NaS effects on nuclear p65 and I κ B α in PNT2 cells

Following the protein expression profiles of nuclear p65 and I κ B α in PNT2 cells, a treatment of 25 ng/mL TNF- α for 0.5 h was selected. Thus, PNT2 cells were treated with 0, 2, 4, 6, 8 and 10 mM NaS for 0.5 or 2 h, followed by exposure to 25 ng/mL TNF- α for 0.5 h in order to study the effect of NaS on the activation of the NF- κ B pathway. In PNT2 cells, expression of the NF- κ B pathway subunit p65 in the nucleus and cytoplasmic I κ B α were analysed by western blots (Figure 4.6 and Figure 4.7). To ensure the nuclear sample was free of contamination of cytoplasmic proteins, α -tubulin, a marker of cytoplasmic proteins, was also analysed. The first blot in Figure 4.8A shows that there was no obvious presence of α -tubulin in the nuclear sample. For nuclear p65, the protein was exported in a dose-dependent manner at both 0.5 and 2 h of co-exposure to NaS and TNF- α .

For 2 h NaS pre-exposure time-point, the cytoplasmic I κ B α level increased as the dose of NaS increased. For both 0.5 and 2 h exposure times, 4 and 6 mM NaS were able to suppress the NF- κ B pathway significantly ($p < 0.01$ and $p < 0.05$ respectively). The top concentrations of NaS resulted in increased protein expression of I κ B α , leading to the suppression of the NF- κ B pathway, due to the sequestration of p65 in the cytoplasm. At 0.5 h exposure of NaS at 10 mM the effect of TNF- α on the NF- κ B pathway was completely lost, as the I κ B α level was not significantly higher when compared to the control group ($p = 0.396$). Likewise, the NF- κ B pathway was suppressed due to the 2 h exposure to 8 and 10 mM NaS ($p > 0.05$). There was no difference between the control (25 ng/mL TNF- α for 0.5 h but no NaS treatment) and the untreated PNT2 cells I κ B α level ($p = 0.210$), indicating that TNF- α can only activate the pathway, but not enhance it. The results of the western blots analysis here show that I κ B α levels increased while nuclear p65 levels decreased when PNT2 cells were treated with NaS prior to TNF- α treatment. It appeared that the TNF- α effect was counteracted at the top dose of NaS (8 and 10 mM) or a longer treatment time (2 h). Hence, NaS is able to suppress the activation of the NF- κ B pathway.

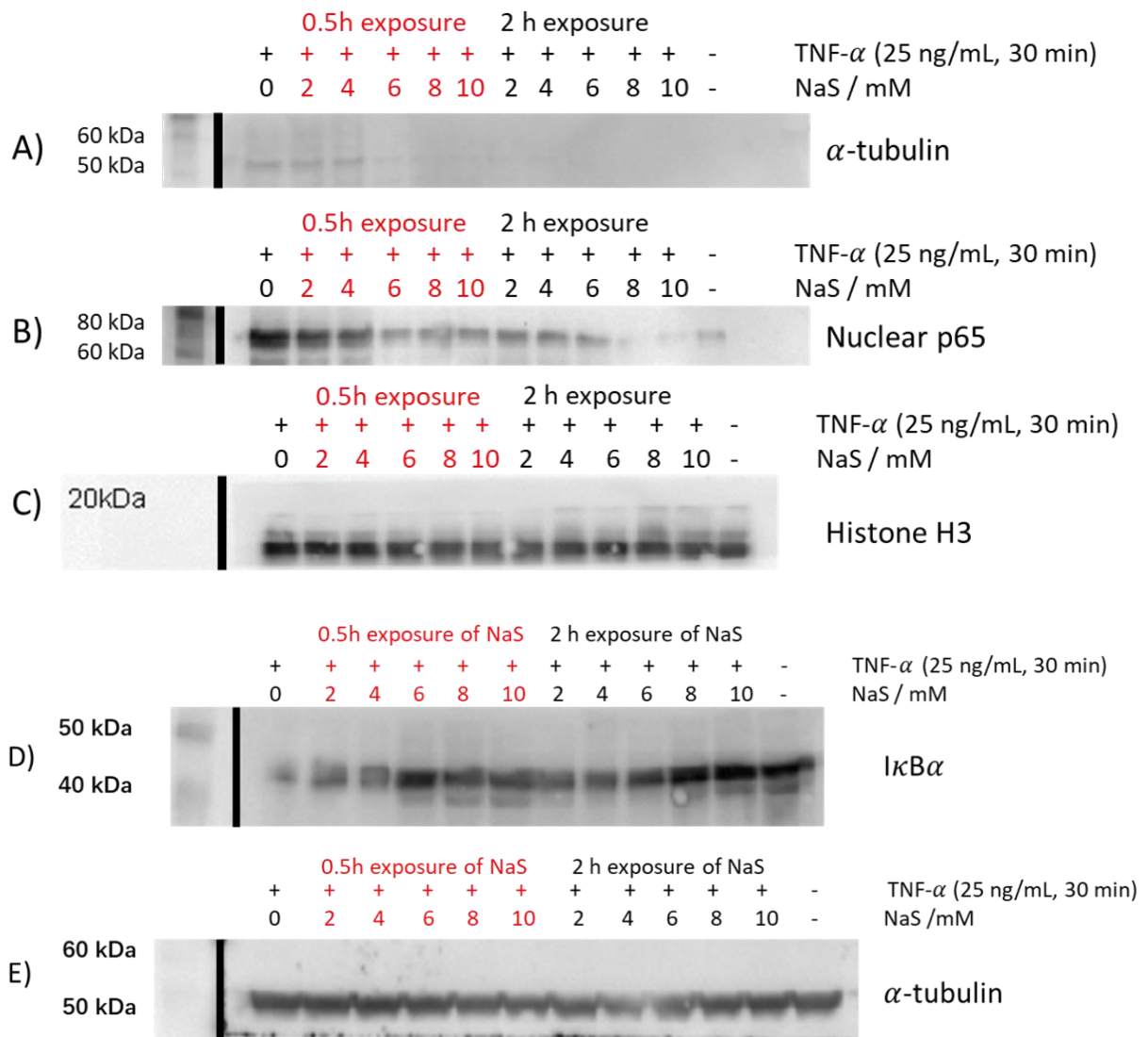


Figure 4.6. Representative example of western blots membrane of NaS role in the activated NF- κ B pathway in PNT2 cells by TNF- α . NaS effects on nuclear p65. In A-C) section, the top membrane (α -tubulin) was to assure there was no contamination of cytoplasmic protein in nuclear samples. The middle membrane was nuclear p65 profile. The bottom membrane was Histone H3, which was the loading control. In D and E) section, the upper membrane section shows a reduction of I κ B α and lower membrane are the control α -tubulin. Black lines around the gels in A-D distinct between different western blots cut to allow for staining as described in the Section 1.2.8.

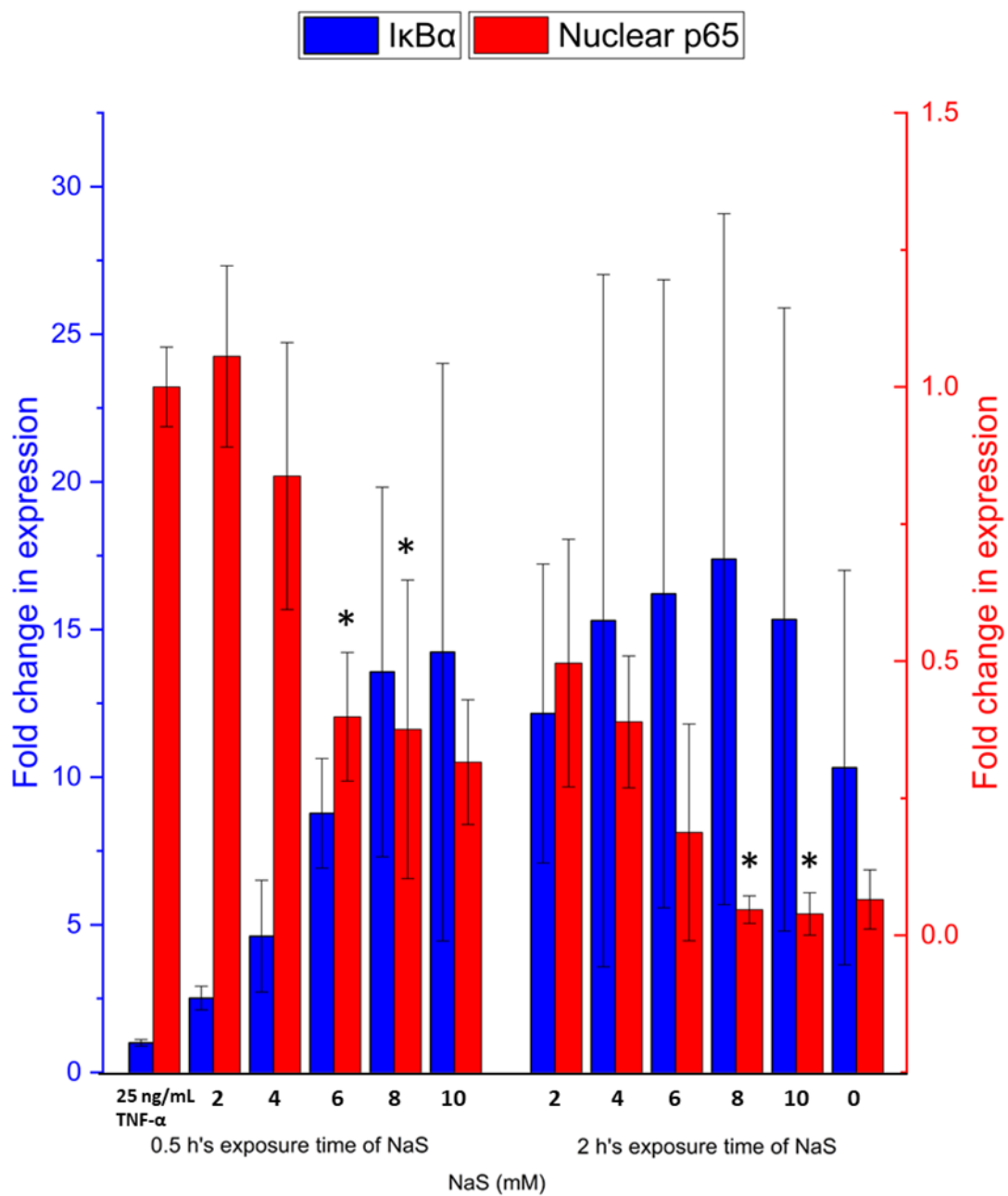


Figure 4.7. NaS role in the activated NF- κ B pathway in PNT2 cells by TNF- α . I κ B α profile with an increasing trend when cells were co-treated with NaS for 0.5 or 2 h of exposure and TNF- α . *, **, and *** indicate significance compared to the control, namely, 25 ng/mL TNF- α for 0.5 h but no NaS treatment, where $p < 0.05$, $p < 0.01$ and $p < 0.001$ respectively, as determined by a one-way ANOVA with the *post hoc*: Dunnett's T3 ($n=3$). Error bars indicate the SD.

4.3.2.4 NaS' effects on nuclear p65 and cytoplasmic I κ B α in the PC3 cell lines

Following the profiles of nuclear p65 and I κ B α in PC3 cells in Section 4.4.2.1, where TNF- α had no effect on the NF- κ B pathway as the pathway was activated constitutively, PC3 cells in the present study design were treated with 0-10 mM NaS alone for 0.5 or 2 h to explore the effect of NaS on the constitutive NF- κ B pathway. Western blot examples and corresponding densitometry data are presented in Figure 4.9 and Figure 4.9 respectively. After the phosphorylation of I κ B α , p65 can then enter nucleus, therefore when measuring their protein levels, significance is not necessarily found simultaneously (i.e. their changes in protein level are not synchronised). Compared to the control, 0.5 h was probably not long enough to increase I κ B α level significantly when the PC3 cells were exposed to NaS. If the exposure time was prolonged to 2 h, 6, 8 and 10 mM NaS were able to increase the expression of I κ B α significantly ($p=0.001$ and 0.001 respectively). When the incubation time was increased to 2 h, significant changes in nuclear p65 levels were present at all concentrations of NaS ($p<0.05$). However, the p -values were only marginally significant at doses 2, 4 and 6mM NaS ($p=0.048$, 0.048 , 0.049 respectively), while only the 8- and 10-mM doses were highly significant. In summary, at higher doses (8 and 10 mM) and longer exposure time, NaS was able to suppress the NF- κ B pathway in the PC3 cell line, where the pathway is activated constitutively.

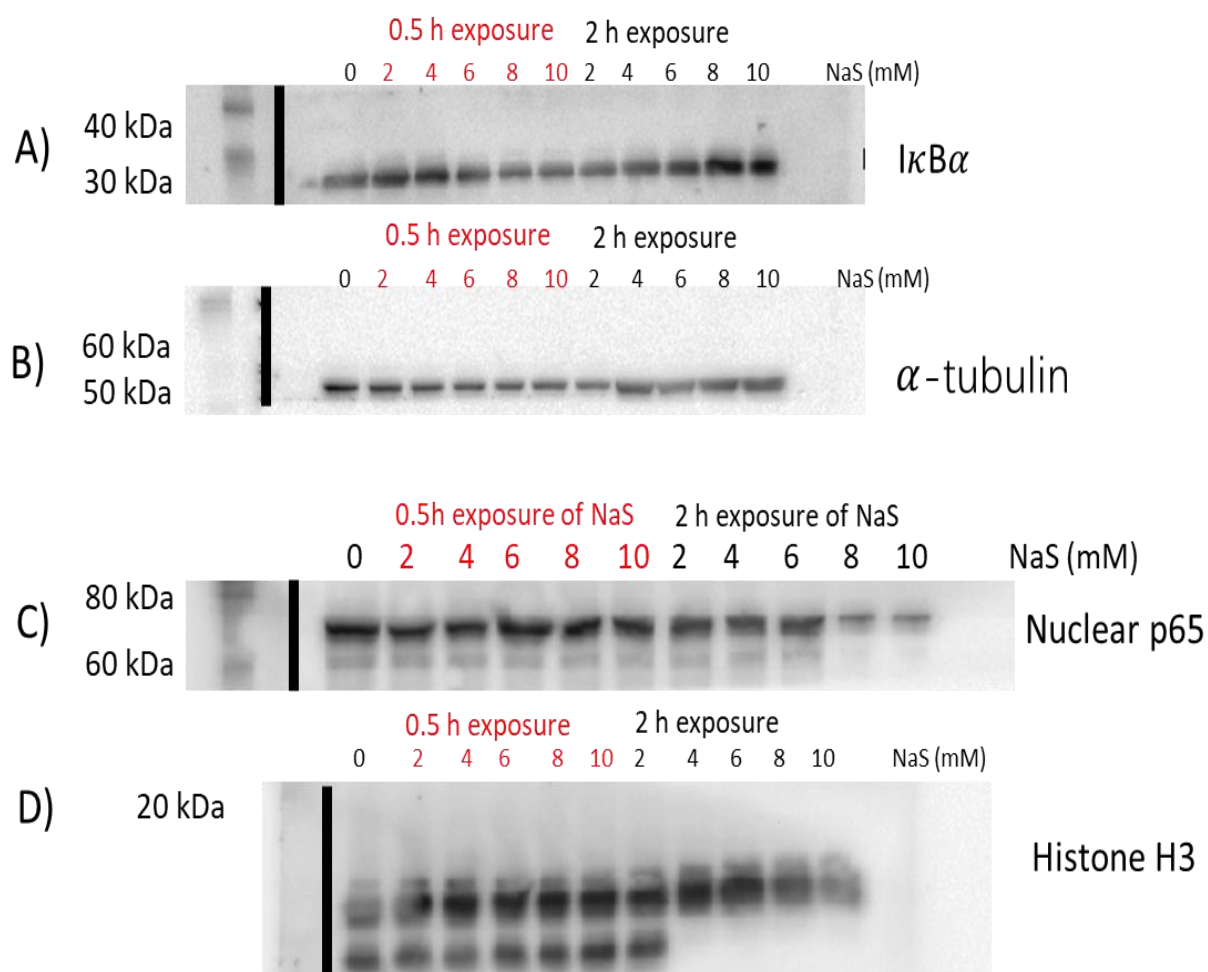


Figure 4.8. Representative image of western blots for PC3 cells exposed to NaS to evaluate nuclear p65 and cytoplasmic IκBα. A-B): NaS effects on IκBα expression. C-D): NaS effects on nuclear p65 expression. Black lines around the gels in A-D distinct between different western blots cut to allow for staining as described in the Section 1.2.8. α-tubulin and Histone H3 are the loading control to IκBα and p65 respectively.

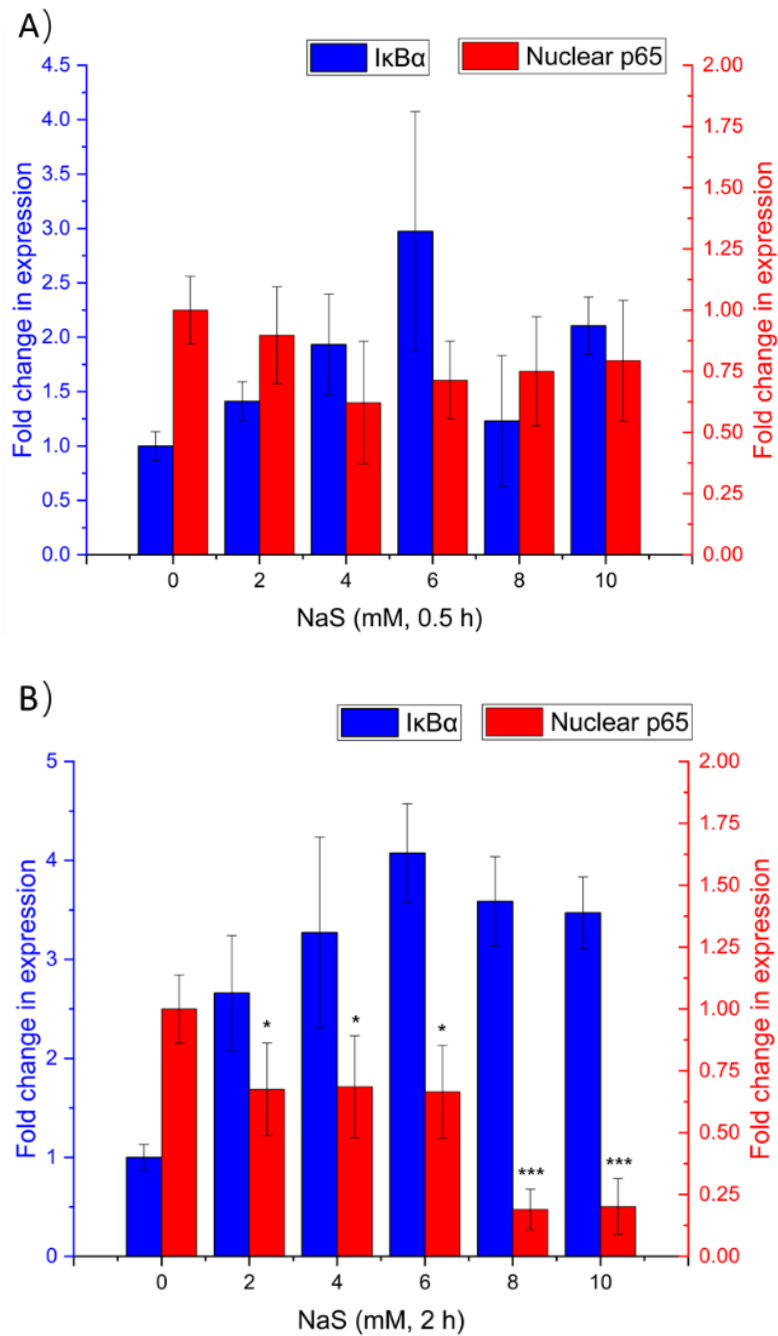


Figure 4.9. NaS role in PC3 cells with constitutive activation of NF- κ B pathway. A) 0.5 h's exposure time. B) 2 h's exposure time. *, and *** indicate significance compared to the control, where $p < 0.05$ and $p < 0.001$ respectively, as determined by a one-way ANOVA with the *post hoc*: LSD for 0.5-h exposure; Dunnett's T3 for 2-h exposure due to homogeneous variance ($n=3$). Error bars indicate: SD.

4.3.3 Impact of NaS toxicity when *COX-2* expression is inhibited

4.3.3.1 *COX-2* mRNA profile after celecoxib pre-treatment

Initially, PNT2 and PC3 cells were treated with 6 μ M celecoxib, a *COX-2* inhibitor, for 72 h, as recommended in the literature and the expression profile of *COX-2* was measured over 5 days (Wang *et al.*, 2012). Figure 4.10 illustrates the profile of *COX-2* gene expression when PC3 cells were treated with celecoxib. PNT2 cells had significantly lower *COX-2* gene expression than the PC3 cells ($p=0.004$) in Figure 3.3. When exposed to celecoxib, PNT2 cells did not respond strongly, with no significant reduction in *COX-2* gene expression over time (albeit a non-significant decreasing trend was observed). In PC3 cells, 24-h exposure to celecoxib was unable to reduce the *COX-2* expression, but once the time was increased to 48h and beyond a significant reduction in gene expression was notable ($p<0.001$). After the treatment of celecoxib was washed off, the *COX-2* mRNA levels were measured on 2 days, i.e. 1 day after wash off and 2 days after wash off in Figure 4.10. *COX-2* mRNA levels were still not back to the normal level (the mRNA level of 1 day after seeding). Thus, for the next set of NaS exposure experiments, a 3-day treatment with celecoxib followed by 24-h recovery after washing off the celecoxib dose was selected as the appropriate study design to take forward.

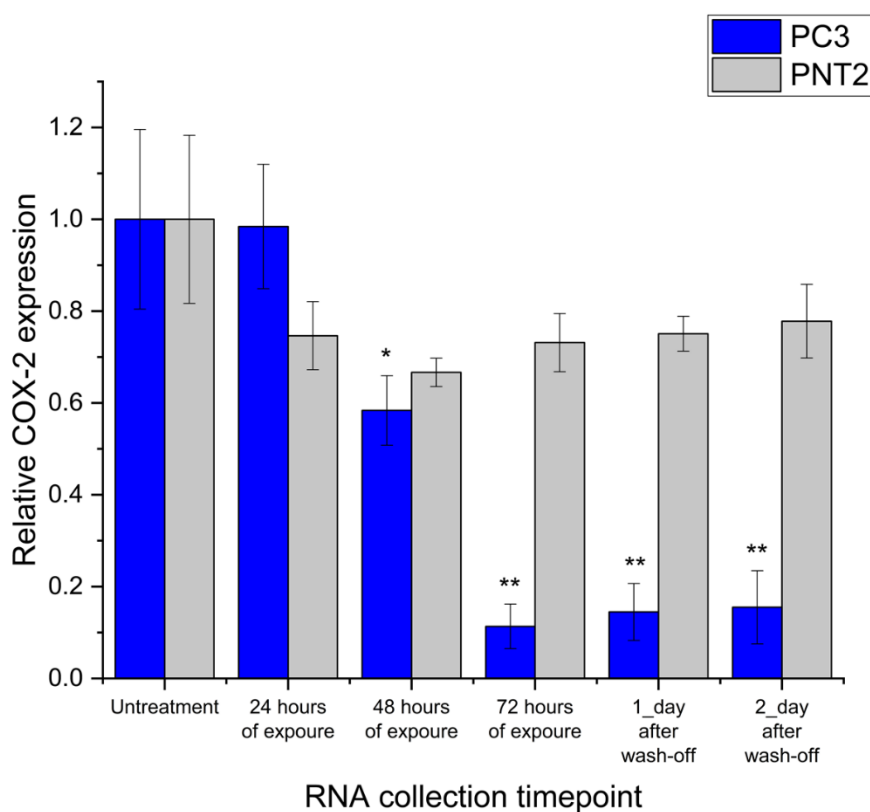


Figure 4.10. *COX-2* gene expression profile after celecoxib treatment in PC3 and PNT2 cells. *, and *** indicate significance compared to the control, where $p < 0.05$ and $p < 0.001$ respectively, as determined by a one-way ANOVA with the *post hoc* LSD ($n=3$). Error bars indicate: SD. *COX-2* in PNT2 cells were approximately 42-fold-change lower than that of PC3 cells; the details can be found in Figure 3.3.

4.3.3.2 PC3 cell toxicity after the depletion of *COX-2* expression

As stated previously, NaS was toxic to both PNT2 and PC3 cells at low and high doses (2 to 10 mM); see Figure 3.2. The cytotoxicity was particularly obvious for PC3 cells at 8 and 10 mM (roughly 120% reduction, which means the cells after 24 h's recovery were less than the seeding density). Here, the *COX-2* gene was assumed as a mediator for NaS effects on PCA cells. When PC3 cells' *COX-2* gene expression was depleted by celecoxib, and the NaS exposure repeated, the RPD values were not reduced significantly ($p > 0.05$) between 2-6 mM in Figure

4.11. However, cytotoxicity in the PC3 cells decreased by approximately 10% with the exposure of 8 and 10 mM NaS ($p=0.047$ and 0.010 respectively), with no significant difference between the two doses ($p=0.412$). Thus, compared to NaS treatment alone, the cytotoxic effects of NaS were partially neutralized when *COX-2* gene expression was removed.

Likewise, in PNT2 cells (the normal cell line), RPD values were also reduced significantly from 6 to 10 mM when they were co-treated with NaS and celecoxib. With solo-treatment of NaS, 2 mM reduced RPD by 20% in PNT2 cells; however, with co-exposure, roughly RPD was reduced by 10% at the top 10 mM dose in the PNT2 cells. A similar trend was noted with the PC3 cells, where again the toxicity imparted by NaS was significantly reduced with the celecoxib co-exposure, albeit to a lesser extent than in PNT2 cells (Figure 4.11). This may be due to the fact that *COX-2* expression in PC3 cells is substantially higher than in PNT2, thus the celecoxib treatment may not be as efficient in PC3 cells, with some *COX-2* expression remaining. The results however indicate that the *COX-2* gene is involved in mediating the cytotoxicity of NaS.

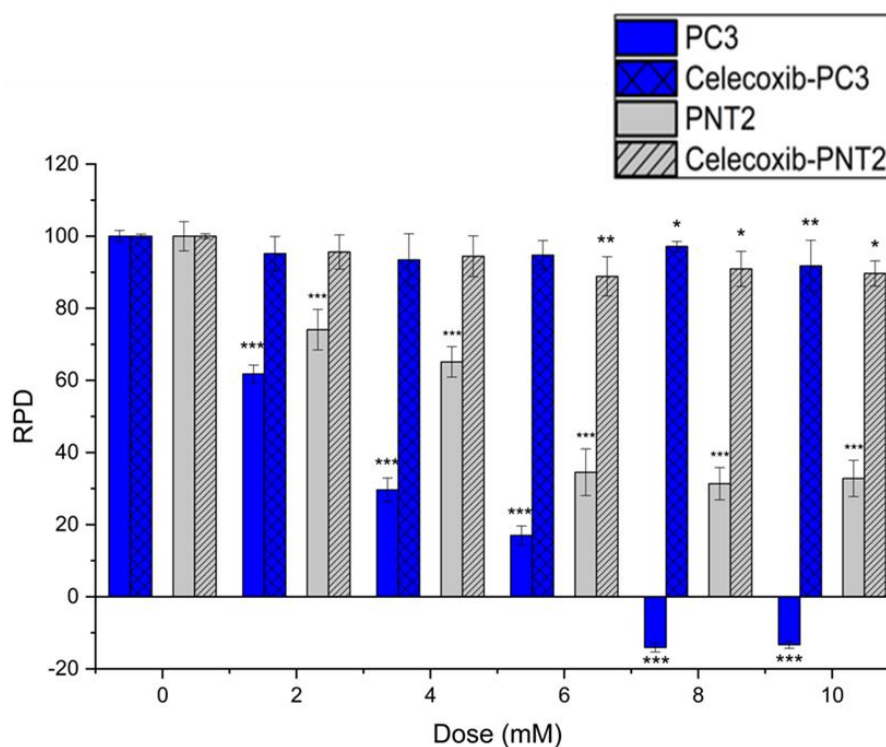


Figure 4.11. Cytotoxic effects of NaS on PC3 and PNT2 cells when pre-treated with celecoxib for 72 h to deplete *COX-2* gene expression. The celecoxib-treated cells were re-seeded at 100000 cells / mL. *, **, and *** indicate significance compared to the control, where $p < 0.05$, 0.01 and 0.001 respectively, as determined by a one-way ANOVA with the *post hoc* LSD ($n=3$). Note: the data the NaS treatment alone in PC3 and PNT2 cells originates from Section 3.3.1. Error bars indicate the SD.

4.3.3.3 INCell morphological and cell cycle analysis

INCell analysis was performed to assess the NaS effects on morphology and cell cycle when *COX-2* was depleted by celecoxib. Colcemid was used as a positive control for changes to nuclear area. The mean nuclear and cell area information collected can be found in Figure 4.12, where the data demonstrates that there were no changes in either measurement when the PC3 cells were pre-treated with celecoxib, followed by NaS. Likewise, when celecoxib pre-treated PNT2 cells were exposed to NaS over a range of doses, nuclear and cell area were not changed significantly ($p > 0.05$).

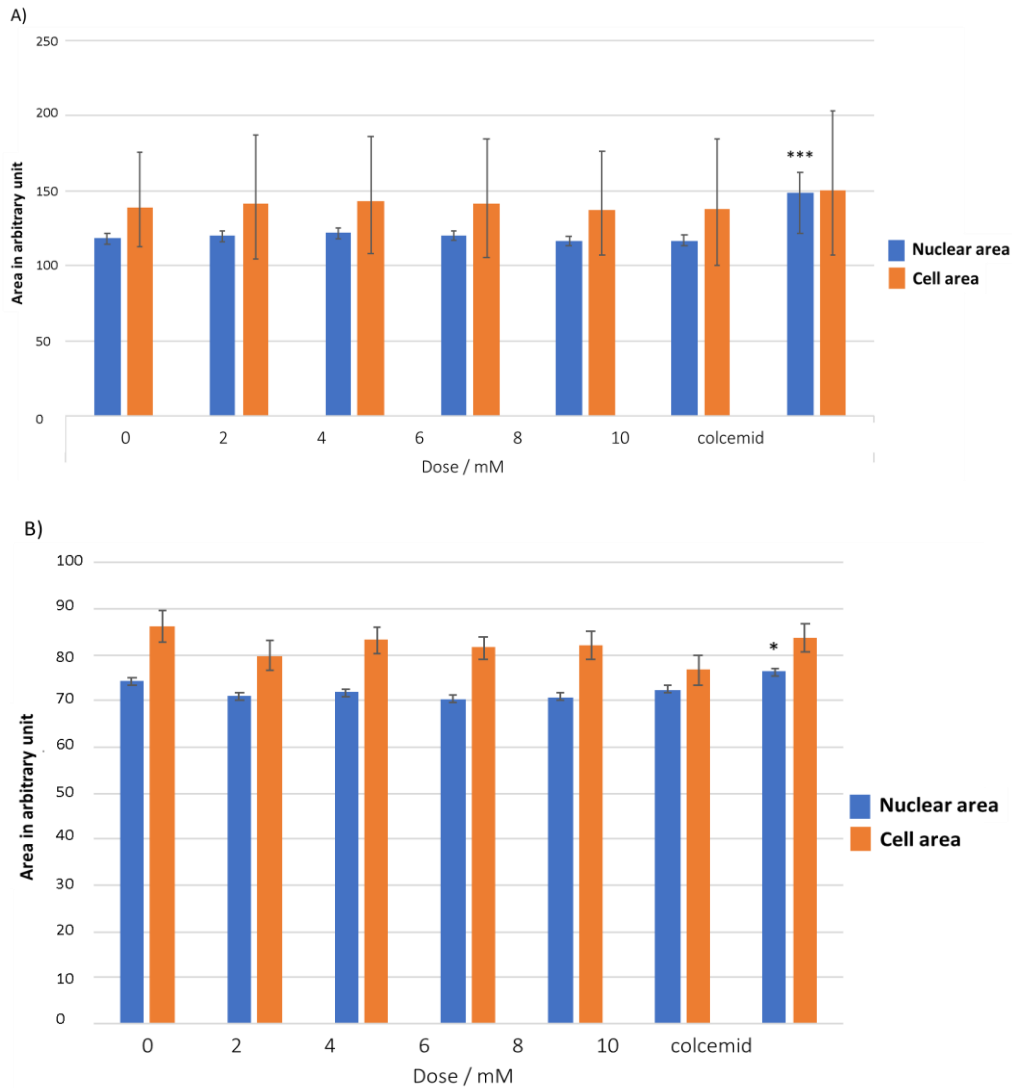


Figure 4.12. Nuclear and cell area in A) PC3 and B) PNT2 cells pre-treated with celecoxib, followed by NaS exposure. Positive control: 24-h exposure of 60 nM colcemid. * indicate significance compared to the control, where $p < 0.05$, as determined by a one-way ANOVA with the *post hoc* LSD for nuclear area ($n=3$) and Dunnett's T3 for cell area due to homogeneous variance ($n=3$). Error bars indicate: SD.

When NaS alone was exposed to the PCA cells, PC3 cells were arrested in the G_0/G_1 stage of the cell cycle in Figure 3.9. When this cell cycle analysis was repeated following co-treatment with celecoxib (as demonstrated in Figure 4.13) the cell cycle profile was very different. With pre-exposure of celecoxib, PC3 cells exhibited no change in terms of percentage of cells at

G₀/G₁ stage ($p>0.05$) following exposure to NaS. However, more cells were shifted to G₂ phase. In previous data from Section 3.3.5.1 (Figure 3.9), there was no change in cell cycle following NaS exposure. Similarly, the inclusion of celecoxib exposure had little effect on the PNT2 cell cycle. There appears to be a trend of increasing percentage of G₀/G₁ cells with increasing dose in PNT2 cells, but this was not significant ($p>0.05$).

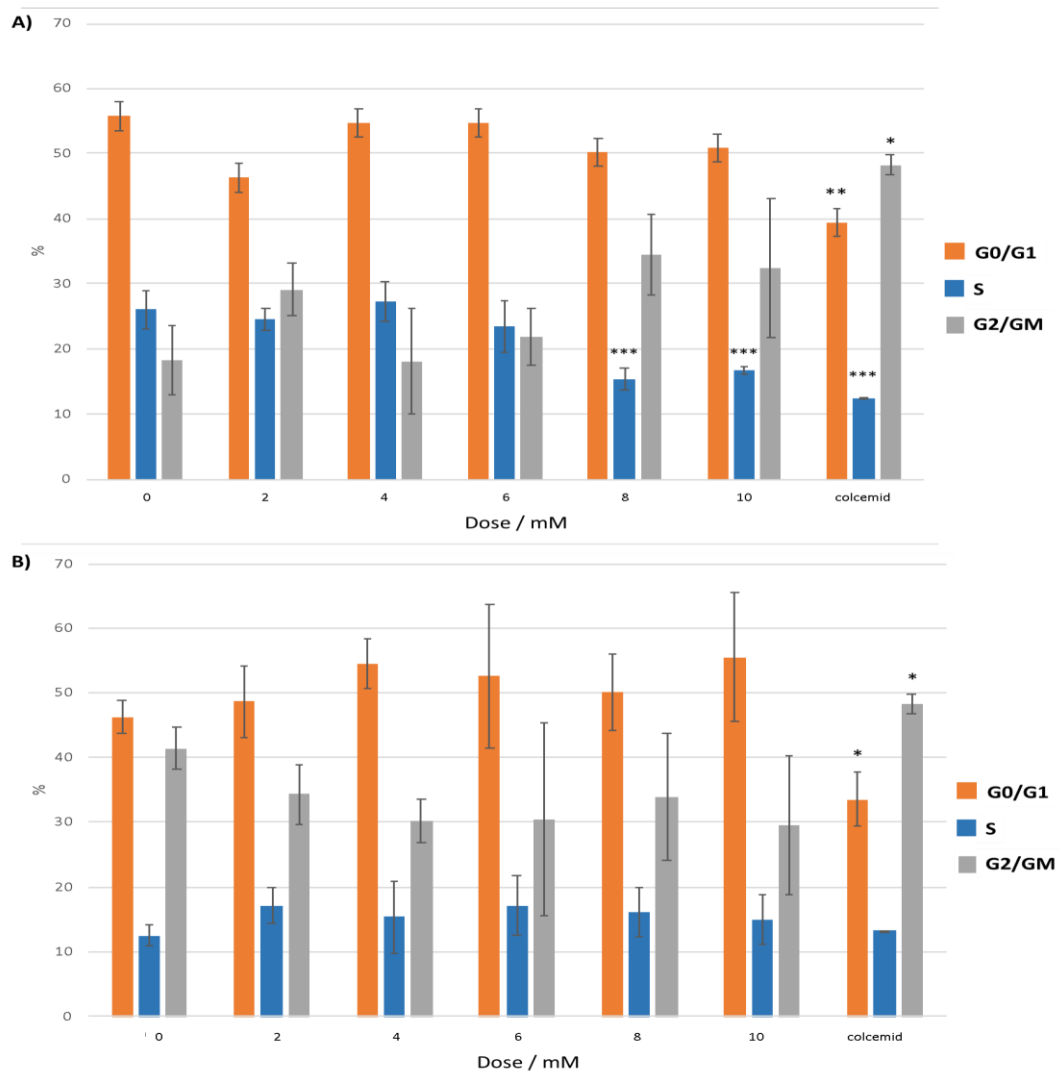


Figure 4.13. Cell cycle analysis in A) PC3 and B) PNT2 with co-exposure of celecoxib and NaS. Positive control: 24-h exposure of 60 nM colcemid. *, **, and ***, indicate significance compared to the control, where $p<0.05$, $p<0.01$ and $p<0.001$ respectively, as determined by a one-way ANOVA with the *post hoc* LSD ($n=3$). Error bars indicate the SD.

4.3.3.4 INCell analysis for Ca²⁺ and mitochondrial health

With the Fluo-8 Calcium Flux Assay Kit - No Wash (ab112129) from Abcam, the level of intracellular Ca²⁺ was measured as an indicator of apoptosis. PNT2 and PC3 cells were treated with 6 μM celecoxib for 72 h followed by 0-10 mM NaS for 24 h, plus 24-h recovery, to investigate if the level of intracellular Ca²⁺ was changed when COX-2 expression was eliminated. The results are depicted in Figure 4.14. Intracellular Ca²⁺ levels in PC3 cells were elevated significantly at the top dose of 10 mM NaS ($p=0.031$) even though COX-2 expression was removed by celecoxib. On the contrary, in celecoxib-treated PNT2 cells, intracellular Ca²⁺ was not changed significantly over the dose-range applied ($p>0.05$).

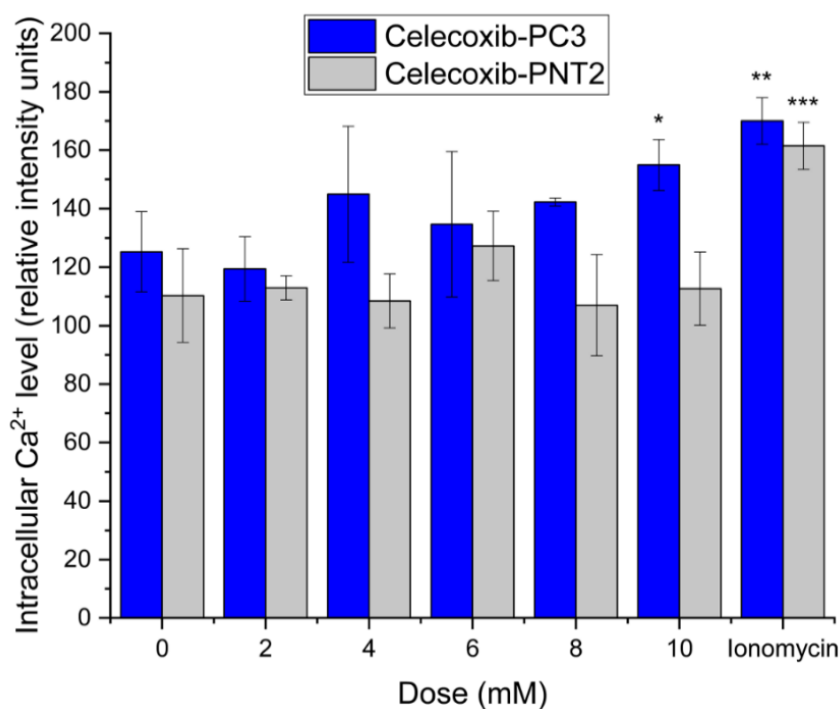


Figure 4.14. Intracellular Ca²⁺ levels in PC3 and PNT2 cells following co-exposure of celecoxib and NaS. Positive control: Ionomycin for 20-min exposure of 20 μM. *, **, and ***, indicate significance compared to the control, where $p<0.05$, $p<0.01$ and $p<0.001$ respectively, as determined by a one-way ANOVA with the *post hoc* LSD ($n=3$). Error bars indicate the SD.

When intracellular Ca^{2+} levels increase dramatically, one of the subsequent results is that the number of mitochondria decreases. Hence, with a Mitochondrial Staining Kit - Orange (Ex405nm) - Cytopainter (ab138897), the mitochondria count (demonstrated in Figure 4.15) was studied in PNT2 and PC3 cells with pre-treatment of celecoxib. In PNT2 cells, the number of mitochondria was not reduced significantly ($p>0.05$). Conversely, when COX-2 expression was diminished in PC3 cells, the 10 mM treatment of NaS induced a significant reduction in mitochondria ($p=0.046$). This result corresponds with the intracellular Ca^{2+} levels which were also increased significantly at this dose in Figure 4.14 ($p=0.031$). In Figure 4.15, p values for 10 mM and FCCP in celecoxib-treated PC3 cells were 0.046 and 0.048, which are closed to the threshold .05, and so is only marginally significant.

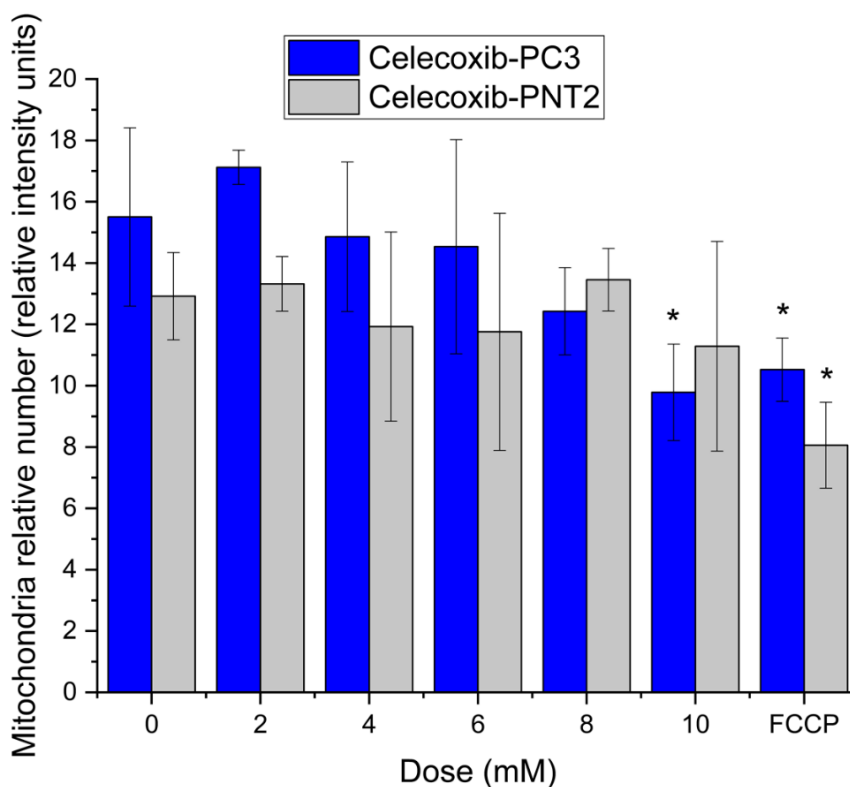


Figure 4.15. Mitochondrial number in PC3 and PNT2 cells following co-exposure to celecoxib and NaS. Positive control: 20-min exposure of 10 μM FCCP for mitochondria. * indicate significance compared to the control, where $p<0.05$, as determined by a one-way ANOVA with the *post hoc* LSD ($n=3$). Error bars indicate the SD.

4.4 Discussion

The effect of aspirin on tumours and the mechanisms underlying its potential anti-cancer properties is currently a hot topic, and a lot of research has been conducted in recent years (Carlson *et al.*, 2013; Langley, 2013). In view of the role of aspirin in inhibiting the growth of prostate cancer cells, it can be used as a prophylactic drug to reduce the incidence of prostate cancer and may also be used in patients with early prostate cancer to reduce mortality (Kashiwagi *et al.*, 2013). However, the specific mechanism of its action and the way of administration of the drugs need further study. In clinical trials, more research is needed to clarify the specific dose, course of treatment, and administration of aspirin in the prevention of prostate cancer. Whilst *in vitro* experiments are required to provide information on aspirin's mode of action, including its impact on the NF- κ B and COX-2 cell signalling pathways, which remains poorly understood.

One objective of this chapter was to study the effects of NaS on the NF- κ B pathway. NF- κ B is a marker of cell activation in inflammation. It consists of members of the Rel protein family in the form of homo/heterodimers (Sun, 2011). p50/p65 heterodimers are the most common. In resting cells, NF- κ B binds to its inhibitory protein I κ B α in the cytoplasm. After stimulation, activation of IKK induces phosphorylation of I κ B α which then dissociates from NF- κ B. The dimer, p65/p50, of the activated NF- κ B is released and translocated into the nucleus where it is involved in the regulation of gene expression (Sun, 2011).

Firstly, a model was established to study NaS effects on the NF- κ B pathway in PNT2 cells where the pathway is not active, as well as the PC3 prostate cancer cell line, where the pathway is constitutively active as confirmed in Figure 4.3. PNT2 cells were activated with TNF- α treatment. The protein levels (nuclear p65 and I κ B α) were not necessarily synchronised; for example, in Figure 4.7, when PNT2 cells were treated with 8 mM NaS, nuclear p65 was reduced significantly but I κ B α levels were comparable to the untreated controls. I κ B α proteins should

be degraded initially then p65 proteins are able to enter the nucleus; given that the translocation may take some time, it is possible that this is reason for this lack of synchronisation between the two proteins (Sun, 2011). Therefore, the two proteins levels were not necessarily synchronised. p65 translocation to the nucleus is the final step of activation in the pathway, hence, changes in levels of nuclear p65 should be seen as the primary indicator of pathway activation, while I κ B α levels are secondary (Campbell *et al.*, 2004; Sun, 2011).

Following this, p65 accumulated in the nucleus within 0.5 h of treatment due to the degradation of I κ B α . In PC3 cells, the NF- κ B pathway is active intrinsically (Garg *et al.*, 2012). Next, PNT2 cells were treated with NaS at different doses prior to TNF- α treatment. It was found that the NF- κ B activation effects of TNF- α were suppressed by the pre-treatment with NaS as cytoplasmic I κ B α was slowly degraded in a dose-dependent manner and less p65 was detected in the nucleus within 0.5 h compared to the control group. When PC3 cells were evaluated, similarly, I κ B α was retained in the cytoplasm and translocation of p65 was reduced in a dose-dependent manner. This data therefore demonstrates that the NF- κ B pathway was suppressed by NaS. The results stating that aspirin inhibits the activity of NF- κ B are well known and aspirin is known to induce apoptosis in many cancers (Yin *et al.*, 1998; Palmer *et al.*, 2017). For example, in DU145, LNCaP and PC3 PCA cells, the NF- κ B pathway was suppressed by 48 h of aspirin treatment (Shi *et al.*, 2017). In this chapter, 2 h's exposure of 8 mM and 10 mM NaS to PC3 cells were the doses that substantially and highly significantly reduced p65 translocation, while 2 h's exposure of 6, 8 and 10 mM treatment were able to prevent the degradation of I κ B α ($p < 0.05$). However, the therapeutic range of aspirin in humans is 0.15-0.30 mg/cm³, which is equivalent to roughly 1-2 mM (Waseem *et al.*, 2017). Thus, it is highly likely that a single use of aspirin at a low dose would not be an effective treatment. Further studies are recommended to investigate this.

The purpose of exploring the NF- κ B pathway in PNT2 cells was because this is a normal

prostate cell line, so it is necessary to conclude if aspirin had the same effect on normal cells as it does on cancer cells. In terms of nuclear p65, 30 minutes exposure of 4 mM or higher NaS reduced NF- κ B-activation in PNT2 cells; while for PC3 under the same conditions, NF- κ B was only suppressed by 6 mM or higher NaS at the same half h exposure time-point. It seems that NF- κ B in PC3 cells are less sensitive and requires a higher dose to suppress the NF- κ B pathway than that of PNT2 cells. For I κ B α expression, there was no change within 0.5-h-exposure in PC3 cells until NaS increased to 4 mM. It is speculated that the reason for this difference is due to the fact that PNT2 was activated artificially by TNF- α , while PC3 cells have a constitutively activated NF- κ B pathway. When the stimuli were removed in PNT2 cells, the pathway cannot be active continuously. Therefore, the NF- κ B pathway in PNT2 cells needs less dose to be suppressed. Normal cells have no NF- κ B activity and the cancer cells have constitutive activity. It can be seen that NF- κ B is crucial in the development of PCA. Furthermore, the pathway can be seen as a therapeutic target for PCA. It is associated with many functions of PCA cells, such as metastasis and proliferation. The research on NF- κ B will help to further understand the mechanism of PCA and provide a theoretical basis for the clinical diagnosis of PCA.

It should be noted that cytotoxicity of NaS is not considered as an interference factor, although massive cytotoxicity was induced by NaS. The exposure times was not the same. With experiments in Chapter 3, the time was 24 h but there were up to 2 h of exposure to NaS in this chapter. Within such a relatively short time, cytotoxicity effects might not be that decisive. Therefore, the toxicity is unlikely to influence the NF- κ B pathway in PCA cells studied in this chapter.

This was not the first study to consider the consequence of inhibition of the NF- κ B pathway in PCA. It has been previously shown that treatment with aspirin led to a NF- κ B inhibition in PCA patients (Lloyd *et al.*, 2003). Shi *et al.* (2017) designed a model to study the effects of aspirin on PCA's invasion. With their model, they found that NF- κ B activation was decreased by the aspirin treatment as the activity of IKK was reduced, which in turn reduced I κ B α

phosphorylation, preventing the translocation of p65 to the nucleus (Shi *et al.*, 2017). Not only aspirin (NaS), but also other anti-cancer drugs, including acacetin, terpenoids, sesamin and cisplatin, were able to suppress the NF- κ B pathway. With an electrophoretic mobility shift assay (EMSA), the binding activity of NF- κ B p65 in the nucleus of DU145 cells was blocked by the treatment of acacetin, which has an inhibiting effect on cancer cells, in a concentration-dependent manner when the cells had been treated for 12 h (Shen *et al.*, 2010). When PC3 cells transfected with the NF- κ B-luciferase reporter gene, were treated with terpenoids, the activity of NF- κ B was suppressed as well (Lin *et al.*, 2015). By western blotting, the expression of the survivin, Bcl-2, Cyclin D1 and c-Myc proteins were reduced after the cells were treated with cisplatin (El-Kady *et al.*, 2011). It has also been found that translocation to the nucleus of the NF- κ B p65 subunit was inhibited by sesamin (Xu *et al.*, 2015). Other investigations of different cancers also support the notion that aspirin is able to suppress the NF- κ B pathway. For example, following 48h 5mM aspirin treatment in U2OS and MG63 cell lines (osteosarcoma cells), NF- κ B activity was reduced as the translocation of p65 was reduced, while downstream targets such as BCL2, CIAP2, Survivin, Livin, and XIAP were all downregulated (Liao *et al.*, 2015).

NF- κ B was originally found to be a B-cell nuclear factor that binds to the kappa chain of immunoglobulins (Sen, 2004). With increased research, it was found that NF- κ B can also be expressed in other cells. It can be seen that NF- κ B is a class of ubiquitous transcription factors. NF- κ B is an activator of immune-activated inflammatory response, cell growth and apoptosis (Liu *et al.*, 2017). It plays the role of promoting tumour cell growth and inhibition of apoptosis. NF- κ B can produce growth factors and angiogenic factors, and directly promote cell cycle progression. NF- κ B can prevent the cell from undergoing apoptosis caused by tumour necrosis factor and ionising radiation (Lam *et al.*, 2015; Brenner *et al.*, 2015). Thus, inhibition of NF- κ B expression can be an important therapeutic target of tumours. Hence, apoptosis can be increased by tumour necrosis factor, and the sensitivity of radiotherapy and chemotherapy on

tumour cells can also be enhanced (Palmer *et al.*, 2017). In the future, apoptosis markers such as caspase levels by western blotting, and nuclear condensation by flow cytometry analysis or microscopy analysis, following treatment could be one of the targets to continue this study in PCA cells. Studies have demonstrated aspirin, as a representative of the NSAIDs, can inhibit the growth of tumour cells, and its mechanism may be related to its inhibition of NF- κ B activity (Ciccoli *et al.*, 2005; Rodrigues *et al.*, 2017). There is growing evidence that NF- κ B acts as a bridge between inflammation and cancer and is one of the important targets of haematological malignancies and solid tumours (Palmer *et al.*, 2017; Manu *et al.*, 2014). As demonstrated in the present study, aspirin can inhibit the activation of NF- κ B induced by TNF and other factors, thereby inhibiting the expression of anti-apoptotic genes and promoting the apoptosis of cancer cells.

The *COX-2* gene is one of the downstream targets of the NF- κ B pathway (Ackerman IV *et al.*, 2008). In the present Chapter it has also been demonstrated that NaS can downregulate the expression of the *COX-2* gene by inhibiting NF- κ B activation, which is possible as the *COX-2* gene promoter has a NF- κ B binding site. Previous studies have found that the *COX-2* promoter (-459~+9) contains two NF- κ B binding sites, and it has been demonstrated that *COX-2* expression is regulated by NF- κ B in the development of prostate cancer, liver cancer and gastric cancer (Garg *et al.*, 2018; Kim *et al.*, 2013; Li *et al.*, 2011). Under the action of various stimuli or other carcinogenic factors, activation of NF- κ B will further promote the expression of *COX-2*, leading to apoptosis, proliferation imbalance and other changes, and eventually induce cancer. It has been found that in colon cancer cell lines, NF- κ B enters the nucleus after being stimulated, and then binds to the specific binding site of the *COX-2* gene's promoter, causing cell proliferation (Mutoh *et al.*, 2007; Li *et al.*, 2011). According to epidemiological surveys, the long-term use of NSAIDs is significantly beneficial to patients with colon, stomach, prostate and breast cancer (Shebl *et al.*, 2014; Tang *et al.*, 2016). COXs including *COX-2* are the targets of NSAIDs. *COX-2* protein is an inducible enzyme, mainly located in the nuclear membrane. When the cells receive an appropriate stimulus, such as inflammatory mediators,

bacterial endotoxin and various carcinogenic factors, *COX-2* expression rapidly increases. In recent years, the role of *COX-2* in the development of a variety of tumours has become a hot topic for research. *COX-2* is not only involved in the early process of tumorigenesis, but also in tumour progression, invasion, and metastasis (Wang *et al.*, 2014; Ko *et al.*, 2017). Therefore, *COX-2* is seen as a promising target for cancer therapy.

In this chapter, it was hypothesized that *COX-2* could be the mediator between aspirin's anti-cancer effects in PCA as it has been found that sensitivities to aspirin seems to be correlated with *COX-2* expression. Hence, PNT2 and PC3 cells were exposed to celecoxib to deplete *COX-2* expression and determine if the anti-cancer effects of NaS observed in Chapter 3 remained. The profile of *COX-2* expression confirmed that *COX-2* was unable to recover to normal levels in the PCA cells over a period of several days despite removal of the drug. Once the appropriate exposure time-lines had been established, the consequence of NaS exposure on cells pre-treated with celecoxib were explored. It was found that only the top doses (8 and 10 mM) of NaS significantly reduced RPD values by only 10% ($p < 0.05$ respectively) in PC3 cells. RPD values in PNT2 cells pre-treated with celecoxib followed by NaS were also significantly decreased by only 10% at 6, 8 and 10 mM ($p < 0.05$). Following this, the morphological assessment showed that the pre-treated cells were not changed by any subsequent NaS dose. Only 10 mM NaS/celecoxib pre-treated PC3 cells induced increased intracellular Ca^{2+} levels at ($p = 0.031$) and mitochondrial number ($p = 0.046$); while NaS/celecoxib pre-treated PNT2 cells did not exhibit any alterations in their Ca^{2+} levels or mitochondrial number, regardless of dose. Finally, with regard to cell cycle analysis, both celecoxib pre-treated PNT2 and PC3 cells were arrested at phase G_0/G_1 at 10 mM NaS ($p < 0.05$).

These results summarised above are highly supportive. Initially, when *COX-2* was absent, growth of PC3 PCA cells were not affected at low and middle doses (0, 2, 4, and 6 mM), indicating that their cell cycle and cell death were not induced by NaS; only the higher doses were capable of inhibiting cell growth, which is likely occurring via a non-*COX-2* related

pathway. With cell cycle analysis, 10 mM NaS arrested PC3 cells at phase G₀/G₁, which is likely linked to the reduced RPD values at 10 mM found in this chapter. When cells were arrested at this phase, where cells are preparing for the DNA synthesis, mitosis was delayed. Thus, the delayed cell cycle resulted in prolonged doubling time. In this chapters' experiments, the selective COX-2 inhibitor, celecoxib almost completely downregulated the expression of COX-2 in PCA cells, which was confirmed by COX-2 gene expression profiling. This drug did not induce any effects on cell proliferation (Denkert *et al.*, 2003; Wang *et al.*, 2012). Recent studies show that COX-2 inhibitors impede proliferation in a variety of tumour cells and induce apoptosis, but their mechanisms are not clear. Celecoxib affects a COX-mediated pathway to induce tumour cell apoptosis and then inhibits the growth of the tumour (Wang *et al.*, 2008). Thus, it can be speculated that COX-2 inhibitors may inhibit the catalytic activity of COX-2, reducing PGE₂ production. Thereby tumour cell growth is inhibited, and apoptosis is enhanced. However, our understanding of the downstream signalling pathway affected is not entirely clear. The results consequently confirm COX-2's role in the effects of NaS on cell growth, morphology and cell cycle distribution as the effects of NaS on these endpoints were largely removed after celecoxib treatment. Only the highest dose, 10 mM, induced increases of intracellular Ca²⁺ level and reduction in mitochondria number. As discussed in the previous Section 3.4, the increase of intracellular Ca²⁺ level and the reduction of mitochondria number is correlated with cell death. It is clear therefore that at the 10 mM dose, the increased intracellular Ca²⁺ levels and reduction in mitochondria number were at least partially responsible for the reduced RPD values recorded at this dose in the cytotoxicity assay.

COX-2 gene is a mediating factor as the effects of aspirin was partially removed when COX-2 was depleted. However, as the top dose of 10 mM NaS was still capable of inhibiting growth of PCA cells, COX-2-dependent and COX-2-independent pathways must be simultaneously involved in the biological activity of aspirin and this correlates with observations made by others in the scientific literature (Denkert *et al.*, 2003; Ricciotti and FitzGerald, 2011). It is key

that *COX*-dependent and *COX*-independent effects of aspirin can be isolated and investigated, so the corresponding cellular targets can be found. In circumstances, where the antitumor effect of aspirin or other drugs for cancer therapy is mediated by *COX*-2, it might be necessary to test the patients' response rate to therapy and *COX*-2 expression prior to therapy, and to consider whether treatment is administered selectively to patients with a high expression of *COX*-2 in tumour tissue (Wang *et al.*, 2012; Wang *et al.*, 2014; Patrignani and Patrono, 2015). On the other hand, if aspirin acts on different cellular targets, for example, *COX*-2-independent pathways, it would be important to screen this target's expression in the tumours of patients' and to use it as a parameter for therapy selection.

In addition to morphology and growth, the *COX*-2 gene is important to prevent metastasis of tumours. Angiogenesis is an important pathological process during the development and metastasis of the malignant solid tumour. The inhibition of angiogenesis is a major part of cancer treatment. The formation of new capillaries is essential to the proliferation of tumour cells, and angiogenesis is a prerequisite for tumour invasion and metastasis. *In vivo* and *in vitro* studies have found that angiogenesis of tumour cells, as well as migration and adhesion, were inhibited by the elimination of *COX*-2 gene expression (Sahin *et al.*, 2014; Xu *et al.*, 2014). The *COX*-2 catalytic products, thromboxane A₂ (TXA₂), prostaglandin I₂ (PGI₂) and PGE₂ have pro-angiogenic effect. PGE₂ can not only increase the expression of the *VEGF* through ERK / JANK1 signalling pathway and protein kinase A, but also promote tumour angiogenesis via the fibroblast growth factor receptor-1 (FGFR -1) (Finetti *et al.*, 2008). There are several studies which confirm that selective *COX*-2 inhibitors can inhibit tumour growth by reducing the level of transcription of *VEGF* gene (Robich *et al.*, 2010; Ben-Batalla *et al.*, 2015; Xu and Croix, 2014). For example, it has been found that *COX*-2 inhibitors such as celecoxib, N-[2-(Cyclohexyloxy)-4-nitrophenyl]methanesulfonamide (NS-398) and 4-[5-(4-Chlorophenyl)-3-(trifluoromethyl)-1H-pyrazol-1-yl]-benzenesulfonamide (SC-236), are able to reduce PGE₂, TXA₂ and other PGs generation by inhibiting the *COX*-2. The release of *VEGF* and basic fibroblast growth factor

(bFGF) can be blocked and thus tumour angiogenesis is suppressed. The same results were obtained by Xu *et al.* (2014a). Early growth response protein 1 (Egr-1) is a transcription factor involved in tumour angiogenesis. It has a very important role in regulating transcription of cytokines and their receptors. Ostrowski *et al.* (2003) found that the selective *COX-2* inhibitor, celecoxib, can inhibit Egr-1 activity in hepatocytes tumour cells in rats, and tumour angiogenesis and metastasis were consequently inhibited. Thus, *COX-2* inhibitors are able to inhibit angiogenesis and metastasis of tumour cells through a variety of ways (Rizzo, 2011) and in the future it would be important to evaluate the mRNA and protein levels of VEGF.

The *COX-2* gene is also involved in intracellular signal transduction pathways that hinder tumour cell metastasis (Feng *et al.*, 2015). The metastasis suppressor gene *KAI-1* (also known as *CD82*) draws attention for its role in tumour development. In a variety of malignant solid tumours in prostate cancer, stomach cancer, laryngeal cancer, and liver cancer studies, researchers found that up-regulation of *KAI1/CD82* could prevent tumour invasion and metastasis (Malik *et al.*, 2009; Scarpino *et al.*, 2013; Feng *et al.*, 2015). Induction of apoptosis and the involvement in adhesion function are the main mechanism to affect motility. In recent years, many studies have confirmed that *COX-2* might be a target for the prevention and treatment of some cancers (Miyashita *et al.*, 2006; Lee *et al.*, 2015). Thus, it is assumed that *COX-2* inhibitors can increase the *KAI-1/CD82* expression and this results in suppression of invasion and metastasis of tumour cells. In thyroid papillary carcinoma cell lines, this hypothesis was accepted. It has been found that inhibition of *COX-2* by NS-398 is connected to upregulation of *KAI-1/CD82* mRNA and this treatment finally led to extrathyroidal extension of the disease and lymph node metastasis (Scarpino *et al.*, 2013). When the gene *KAI-1/CD82* was re-expressed via transfection, the cells' migratory and invasive capacities were reduced. Hence, it is believed that regulation of *KAI-1/CD82* with *COX-2* inhibitors is one of the molecular mechanisms which reduce invasive and metastatic potential of cancer cells (Scarpino *et al.*, 2013). However, in other research there was no such correlation between

COX-2 inhibitor and *KAI-1/CD82* (García-González *et al.*, 2005; Krawczyk-Rusiecka *et al.*, 2014). This is worth further exploration. In the future, aspirin's effects on the invasion and migratory ability should be evaluated when *COX-2* expression has been eliminated by a compound such as celecoxib.

In the present Chapter, a significant element of the work conducted was reliant on the western blotting technique to evaluate protein levels. It is however important to note that western blots are a semi-quantitative means of evaluating protein expression changes. There are also technical limitations as it is not possible to collect all nuclei from the treated cells due to loss during the sample preparation stages. These issues represent drawbacks associated with the methodologies involved in Chapter 4, because the use of statistical analysis on densitometry data has limitations and should be interpreted with some caution, particularly when the level of significance is borderline. Nonetheless, the data demonstrates that *COX-2* and NF- κ B pathways are involved in underlying the anti-cancer effects of NaS' on PC3 cells, representing a starting point for future work to further evaluate these mechanistic pathways. Although the data in this Chapter indicates p65 enters the nucleus, western blotting is unable to demonstrate if those p65 protein bind to the DNA. In order to corroborate the results that have been found here, additional research is required. Chromatin Immunoprecipitation (ChIP) would be a very useful supportive technique to apply in order to demonstrate the binding ability of p65 protein to the DNA. In addition, Enzyme-linked immunosorbent (ELISA) assays could be used to detect the expression levels of key proteins involved in apoptosis such as Bcl-2 and caspases to validate the results generated in this Chapter and better understand NaS' effects on PC3 cells when *COX-2* gene expression was depleted.

In summary, NF- κ B is the regulatory factor for inflammation and apoptosis. NF- κ B can regulate and control cells' growth, including inhibition of apoptosis, producing growth factors and angiogenic factors, and directly promoting cell cycle progression. In this chapter, it has been found that NaS affected PCA cells via the NF- κ B pathway. The mechanism can be summarised

as follows: aspirin firstly inhibits IKK activity, and thus, I κ B α degradation/ phosphorylation is blocked. Subsequently, p65 cannot enter the nucleus, and thus, inhibition of the expression of NF- κ B-regulated *COX-2* results in inhibition of tumour cell proliferation in a dose-dependent manner (Takada *et al.*, 2004; Christian *et al.*, 2016; Shi *et al.*, 2017). Our study shows that specific inhibition of *COX-2* by celecoxib can largely remove the effects of NaS on PCA cells and normal PNT2 cells. Furthermore, our results suggest that cell cycle arrest, increase in Ca²⁺ levels and disruption of mitochondria are primary mechanisms responsible for the antiproliferative effects of NaS on PCA cells, and that this effect is not mediated solely by inhibition of *COX-2*.

Chapter 5 Development and Characterisation of Prostate Cancer 3D Spheroids and Evaluation of Sodium Salicylate Impacts on Spheroids Cells

5.1 Introduction

Cells behave differently when they are cultured in three-dimensions (3D) as compared to two-dimensions (2D). In terms of cell growth, 3D cultures can more accurately simulate the proliferation and differentiation of cells *in vivo* and the process of tissue formation (Page *et al.*, 2013; Edmondson *et al.*, 2014). 3D cell culture involves growth of cells under conditions that result in a more similar tissue structure, which can provide a microenvironment that is more representative of the *in vivo* situation, thus improving on current 2D culture systems (Herrmann *et al.*, 2014). Currently, 3D cell culture technology has been applied in tissue engineering, oncology (Yu *et al.*, 2014), regenerative medicine and cancer research (Zhang *et al.*, 2016; Antoni *et al.*, 2015). This section reviews the recent development of 3D cell culture techniques and its applications in cancer-based studies.

5.1.1 Advantages and limitations of 3D versus 2D *in vitro* cell culture

In 1885, a German scientist named Willhelm Roux isolated cells from embryos, which was considered as the beginning of the tissue culture technique (Heams, 2012). In 1907, Harrison, and shortly after in 1912, Carrel and Ingebrigtsen, began to study animal cell culture methods *in vitro* which marks the birth of modern cell culture technology (Harrison, 1908; Carrel and Ingebrigtsen, 1912). With over 100 years of continued development of the *in vitro* cell culture technology, 2D culture is widespread and does have its advantages (Imamura *et al.*, 2015). The techniques involved are simple. People only need basic skills in tissue culture and basic laboratory equipment. Furthermore, the experimental design is straightforward as exogenous

agents can be easily applied; and the cells grow more rapidly than the same cells grown in 3D culture environments (Chitcholtan *et al.*, 2013).

However, the experimental results obtained in many cases by 2D culture are not always wholly representative of biological responses seen *in vivo* (Jacobi *et al.*, 2017; Kapałczyńska *et al.*, 2018). The main reason for this difference between the results generated in *in vitro* and *in vivo* experiments is that, although 2D cultured cells can proliferate and differentiate *in vitro*, there is a huge difference between the environmental conditions *in vivo* and *in vitro*, which therefore leads to gene expression and morphological characteristics that vary considerably (Edmondson *et al.*, 2014; Antoni *et al.*, 2015). As current 2D cell systems do not adequately represent the *in vivo* environment, there is increased reliance on experimental animal models in medical research, which are also not ideal, as there are substantial differences in biology between rodents and humans (Bracken, 2009; Perlman, 2016). Animal model experiments are time consuming, laborious and expensive. Development of diseases can significantly differ between humans and the artificial setting in animal models, where response to drugs can occur via different pathways and mechanisms are more difficult to explore (Bartel *et al.*, 2013; Page *et al.*, 2013).

Given these limitations, in recent years 3D cell culture technology (3D cell culture) has been developed (Heams, 2012). Cells obtained with this culture method are significantly different in morphology, proliferation, differentiation, gene expression and functional activity, and other aspects, compared to the cells from 2D culture, as demonstrated in Table 5.1 (Yeatts *et al.*, 2012 ; Shin *et al.*, 2013; Llorens *et al.*, 2015; Thoma *et al.*, 2014). 3D cell culture not only retains the foundation of material structure for a natural cellular microenvironment, but better simulates the *in vivo* microenvironment for cell growth as well (Zhang *et al.*, 2016). 3D culture therefore overcomes many of the deficiencies of 2D culture and *in vivo* experimentation and offers a more valid and reliable method.

Table 5.1. Comparison of key growth and functional characteristics of cells cultured using 3D versus 2D technologies.

Characteristics	2D cell culture	3D cell culture	Reference
Morphology	Cells in planar growth, showing spindle or flat round shape, adherent growth, and small nucleolus.	Cells grow in the 3D space and are irregular polygons or spheres, with layered growth, and large nucleolus.	Tit-Oon <i>et al.</i> , 2014
Cell junction	Most cells grow as a monolayer; a few cells aggregate.	3D network forms with large numbers of cell-matrix and cell-cell interactions. A large number of cells aggregate into clusters.	Roohani-Esfahani <i>et al.</i> , 2010
Gene expression and metabolism	Less secretory factors; generally lower expression of metabolic enzymes with different transcriptomic profiles as compared to those <i>in vivo</i> .	Enhanced expression of key growth factors and secretion of more key functional proteins.	Chitcholtan <i>et al.</i> , 2013 ; Leslie <i>et al.</i> , 2010; Becerra-Bayona <i>et al.</i> , 2012
Proliferation	Apoptosis begins after approximately 5 days if cells are not sub-cultured. However, depends on cell lines, they grow rapidly with less cell death	Longer-term proliferation potential, but some 3D models have a necrotic core due to hypoxia, so only outer cells grow	Thoma <i>et al.</i> , 2014; Llorens <i>et al.</i> , 2015; Yeatts <i>et al.</i> , 2012
Differentiation	Weak differentiation potential.	Greater differentiation potential.	Yeatts <i>et al.</i> , 2012 ; Shin <i>et al.</i> , 2013
Drug sensitivity	High sensitivity.	Low sensitivity.	Chetty <i>et al.</i> , 2013

At present, there is increasing experimental evidence that 3D culture of cells is more suitable

for screening anti-cancer drugs, and that such models are able to better predict the mechanism associated with tumorigenesis. In recent years, 3D cell culture techniques have been widely used in oncology, stem cell biology and organ reconstruction (Baker and Chen, 2012). For example, a 3D culture system was superior to the 2D culture system for study of the growth patterns, signal expression and metabolic status of endometrial cells (Chitcholtan *et al.*, 2013). Some signalling pathways (such as the STAT3 pathway), proteins (e.g. IL-6 in breast epithelial cells), and extracellular matrix are more active in 3D culture systems (Leslie *et al.*, 2010; Tit-Oon *et al.*, 2014). Furthermore, cells cultured in 3D demonstrate sensitivity to drugs that is more representative of the tumour cell sensitivity observed *in vivo* (Chetty *et al.*, 2013). Therefore, based on the current literature, it is believed that 3D culture is conducive to the study of cancer cells' growth and behaviour (Tit-Oon *et al.*, 2014).

Compared with monolayer culture, the main advantage of 3D culture is the ability to co-culture multiple cell types and matrices to simulate the formation of a tissue-like structure, with intercellular relations between cells and matrix (Tit-Oon *et al.*, 2014 ; Holton *et al.*, 2014; Kaisani *et al.*, 2014; van Zijl and Mikulits, 2010). The tumour microenvironment is complex containing a mixture of normal epithelial cells, highly heterogeneous malignant cells, stromal cells and extracellular matrix. Studies in the 1970s showed that tumorigenesis is closely related to its microenvironment and we now understand that signalling between cells and matrix and signals from stromal cells to cancer cells are an important aspect of tumour development (Verloes and Kanarek, 1976 ; Zhang *et al.*, 2015a). The components of the tumour microenvironment interact with the tumour cells to stimulate the proliferation and metastasis of tumour cells (Dvorak *et al.*, 2011). The growth of cells, specifically the direction of their development, is closely related to their microenvironment. Liver tumour cells in a 3D growth state are tolerant to treatment and their drug resistance characteristics are similar to solid tumours *in vivo* (Sakai *et al.*, 2012; Tsai *et al.*, 2012). Similarly, breast cancer MCF-7 cells grown in 3D scaffolds were more resistant to the endocrine therapy drug tamoxifen than

monolayer cultured tumour cells (Dhiman *et al.*, 2005). These studies all reflect that the microenvironment in which the tumour cells are located will significantly alter their response to drugs (Sakai *et al.*, 2012). Hence, due to the fact that many central cells in a 3D structure were unlikely to be as exposed as the periphery cells, 3D cell culture techniques can better support investigations into the relationship between the malignant phenotype of tumour cells and its microenvironment, while conventional 2D cell culture techniques cannot simulate the morphological characteristics of the tumour.

5.1.2 3D cell culture techniques

In the 1980s, Mina Bissell and William Ole Peterson from Lawrence Berkeley National Laboratory invented the 3D cell culture techniques whilst studying breast cancer. They found that normal mammary epithelial cells cultured in 3D assembled into acinar structures and established a *de novo* basement membrane (Baker and Chen, 2012).

From the research over the last 30 years, 3D culture technology has made tremendous progress. Currently, 3D cell culture techniques are generally divided into culture with scaffolds and culture without scaffolds. The main methods and their comparison are described in Table 5.2. The main scaffolds are collagen, and so the cost is relatively cheap and the technique is easy to operate compared to other techniques (e.g. Rotary cell culture system) (Breslin and O'Driscoll, 2013a; Kim, 2005). However, the scaffolds are still more expensive than other methods, such as hanging drop and overlaid culture techniques. The method based on scaffolds involves growth of cells in a scaffold, so the cells adhere to the scaffold fibre and divide to form a 3D structure (Mitsiades *et al.*, 2000; Tan *et al.*, 2011).

3D culture technique without scaffolds are achieved by physical methods. Although use of scaffolds is most popular, other non-scaffold approaches exist based on, for example, magnetic microcarriers, levitation or hanging drop plates. When the adhesion between the

cells is greater than the adhesion to the substrate, the cells can aggregate into a 3D structure that often appears as a spherical body (Fennema *et al.*, 2013; Weiswald *et al.*, 2015). Overlay culture requires the growth substrate to be covered with agarose, Matrigel or another collagen to prevent cell adhesion to the bottom of the culture plastic-ware (Yuhas *et al.*, 1977; Lin and Chang, 2010; Fennema *et al.*, 2013). This is the simplest system and often involves the tumour cell lines spontaneously aggregating into a globular structure, as previously demonstrated with breast cancer, prostate cancer and other tumour cells (Glinsky *et al.*, 2000; Kim, 2005; Page *et al.*, 2013). Interestingly, the growth rate, gene expression profile and proliferation of tumour cells in tumour spheroids are similar to solid tumour cells (Hsu and Huang, 2013; Lu *et al.*, 2012). In addition, as with the *in vivo* tumour microenvironment, there is a gradient of pH, nutrients and gas diffusion across the spheroid body (Kim *et al.*, 2011). Therefore, such 3D models represent improved systems for investigating the mechanisms underlying tumorigenesis.

Other more expensive methods include the use of gyratory and spinner flasks in a stirred tank or bioreactor. Such systems maintain the cell suspension in culture through the rotation of the impeller agitation and is conducive to nutrient transport and waste exclusion (Sutherland *et al.*, 1970; Kim, 2005; Montanez-Sauri *et al.*, 2015). Currently microcarrier systems that are used widely include liquid microcarriers, large well gelatine microcarriers, polystyrene microcarriers and PHEMA microcarriers (Hutmacher *et al.*, 2004). A rotary cell culture system (RCCS) is a bioreactor based on the simulation of the effects of microgravity that has been designed by The National Aeronautics and Space Administration (NASA). It is currently the most advanced 3D cell culture technique. RCCS has three main features namely a simulated microgravity environment; minimises turbulence and shear forces; permits gas exchange (Mitteregger *et al.*, 1999; Mattei *et al.*, 2018).

With increasing complexity, increasing cost and difficulty in preparation comes. Therefore, the choice of which system to use is dependent upon the cells and also the biological endpoints

to be investigated. For the purposes of the present study, an overlay culture system based on agarose-coated well-plate was selected to establish a 3D culture model for prostate cancer. This approach was utilised as it readily allowed investigation of many of the endpoints evaluated in earlier Chapters. Although the simpler hanging-drop method initially was trialled, this method failed to produce viable PC3 spheroids and thus further optimisation demonstrated the overlay culture system was more promising.

5.1.3 Aims

The aim of this chapter was to develop, optimise and characterise the growth of 3D prostate cancer spheroids, to provide a new model for evaluating aspirin's mode of action. To achieve this aim, the Chapter includes focus upon the following three key objectives:

- Establish an overlay culture system for the 3D culture of PC3 PCA cells, determine the optimal growth time that results in minimal necrosis in the centre of the models and the most appropriate dosing time frame;
- Evaluate the cytotoxic profile and the changes in *COX-2* expression profiles following exposure of 3D PC3 models to NaS, to enable direct comparison between 2D & 3D model response to the drug;
- Investigate NaS' impact on the NF- κ B pathway in both 2D and 3D systems.

Table 5.2. Advantages, disadvantages and examples of different 3D culture systems available.

3D culture system	Description	Advantages and disadvantages
Spontaneous cell aggregation	Cells aggregate spontaneously form in Hanging drop plates (petri dish).	Simple to utilise, but not all cell lines can form spontaneous aggregates. The method can also be used to co-culture two (or more) different cell populations simultaneously.
Overlay culture	Cells are cultured on pre-coated well plates to allow them to form spheroids.	Simple to establish if the adhesion between the cells is greater than the adhesion to the substrate. Used for example, it is applied to aggressive cancer cell lines, e.g. DU145 (prostate cancer cells) and MCF10.DCIS (breast cancer cells). It is also applicable for co-culture.
Gyratory and spinner flasks	Cells are cultured in stirred tank bioreactors and maintained with impellers.	Gyratory and spinner flasks are suitable for long-term culture/co-culture, and precise control of a number of physical and chemical parameters. The shearing forces are high, so it is easy to destroy the structure of a sphere.
Microcarrier beads	Cells are attached to microcarriers and then are applied to the culture medium with continuous agitation keep cells suspended.	Magnetic microcarriers are the most common application of this technique. It is easy to conduct co-culture. However, microcarriers' surfaces receive uneven fluid stresses and change with the movement and magnetic fields of suspended carriers. High expense.

Pre-fabricated engineered scaffolds	Cells are embedded in scaffolds to promote 3D growth characteristics. There are hydrogels, such as collagen scaffolds, and non-gel scaffolds, such as bioglass or bioceramic and porous metallic scaffolds.	They can promote growth or supplement regulatory factors and provide physical support to promote <i>in vivo</i> -like differentiation and transcriptional profiles of cells. This culture process is relatively simple, but the associated process is expensive. It can be applied to co-culture.
Rotary cell culture system (RCCS)	Cells are cultured in a bioreactor, which is able to simulate microgravity. This is the most advanced 3D culture system.	Cell clusters grow in microgravity. This offers the most realistic simulation and enables co-culture of a variety of cell types to form a complex 3D heterologous structure <i>in vitro</i> (both on earth or in space). However, it is the most expensive technique.
Organoids	One or a few cells derived from a tissue, embryonic stem cells or induced pluripotent stem cells, can self-organize in 3D culture.	The greatest advantage of organoids is that they can be derived from primary cells. However, the information they can provide is quite limited because organoids encounter supply problems (associated with success of organoid generation from harvested tissue) and donor variability. Organoids often consist of many types of cells.

5.2 Method and materials

5.2.1 Chemicals and kits used

The materials that have been used for all the experiments in this chapter are listed in Table 5.3.

Table 5.3 Chemicals and kits used in Chapter 5.

Chemicals	Manufacturer	Catalogue Number
Alexa Fluor [®] 488 Phalloidin	Thermo Fisher Scientific, UK	A12379
Chloroform	Sigma-Aldrich, UK	C2432-1L
Hoechst 33342	Sigma-Aldrich, UK	38733
miRNeasy Mini Kit	Qiagen, DE	217004
miScript II RT Kit (12)	Qiagen, DE	218160
Propidium iodide (PI)	Sigma-Aldrich, UK	P4170
Tris(4,7-diphenyl-1,10-phenanthroline)ru [ru(dpp)]	Santa Cruz, US	SC-213125

5.2.2 Cell culture

In this chapter, to avoid any interference from the culture media for imaging purposes, PC3 cells were cultured in Dulbecco's Modified Eagle's Medium (DMEM) without phenol red supplemented with 1% Glutamine, 10% FBS and 1% Pen / Strep. The cell line was incubated at 37°C, and 5% CO₂ in a humidified environment. All other techniques for tissue culture in 2D followed the protocols outlined in Section 2.4.

5.2.3 PC3 Spheroid fabrication and size determination

A total of 0.15 g agarose was dissolved in 10 mL of DMEM without phenol red media and autoclaved. All 96-well plates to be used were coated with 50 μL of 1.5% agarose. The coated plate can be used as soon as agarose is solidified. A concentration of 10,000, 20,000, 50,000 and 100,000 PC3 cells / cm^3 in 100 μL were seeded into each well of the agarose coated plates and incubated at 37 $^{\circ}\text{C}$, 5% CO_2 in a humidified environment. The standard PC3 cell culture medium was changed very gently every two days so as not to disturb the PC3 spheroids, by removing 50 μL of old medium and applying fresh 50 μL medium to the well. PC3 spheroids were cultured for up to 14 days depending upon the experimental requirements. The diameter of the PC3 spheroids were determined on an Axiocam ERc 5s Microscope (Zeiss) together with the software ZEN (blue edition) from Zeiss.

5.2.4 NaS dosing

A total of 0.16 g NaS was dissolved in 10 mL Tris-HCl resulting in a 0.1 M stock concentration of NaS, which was used for all subsequent dosing experiments.

5.2.5 RNA extraction, cDNA synthesis and RT-PCR

Total RNA was collected per the instruction of the manufacturer. The quantity and quality of all RNA samples were determined with a Nanodrop and they were stored at -80 $^{\circ}\text{C}$ until use, as described in Section 2.6. cDNA synthesis and RT-qPCR were conducted according to the methods in Section 2.7 and 2.8 respectively.

5.2.6 COX-2 expression analysis

COX-2 expression analysis was conducted as described previously in Section 3.2.4 and the housekeepers were *RPL-19* and *β-actin*. Their sequence as well as COX-2's can be found in Table 4.2.

5.2.7 miRNA extraction

Protocols followed here were described in manuals from the manufacturer. The miRNeasy Mini Kit is designed for purification of total RNA, including miRNA. PC3 cells in monolayer were seeded at 1×10^5 cell /cm³; the cells were harvested after 24 h of culture (monolayer cells) or on Day 1 to 7 (PC3 spheroids) by centrifuging at 300 x g. The cells were disrupted by adding 700 μL QIAzol Lysis Reagent (contained in the miRNeasy Mini Kit) using a pipette to mix, ensuring that no cell clumps were visible. Cells were then homogenized by vortexing for 1 min. The homogenate in the tubes were placed on the benchtop at room temperature (15–25°C) for 5 min to promote dissociation of nucleoprotein complexes. A total of 140 μL chloroform was added to the tubes containing the homogenate, the cap was applied securely, and the tube was shaken vigorously for 15 s. The tube was then placed on the benchtop for 3 min and centrifuged for 15 min at 12,000 x g at 4°C. After centrifugation, the tube was warmed up to room temperature (15–25°C) on the bench top. After centrifugation, the sample separated into 3 phases: an upper colourless aqueous phase containing RNA; a white interphase; and a lower red organic phase. The volume of the aqueous phase should be approximately 350 μL. The upper aqueous phase was transferred to a new collection tube (supplied) and 1.5 volumes (usually 525 μL) of 100% ethanol was added and mix thoroughly by pipetting up. Without any delay, 700 μL of the sample, including any precipitate was transferred into an RNeasy Mini spin column in a 2 mL collection tube (supplied) and centrifuged at 8000 x g ($\geq 10,000$ rpm) for 15 s at room temperature (15–25°C). The flow-through was discarded. This centrifugation was repeated once. A total of 700 μL Buffer RWT (supplied) and 30 mL ethanol (96%–100%) was

mixed with the buffer) was added to the RNeasy Mini spin column and centrifuged for 15 s at 8000 x g ($\geq 10,000$ rpm) to wash the column. The flow-through was discarded. A total of 700 μ L Buffer RPE (supplied and 44 mL ethanol (96% - 100%) was mixed with the buffer) was added to the RNeasy Mini spin column and centrifuged for 1 min at 8000 x g ($\geq 10,000$ rpm) to wash the column. The flow-through was discarded. Another 700 μ L Buffer RPE was added to the RNeasy Mini spin column and centrifuge for 1 min at 8000 x g ($\geq 10,000$ rpm) to wash the column to dry the RNeasy Mini spin column membrane. The RNeasy Mini spin column was replaced with a new 1.5 mL collection tube (supplied). A total of 30 μ L RNase-free water was added directly onto the RNeasy Mini spin column membrane and centrifuged for 1 min at 8000 x g ($\geq 10,000$ rpm) to elute the RNA. Quantification of the sample concentration and purity was determined with a Nanodrop. The ratio of the readings at 260 nm and 280 nm (A_{260}/A_{280}) provides an estimate of the purity of RNA, with a ratio between 1.9 and 2.1 considered acceptable. RNA was stored in aliquots at -80°C until use and was freeze-thawed no more than twice.

5.2.8 cDNA synthesis

miScript II RT Kit (12) was used for cDNA synthesis. The miScript kit uses total RNA that contains miRNA as the starting material for cDNA synthesis, and separate enrichment of small RNA is not needed. Template RNA, 10x miScript Nucleics Mix, RNase-free water, and 5x miScript HiSpec Buffer were thawed on the ice. The reverse transcription master mix was prepared on ice according to Table 5.4.

Table 5.4. Reverse transcription reaction components.

Component	Volume/reaction (μL)
5x miScript HiSpec Buffer	4
10x miScript Nucleics Mix	2
miScript Reverse Transcriptase Mix	2
Template RNA	$\frac{1000 \text{ ng}}{\text{concentration of RNA (ng/}\mu\text{L)}}$
RNase-free water	The waster was added to make up to 20 μL of solution
Total	20

The tube was mixed gently, then it was briefly centrifuged and stored on ice. The tube was incubated for 60 min at 37 °C followed by an incubation for 5 min at 95 °C to inactivate the miScript Reverse Transcriptase Mix. Next, the tube was placed on ice and 200 μL RNase-free water (supplied) was added to dilute the 20 μL reverse transcription reaction. The 220 μL diluted cDNA was dispensed into 5 aliquots (44 μL each) and transferred to a -20 °C freezer.

5.2.9 miRNA RT-PCR

Real-time miRNA PCR was run on a CFX Connect™ Real-Time PCR Detection System with the miScript SYBR® Green PCR Kit. All samples were performed in triplicate template cDNA, 2x QuantiTect SYBR Green PCR Master Mix (contained in the kit), 10x miScript Universal Primer (contained in the kit), primers and RNase-free water (contained in the kit) were thawed on ice. With the reagents above, the master mix was prepared. The recipe is listed in Table 5.5.

Table 5.5. Reaction setup for real-time PCR.

Component	Volume (μL) / reaction
2x QuantiTect SYBR Green PCR Master Mix	12.5
10x miScript Universal Primer	2.5
Primers (<i>hsa-miR-210</i> , <i>RNU48</i> or <i>hsa-miR-191-5p</i>)	3
RNase-free water	4.5
Template cDNA	2.5
Total volume	25

Primers (Table 5.6) were ordered from MystiCq[®] microRNA qPCR Assay Primer (Sigma-Aldrich): *hsa-miR-210* and values for miRNA were finally normalized to expression levels of housekeeping gene miRNA gene *RNU48* and *hsa-miR-191-5p*.

Table 5.6. Primers for mRNA RT-qPCR.

Primer	Sequence	Annealing temperature / $^{\circ}\text{C}$
<i>hsa-miR-210</i>	CUGUGCGUGUGACAGCGGCUGA	55
<i>RNU48</i>	AGUGAUGAUGACCCCAGGUAACUCU GAGUGUGUCGUCUGAUGCCAUCACCG CAGCGCUCUGACC	55
<i>hsa-miR-191-5p</i>	CAACGGAAUCCCAAAGCAGCUG	55

miR-210 is one of the most frequently identified hypoxia responsive microRNA genes (Devlin *et al.*, 2011). The stem-loop structure sequence of *miR-210* is located in the intron of the non-coding RNA that is transcribed from the AK123483 gene on the 11p15.5 locus on chromosome (Huang *et al.*, 2010). *miR-210* is regulated by HIF-1 α and Hypoxia-inducible factor 2 α (HIF-2 α). HIF-1 α binds directly to the 400-bp hypoxia response element upstream of the promoter of *miR-210* (Huang *et al.*, 2010; Huang *et al.*, 2009). In addition to HIF, NF- κ B is also able to bind

to κ B binding site about 200bp upstream of the *miR-210* promoter, inducing the up-regulation of *miR-210* (Zhang *et al.*, 2012). It has been confirmed the expression of *miR-210* under hypoxia can be induced in many cell lines, such as breast, head and neck, lung, colon, and renal cancer cell lines (Kulshreshtha *et al.*, 2007).

When the master mix was prepared, template cDNA was dispensed and mixed with the master mix thoroughly and then added to the plate. The plate was sealed with film and centrifuged at 1000 g at room temperature to remove bubbles. The real-time cycler was programmed as follows: the sample was initially incubated at 95 °C for 15 min to activate the HotStarTaq DNA Polymerase, followed by 40 cycles of 15s-denaturation at 94 °C, annealing and extension steps were conducted at 55 °C and 70 °C respectively for 30 s each and finally, a melt curve analysis was performed by successively increasing the temperature from 50 to 95 °C at the ramp rate of 0.5 °C/s. Finally, data were analysed using $2^{-\Delta\Delta Ct}$ method performed by the CFX Manager software coming with CFX Connect™ Real-Time PCR Detection System.

5.2.10 MTT assay

The MTT ((3-(4,5-Dimethylthiazol-2-yl)-2,5-diphenyltetrazolium bromide) assay was used for cell viability assessment. MTT is a tetrazolium salt that is transformed to purple formazan granules in live cells when the formazan is dissolved in DMSO. The absorbance readings at an excitation of 590 nm are directly proportional to the number of live cells in the sample.

A total of 100 μ L medium was removed from the well firstly, and PBS was used to wash the PC3 spheroids twice. When washing the plate, medium was pipetted off carefully and 100 μ L PBS was slowly added. Cells were then incubated for 4 h with 100 μ L MTT solution diluted to 1 mg / mL in PBS. Next, each well was washed with PBS twice after the MTT solution was removed. The formazan was then dissolved by removing the PBS solution and replacing it with

100 μ L DMSO. The plate was placed into a spectrometer and the absorbance read at 590 nm using a micro-plate reader (POLAR star Omega, BMG Labtech, UK). In addition to the test samples, blank wells without cells were included, and negative control wells included cells treated with Tris-HCl in the absence of NaS. Cell viability = $\frac{A_s - A_b}{A_c - A_b} \times 100\%$, where A_s is the optical density of the sample, A_b is the optical density of the blank wells, and A_c is the optical density of the control wells. All samples were performed in triplicate.

5.2.11 Cell culture for imaging purposes

Cell culture followed the methods in this Section 5.2.2 and 5.2.3. However, when PC3 spheroids were cultured for confocal microscopy analysis, 15 μ -slide angiogenesis plates (ibidi, DE) were used instead of 96-well-plate. All wells in the 15 μ -slide angiogenesis plate were coated with 10 μ L of 1.5% agarose. A 50 μ L aliquot of PC3 cell suspension at concentration of 50,000 cells / cm^3 were seeded into each well of the agarose coated plates and incubated at 37 $^{\circ}\text{C}$, 5% CO_2 in a humidified environment. The standard PC3 cells culture DMEM medium was changed very gently every two days so as not to disturb the PC3 spheroids, by removing 25 μ L of old medium and applying fresh 25 μ L medium to the well. PC3 spheroids were cultured for up to 7 days. All samples were performed in replicates.

5.2.12 Confocal microscopy

PC3 spheroids cultured for up to 7-days were stained with Hoechst 33342 (Sigma-Aldrich, UK) and propidium iodide (PI, Sigma-Aldrich, UK) for live-dead cell imaging. Hoechst and PI are both DNA stains, but PI can only enter the nuclei of dead cells. In order to identify the formation of potential lumen structures, phalloidin was used as a cell body stain; it binds to F-actin. Oxygen bioavailability in 3D PC3 spheroids was assessed with Tris(4,7-diphenyl-1,10-phenanthroline) ruthenium (II) dichloride complex (Ru(ddd)) dye, when oxidised loses its fluorescence.

The PC3 spheroids were imaged on a confocal microscope (Zeiss LSM 710, Germany) and its imaging software (ZEN) was utilised to acquire the images.

PC3 spheroids were incubated with Hoechst and PI for live / dead imaging for five minutes. A concentration of 10 $\mu\text{g}/\text{mL}$ was used for both stains. A DAPI filter and TRITC filter were applied to view the Hoechst and PI signals respectively.

For structural spheroid imaging, PC3 spheroids were stained with Hoechst and phalloidin for 4 h at 37°C. The Hoechst concentration was 10 $\mu\text{g}/\text{mL}$. Phalloidin staining was achieved by following the instructions of the manufacturer. The vial contents were dissolved in 1.5 mL methanol. On each day from day 1 to day 7, the PC3 spheroids were washed with PBS at room temperature twice and then fixed with 4% paraformaldehyde (PFA) at room temperature for 15 min. The PFA was washed off three times with PBS. Then 0.1% Triton X-100 was applied to the cells in PBS for 5 minutes at room temperature. Cells were stained with 6.6 nM Alexa Fluor® 488 Phalloidin for cell body outline (1 μL into 1000 μL PBS) for 2 h and then 10 $\mu\text{g}/\text{mL}$ Hoechst (nuclei stain) was added to the wells for 20 min. Three representative images were taken for each sample. DAPI and FITC filters were utilised to view the Hoechst and phalloidin signals respectively in order to examine the structure of spheroids.

To explore oxygen bioavailability, the PC3 spheroids were cultured in 1×10^{-4} μM Ru(ddd) containing culture medium for 4 h at 37°C. Bright field and the TRITC filter were applied to view the outline of the PC3 spheroids and O_2 when oxygen availability was observed. All experiments above were performed in replicates.

5.2.13 Western blots

After the PC3 spheroids has been allowed to grow for 3 days, they were treated with NaS for either a 2h or 30 min period as required prior to protein extraction and quantification as described in Section 2.12 and 2.13 respectively. Western blotting was performed according to the methods described in Section 2.14 accordingly. Antibodies used were the same as those described in Section 4.2.8. All experiments above were performed in triplicates.

5.2.14 Statistical analysis

Shapiro-Wilk test confirmed the normal distribution if the $p \geq 0.05$. All data expressed are the mean of 3 independent experiments (\pm SD). The T-test was used for the difference in growth of spheroids over 7 days in Section 5.3.1.2. A one-way ANOVA was used to test significance for all other assays applied in this Chapter. If variance is homogeneous ($p > 0.05$), the LSD *post hoc* test was applied; otherwise, the Dunnett's T3 *post hoc* test was utilised. Data were considered significant if $p > 0.05$.

5.3 Results

To explore the effects of aspirin in a model system that more closely represented the *in vivo* situation, an optimised novel 3D spheroid system needed to be developed and characterised. The PC3 cells took on a spheroid format when cultured in agarose coated plates that prevented them from adhering to the bottom of the culture flask. In addition to determining the optimal seeding density, the length of time that they remained viable for had to be established. Finally, the difference in cytotoxicity, COX-2 gene expression, and NF-κB pathway were compared in PC3 spheroids against the same cells grown in 2D monolayer format.

5.3.1 Evaluation of spheroid growth and viability over time

5.3.1.1 Size changes in PC3 spheroids according to seeding density over time

The impact of seeding density on PC3 spheroid growth were explored by establishing the cultures with 10,000, 20,000, 50,000 and 100,000 cells / cm³ as illustrated in Figure 5.1. Among the four groups of spheroids, the size was dependant on seeding density. Their growth was evaluated over 7 days. During this period, the spheroid diameter declined significantly from 1,392.601 μm on day 1 to 1,089.456 μm on day 7 when the PC3 spheroids were seeded at concentration of 100,000 cells / cm³ ($p=0.017$). However, there was a roughly 9 μm-decrease in PC3 spheroids seeded at 10,000 cells / cm³, about 20 μm-decrease at 20,000 cells / cm³ and approximate 5 μm-decrease at 50,000 cells / cm³, none of which were significant ($p>0.05$).

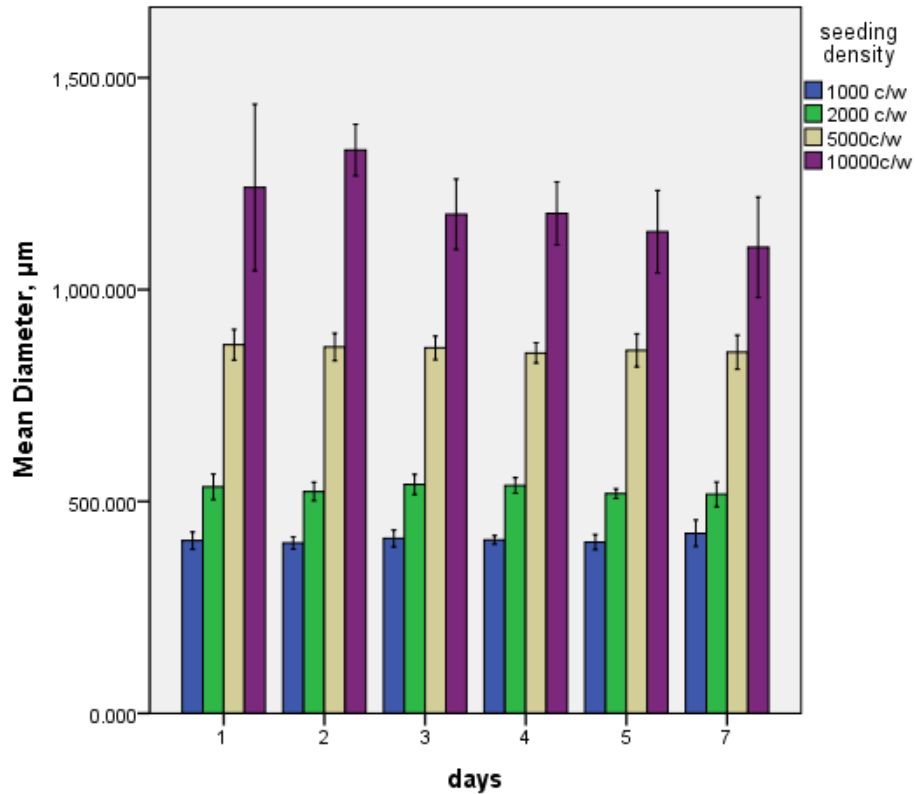


Figure 5.1. Variation in diameter of PC3 spheroids over a 7-day culture period. Horizontal axis is the indicated culture time while the Y-axis shows the mean spheroid diameter. Error bars represent standard deviation (SD) (n=3).

5.3.1.2 PC3 spheroid viability

The MTT assay measures the metabolic activity of PC3 spheroids in 3D culture. MTT readings are thus positively correlated with number live cells. For 3D culture, the maximal reading was 0.5 approximately while the maximal of 2D culture was 2 using arbitrary units. Overall, for cells grown in 2D, the cells grew exponentially with similar growth rates and an S-shaped growth curves. In contrast, the 3D models had a slow growth rate as compared to standard 2D cultured cells. In PC3 spheroids seeded at 50,000 cells / cm³, the viability of the PC3 cells was maintained over a 5-day period and then dropped substantially from day 7. The PC3 spheroids seeded at 100,000 cells / cm³ had a similarly high initial cell number to those seeded at 50,000

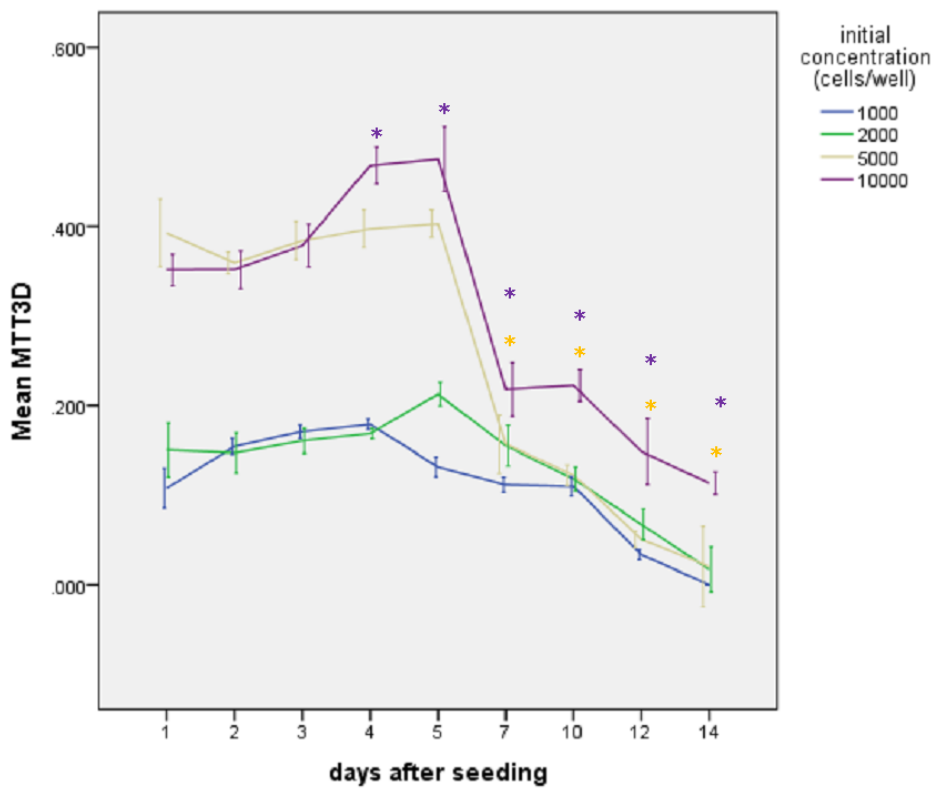
cells / cm³, but exhibited some growth between Day 3 to 5, followed by a sharp drop in viability from Day 7. PC3 spheroids seeded at 10,000 and 20,000 cells / cm³ demonstrated little drop in viability over time, but there was nearly half the number of viable cells in these spheroids as compared to those with a starting seeding density of 50,000 cells / cm³. Based on this data, either the 50,000 or 100,000 cells / cm³ seemed the best concentration for seeding and it was clear the spheroids could not be used beyond 7 days given the increasing degree of cell death noted after this point.

5.3.1.3 Evaluation of necrosis in PC3 spheroids

Combined Hoechst and propidium iodide (PI) staining were used to assess the level of necrosis in the middle of the PC3 spheroids over time using a confocal microscopy approach. The complete series of z-stack videos are located in Appendix 5. Figure 5.3 presents the comparison between the first day of culture, the 3rd day, the 7th day and the 12th day at all seeding densities trailed and they clearly demonstrate the increase in necrosis over time within the PC3 spheroids. More PI staining indicates cell death allowing uptake of the stain into the cells.

From the 1st to 3rd day, 10,000 cells / cm³, 20,000 cells / cm³ and 50,000 cells / cm³ PC3 spheroids showed fewer dead cells at the bottom and the middle of the cellular structure as compared with the 100,000 cells / cm³ spheroids. With respect to Figure 5.2, 10,000 and 20,000 cannot offer sufficient live cells. Therefore, PC3 spheroids with an initial concentration of 50,000 cells / cm³ were finally selected for all further stages of work given the high necrosis demonstrated in the spheroids that were seeded with 100,000 cells / cm³ (Figure 5.3).

A)



B)

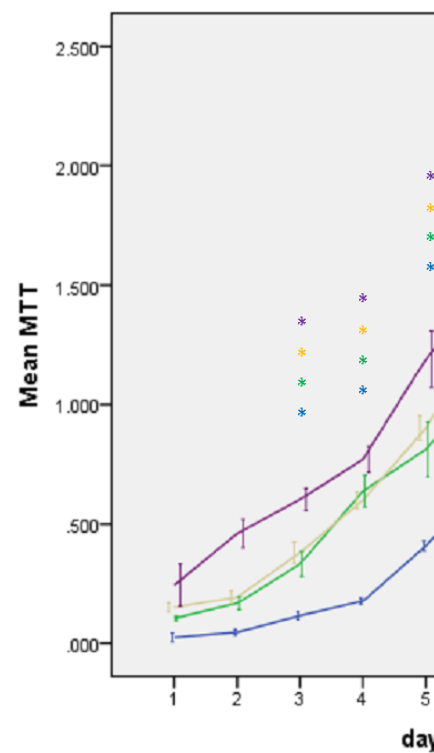


Figure 5.2. Cell viability of PC3 spheroids and 2D monolayer cell culture over time. A, Line chart presenting MTT assay results for live PC3 cells number cultured in 2D. Error bars indicates +/-SD. The Y-axis shows the mean MTT Absorbance at 550nm. Asterisks indicate the viability on Day 1 where $p < 0.05$, as determined by a T-test ($n=3$). Purple *, yellow *, green * and blue * are corresponding to spheroid concentrations of 10,000 cells / cm^3 respectively.

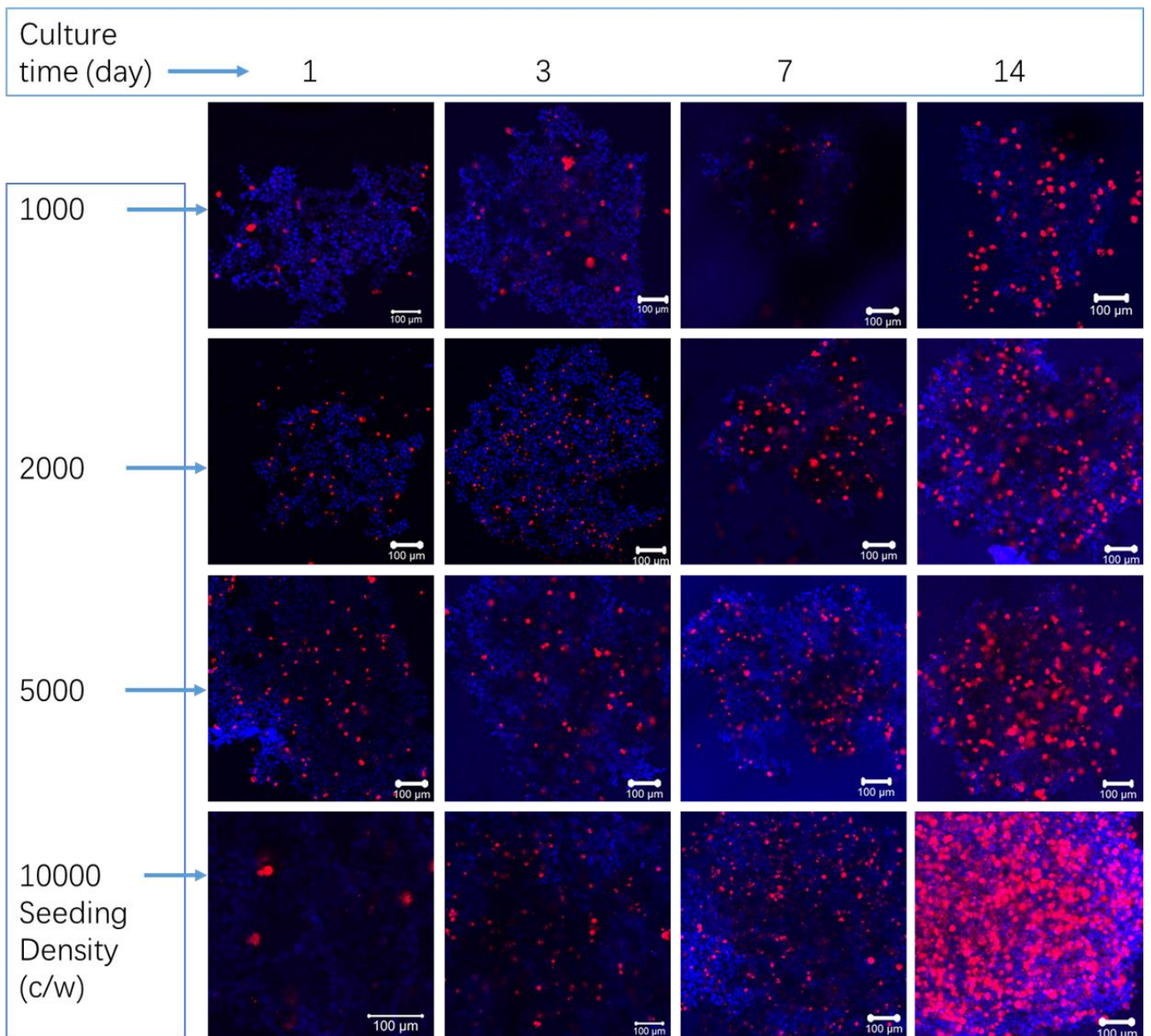


Figure 5.3. Confocal imaging comparing live cells and dead cells between the first day of culture and the 12th day at differing starting seeding densities. Blue indicates the live cells (Hoechst) and red represents the dead cells (PI). Scale bar: 100 μm .

5.3.2 Cell survival analysis of PC3 cells grown as spheroids

5.3.2.1 Oxygen availability analysis

Oxygen availability was monitored with Ru(ddd). The z-stack images can be found in Appendix 5. These “Z stacks” are generated by several images taken by a focal drive incrementally stepping through a sample. For the first three days there was no notable change in the degree of red stain within the PC3 spheroids, indicating no limitation in oxygen content in the centre of the 3D structures. However, as culture continued beyond day-3, increasing hypoxia was evident as indicated by the increasing degree of red stain present within the PC3 spheroids from the 4th day of culture (Figure 5.4).

5.3.2.2 *miR-210* expression

As the Ru(ddd) experiment indicated it was likely that the PC3 spheroids were developing a hypoxic core over time, *miR-210* gene expression was subsequently measured to further investigate this effect. *miR-210* is a gene expressed when hypoxia exists (Devlin *et al.*, 2011).

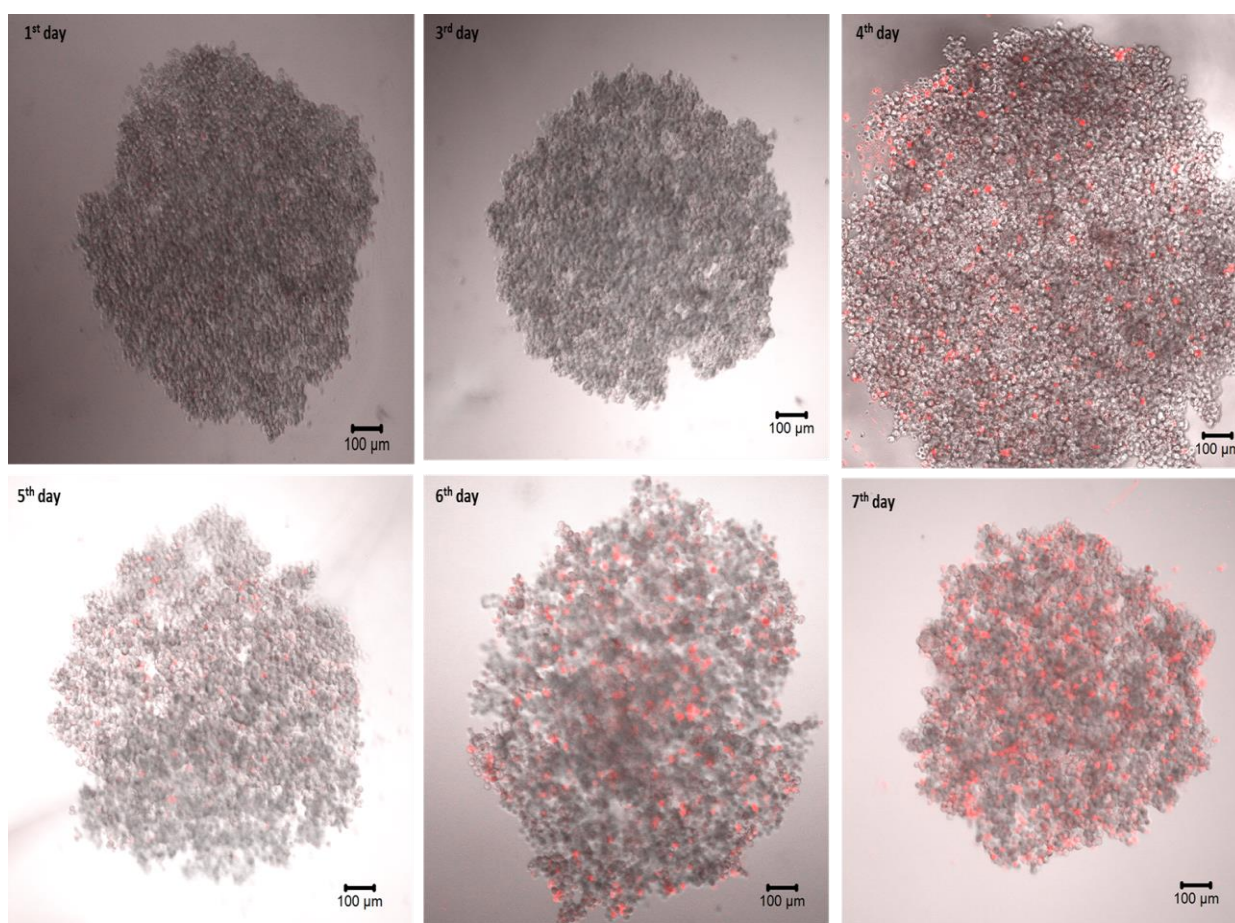


Figure 5.4. Images of oxygen availability in PC3 spheroids over 7 days of culture. The scale bar represents 100 μm . The presence of hypoxia was represented by the red Ru(ddp) signal observed in the images from Day 4. This is not serial imaging of the same spheroid, but instead is representative example images of separate PC3 spheroids taken on each day. N.B. for higher resolution of the images and the scale bar, please refer to the images in Appendix 5.

The *miR-210* gene expression over a 7-day period in PC3 spheroids and PC3 cells cultured in 2D is illustrated in Figure 5.5. Comparing to PC3 cells in 2D, there were no significant changes in the gene expression on Day 1 and Day 2 ($p > 0.05$). However, from the third day, *miR-210* expression levels in the PC3 spheroids increased significantly in a time-dependent manner. Comparing to Day 1, *miR-210* expression was 1.7-fold higher on Day 3 in the PC3 spheroids, but was significantly (7-fold) higher by Day 4 ($p < 0.05$). From day 6 the *miR-210* expression levels dropped substantially, but this was likely due to the increased necrosis occurring in the

centre of the spheroids by this time period.

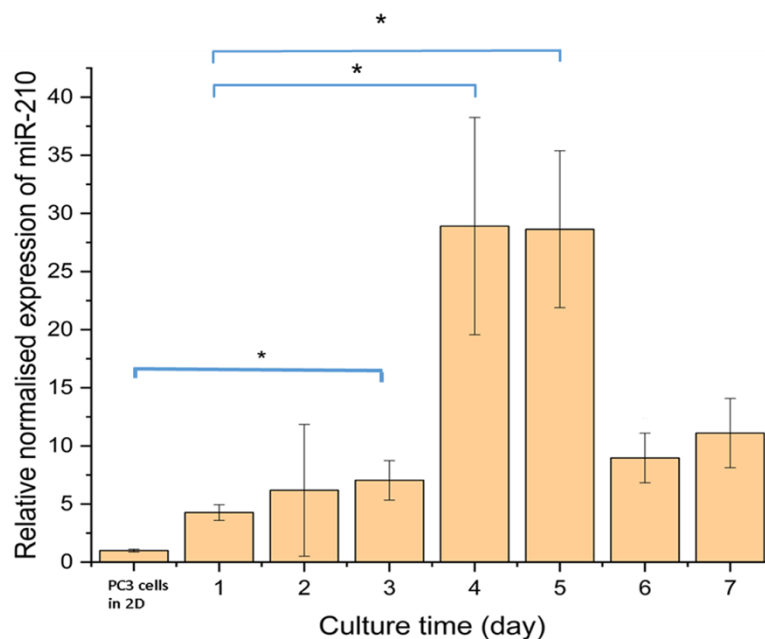


Figure 5.5. *miR-210* gene expression in PC3 spheroids over 7 days of culture. *, indicate significance compared to the viability in either PC3 cells cultured in 2D or on Day 1 of 3D spheroid culture where $p < 0.05$, as determined by a one-way ANOVA and the *post hoc* LSD ($n=3$). Error bars indicate SD. Note: *miR-210* expression in PC3 cells in 2D were measured after 24 h of culture.

5.3.3 Structural analysis of PC3 spheroids

In order to more clearly understand the structural formation of the 3D spheroid by the PC3 cells, they were stained with Hoechst and phalloidin and evaluated by confocal microscopy as illustrated in Figure 5.6. This imaging analysis demonstrated the spheroids were composed of a dense structure with clear cell-cell contacts. However, over time, it was noticeable that, lumen-type structures appeared to form in the PC3 spheroids (Fig 5.6B). The number of lumens in the core or periphery developed per spheroid were scored per day of culture in three replicate samples; in total 15 spheroids were analysed for lumen formation per sample

group. On the first day, 2.9% of PC3 spheroids were found with lumen structure. This increased to 61.8%, 97.2% and 99.1% of PC3 spheroids with luminal structures on days 2, 3 and 4 respectively indicating maturity of the spheroids over time.

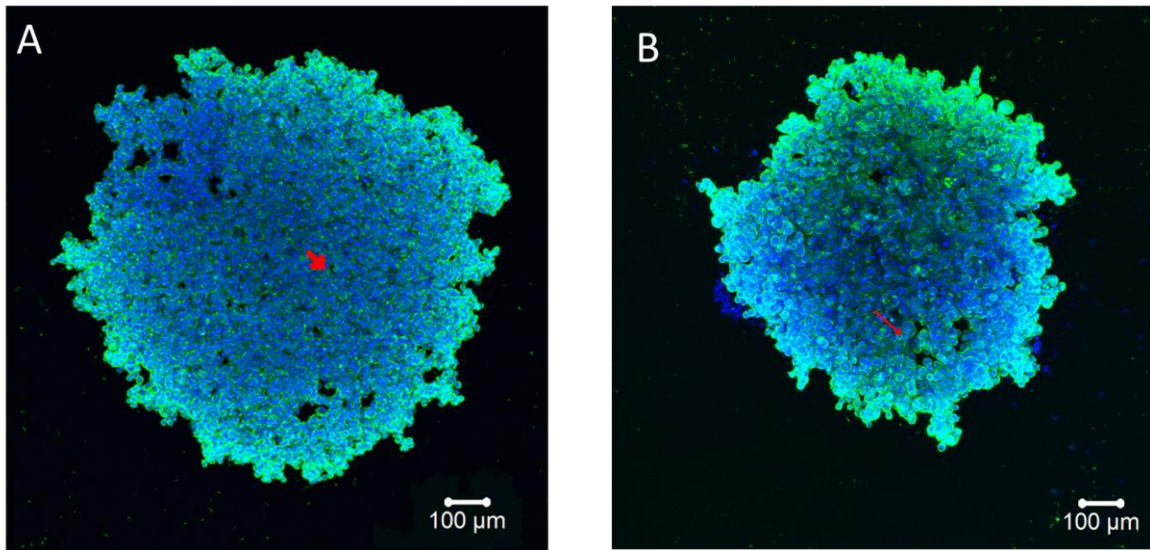


Figure 5.6. Morphological evaluation of PC3 spheroids. A. Spheroid lacking a luminal structure (image taken on day 1 of culture); B. Spheroid containing a lumen as indicated by the red arrow (image taken on day 7 of culture). Images were stained by Hoechst (blue) and phalloidin (green). Scale bars in these images are 100 μm .

5.3.4 Profile of *COX-2* gene expression in 3D PC3 spheroids over time

As the 3D PC3 spheroids mature with time, their *COX-2* expression profile during their growth needed to be established over 7 days of culture in order to compare the response to NaS in 3D against 2D culture. As illustrated in Figure 5.7, the *COX-2* expression levels in the PC3 spheroids were substantially higher than that of the same cells cultured in 2D. All the PC3 spheroids had at least a two-fold increase in *COX-2* expression compared with that of cells cultured in 2D. However, PC3 spheroids cultured for 3- 4 days had the highest expression of

COX-2 compared to PC3 grown in monolayer culture with a 2.5 - 3-fold- increase ($p < 0.0001$). Although a significant difference in COX-2 gene expression levels was noted between the cells grown in 2D versus 3D format, there was no significant change in COX-2 expression levels across the 7-days of culture.

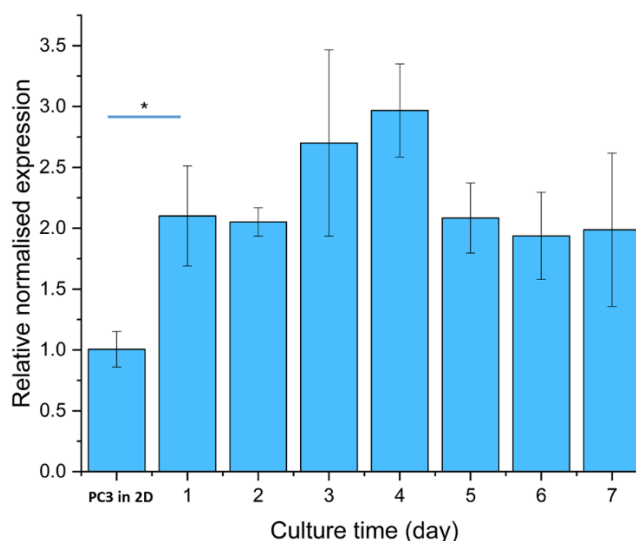


Figure 5.7. Profile of COX-2 gene expression in 3D PC3 spheroids compared to PC3 cells in 2D culture. All the expression is normalised to the expression of PC3 in 2D culture. *, indicate significance compared to the viability on Day 1 where $p < 0.05$, as determined by a one-way ANOVA and the *post hoc* LSD ($n=3$). Note: The COX-2 in PC3 cells were extracted after 24 h of culture.

5.3.5 NaS effects on cell viability in 3D PC3 models as compared to 2D monolayer cultures

In order to compare the difference in response of PC3 spheroids to NaS versus PC3 cells grown in 2D, the MTT assay was utilised to measure cell viability of PC3 cells grown in both 2D and 3D spheroid format. PC3 cells and PC3 spheroids were seeded at 50,000 cells / cm^3 . After 72 h (3 days) of incubation, PC3 monolayers (2D) and spheroids (3D) were treated with NaS at concentrations ranging from 2 to 10 mM for 24h and then the MTT assay was conducted to

evaluate cell viability. As illustrated in Figure 5.8, in 2D culture, a dose dependent decrease in cell viability was observed with the first significant reduction in viability arising at 2 mM, and with 10 mM NaS resulting in a significant 50% reduction of cell viability ($p < 0.001$). The PC3 cells grown in spheroid format were in contrast far less sensitive to toxicity induced by NaS with very little reduction in cell viability over the dose range applied. A significant reduction in viability was not observed until the higher doses of 8 and 10 mM were applied, which reduced cell viability by approximately 6.7% and 8.4% respectively ($p = 0.009$ and 0.005). This data clearly demonstrated that when PC3 cells are grown in spheroid format, they are far more resistant to the cytotoxic effects of NaS than when the same cell type is grown as a 2D monolayer.

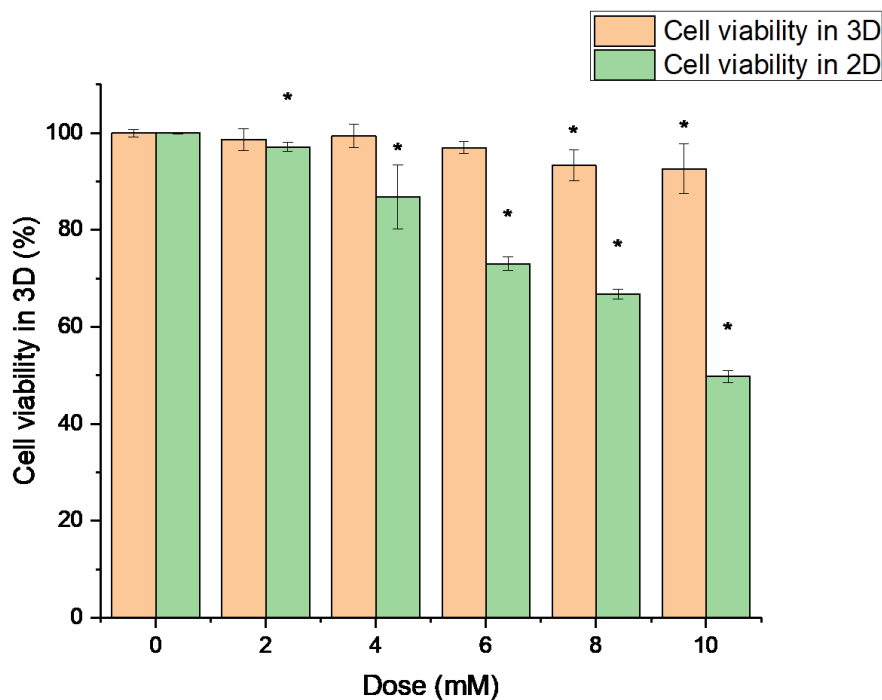


Figure 5.8. Cell viability of PC3 in 3D culture vs. 2D culture when cells and spheroids were treated with NaS. Viability measures were made after treatment on day 3 of culture. *, indicate significance compared to negative control, where $p < 0.05$, as determined by a one-way ANOVA and the *post hoc* LSD ($n = 3$). Error bars represent SD.

5.3.6 NaS effects on the NF- κ B pathway in 3D PC3 cultures

5.3.6.1 Purity check for contamination of cytoplasmic extracts in nuclear extracts in PC3 spheroids

p65 is a subunit of the NF- κ B pathway and the amount of nuclear p65 is positively linked to the activity of the pathway. If the pathway is active, p65 will be released from I κ B and enters the nucleus. In order to study nuclear p65 of NF- κ B pathway, the purity of nuclear extracts should be established and thus this quality control was undertaken in the present study. In Figure 5.9, α -tubulin was only expressed in the cytoplasmic extract, which were obtained from PC3 spheroids treated with 2 mM NaS for 2 h. In contrast, no α -tubulin expression was present in any of the nuclear extracts, demonstrating their purity.

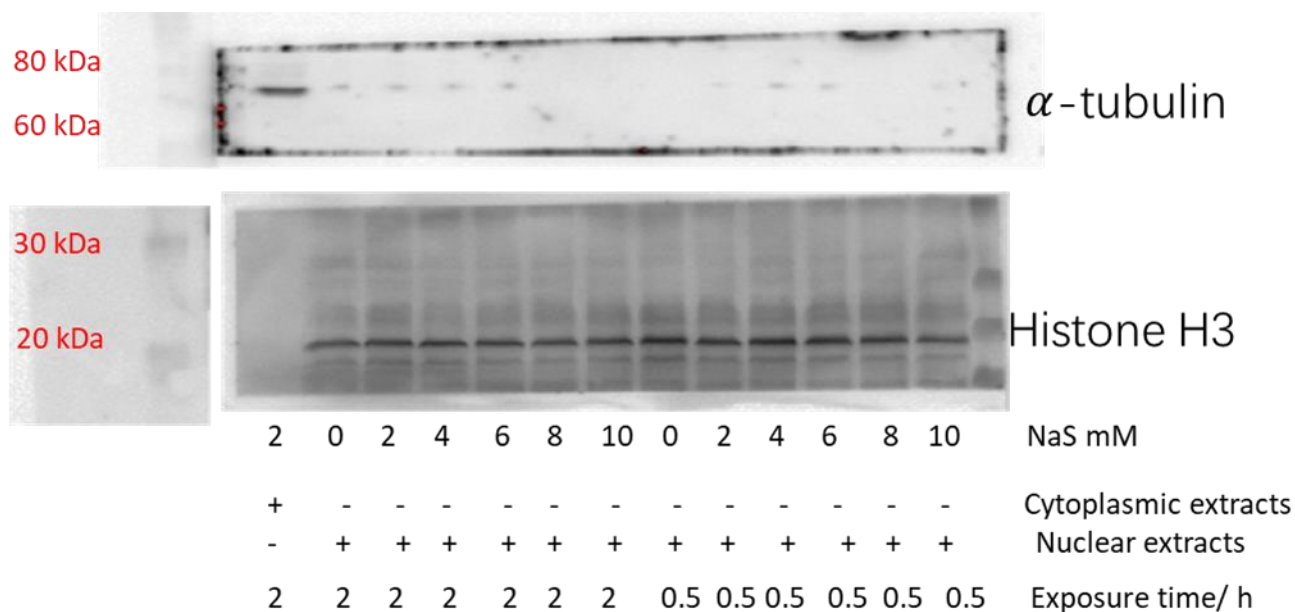


Figure 5.9. α -tubulin expression in nuclear extracts of PC3 spheroids to detect contamination of cytoplasmic extracts. The blots here are representative examples. First lane is the cytoplasmic extracts and the rest of the lanes were loaded with nuclear extracts.

5.3.6.2 Profiling of nuclear p65 and cytoplasmic *I κ B α* expression following 3D PC3 spheroid treatment with NaS

Following the purity check for contamination of cytoplasmic extracts in nuclear extracts in PC3 spheroids, nuclear p65 and cytoplasmic *I κ B α* expressions were then profiled. However, TNF- α did not increase nuclear p65 level as constitutive expression was high in PC3 cells according to the previous results in Section 4.7.2.2. Hence, there was no need to pre-treat the PC3 spheroids to activate the NF- κ B pathway. Thus, NaS induced effects on the abundance of nuclear p65 and cytoplasmic *I κ B α* were then investigated after PC3 spheroids or PC3 cells in 2D were treated with NaS or with Tris-HCL alone as the negative background vehicle control. As demonstrated in Figure 5.2 and Figure 5.3, there was not many dead cells in the cores on the day the proteins were collected. Example western blots of the resultant experimental outputs are illustrated in Figure 5.10. In the quantitative data demonstrated in Figure 5.11, as the concentration of NaS was increased with a 30min exposure time, *I κ B α* and p65 expression remained the same; but the 10 mM indeed reduced nuclear p65 and increased the level of *I κ B α* in the cytoplasm. When spheroids were treated with NaS for 2 h, the top doses (8 and 10 mM) resulted in a significant increase of *I κ B α* expression ($p < 0.05$), which were both 1.3-fold higher than the vehicle control respectively. Additionally, the higher doses (8 and 10 mM) of NaS significantly reduced nuclear p65 expression, with fold change of -0.60 ($p < 0.05$) and -0.52 ($p < 0.05$) respectively.

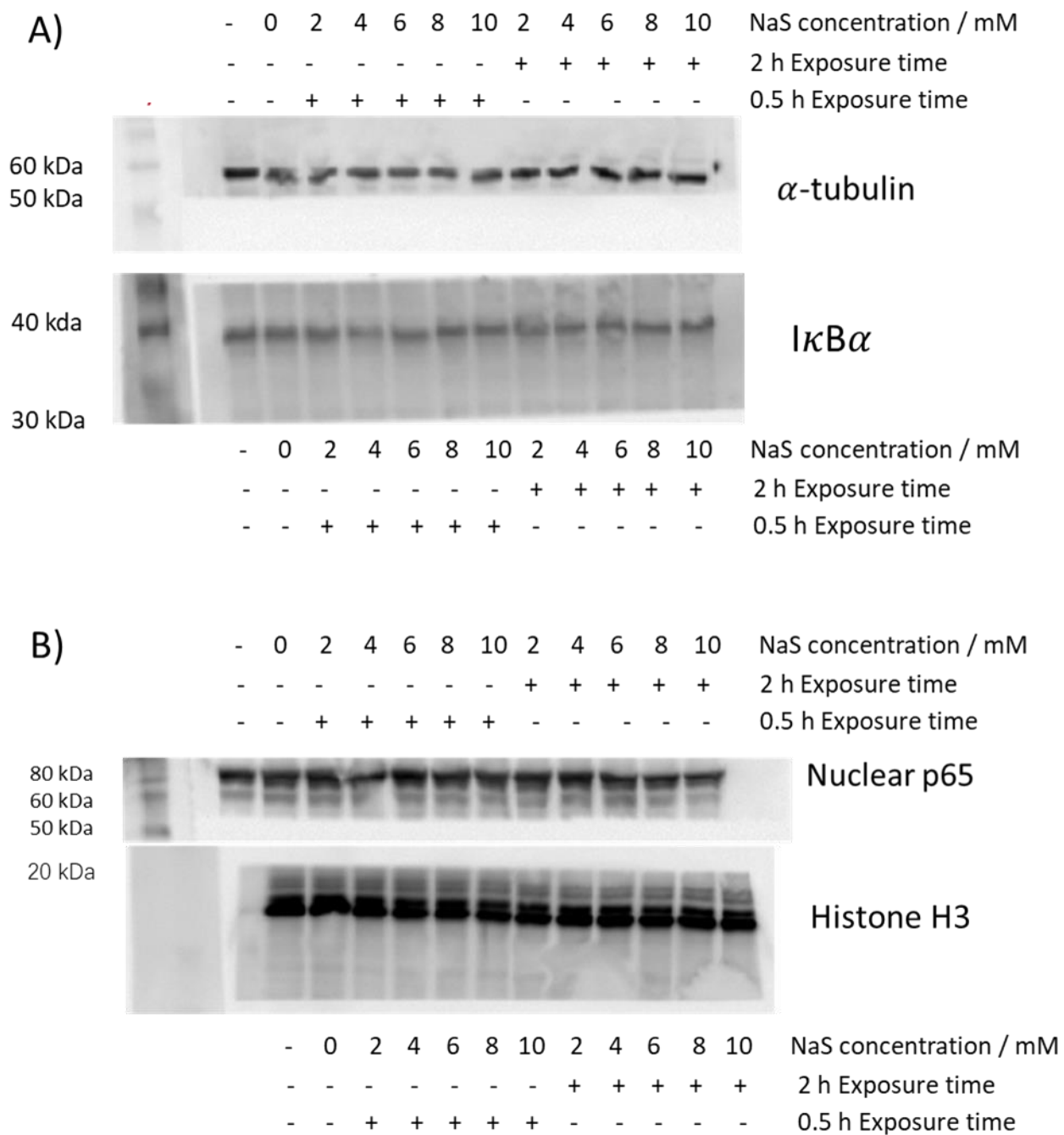


Figure 5.10. Examples of a representative western blot of A) cytoplasmic $I\kappa B\alpha$ expression, and B), Nuclear p65 in PC3 spheroids treated with NaS.

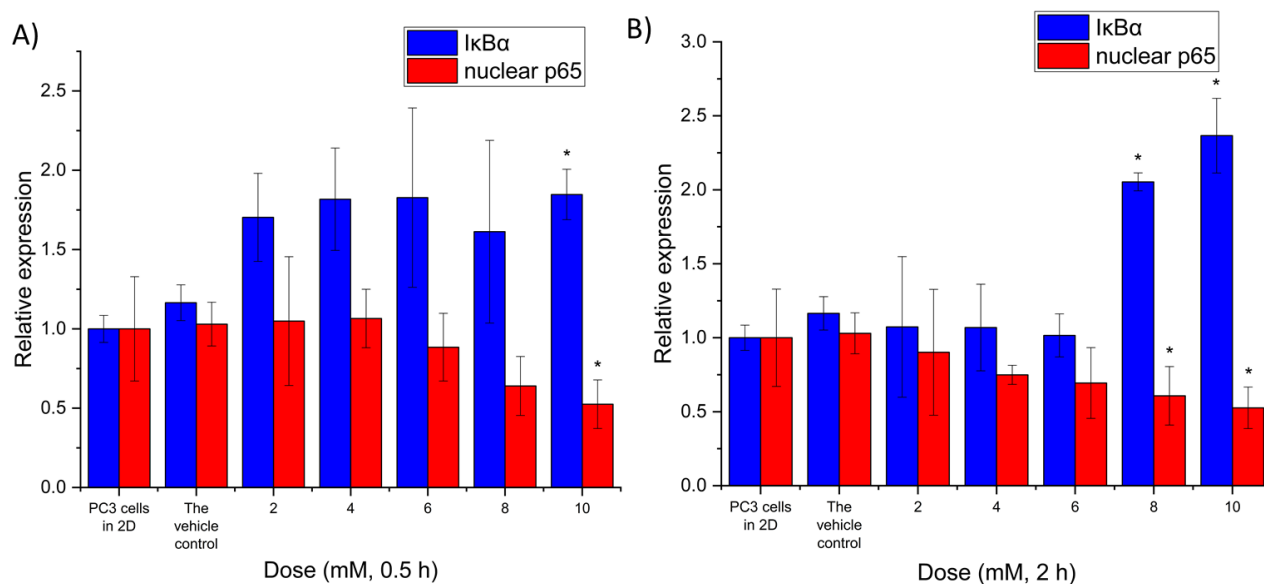


Figure 5.11. Nuclear p65 and cytoplasmic *IκBα* expression in PC3 spheroids treated with NaS. Relative expression of nuclear p65 and cytoplasmic *IκBα*, which was densitometry based on ‘adjusted volume’. A) NaS exposure time was 0.5 h and B) the time was 2 h. *, indicate significance compared to the control, where $p < 0.05$, as determined by a one-way ANOVA and the *post hoc* LSD ($n=3$). Both A and B have the same control as these experiments were conducted in simultaneously. Error bar indicates SD.

5.3.7 NaS effects on *COX-2* expression in 3D PC3 spheroids compared to 2D PC3 culture

COX-2 gene expression in PC3 spheroids was investigated following NaS exposure for 24 h. Spheroids were seeded at 50,000 cells / cm³ and treated with NaS on the 3rd of culture. One day later, total RNA was harvested from the spheroids for measurement of *COX-2* expression by RT-qPCR. As demonstrated in Figure 5.12, it was noticeable that the PC3 spheroids had 1.5-fold higher *COX-2* expression levels than that of PC3 cells in 2D ($p < 0.001$). Both PC3 cells from 2D culture or 3D culture had higher *COX-2* expression than in PNT2 cells grown in 2D ($p < 0.001$).

In addition, there was a 2-fold change in *COX-2* gene expression between PC3 cells in 2D and the PC3 spheroids ($p < 0.001$).

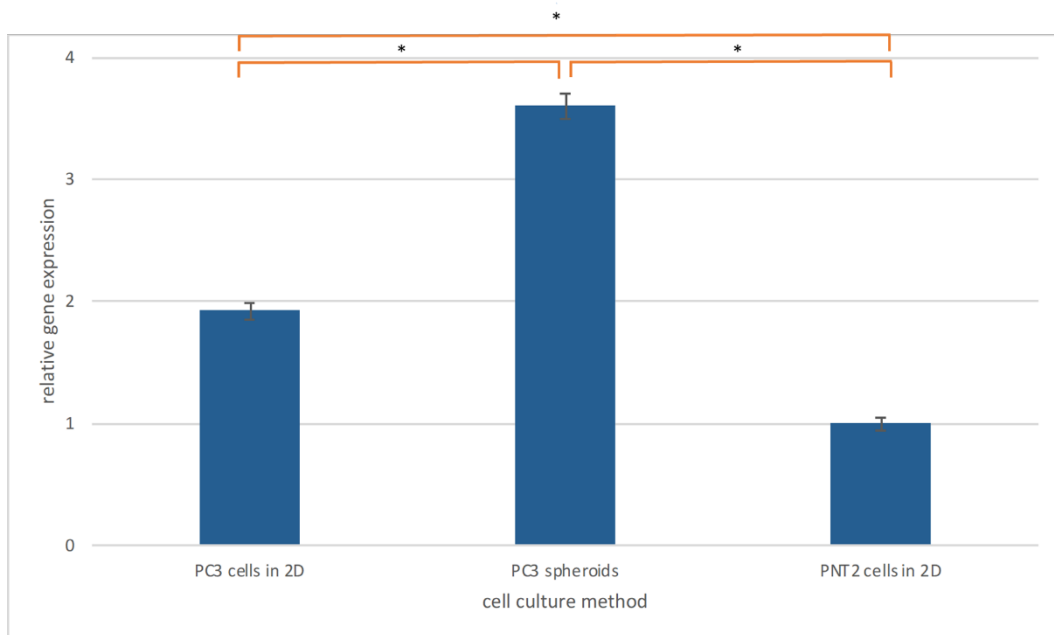


Figure 5.12. Baseline analysis for *COX-2* gene expression levels in PC3 spheroids, PC3 cells in 2D and PNT2 cells in 2D. *, indicate significance where $p < 0.05$, as determined by a one-way ANOVA and the *post hoc* LSD ($n=3$). Error bars represent SD.

Once the base-line levels of *COX-2* expression were established in the 3D PC3 spheroid models, they were then exposed to NaS for 24h and the *COX-2* expression levels determined again. As illustrated in Figure 5.13, NaS had little effect on the expression profile of *COX-2* in the spheroids, until the top 10 mM dose, where there was a reduction of roughly 3-fold in *COX-2* gene expression ($p=0.001$).

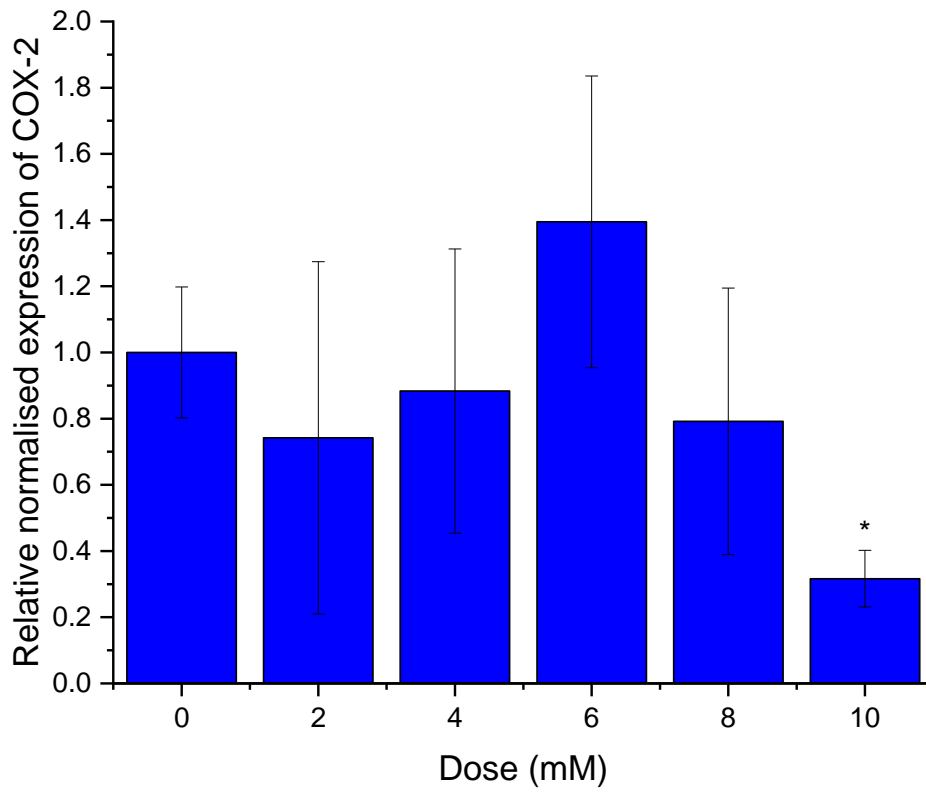


Figure 5.13. Effect of NaS exposure on COX-2 gene expression levels in PC3 spheroids. *, indicate significance compared to the control, where $p < 0.05$, as determined by a one-way ANOVA and the *post hoc* Dunnett's T3 ($n=3$). Error bars represent SD.

5.4 Discussion

In this chapter, the aim was to develop a new test system to explore the potential mode of action of aspirin in a more realistic cell model. Thus, a 3D PCA spheroid model was developed, optimised and characterised for its growth, structure, and profiles of *COX-2* gene expression and NF- κ B pathway activation with/without NaS treatment. In this study, 3D culture of prostate cancer cells (PC3) was based on agarose pre-coated 96-well plates. Agarose is a linear polysaccharide extracted from algae which demonstrates biosafety (non-cytotoxic) and histocompatibility (Jeon *et al.*, 2005). It is rich in resources, so is low cost. Cell adhesion is strongly reduced by agarose that forms a stiff inert hydrogel, which prevents the cells from adhering to the plastic-ware and instead forces them to aggregate together (Amedee *et al.*, 1994; Strobel *et al.*, 2018).

When this system was being monitored, it was found that the size of spheroids fabricated was linked to the seeding density. The 50,000 cells / cm³ was decided as initial seeding concentration. At this starting concentration of cells, the spheroids' viability reached a peak by the 4th day of the culture and after this point, increasing necrosis and hypoxia was found in the core of the PC3 spheroids, with it being most notable from day 7. Lumens were formed by the 3rd day of culture, indicating functionality and maturation of the PC3 spheroids. Interestingly, the 3D structure promoted elevated expression of *COX-2* as compared with conventional monolayer culture, with consistently high expression over 7 days of culture. For the NaS treatment regime, it was established that dosing had to be conducted by no later than day 4 as this allowed sufficient time for formation of a mature spheroid, while still ensuring the spheroids were viable for the experimental period. Finally, NaS' effects on growth, *COX-2* expression profiles, and the NF- κ B pathway in the 3D PC3 models were investigated. The

outcome of these investigations confirmed the anti-cancer effects of NaS, but they were not as prominent as noted when PC3 cells cultured in 2D were exposed to NaS (Chapter 4).

5.4.1 Rationale for selection of seeding density and dosing time point

Currently, *in vitro* drug-sensitivity experiments generally use traditional monolayer culture, while the target of the drug *in vivo* is usually a solid tumour with a 3D organizational structure. Heterogeneity of tumour cells are very well understood (Singh *et al.*, 2016; Breslin and O'Driscoll, 2013), where a wide range of interactions are known to occur between different cell types, matrix and cells, cells and media, and cell and gravity. Therefore, the growth status of monolayer cultured tumour cells is not very representative of the *in vivo* situation; tumour cells grown in 3D *in vitro* culture are however better able to simulate the real situation, to improve our understanding of tumour biology and drug's efficacy with less reliance on animal testing (Hosseinkhani, 2012; Breslin and O'Driscoll, 2013b; Edmondson *et al.*, 2014).

In this study, when single cell suspension was inoculated into the coated-96-well plate, cells in each well aggregated and fused with each other and then spontaneously formed tumour spheroids in a short time (less than 24 h). This method to fabricate spheroids can produce them with similar consistency, whereas spinner flasks, NASA rotary system and hanging drop methods tend to generate spheroids with variation in size and shape (Singh *et al.*, 2016). As illustrated in Figure 5.1, the size of the PC3 spheroids seeded at 50,000 cells / cm³ was usually consistent ($\pm SD \leq \sim 10\%$) across Day 1 to Day 5, which is important for obtaining reproducible results in any further research work using the test systems (Singh *et al.*, 2016). The non-homogeneity in relation to spheroid sizes can result in inconsistency such as in the tumour cell microenvironment, including variation in nutrient/oxygen gradients, hypoxia and metabolic

stress (Gong *et al.*, 2015). Consequently, these could affect the models' response to drugs and its biological behaviour (Singh *et al.*, 2016). The 3D *in vitro* model generation method utilised in the present study has also been demonstrated by others to be more promising in mimicking the *in vivo* environment to screen for drug efficacy (Gong *et al.*, 2015).

In this chapter, the purpose for establishing the optimal seeding density was complimentary and supported the rationale for selection of starting seeding concentration as well as the window for exposures. MTT assay results confirmed that cell viability of spheroids seeded at 50,000 cells / cm³ and 100,000 cells / cm³ was optimal until the 7th day of culture. This was supported by confocal microscopy with Hoechst and PI, where necrosis in the core of PC3 spheroids increased dramatically after the 7th day in spheroids seeded at 50,000 cells / cm³, while the 100,000 cells / cm³ spheroids exhibited substantial necrosis from day 4. This data supported the use of 3D models generated using a 50,000 cells / cm³ seeding density. In our culture model, by the 3rd day of culture, 97% PC3 spheroids were found with one or two lumens. This formation is based on generation of a functional lumen driven by the cellular machinery (Fatehullah *et al.*, 2013). The lumens within the prostate is filled with fluids of the organ secreted by surrounding epithelial cells. Although a distinguished lumen space or gland might be difficult to see in tissues with higher Gleason score, lumens have been seen as a target of treatment. Drugs such as aspirin or other anti-inflammatory drugs are thought to be more effective in treating prostate cancer if they are able to reach and stay in the lumens within the prostate for a sufficient period of time (Nelson *et al.*, 2012). Thus, the formation of these structures in the spheroids was particularly pertinent and exposure to NaS was designed to occur after the 3D models had matured sufficiently to form these lumens. When *COX-2* base-line gene expression levels were investigated in the spheroids, it was roughly 2-fold-

higher than the *COX-2* levels PC3 cells grown in 2D, although there was no difference amongst spheroids from Day 1 to 7 of culture. The reason for the difference could be the microenvironment (Taddei *et al.*, 2013). To sum up, the optimal seeding density for the 3D PC3 spheroids was 50,000 cells / cm³ and they were treated on the 3rd day of culture.

5.4.2 Oxygen availability in spheroids

The O₂ availability inside the PC3 spheroids was determined by Ru(ddd) staining followed by confocal microscopy-based imaging. It was found that an increase in fluorescence signal occurred in the core of PC3 spheroids from the 4th to 7th day of culture (Figure 5.4, and Z-stack images can be found in Appendix 5). As Ru(ddd) staining is not quantitative, this data was supported by an RT-PCR approach to evaluate the expression levels of *miR-210*. Which also confirmed that *miR-210* gene expression was upregulated by the 4th day of culture ($p=0.02$).

We mainly consider the following reasons for the drop-in cell viability and increased necrosis with increasing time of 3D culture growth: lack of oxygen, nutrition, and accumulation of metabolites in the core of the PC3 spheroids. Our results show that the live cell number in the 3D environment gradually increased in the initial stage, and the number of live cells decreased as the incubation time prolongs while the size decreased. This decrease in diameter is likely due to the formation of tightening cell spheres coupled to necrosis in the core over time. Thus, this study demonstrates that the PC3 cancer cells located in the outermost layer of the PC3 spheroids were live and were able to proliferate, but with time, the PC3 spheroids became more compact and the centre of the 3D structure began to experience hypoxia. This coupled to an inadequate supply of nutrients in the centre of spheroids result in the cells within the core becoming quiescent, and eventually necrotic, which has also been observed in the scientific literature (Ma *et al.*, 2012). This is very similar to the microenvironment in tumour

tissue *in vivo*, especially during the pre-angiogenesis stage of tumorigenesis. Cancer cells in the centre of tumours suffer from hypoxia and inadequate supply of nutrients and oxygen, and metabolic waste cannot be discharged rapidly (Parks *et al.*, 2017). The local microenvironment is not suitable for cancer cells' survival. Cells grow slowly or even become necrotic. However, tumour cells at the junction of tumour tissue and normal tissue grow actively, indicating the dependence of cancer cells on adjacent non-neoplastic cells (Hamilton, 1998; Tarin, 2012). In many solid tumours, hypoxia is common and is closely associated with tumorigenesis. Figure 5.3 shows PI-positive (dead) cells in the central core and live cells at the periphery. This distribution of live and necrotic cells in this chapter are therefore representative of solid tumours *in vivo*.

5.4.3 Response of PC3 spheroids to NaS

The efficacy and behaviour of NaS was compared between the 3D PC3 models and the response of the same cells cultured in 2D. In this study, the MTT assay was utilised to investigate NaS' effects on PC3 cell growth. The top aspirin doses (8 and 10 mM) significantly reduced cell viability in PC3 spheroids by 6.7% and 8.4% respectively ($p=0.049$ and 0.048), while a lower dose of 4mM caused a 13% reduction of viability in 2D culture ($p<0.001$). Thus, compared with 2D cultured cells, PC3 cells grown in a 3D spheroid format were less sensitive to NaS. This correlates with other reports in the literature where cell lines such as the ovarian carcinoma cell lines (including 1847^{AD}, FUOV1, and OV2008), hepatocarcinoma (HepG2) and prostate cancer (PC3 and LNCaP) demonstrate an increase in drug resistance in 3D culture environment, where the degree of differentiation of the tumour cells is more similar to the tumour tissue (Lee *et al.*, 2013; Fitzgerald *et al.*, 2015; Xu *et al.*, 2013b; Lv *et al.*, 2017). It should however be noted that where viability was reduced in the 3D models, it generally was

marginal. For example, in Figure 5.8, at 10 mM dose, viability was only slightly reduced at $92 \pm 5.09\%$. Although, statistically this was significant, the p value was 0.048; thus, it only just reached statistical significance and is unlikely to be biologically significant given this minor reduction in viability at the top 10 mM dose.

It has been argued that the experimental results of drug susceptibility testing in a 3D culture environment can more truly reflect the drug efficacy *in vivo* and is therefore an important tool for *in vitro* efficacy studies to minimise the requirement for *in vivo* testing (Lee *et al.*, 2013). The mechanism underlying the increased tolerance to drugs in 3D culture systems is not yet clear, but this has drawn wide attention. It has been reported in the literature that it may be related to the different gene expression profiles in 3D culture (as compared to the same cells in a 2D environment), hypoxia (which is more representative in 3D culture and rarely happens in 2D unless a specialist incubator is utilised) and more *in vivo* like interaction with extracellular matrix components in 3D culture (Liu *et al.*, 2015b).

In the present study, the MTT assay was selected to evaluate cytotoxicity. This assay is based on reduction of MTT to formazan in the living cells' mitochondrial dehydrogenase (such as succinate dehydrogenase) while the dead cells are not capable of this. In the present Chapter, NaS was found to reduce the viability of PC3 cell spheroids by approx. 10% using the MTT assay. It is however important to note that in Chapter 3, NaS was found to disrupt mitochondria at doses of 8 and 10 mM in PC3 cells. It is therefore difficult to determine if the reduced viability is a direct cause of mitochondrial loss or if another pathway involved in promoting cytotoxicity could be involved. Mitochondria disruption is an early event in apoptosis (Yasugi *et al.*, 2002; Tait and Green, 2013; Carlson *et al.*, 2014). In the future, it would be useful to further evaluate the cytotoxicity pathways involved using other supportive assays

that are not reliant on mitochondrial fidelity. For example, investigation of the caspase pathways by both western blots and ELISA together would be an alternative. The trypan blue assay is another option to explore apoptosis but this method is more time intensive.

In the current study, varying transcriptional profiles and greater hypoxia in the 3D tissue mode are also likely to be responsible for the differences in response to NaS for PC3 spheroids vs. PC3 cells in 2D. However, the influence of these factors when comparing the specific mechanism underlying the difference between 2D vs 3D models remains to be further explored. Additionally, it is important to note that the 3D model utilised here only consists of a single cell type and so does not completely reflect the *in vivo* microenvironment where multiple cell types communicate with each other. This could also be very important in governing the impact of NaS exposure and its potential anti-cancer properties. Further investigation in this area could involve the development of co-culture 3D models. For example, PC3 cells could be co-cultured with hFOB 1.19 osteoblast cells in 2D and in 3D on pre-coated plates or collagen scaffolds simulating the bone microenvironment (ratio 1:1 or as determined by optimisation). Then the response of these co-cultures to NaS could be evaluated to understand its impact on the response to NSAIDs.

5.4.3.1 Aspirin effects on NF- κ B pathway in 3D culture

The activation of NF- κ B plays an important role in the development of tumours. It is known that NF- κ B activation is closely related to tumour formation, angiogenesis, distant metastasis, anti-apoptosis and chemoresistance (Pikarsky *et al.*, 2004). Aspirin anti-inflammatory activity has been reported to function through inhibition of NF- κ B and COX-2 (Liu *et al.*, 2008; Shi *et al.*, 2017). Additionally, aspirin is thought to constrain the activity of NF- κ B and via this

mechanism, potentially repress the growth of prostate cancer cells *in vitro* and *in vivo* (Liao *et al.*, 2015).

As the NF- κ B pathway is activated constitutively in PC3 cells, the PC3 spheroids were not treated with TNF- α as a pre-treatment to activate the pathway as is often required in *in vitro* studies (Garg *et al.*, 2012). To investigate the effect of aspirin on NF- κ B signalling in a 3D environment and to compare the effects with the 2D environment, the NF- κ B activity was explored in this investigation using western blots measuring nuclear p65 and cytoplasmic I κ B α when PC3 spheroids were treated with NaS. As a result, it was found that in the 3D environment, I κ B α expression was increased after 2-h's exposure to 8 and 10 mM NaS ($p < 0.05$) as well as the 0.5h's exposure to 10 mM NaS, while p65 expression was decreased by 8 and 10 mM NaS 2h exposures ($p < 0.05$) and 0.5-h-exposure of 10 mM NaS. It should however be acknowledged that western blots are semi-quantitative and so statistical analysis of this data has limitations. For example, in Figure 5.10, there appeared little difference in nuclear p53 expression, but when densitometry analysis was applied, as illustrated in Figure 5.11, nuclear p65 expression was significantly reduced at 0.5 h for 10 mM NaS and at 2 h for 8 and 10 mM NaS. This significance was borderline and given the limited visual difference in the western blot itself, this outcome should be interpreted with caution. Thus, in order to corroborate this result, further experimentation using alternative techniques that are less subjective than western blotting is required. One option for future work is to use an ELISA approach to evaluate down-stream protein expression levels that are key targets for the NF- κ B pathway, such as IL-1 β in relation to metastasis, as found in Chapter 3. This would provide additional supportive data for the activation of the pathway in response to NaS. CHIP would also be a useful technique to more specifically determine the activity of the p65 protein

binding to relevant genes in order to demonstrate if the reduction of *COX-2* gene expression is directly related to regulation of NF- κ B.

When NF- κ B is activated, the *I* κ B kinase (IKK) promotes phosphorylation of *I* κ B α utilising ATP. This results in *I* κ B α degradation, releasing p65 from the p50-*I* κ B complex, thus promoting p65 nuclear entry. There is evidence that aspirin inhibits the activity of the NF- κ B signalling pathway through blocking IKK- β . Aspirin or NaS is able to directly bind IKK β and IKK loses the ability to bind ATP; therefore, the kinase activity of IKK is inhibited (Gamble *et al.*, 2012). As a result, phosphorylation activity of *I* κ B α is attenuated (Shi *et al.*, 2017). Therefore, following the NaS treatment, more *I* κ B α in cytoplasm was detected, preventing release of p65 and its nuclear entry. The evidence therefore indicates that NaS is able to suppress the activation of NF- κ B in the 3D PC3 spheroids and the mechanism is summarised in Figure 5.14.

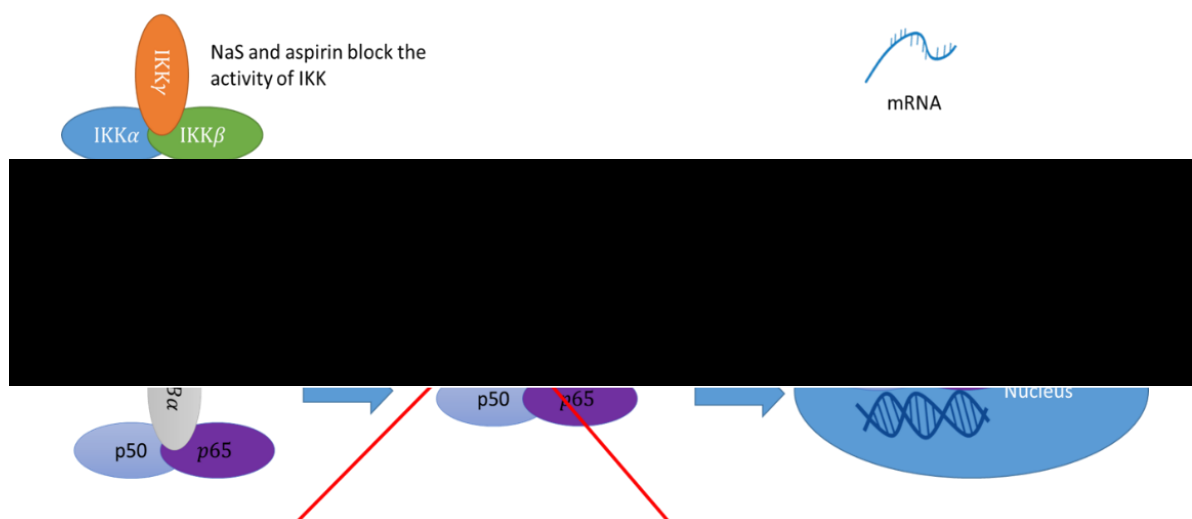


Figure 5.14. Schematic representation of NF- κ B suppression due to NaS treatment. NaS suppression blocks the phosphorylation of IKK, therefore, the dimer p50-p65 cannot be released. Finally, there will no p50-p65 to enter the nucleus. Source: Xia *et al.*, 2014; Imani Fooladi *et al.*, 2012.

There are several publications in the scientific literature that suggest aspirin or NaS are able to suppress the NF- κ B pathway. However, no reports have explored this connection in 3D culture models; thus, the data generated in the present study is highly novel. When aspirin was exposed to other PCA cell lines including DU145 and LNCaP, a strong reduction in activation of NF- κ B was reported (Shi *et al.*, 2017; Bilani *et al.*, 2017). Activity of I κ B kinase (IKK)- β was firstly weakened and then they also found that phosphorylation of I κ B α , as well as translocation of NF- κ B p65 to the nucleus was suppressed following aspirin treatment (Shi *et al.*, 2017). The study of the inhibition of NF- κ B by NSAIDs *in vivo* and *in vitro*, indicates that the effect of NSAIDs on NF- κ B, cell proliferation and immune activation are potential factors for preventing malignant transformation (Chattopadhyay *et al.*, 2010). Nitric oxide-aspirin reduces NF- κ B protein levels, while aspirin also inhibits the growth of HT-29 human colon cancer cells (Chattopadhyay *et al.*, 2010). A reduction in NF- κ B activity has also been observed in a range of cell lines following aspirin treatment including U2OS and MG63 osteosarcoma cells, colorectal cancer cells and colon cancer cells (Liao *et al.*, 2015; Chen and Stark, 2017; Pathi *et al.*, 2012). It should be noted that all the results cited above were obtained in monolayer culture systems. As mentioned earlier, 3D culture is often able to offer increased resistance to drugs, thus, it is probable that if those experiments were carried out in 3D culture models, the effects observed may have been weakened.

5.4.3.2 Aspirin effects on COX-2 expression in 3D compared to 2D culture

COX-2 is overexpressed in prostate cancer, which can promote the proliferation of prostate cancer cells, and inhibit the apoptosis of prostate cancer cells (Liao *et al.*, 2015). COX-2 also promotes the angiogenesis, metastasis, and infiltration of cancer cells including breast cancer cells and prostate cancer cells (Gan *et al.*, 2016; Rajabi and Mousa, 2017). As COX-2 plays an

important role in the development of prostate cancer, *COX-2* inhibitors also play a role in the treatment of prostate cancer (Wang *et al.*, 2012; Mutter *et al.*, 2009). To better understand the potential mechanisms underlying aspirin's potential anti-cancer effects in PCA, we treated the 3D cultured PC3 spheroids with NaS and observed their sensitivity to the drug, as compared to PC3 cells cultured in a monolayer. The baseline analysis of *COX-2* gene expression for 2D versus 3D results in this chapter showed that PC3 in 3D culture had higher levels of *COX-2* mRNA than that of the traditional monolayer cultures. These results are in agreement with Sha *et al.* where they also reported that *COX-2* expression is elevated in 3D prostate cancer models (Sha *et al.*, 2013). They established a 3D culture model based on DU145 cells and found that *COX-2* expression was 9 fold-higher in DU145 spheroids after 3 days of culture than DU145 cell grown in 2D (Sha *et al.*, 2013). The reason for the difference between 2D and 3D expression patterns of *COX-2* is speculated to involve microenvironmental signals of necrosis in the core that may also orchestrate gene expression changes in the tumour cells (Sha *et al.*, 2013; Ma *et al.*, 2012). *COX-2* expression levels did not increase when a monolayer culture method was used to grow DU145 cells in glucose-free DMEM medium or in a hypoxia environment; however, when DU145 cells were co-cultured in a 2D environment with the core of necrotic DU145 cells, the *COX-2* expression level was indeed increased (Sha *et al.*, 2013). Therefore, the increased expression of *COX-2* in 3D environment may be related (in part) to the central necrosis cells.

When NaS was exposed to PC3 spheroids, only the 10 mM NaS dose was found to cause a significant reduction in *COX-2* mRNA levels ($p=0.005$, in Figure 5.13). This is linked to the MTT assay results where 8 and 10 mM NaS caused significant loss of cell viability (Figure 5.8). These results are consistent with a study where celecoxib treatment in *COX-2* transgenic mice with

pancreatic ductal adenocarcinomas, completely eliminated *COX-2* gene expression and inhibited the tumour formation (Wang and DuBois, 2010). Aspirin eugenol ester (AEE), which has similar efficacy to aspirin and eugenol was synthesized to avoid side effects. When this AEE was fed to Wistar male rats, their *COX-2* expression decreased substantially (Ma *et al.*, 2017). There are limited studies that have evaluated the relationships between NSAIDs and *COX-2* gene expression in 3D culture or *in vivo*. However, there are many experiments in 2D culture systems that have demonstrated *COX-2* expression can be reduced by aspirin or salicylate (Sharma and Sharma, 1997; Hugo *et al.*, 2015; Oates *et al.*, 2015; Yuan *et al.*, 2016).

In this Chapter, NaS was found to be less effective in 3D PC3 cell cultures than when the same cells are cultured in 2D. There are several possible reasons for this difference, with a key one being the difference in *COX-2* gene expression profiles between the two culture formats. Despite the greater levels of *COX-2* gene expression, the same concentrations of NaS were applied to the 2D and 3D PC3 cell cultures. It is, therefore, possible, that a higher concentration of NaS is required in the 3D cultures to see a more effective anti-cancer effect due to the higher nascent *COX-2* gene expression profile. Moreover, the compact 3D cell format should not be forgotten. This compact structure, in fact, makes it more difficult for the NaS to reach all the cells in the spheroid efficiently. Conversely, in 2D culture, PC3 cells were grown flat at the bottom of a flask, leaving a large cell surface area is exposed to the NaS. Thus, NaS may be more readily internalised in a more significant proportion of cells in 2D than in a 3D spheroid, resulting in a greater toxic effect in 2D culture. In addition, in this Chapter, the centre of the PC3 cell spheroids were noted to be hypoxic, which could further contribute to the difference between the 2D and 3D cell response to NaS.

In summary, the agarose-based PC3 spheroid culture model utilised in this study offers uniform-sized PC3 spheroids that can be reproducibly constructed. From the 3rd day of culture, the PC3 spheroids are seen as a functioning and mature model for undertaking molecular studies into PCA. Decreased drug penetration, hypoxia, and altered *COX-2* gene expression profiles were observed in PC3 cells cultured as spheroids when compared to the same cell line cultured in a 2D format. NaS had less efficacy in the 3D PC3 models as compared to the 2D monolayer culture of these cells with only the top dose (10 mM) able to reduce *COX-2* expression, while p65 nuclear localisation was reduced by doses ranging from 6 to 10 mM.

Chapter 6 General Discussion

Prostate cancer is one of the most common malignancies in the male reproductive system. The onset of disease increases with age, and its incidence is markedly regional, accounting for the second largest number of male cancer deaths (Pandeya *et al.*, 2010). At present, the cause of prostate cancer is not yet clear, and may be related to factors such as heredity, environment, and sex hormones. A total of 98% of prostate cancers are adenocarcinomas and often occur in the peripheral part of the prostate. Most of them are multifocal cancers (Rothwell *et al.*, 2012). Many patients with prostate cancer have no obvious clinical symptoms in the early stage and the cancer is often found following rectal examinations, serum PSA tests, or histological examination of biopsies. Pathological grading of prostate cancer is based on the Gleason grading system (Gleason, 1977; Baig *et al.*, 2015; Beauval *et al.*, 2016). The staging of prostate cancer can guide the choice of treatment methods and the evaluation of prognosis. The staging can be determined by the results of DRE, CT, MRI, ECT, PSA, and lymph node dissection for TNM staging. The T stage represents the location of the primary tumour, which is mainly determined by DRE, MRI, and positive biopsies. N stage represents lymph node status as determined by localised diagnosis of lymph node dissection, including open or laparoscopic resection. While, the M-staging refers to the presence of metastasis, which can be confirmed by whole-body radionuclide bone imaging or MRI.

In the past decade, the treatment of prostate cancer has made great progress. Radical prostatectomy is one of the most effective ways to cure localised prostate cancer, but patients may still suffer recurrence or distant metastasis (Shipley *et al.*, 2017; Struss and Black, 2017). In addition to radical surgery, external radiation therapy and close-beam irradiation therapy

are the selected radical treatment for localised prostate cancer. The latter in particular can improve the localised dose to the prostate and reduce the radiation dose to the surrounding rectum and bladder, which are associated with radiation side effects.

Aspirin, also known as acetylsalicylic acid, has antipyretic, analgesic, anti-inflammatory, platelet aggregation and antithrombotic effects, and is increasingly used in clinical practice. In recent years, the anticancer effect of aspirin has received extensive attention. In particular, the prevention or inhibition of prostate cancer has become a hot topic. Studies have demonstrated that long-term use of aspirin can significantly reduce the incidence of multiple cancers, including prostate cancer (Lee *et al.*, 2008; Piazuelo *et al.*, 2016; Shiao *et al.*, 2017; Hua *et al.*, 2018). A retrospective cohort study examined the preventive effect of low-dose aspirin on prostate cancer. The study included 13,453 subjects and the use of low-dose aspirin reduced the incidence of prostate cancer by 54% (HR = 0.46). Benefits were more common in subjects who used low-dose aspirin more than twice weekly (HR = 0.60). In addition, the study demonstrated a 57% reduction in the incidence of prostate cancer with low-dose aspirin \geq 5 years (HR = 0.43) (Lapi *et al.*, 2016). The study of Yang *et al.* (2016) also found that aspirin can reduce the incidence of prostate cancer and delay the transition from prostate hyperplasia to prostate cancer. A further investigation in the United States demonstrated that anticoagulant therapy (especially use of aspirin) was associated with lowering prostate cancer-specific mortality (PCSM) in patients undergoing radical prostatectomy or radiation therapy, which was published in 2012 (Choe *et al.*, 2012). The study included 5,955 patients with localised prostate cancer who underwent radical prostatectomy or radiotherapy, and 37% received anticoagulation treatment. At a median follow-up of 70 months, the 10-year PCSM in the anticoagulant group was significantly lower (3% to 8%) than in the non-anticoagulant group.

The benefit was more pronounced in high-risk patients; multivariate analysis suggested an independent correlation between aspirin and reduction in PCSM risk (HR=0.43, $p=0.02$) (Choe *et al.*, 2012). Despite these clear benefits of aspirin use, our understanding of aspirin's underlying mechanisms of action on cancer cells are limited. Enhancing our knowledge in this area is of importance to better understand the advantages and limitations of aspirin's use to support the clinical management of prostate cancer patients. Hence, the overall aim of this thesis was to explore the functional and mechanistic effects of aspirin on PCA cells.

The first line of analysis undertaken was the investigation of the effects of NaS on prostate cancer cells, including growth, *COX-2* expression, morphological changes, cell cycle and wider gene expression changes in PCA cells in Chapter 3. In this chapter, NaS was able to reduce RPD values of PNT2, DU145 and PC3 cell lines, resulted in increased Ca^{2+} levels, as well as reduced number of mitochondria in PCA cells. Baseline *COX-2* gene expression levels were found to differ in the three cell lines included in this study; PC3 had the highest level of *COX-2* while there was barely expression in PNT2. Interestingly, following NaS exposure, *COX-2* expression was reduced in both DU145 and PC3 cell lines. NaS treatment also reduced the nuclear area in PC3 and DU145 cells, and at higher doses increased MN formation, which was associated with aneugenicity. Finally, a PCR array was performed in order to identify potential mechanistically important signalling pathways induced or repressed by NaS exposure. Only one replicate was performed with the PCR array as this array system was simply used as an indicator, to identify key genes that would undergo further, more robust analysis by RT-qPCR. The limitation with this approach was that individual sample variation was not taken into consideration with the PCR array and so it meant that genes were identified as up-/down-regulated in the array, which did not subsequently correlate with the more robust RT-qPCR

analysis. In an ideal world, a triplicate PCR array would have provided more reliable target genes for further analysis, but nonetheless this approach did identify *CXCR2*, *IL-61* and *NR4A3* in PC3 cells as interesting downstream target of NaS.

NaS is one of the clinical NSAIDs. Its main mechanism of action is to reduce prostaglandin secretion by inhibiting COX activity. In recent years, studies have found that in addition to anti-inflammatory effects and anticoagulant effects, NaS also has a certain anti-cancer effect, that is the inhibition of tumour cell proliferation induced apoptosis (Ruan and So, 2014). At the same time, some scholars have pointed out that NaS can assist the treatment of many cancers by increasing the sensitivity of tumour cells to chemotherapeutic drugs. For example, it has been found that the incidence of rectal cancer was significantly reduced in people taking long-term NaS and it has also been found that NaS can effectively reduce the incidence of endometrial cancer in obese women (Gómez *et al.*, 1997; Kutuk and Basaga, 2004; Ding *et al.*, 2014). Therefore, NaS is worthy of further clinical research because of its anti-cancer effect. Numerous studies have demonstrated that chronic inflammation featured with over-expression of *COX-2* is closely related to the occurrence and development of various tumours (Vendramini-Costa and Carvalho, 2012). Evidence from genetic and clinical studies suggests that increased *COX-2* expression is one of the key steps in carcinogenesis (Kim *et al.*, 2011; Vendramini-Costa and Carvalho, 2012). Most studies have found that *COX-2* is also over-expressed in prostate cancer tissues and is closely related to stage and prognosis (Shao *et al.*, 2012; Bonkhoff, 2012).

In Chapter 4, the MoA of aspirin as well as the role of the *COX-2* and NF- κ B pathways was studied. In Chapter 3, it seemed that sensitivity to NaS was related to *COX-2* expression levels in the PCA cell lines. As a transcription factor, NF- κ B is directly involved in the regulation of

COX-2 expression. Di *et al.* (2010) demonstrated that Toll-like receptor 9 (TLR9) can stimulate NF- κ B-dependent *COX-2* expression in the PC3 cell line in a time and dose dependent manner under the action of agonist CpG oligodeoxynucleotides. In addition, the study evaluated three prostate cell lines (RWPE-1, LNCaP and PC3) and demonstrated that vasoactive intestinal polypeptide (VIP) could stimulate *COX-2* expression and accelerate transformation from normal androgen-dependent prostate tissue to androgen-independent prostate cancer (Fernández-Martínez *et al.*, 2007). Further, by detecting the level of NF- κ B p50 in each cell line, VIP can stimulate the transfer of p50 from the cytoplasm to nucleus in LNCaP cells and PC3 cells (Fernández-Martínez *et al.*, 2007a). This suggests that *COX-2* expression induced by VIP stimulation in prostate cancer cell lines is achieved by activating the NF- κ B pathway. Zhi *et al.* (2009) has demonstrated that guanine nucleotide exchange factor SmgGDS (an activator of many small GTPases in Ras and Rho family) can up-regulate the gene expression of *COX-2* which is related to the NF- κ B pathway, thereby promoting the occurrence and development of prostate cancer. In the present study, it was consequently assumed that *COX-2* was one of the mediators for the anti-tumour effects of NaS via the NF- κ B pathway. Indeed, in Chapter 4, when the *COX-2* gene expression was diminished by celecoxib treatment, NaS effects on growth, cell cycle arrest and morphological changes, which were found previously in Chapter 3, were removed at lower doses (0-6 mM). However, the very high dose of 10 mM NaS was still able to cause significant, albeit low-level changes ($p < 0.05$). To explore NaS effects on NF- κ B, we utilised two cell lines. PNT2's NF- κ B pathway was activated by TNF- α while PC3 cells' NF- κ B was intrinsically active. NaS was able to suppress the activation of the NF- κ B pathway regardless of whether the cells were activated artificially or intrinsically.

The results presented in Chapter 3 and 4 demonstrate that PCA cells are mostly in G₀/G₁ phase.

Following aspirin exposure, the proportion of cells at the G₀/G₁ phase of the cell cycle significantly increased at the 6, 8 and 10 mM dose groups over untreated controls ($p < .05$). Thus, PCA cell growth was delayed and suppressed by NaS intervention. The literature indicates that NF- κ B p65 is ubiquitous in the cytoplasm of cells. When related stimuli (such as TNF) activate their biological activity, NF- κ B p65 will enter the nucleus and exert its regulation of proliferation. In this study, NaS significantly reduced the expression of NF- κ B p65 ($p < 0.05$) in PCA, and the degree of inhibition demonstrated a correlation with NaS concentration. At the same time, the number of mitochondria decreased significantly ($p < .05$), indicating that NaS can also influence cellular metabolism and further promote apoptosis. Consequently, aspirin promotes cell death by stalling mitosis and reducing the energy source that is required for both cell proliferation and metabolism.

In Chapter 4, NaS treatment suppressed NF- κ B activation, I κ B α phosphorylation, translocation of NF- κ B p65 to the nucleus and IKK- β activation in PC3 cells. This was associated with a reduction in invasion and migration capacity of these cells. These results correlated with previous studies which have demonstrated that the inhibition of NF- κ B significantly decreases cell invasion and angiogenesis in a prostate cancer animal model (Zhi *et al.*, 2009; Fernández-Martínez *et al.*, 2007a). The molecular mechanisms underlying aspirins' influence on NF- κ B-mediated invasion in prostate cancers cells have not been fully defined, although some useful insight exists in the literature. One study in PC3 cells reported that the inhibitory effect of aspirin on NF- κ B resulted in diminished secretion of urokinase-type plasminogen activator (uPA), which is thought to be a crucial molecule involved in cancer metastasis (Lloyd *et al.*, 2003; Shi *et al.*, 2017). Furthermore, IKK- β overexpression reversed the inhibitory effects of aspirin on cell invasion (Shi *et al.*, 2017).

The traditional *in vitro* planar cell culture models (2D model) are limited by the cell growth arrangement and the absence of extracellular matrix (ECM). Standard cell 2D culture therefore does not mimic the tumour microenvironment well (Montanez-Sauri *et al.*, 2015). Prostate cancer cell lines have been sub-cultured for decades and therefore are likely far removed from primary tumours and the artificial monolayer structure limits the validity of 2D cell models in individualised therapeutic research. On the other hand, commonly used transgenic animal models, such as TRAMP mice, have expensive breeding costs, longer modelling cycles, and non-human homologous prostate tissue sources which make the animal models difficult to widely apply (Hurwitz *et al.*, 2001; Hensley and Kyprianou, 2012). Therefore, in order to investigate NaS effects on PC3 cells in a more physiologically relevant environment and compare it against 2D culture, a culture system with a 3D format was needed. Thus, Chapter 5 was in part, aimed at establishing a 3D model system utilising PC3 cells. This model was developed and its features were characterised, including growth rate, morphology, survival time, necrosis and *COX-2* expression profile. Once a robust model had been developed, NaS effects on cells cultured in the 3D system were compared to cells grown in monolayer. The PC3 spheroids did not grow as rapidly as the cells cultured in monolayer and their cells' viability reached a peak by the 4th day of the culture. The spheroids exhibited higher expression of the *COX-2* gene than cells cultured in a 2D system and the expression was consistent over 7 days of culture. It was also found that lumens were formed by the 3rd day of culture, indicating functionality of spheroids. However, the potential luminal structures found in the PC3 spheroids need further investigation and characterisation. Thus, future work should utilise an immunohistochemistry-based approach with an antibody specific to prostate-specific membrane antigen (PSMA) to determine and verify if the structures observed in this study are indeed lumen. PSMA immunoreactivity is typical of luminal structures in the human prostate,

thus, it is hypothesised that membranous subluminal staining would be observed in the luminal structures of the 3D spheroids developed within Chapter 5. Although some preliminary work was undertaken in the present study attempting to embed the PC3 spheroids in paraffin wax to allow for immunohistochemical analysis, this embedding process was not successful as the PC3 spheroids could not be removed from the agarose layer without causing damage (data not shown). Thus, further optimisation is required to support immunohistochemical analysis of the 3D PC3 spheroid structure in the future, in order to more comprehensively characterise their histology.

The characterisation work provided the time frame for NaS treatment, namely from 3rd day to 5th day of culture with a seeding density of 50,000 cells / cm³, as defined by sufficient cell viability and limited hypoxia in the spheroid core during this period. Upon NaS treatment, the viability of spheroids was reduced significantly at higher doses of 8 and 10 mM. COX-2 expression was only down-regulated by 10 mM NaS. However, the NF-κB pathway was not affected by NaS exposure in the 3D culture system. For example, 0.5 h-exposure of NaS at 6 mM was able to prevent p65 translocation to nuclear region in PC3 cells, while even higher doses failed to do so in 3D culture. Thus, in Chapter 5, it was found that NaS effects on spheroids were not as prominent as the effects on cells cultured in 2D culture systems. This is of importance given that the 3D culture system is more similar to the *in vivo* situation, and is clearly less sensitive than the standard 2D cell culture format due to limitations in access of the drug to all cells in the model.

In Chapters 4 and 5, much of the data generated was based on western blots. Western blots typically employ densitometry analysis with proprietary software based on three replicates, thus it is a semi-quantitative form of analysis. In both Chapters, there were several

densitometry data points that were borderline significant (*e.g.* $P=0.048$) but did not appear to be a prominent change in protein expression when reviewing the associated western blots. These data points need to be considered with some caution because of the semi-quantitative nature of the technique. In the future, it is therefore important to further corroborate the western results generated for p65 and I κ B α , in follow-up studies utilising protein analysis methods that generate either complimentary semi-quantitative or more quantitative techniques. For example, *in situ* fluorescent imaging approaches using secondary antibodies conjugated to a fluorescent fluorophore would be very useful in providing further visual data on subcellular localisation of the proteins under investigation. This technique has a greater upper linear range of detection than that of chemiluminescent-based methods used for western blotting and so would provide greater quantitative power, which was lacking in the present study (Bass *et al.*, 2017).

The findings in Chapter 5 are of interest because a previous study found that only long-term administration of aspirin was an effective clinical method for prostate cancer or other cancers (Lapi *et al.*, 2016; Choe *et al.*, 2012; Bilani *et al.*, 2017). Aspirin is used in different doses and dosage forms; therefore, its effect on preventing and treating tumours also varies. It has been found that the use of aspirin to prevent tumours was dose-dependent (Cao *et al.*, 2016). The relative ratio (RR) was 0.99 if aspirin is administered weekly from 162.5 to 487.5 mg while RR is increased to 0.94 when patients took over 4,875 mg of aspirin weekly. The risk of developing a tumour also decreases with increasing dose. A meta-analysis included 71 randomised controlled trials and 104,101 subjects followed for an average of 60 months. Paired analysis demonstrated that 100 mg of aspirin per day was the optimal dose to reduce tumour morbidity and mortality while reducing the incidence of adverse events such as bleeding. In

addition to dose, the form of the drug also matters. Aspirin capsules have a better effect on the reduction of tumour morbidity and mortality, while aspirin-controlled release tablets have a better preventive effect on cerebrovascular diseases (Lotrionte *et al.*, 2016). The effect of aspirin on the prevention and treatment of tumours is also related to the time and frequency of administration. Wu *et al.* conducted a dose-response analysis of 24 studies and found that the use of aspirin or other NSAIDs ≥ 2 years reduced the risk of gastric cancer by 5% and 11%, respectively (Wu *et al.*, 2016). The use of aspirin 5 times a week is the threshold for the prevention of gastric cancer. With the continuous use of aspirin for 10 to 19 years, the incidence of colon cancer decreased by 40% (RR = 0.60), and the risk of colon cancer death decreased by 33% (RR = 0.67) with a continuous use for 20 years (Chubak *et al.*, 2016).

Similarly, to the present study, in multi-tumour epithelial ovarian cancer cell microspheres formed in the 3D culture environment, the degree of differentiation of the tumour cells was higher, which more closely replicates the human body than that of the tumour cells in 2D. Therefore, the study authors believe that the experimental results of drug sensitivity testing in a 3D environment can more realistically reflect the drug tolerance of cells *in vivo* (Lee *et al.*, 2013). It should not be neglected to mention that NaS was indeed toxic to the normal cell line, PNT2 cells, in 2D culture. However, owing to the increased sensitivity of 2D culture to drugs, it is likely that a longer exposure time or higher dose is actually required to adversely affect normal prostate cells. Nonetheless, this requires further research, and both the administration dose and time of aspirin delivery would be vital to carefully establish if aspirin was applied clinically for prostate cancer treatment.

It is widely believed that *COX-2* is linked to drug resistance in cancer (Sui *et al.*, 2011; Kalle and Rizvi, 2011). In Chapter 3, DU145 had lower *COX-2* expression than PC3 as well as lower

sensitivity to NaS than PC3 cells. In Chapter 5, there was a 1.5-fold-higher level of *COX-2* gene expression in spheroids cells compared to 2D cells. Drug resistance is one of the most important factors affecting the efficacy of clinical therapies for cancer. The mechanism of resistance is complicated. The P-glycoprotein (P-Gp) encoded by the *multidrug resistance gene* (*MDR*) plays an important role in drug resistance (Pajak and Orzechowski, 2006; Miller *et al.*, 2006; Zhang *et al.*, 2015b). A study found that *COX-2* is closely related to *MDR1/P-gp* and other resistance-related genes and can regulate the expression of *MDR* gene in tumour cells (Bassiouny *et al.*, 2010). In order to further confirm this idea, RT-PCR and Western blot could be used in the future to evaluate the expression profile of *MDR1* and *P-gp* mRNA after *COX-2* intervention by NaS. The relationship between *COX-2* gene expressions with *MDR1/P-gp* transcriptional levels in PCA cells may point to the importance of drug resistance linked to aspirin treatment.

One of the advantages in 2D culture systems is the ability to use them for rapid screening; while the 3D models can more accurately reproduce the action mode and effect of anticancer drugs in the *in vivo* model, and exhibit tumour cell resistance similar to the *in vivo* model (Xu *et al.*, 2014c). Thus, there is benefits to using both systems in the field of drug development. For example, Härmä *et al.* (2015) used the prostate cancer 2D model to select 25 species of betulin derivatives with stronger anti-invasive and metastatic potential from 93 compounds and then used a 3D model for rescreening to study cell viability and proliferation effects on the cell cycle and its non-specific cytotoxicity. Furthermore, the phenotypic analysis of tumour microspheres was carried out to verify the target of the compound. There are also efforts to increase the throughput of 3D models, which are traditionally quite limited when it comes to high-throughput evaluations. In this area, Chambers *et al.* (2014) established a high-

throughput drug test platform that used a mould to form a microwell array on a polydimethylsiloxane plate, followed by injection of a mixed suspension of prostate cancer cells and high-speed centrifugation. The cells agglomerated in the microwells to form microspheres. In this system, microspheres formed by prostate cancer cells survived successfully and exhibited cell morphology and drug resistance similar to those *in vivo*. Using this test platform, up to 600 microwells can be constructed per square meter, and up to 34,000 microspheres can be generated in a 96-well plate. Combined with a microfluidic device, it is suitable for high-throughput drug screening tests. At present, the traditional 2D model is still dominant in prostate cancer research because of its wide recognition and low price. However, with the development of biomaterials and engineering technology and a deeper understanding of 3D cell culture systems, it is believed that the 3D tumour model will be recognised by more researchers and will be increasingly used as a research tool.

From the data gained from the Chapters 3, 4 and 5, the mechanism for aspirin effects on PCA can be summarised as illustrated in Figure 6.1. Firstly, NaS is able to reduce *COX-2* gene expression via the inhibition of the NF- κ B pathway. The NF- κ B pathway in PCA promotes the growth of cells. When this pathway is suppressed, growth of the PCA cells was therefore inhibited. This inhibition of growth was partially due to cell cycle arrest at the G_0/G_1 phase via the *COX-2* gene. The arrest resulted in prolonged cell cycle and a decrease in nuclear area, hence, the nuclear area and RPD values were reduced. NaS caused DNA damage (MN) and increased Ca^{2+} in the cells, which resulted in rupture of the mitochondria. The *COX-2* gene also regulates other related genes, relevant genes, such as MMPs, which are involved in driving metastasis; thus, its suppression minimises these phenotypic changes in the cancer cells. Finally, PCA cells were less capable of exhibiting migration and invasion. However, within the

microenvironment of 3D culture, the above effects of NaS were somewhat reduced at equivalent doses, indicating that higher doses or longer-term exposures may be required *in vivo*.

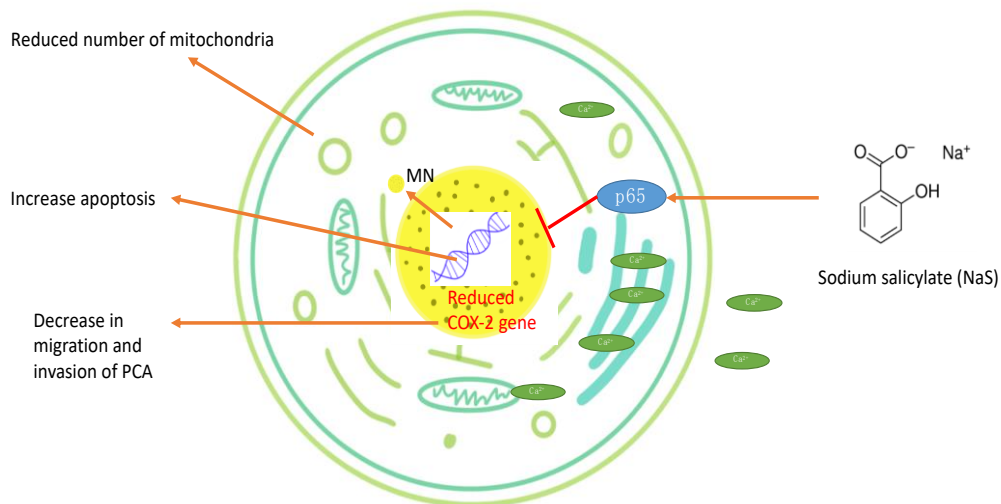


Figure 6.1. NaS affects *COX-2* gene expression profiles via the NF-κB pathway. NaS suppresses the pathway by inhibiting p65 translocation. Then, *COX-2* expression cannot be induced by the NF-κB pathway, leading to PCA cell toxicity.

From the literature and the results above, aspirin or NaS would be a promising drug for prostate cancer. However, aspirin has side effects, which have been reported in the literature. Oral administered aspirin is absorbed rapidly, with a half-life of 6 to 15 minutes. After oral administration of 500 to 600 mg, the blood concentration can quickly reach 40 to 60 μg/mL (Osterhoudt and Penning, 2011). Long-term use of aspirin increases the risk of ulcers and bleeding. Aspirin acts directly on the gastric mucosa, destroys the protective barrier of the gastric mucosa, promotes the release of cytotoxic substances such as leukotrienes, and damages the gastric mucosa. Even at low doses (75 mg/day), the risk of complications such as

gastrointestinal injury and ulceration increased. The risk of bleeding and ulceration was significantly higher in patients older than 70 years (Robertson, 2013). Specific aspirates can cause allergic reactions such as rash, angioneurotic oedema, and asthma after taking aspirin (Stevens *et al.*, 2015; Topaz *et al.*, 2016). When the dosage is too high, mental confusion, convulsions, or even coma can occur. Symptoms can however be completely removed within 2-3 days after drug withdrawal (VanWormer *et al.*, 2012).

As discussed in previous Chapters, further research could be done to support the study on NaS or aspirin in the clinical management of prostate cancer if time permitted. Several options for further research have been discussed above, but in addition, the effects of NaS on the invasion ability and migratory ability should be evaluated when *COX-2* is completely knocked out. To facilitate this knock-out, siRNA or CRISPR/Cas9 technology could be utilised to remove *COX-2* expression and then the NaS exposure experiments in this thesis could be repeated. MMP-2 expression and / or MMP-9 are related to metastasis. The Amersham Biotrak™ assays or Enzyme-linked immunosorbent assay (ELISA) can be used to measure specific MMP proteins following NaS treatment when *COX-2* is expressed or knocked-out. Future work should also focus on the relationships between the mRNA and protein levels of VEGF and NaS when *COX-2* is expressed or knocked-out. The influence of the microenvironment should not be neglected. This could be evaluated through the development of a 3D co-culture system. For example, PC3 cells or other PCA cell lines could be co-cultured with osteoblast cells, such as hFOB 1.19, both in 2D and in 3D on pre-coated plates or collagen scaffolds, which simulates the bone microenvironment. Under this microenvironment, the experiments could be repeated again to understand the impact of aspirin on highly aggressive PCA cells, as highly invasive prostate cancer is substantially more difficult to treat and has poorer outcome with

higher morbidity, compared to the those men with low- and moderate localised PCA (Mossanen *et al.*, 2018).

Another important aspect for future work is a more thorough evaluation of cancer cell apoptosis induced by NaS. In Chapter 3, Ca^{2+} levels and mitochondria numbers were reduced due to exposure of NaS, which are related to the induction of apoptosis. However, to more comprehensively evaluate this endpoint, additional investigation is required as these measurements are not direct indicators of apoptosis. There are many different ways of detecting apoptosis, each with their advantages and disadvantages. In the past, the examination of apoptosis by microscopy or confocal microscopy following nuclear staining was considered to be an intuitive, simple, and reliable method, but it is time consuming and laborious (Elmore, 2007; Wlodkowic *et al.*, 2011). Nuclear debris and apoptotic condensed chromatin can be localized by laser confocal microscopy. However, the evaluation of large samples numbers is difficult with such manual morphological analysis, it is not quantitative, and the judgment criteria are subjective, varying from person to person. An alternative imaging technique is the use of fluorescent markers (such as those sensitive to caspase activation and mitochondrial transmembrane potential ($\Delta \psi_m$) decrease) for the detection of various internal changes in the signal transduction and intracellular environment of cells, which are associated with apoptosis (Lant and Derry, 2013). This technique is relatively simple and is low cost, plus the additional advantage of observation by microscopy is that it is a quantitative indicator. Therefore, observation by microscopy is one of most commonly used methods for apoptosis detection. However, quantification relies on manually counting different nuclear patterns within multiple fields of views, representing a limitation. Analysis of DNA separation in an agarose gel is another method for detecting apoptosis. Activated

endonucleases associated with initiating apoptosis cleaves the DNA strand to form nucleic acid fragments of about 180 to 200 bp length (He *et al.*, 2009; Iglesias-Guimaraes *et al.*, 2012). Although, this phenomenon is a key stage in cell apoptosis, there are many factors that affect the quality of the experimental results; for example, the timing of collecting samples and whether the cell population has been adequately synchronized prior to initiating the experiment have a heavy influence on the subsequent data quality. Therefore, from a qualitative point of view, this method is not as accurate as microscopy and it cannot be used for quantitative purposes. Other techniques take advantage of the phenomenon whereby phosphatidylserine (PS) on the inner side of the cell membrane migrates to the outside of the cell membrane in the early stage of apoptosis (Kay and Grinstein, 2011). The phospholipid binding protein Annexin V has a high affinity for PS. Apoptosis can therefore be detected by flow cytometry after labelling Annexin V with fluorescein together with PI staining to identify dead cells. In order to enable flow cytometric analysis, it is necessary to prepare a single-cell suspension. Although this is a powerful quantitative technique for apoptosis, apoptotic cells are easily lost during the digestion and suspension stages of sample preparation, thereby affecting the experimental results and increasing the data variability (Wlodkowic *et al.*, 2009; Demchenko, 2013). Last but not least, active Caspase-3 is only present in apoptotic cells (Crowley and Waterhouse, 2016) and so fluorescent probes for detecting caspase activity can be imaged and quantified with flow cytometry. Another commonly used apoptotic molecule marker is the poly (ADP-ribose) polymerase (PARP) protein splicing because it is one of the substrates for Caspase-3 (Boulares *et al.*, 1999; Chaitanya *et al.*, 2010). Caspas-3 based apoptosis detection is therefore a very popular method at present, but it is important to note that occasionally, apoptosis is not dependent on the Caspase pathway (Kroemer and Martin, 2005; Fitzwalter and Thorburn, 2017). Hence, a combination of nuclear staining coupled to

microscopy analysis, together with a Caspase-3 based assay utilising flow cytometry is a powerful combination to detect apoptosis. Complementary techniques are required to generate a robust overview of the induction of apoptosis following exposure to an exogenous agent.

Another important point to note is that aspirin consist two groups of molecules, namely, the acetyl and salicylate groups. Most studies *in vivo* focus on the use of aspirin, as it is subsequently metabolised in the body. However, *in vitro* systems often do not have efficient metabolic capacity. Thus, when aspirin is used *in vitro*, it may not be efficiently metabolised and so in the present study, NaS was selected as the metabolite of choice to evaluate. However, evidence in the literature suggests that both constituent groups of aspirin (the acetyl and salicylate) may together contribute to its anticancer effects (Alfonso *et al.* 2014). The mechanisms proposed in this thesis are therefore only valid for effects induced specifically by the NaS metabolite. In the future, it will therefore be interesting to also explore the role of the acetyl group on prostate tumorigenesis to better understand how the two metabolites contribute to the anti-cancer properties associated with aspirin.

In conclusion, research on aspirin and cancer prevention has been carried out for over a decade. A large number of studies have demonstrated that long-term use of aspirin reduces the incidence and mortality of cancer, and inhibits the occurrence, development, recurrence and metastasis of cancer. It has been found that aspirin contributes to the prevention of prostate cancer, but studies in this area remain limited, particularly those exploring the underlying mechanisms of action. The results within this thesis have provided important data to demonstrate that aspirin induces anti-cancer effects on PCA cells. This predominantly occurs through an NF- κ B and COX-2 mediated pathway. Although the best applicable

population, effective dose, and duration of continuous administration require further clinical research, this study provides confidence in the potential value of aspirin in the clinical management of prostate cancer patients.

References

- Abd, T. T., Goodman, M., Hall, J., Ritenour, C. W., Petros, J. A., Marshall, F. F. & Issa, M. M. 2011. Comparison of 12-core versus 8-core prostate biopsy: multivariate analysis of large series of US veterans. *Urology*, 77, 541-547.
- Abiru, S., Nakao, K., Ichikawa, T., Migita, K., Shigeno, M., Sakamoto, M., Ishikawa, H., Hamasaki, K., Nakata, K. & Eguchi, K. 2002. Aspirin and NS-398 inhibit hepatocyte growth factor-induced invasiveness of human hepatoma cells. *Hepatology*, 35, 1117-1124.
- Ackerman IV, W. E., Summerfield, T. L., Vandre, D. D., Robinson, J. M. & Kniss, D. A. 2008. Nuclear factor-kappa B regulates inducible prostaglandin E synthase expression in human amnion mesenchymal cells. *Biology of reproduction*, 78, 68-76.
- Afifi, N., Abdel-Hamid, E., Baghdadi, H. & Mohamed, A. 2012. Nuclear Area Factor as a Novel Estimate for Apoptosis in Oral Squamous Cell Carcinoma-Treated Cell Line: A Comparative in-vitro Study with DNA Fragmentation Assay. *J Clinic Experiment Pathol*, 2, 2161-0681.1000107.
- Alfonso, L., Ai, G., Spitale, R. & Bhat, G. J. B. j. o. c. 2014. Molecular targets of aspirin and cancer prevention. 111, 61.
- Alfonso, L. F., Srivenugopal, K. S., Arumugam, T. V., Abbruscato, T. J., Weidanz, J. A. & Bhat, G. J. 2009. Aspirin inhibits camptothecin-induced p21CIP1 levels and potentiates apoptosis in human breast cancer cells. *International journal of oncology*, 34, 597-608.
- Algra, A. M. & Rothwell, P. M. 2012. Effects of regular aspirin on long-term cancer incidence and metastasis: a systematic comparison of evidence from observational studies versus randomised trials. *The lancet oncology*, 13, 518-527.
- Amedee, J., Bareille, R., Jeandot, R., Bordenave, L., Remy, M., Rouais, F. & Baquey, C. 1994. Evaluation of cell colonization on biomaterials: preventing cell attachment to plastic containers. *Biomaterials*, 15, 1029-1031.
- American Cancer Society. 2018. *Initial Treatment of Prostate Cancer, by Stage* [Online]. Available: <https://www.cancer.org/cancer/prostate-cancer/treating/by-stage.html> [Accessed 19 Dec 2018].
- Anilkumar, U., Weisova, P., Schmid, J., Bernas, T., Huber, H. J., Dössmann, H., Connolly, N. M. & Prehn, J. H. 2017. Defining external factors that determine neuronal survival, apoptosis and necrosis during excitotoxic injury using a high content screening imaging platform. *PLoS one*, 12, e0188343.
- Antoni, D., Burckel, H., Josset, E. & Noel, G. 2015. Three-dimensional cell culture: a breakthrough in vivo. *International journal of molecular sciences*, 16, 5517-5527.
- Aoki, T. & Narumiya, S. 2017. Prostaglandin E(2)-EP2 signaling as a node of chronic inflammation in the colon tumor microenvironment. *Inflammation and Regeneration*, 37, 4.
- Araki, Y., Okamura, S., Hussain, S. P., Nagashima, M., He, P., Shiseki, M., Miura, K. & Harris, C. C. J. C. r. 2003.

- Regulation of cyclooxygenase-2 expression by the Wnt and ras pathways. *63*, 728-734.
- Araujo, J. L., Altorki, N. K., Sonett, J. R., Rodriguez, A., Sungur-Stasik, K., Spinelli, C. F., Neugut, A. I. & Abrams, J. A. 2016. Prediagnosis aspirin use and outcomes in a prospective cohort of esophageal cancer patients. *Therapeutic Advances in Gastroenterology*, *9*, 806-814.
- Arnold, M., Razum, O. & Coebergh, J.-W. 2010. Cancer risk diversity in non-western migrants to Europe: an overview of the literature. *European journal of cancer*, *46*, 2647-2659.
- Aslan, G., İrer, B., Kefi, A., Çelebi, İ., Yörükoğlu, K. & Esen, A. 2005. The value of PSA, free-to-total PSA ratio and PSA density in the prediction of pathologic stage for clinically localized prostate cancer. *International urology and nephrology*, *37*, 511-514.
- Atan, A. & Güzel, Ö. 2013. How should prostate specific antigen be interpreted? *Turkish journal of urology*, *39*, 188-193.
- Aune, D., Rosenblatt, D. A. N., Chan, D. S., Vieira, A. R., Vieira, R., Greenwood, D. C., Vatten, L. J. & Norat, T. 2015. Dairy products, calcium, and prostate cancer risk: a systematic review and meta-analysis of cohort studies. *The American journal of clinical nutrition*, *ajcn*. 067157.
- B Vendramini-Costa, D. & E Carvalho, J. 2012. Molecular link mechanisms between inflammation and cancer. *Current pharmaceutical design*, *18*, 3831-3852.
- Baig, F. A., Hamid, A., Mirza, T. & Syed, S. 2015. Ductal and Acinar Adenocarcinoma of Prostate: Morphological and Immunohistochemical Characterization. *Oman Medical Journal*, *30*, 162-166.
- Baker, B. M. & Chen, C. S. 2012. Deconstructing the third dimension—how 3D culture microenvironments alter cellular cues. *J Cell Sci*, *125*, 3015-3024.
- Balkwill, F. & Mantovani, A. 2001. Inflammation and cancer: back to Virchow? *The lancet*, *357*, 539-545.
- Baron, J. A., Cole, B. F., Sandler, R. S., Haile, R. W., Ahnen, D., Bresalier, R., McKeown-Eyssen, G., Summers, R. W., Rothstein, R. & Burke, C. A. 2003. A randomized trial of aspirin to prevent colorectal adenomas. *New England Journal of Medicine*, *348*, 891-899.
- Bartel, C., Tichy, A., Schoenkypl, S., Aurich, C. & Walter, I. 2013. Effects of steroid hormones on differentiated glandular epithelial and stromal cells in a three dimensional cell culture model of the canine endometrium. *BMC veterinary research*, *9*, 86.
- Bass, J. J., Wilkinson, D. J., Rankin, D., Phillips, B. E., Szewczyk, N. J., Smith, K. & Atherton, P. J. 2017. An overview of technical considerations for Western blotting applications to physiological research. *27*, 4-25.
- Bassiouny, A. R., Zaky, A. & Neenaa, H. M. 2010. Synergistic effect of celecoxib on 5-fluorouracil-induced apoptosis in hepatocellular carcinoma patients. *Ann Hepatol*, *9*, 410-418.
- Beauval, J.-B., Roumiguié, M., Filleron, T., Benoit, T., de la Taille, A., Malavaud, B., Salomon, L., Soulié, M. & Ploussard, G. 2016. Biochemical recurrence-free survival and pathological outcomes after radical prostatectomy for high-risk prostate cancer. *BMC Urology*, *16*, 26.
- Begley, L. A., Kasina, S., Mehra, R., Adsule, S., Admon, A. J., Lonigro, R. J., Chinnaiyan, A. M. & Macoska, J. A. 2008. CXCL5 promotes prostate cancer progression. *Neoplasia*, *10*, 244-254.

- Ben-Batalla, I., Cubas-Cordova, M., Udonta, F., Wroblewski, M., Waizenegger, J. S., Janning, M., Sawall, S., Gensch, V., Zhao, L., Martinez-Zubiaurre, I., Riecken, K., Fehse, B., Pantel, K., Bokemeyer, C. & Loges, S. 2015. Cyclooxygenase-2 blockade can improve efficacy of VEGF-targeting drugs. *Oncotarget*, 6, 6341-6358.
- Bilani, N., Bahmad, H. & Abou-Kheir, W. 2017. Prostate Cancer and Aspirin Use: Synopsis of the Proposed Molecular Mechanisms. *Frontiers in Pharmacology*, 8, 145.
- Bill-Axelsson, A., Holmberg, L., Garmo, H., Rider, J. R., Taari, K., Busch, C., Nordling, S., Häggman, M., Andersson, S.-O. & Spångberg, A. 2014. Radical prostatectomy or watchful waiting in early prostate cancer. *New England Journal of Medicine*, 370, 932-942.
- Bill-Axelsson, A., Holmberg, L., Ruutu, M., Häggman, M., Andersson, S.-O., Bratell, S., Spångberg, A., Busch, C., Nordling, S. & Garmo, H. 2005. Radical prostatectomy versus watchful waiting in early prostate cancer. *New England Journal of Medicine*, 352, 1977-1984.
- Blobaum, A. L. & Marnett, L. J. 2007. Structural and Functional Basis of Cyclooxygenase Inhibition. *Journal of Medicinal Chemistry*, 50, 1425-1441.
- Böhmer, D., Wirth, M., Miller, K., Budach, V., Heidenreich, A. & Wiegand, T. 2016. Radiotherapy and Hormone Treatment in Prostate Cancer. *Deutsches Arzteblatt international*, 113, 235-241.
- Bolla, M., De Reijke, T. M., Van Tienhoven, G., Van den Bergh, A. C., Oddens, J., Poortmans, P. M., Gez, E., Kil, P., Akdas, A. & Soete, G. 2009. Duration of androgen suppression in the treatment of prostate cancer. *New England Journal of Medicine*, 360, 2516-2527.
- Bonkhoff, H. 2012. Factors implicated in radiation therapy failure and radiosensitization of prostate cancer. *Prostate cancer*, 2012.
- Bonnans, C., Chou, J. & Werb, Z. 2014. Remodelling the extracellular matrix in development and disease. *Nature reviews. Molecular cell biology*, 15, 786-801.
- Borthwick, G. M., Johnson, A. S., Partington, M., Burn, J., Wilson, R. & Arthur, H. M. 2006. Therapeutic levels of aspirin and salicylate directly inhibit a model of angiogenesis through a Cox-independent mechanism. *The FASEB Journal*, 20, 2009-2016.
- Bosetti, C., Rosato, V., Gallus, S. & C., L. V. 2014. Aspirin and prostate cancer prevention. *Recent Results Cancer Res*, 202, 93-100.
- Boulares, A. H., Yakovlev, A. G., Ivanova, V., Stoica, B. A., Wang, G., Iyer, S. & Smulson, M. J. J. o. B. C. 1999. Role of poly (ADP-ribose) polymerase (PARP) cleavage in apoptosis Caspase 3-resistant PARP mutant increases rates of apoptosis in transfected cells. 274, 22932-22940.
- Bracken, M. B. 2009. Why animal studies are often poor predictors of human reactions to exposure. *Journal of the Royal Society of Medicine*, 102, 120-122.
- Brasky, T. M., Velicer, C. M., Kristal, A. R., Peters, U., Potter, J. D. & White, E. 2010. Non-steroidal anti-inflammatory drugs and prostate cancer risk in the VITamins And Lifestyle (VITAL) cohort. *Cancer Epidemiology and Prevention Biomarkers*, cebp. 0942.2010.
- Bremnes, R. M., Al-Shibli, K., Donnem, T., Sirera, R., Al-Saad, S., Andersen, S., Stenvold, H., Camps, C. & Busund, R. T. 2015. Aspirin and survival in early-stage prostate cancer: a randomized, controlled trial. *Journal of Clinical Oncology*, 33, 1175-1182.

- L.-T. 2011. The Role of Tumor-Infiltrating Immune Cells and Chronic Inflammation at the Tumor Site on Cancer Development, Progression, and Prognosis: Emphasis on Non-small Cell Lung Cancer. *Journal of Thoracic Oncology*, 6, 824-833.
- Brenner, D., Blaser, H. & Mak, T. W. 2015. Regulation of tumour necrosis factor signalling: live or let die. *Nature Reviews Immunology*, 15, 362.
- Breslin, S. & O'Driscoll, L. 2013a. Three-dimensional cell culture: the missing link in drug discovery. *Drug discovery today*, 18, 240-249.
- Breslin, S. & O'Driscoll, L. J. D. d. t. 2013b. Three-dimensional cell culture: the missing link in drug discovery. 18, 240-249.
- Bundred, N. & Barnes, N. 2005. Potential use of COX-2–aromatase inhibitor combinations in breast cancer. *British journal of cancer*, 93, S10.
- Campbell, K. J., Rocha, S. & Perkins, N. D. 2004. Active repression of antiapoptotic gene expression by RelA (p65) NF- κ B. *Molecular cell*, 13, 853-865.
- Cao, Y., Nishihara, R., Wu, K., Wang, M., Ogino, S., Willett, W. C., Spiegelman, D., Fuchs, C. S., Giovannucci, E. L. & Chan, A. T. 2016. Population-wide impact of long-term use of aspirin and the risk for cancer. *JAMA oncology*, 2, 762-769.
- Carlson, E. A., Yan, S. S. J. I. C. S. & Therapeutics 2014. Disrupting cancer cell function by targeting mitochondria. 1.
- Carlson, L.-M., Rasmuson, A., Idborg, H., Segerström, L., Jakobsson, P.-J., Sveinbjörnsson, B. & Kogner, P. 2013. Low-dose aspirin delays an inflammatory tumor progression in vivo in a transgenic mouse model of neuroblastoma. *Carcinogenesis*, 34, 1081-1088.
- Carrel, A. & Ingebrigtsen, R. 1912 THE PRODUCTION OF ANTIBODIES BY TISSUES LIVING OUTSIDE OF THE ORGANISM. *J Exp Med*, 287–291.
- Cell Signalling. 2015. *NF- κ B Signaling Pathway* [Online]. Cell Signalling. Available: http://media.cellsignal.com/www/pdfs/science/pathways/NF_kappaB.pdf [Accessed 28th May 2017].
- Celsi, F., Pizzo, P., Brini, M., Leo, S., Fotino, C., Pinton, P. & Rizzuto, R. 2009. Mitochondria, calcium and cell death: A deadly triad in neurodegeneration. *Biochimica et biophysica acta*, 1787, 335-344.
- Ceylan, C., Doluoglu, O. G., Aglamis, E. & Baytok, O. 2014. Comparison of 8, 10, 12, 16, 20 cores prostate biopsies in determination of prostate cancer and importance of prostate volume. *Canadian Urological Association Journal*, 8, 81-5.
- Chaffer, C. L. & Weinberg, R. A. 2011. A perspective on cancer cell metastasis. *Science*, 331, 1559-1564.
- Chaitanya, G. V., Steven, A. J. & Babu, P. P. 2010. PARP-1 cleavage fragments: signatures of cell-death proteases in neurodegeneration. *Cell communication and signaling : CCS*, 8, 31-31.
- Chambers, K. F., Mosaad, E. M., Russell, P. J., Clements, J. A. & Doran, M. R. 2014. 3D cultures of prostate cancer cells cultured in a novel high-throughput culture platform are more resistant to chemotherapeutics compared to cells cultured in monolayer. *PloS one*, 9, e1111029.

- Chan, A. T., Giovannucci, E. L., Meyerhardt, J. A., Schernhammer, E. S., Curhan, G. C. & Fuchs, C. S. 2005. Long-term use of aspirin and nonsteroidal anti-inflammatory drugs and risk of colorectal cancer. *Jama*, 294, 914-923.
- Chan, A. T., Ogino, S. & Fuchs, C. S. 2007. Aspirin and the risk of colorectal cancer in relation to the expression of COX-2. *New England Journal of Medicine*, 356, 2131-2142.
- Chao, T., Furth, E. E. & Vonderheide, R. H. 2016. CXCR2-dependent accumulation of tumor-associated neutrophils regulates T-cell immunity in pancreatic ductal adenocarcinoma. *Cancer immunology research*, 4, 968-982.
- Chapman, K. E., Doak, S. H. & Jenkins, G. J. 2015. Acute Dosing and p53-Deficiency Promote Cellular Sensitivity to DNA Methylating Agents. *Toxicological Sciences*, 144, 357-365.
- Chattopadhyay, M., Goswami, S., Rodes, D. B., Kodela, R., Velazquez, C. A., Boring, D., Crowell, J. A. & Kashfi, K. 2010. NO-releasing NSAIDs suppress NF- κ B signaling in vitro and in vivo through S-nitrosylation. *Cancer letters*, 298, 204-211.
- Cheever, M. A. & Higano, C. S. 2011. PROVENGE (Sipuleucel-T) in prostate cancer: the first FDA-approved therapeutic cancer vaccine. *Clinical Cancer Research*, 17, 3520-3526.
- Chen, J. & Stark, L. A. 2017. Aspirin Prevention of Colorectal Cancer: Focus on NF- κ B Signalling and the Nucleolus. *Biomedicines*, 5, 43.
- Cheng, G., Shan, X.-F., Wang, X.-L., Dong, W.-W., Li, Z., Liu, X.-H., Zhang, W., Xing, K. & Chang, F.-J. 2017. Endothelial damage effects of circulating microparticles from patients with stable angina are reduced by aspirin through ERK/p38 MAPKs pathways. *Cardiovascular therapeutics*, 35.
- Cheng, L., Montironi, R., Bostwick, D. G., Lopez-Beltran, A. & Berney, D. M. 2012. Staging of prostate cancer. *Histopathology*, 60, 87-117.
- Chetty, A. S., Vargha, V., Maity, A., Moolman, F. S., Rossouw, C., Anandjiwala, R., Boguslavsky, L., Mancama, D. & Focke, W. W. 2013. Development of thermoresponsive poly(propylene-g-N-isopropylacrylamide) non-woven 3D scaffold for smart cell culture using oxyfluorination-assisted graft polymerisation. *Colloids and Surfaces A: Physicochemical and Engineering Aspects*, 419, 37-45.
- Chiang, S.-L., Velmurugan, B. K., Chung, C.-M., Lin, S.-H., Wang, Z.-H., Hua, C.-H., Tsai, M.-H., Kuo, T.-M., Yeh, K.-T., Chang, P.-Y., Yang, Y.-H. & Ko, Y.-C. 2017. Preventive effect of celecoxib use against cancer progression and occurrence of oral squamous cell carcinoma. *Scientific Reports*, 7, 6235.
- Chitcholtan, K., Asselin, E., Parent, S., Sykes, P. H. & Evans, J. J. 2013. Differences in growth properties of endometrial cancer in three dimensional (3D) culture and 2D cell monolayer. *Exp Cell Res*, 319(1), 75-87.
- Choe, K. S., Cowan, J. E., Chan, J. M., Carroll, P. R., D'Amico, A. V. & Liauw, S. L. 2012. Aspirin use and the risk of prostate cancer mortality in men treated with prostatectomy or radiotherapy. *Journal of Clinical Oncology*, 30, 3540.
- Choi, B.-H., Chakraborty, G., Baek, K. & Yoon, H. S. 2013. Aspirin-induced Bcl-2 translocation and its phosphorylation in the nucleus trigger apoptosis in breast cancer cells. *Experimental & molecular*

medicine, 45, e47-e47.

- Choudhary, C., Kumar, C., Gnad, F., Nielsen, M. L., Rehman, M., Walther, T. C., Olsen, J. V. & Mann, M. 2009. Lysine acetylation targets protein complexes and co-regulates major cellular functions. *Science*, 325, 834-840.
- Christian, F., Smith, E. L. & Carmody, R. J. 2016. The Regulation of NF- κ B Subunits by Phosphorylation. *Cells*, 5, 12.
- Chubak, J., Whitlock, E. P., Williams, S. B., Kamineni, A., Burda, B. U., Buist, D. S. & Anderson, M. L. 2016. Aspirin for the prevention of cancer incidence and mortality: systematic evidence reviews for the US Preventive Services Task Force. *Annals of internal medicine*, 164, 814-825.
- Ciccoli, R., Sahi, S., Singh, S., Prakash, H., Zafiriou, M.-P., Ishdorj, G., Kock, J. L. & Nigam, S. 2005. Oxygenation by COX-2 (cyclo-oxygenase-2) of 3-HETE (3-hydroxyeicosatetraenoic acid), a fungal mimetic of arachidonic acid, produces a cascade of novel bioactive 3-hydroxyeicosanoids. *Biochemical Journal*, 390, 737-747.
- Clarke, M. S., Sundaresan, A., Vanderburg, C. R., Banigan, M. G. & Pellis, N. R. 2013. A three-dimensional tissue culture model of bone formation utilizing rotational co-culture of human adult osteoblasts and osteoclasts. *Acta biomaterialia*, 9, 7908-7916.
- Clements, M., Millar, V., Williams, A. S. & Kalinka, S. 2015. Bridging functional and structural cardiotoxicity assays using human embryonic stem cell-derived cardiomyocytes for a more comprehensive risk assessment. *Toxicological Sciences*, 148, 241-260.
- Colloca, G. & Venturino, A. 2011. The evolving role of familial history for prostate cancer. *Acta Oncologica*, 50, 14-24.
- Corvi, R. & Madia, F. 2017. In vitro genotoxicity testing—Can the performance be enhanced? *Food and Chemical Toxicology*, 106, 600-608.
- Costa, E. C., Gaspar, V. M., Coutinho, P. & Correia, I. J. 2014. Optimization of liquid overlay technique to formulate heterogenic 3D co-cultures models. *Biotechnology and bioengineering*, 111, 1672-1685.
- Coussens, L. M. & Werb, Z. 2002. Inflammation and cancer. *Nature*, 420, 860.
- Crowley, L. C. & Waterhouse, N. J. J. C. S. H. P. 2016. Detecting cleaved caspase-3 in apoptotic cells by flow cytometry. 2016, pdb. prot087312.
- CRUK. 2014a. *Cancer incidence for common cancers* [Online]. Cancer Research UK: Cancer Research UK. Available: <http://www.cancerresearchuk.org/health-professional/cancer-statistics/incidence/common-cancers-compared#heading-Zero> [Accessed 19 Dec 2015].
- CRUK. 2014b. *Prostate cancer incidence statistics* [Online]. Cancer Research UK: Cancer Research UK. Available: <http://www.cancerresearchuk.org/health-professional/cancer-statistics/statistics-by-cancer-type/prostate-cancer/incidence#heading-One> [Accessed 19 Dec 2015].
- CRUK. 2014c. *Worldwide cancer incidence statistics* [Online]. Cancer Research UK: Cancer Research UK. Available: <http://www.cancerresearchuk.org/health-professional/cancer-statistics/worldwide-cancer/incidence#heading-Zero> [Accessed 19 Dec 2015].
- CRUK. 2014d. *Worldwide cancer incidence statistics* [Online]. Cancer Research UK. Available: <http://www.cancerresearchuk.org/health-professional/cancer-statistics/worldwide-cancer/incidence#heading-Zero>

[cancer/incidence#heading-Zero](#) [Accessed 22nd March 2017].

- CRUK. 2016. *Types and Grade* [Online]. Cancer Research UK: Cancer Research UK. Available: <http://www.cancerresearchuk.org/about-cancer/prostate-cancer/types-grades> [Accessed 19 Dec 2017].
- Dai, X., Yan, J., Fu, X., Pan, Q., Sun, D., Xu, Y., Wang, J., Nie, L., Tong, L. & Shen, A. 2017. Aspirin inhibits cancer metastasis and angiogenesis via targeting heparanase. *Clinical Cancer Research*, 23, 6267-6278.
- De Simone, V., Franze, E., Ronchetti, G., Colantoni, A., Fantini, M., Di Fusco, D., Sica, G., Sileri, P., MacDonald, T. & Pallone, F. 2015. Th17-type cytokines, IL-6 and TNF- α synergistically activate STAT3 and NF- κ B to promote colorectal cancer cell growth. *Oncogene*, 34, 3493.
- DeCoster, M. A. 2007. The nuclear area factor (NAF): a measure for cell apoptosis using microscopy and image analysis. *Modern research and educational topics in microscopy*, 378-384.
- Demchenko, A. P. 2013. Beyond annexin V: fluorescence response of cellular membranes to apoptosis. *Cytotechnology*, 65, 157-172.
- Denkert, C., Fürstenberg, A., Daniel, P. T., Koch, I., Köbel, M., Weichert, W., Siegert, A. & Hauptmann, S. 2003. Induction of G0/G1 cell cycle arrest in ovarian carcinoma cells by the anti-inflammatory drug NS-398, but not by COX-2-specific RNA interference. *Oncogene*, 22, 8653.
- Devita Jr, V. T., Lawrence, T. S. & Rosenberg, S. A. 2015. *DeVita, Hellman, and Rosenberg's cancer: principles & practice of oncology*, Lippincott Williams & Wilkins.
- Devlin, C., Greco, S., Martelli, F. & Ivan, M. 2011. miR-210: More than a silent player in hypoxia. *IUBMB life*, 63, 94-100.
- Dhanoya, T. & Burn, J. 2016. Colon cancer and Salicylates. *Evolution, medicine, and public health*, 2016, 146-147.
- Dhiman, H. K., Ray, A. R. & Panda, A. K. 2005. Three-dimensional chitosan scaffold-based MCF-7 cell culture for the determination of the cytotoxicity of tamoxifen. *Biomaterials*, 26, 979-986.
- Di, J.-m., Pang, J., Pu, X.-y., Zhang, Y., Liu, X.-p., Fang, Y.-q., Ruan, X.-x., Gao, X. J. C. g. & cytogenetics 2009. Toll-like receptor 9 agonists promote IL-8 and TGF- β 1 production via activation of nuclear factor κ B in PC-3 cells. 192, 60-67.
- Di, J. M., Pang, J., Sun, Q. P., Zhang, Y., Fang, Y. Q., Liu, X. P., Zhou, J. H., Ruan, X. X. & Gao, X. 2010. Toll-like receptor 9 agonists up-regulates the expression of cyclooxygenase-2 via activation of NF- κ B in prostate cancer cells. *Molecular biology reports*, 37, 1849-1855.
- Diamandis, E. P., Helle, S. I., Yu, H., Melegos, D. N., Lundgren, S. & Lonning, P. E. 1999. Prognostic value of plasma prostate specific antigen after megestrol acetate treatment in patients with metastatic breast carcinoma. *Cancer*, 85, 891-898.
- Dikshit, P., Chatterjee, M., Goswami, A., Mishra, A. & Jana, N. R. 2006. Aspirin induces apoptosis through the inhibition of proteasome function. *Journal of Biological Chemistry*, 281, 29228-29235.
- Ding, J. h., Yuan, L. y., Huang, R. B. & Chen, G. a. 2014. Aspirin inhibits proliferation and induces apoptosis of multiple myeloma cells through regulation of Bcl-2 and Bax and suppression of VEGF. *European journal of haematology*, 93, 329-339.

- Dörsam, B. 2017. *Role of PARP-1 in Colitis-associated Colorectal Cancer Induced by Alkylating N-nitroso Compounds*. Universitätsbibliothek Mainz.
- Dovizio, M., Bruno, A., Tacconelli, S. & Patrignani, P. 2013. Mode of action of aspirin as a chemopreventive agent. *Prospects for chemoprevention of colorectal neoplasia*. Springer.
- Dvorak, H. F., Weaver, V. M., Tlsty, T. D. & Bergers, G. 2011. Tumor microenvironment and progression. *Journal of surgical oncology*, 103, 468-474.
- Edge, S. B. & Compton, C. C. 2010. The American Joint Committee on Cancer: the 7th edition of the AJCC cancer staging manual and the future of TNM. *Annals of surgical oncology*, 17, 1471-1474.
- Edmondson, R., Broglie, J. J., Adcock, A. F. & Yang, L. 2014. Three-dimensional cell culture systems and their applications in drug discovery and cell-based biosensors. *Assay and drug development technologies*, 12, 207-218.
- El-Kady, A., Sun, Y., Li, Y.-x. & Liao, D. J. 2011. Cyclin D1 inhibits whereas c-Myc enhances the cytotoxicity of cisplatin in mouse pancreatic cancer cells via regulation of several members of the NF- κ B and Bcl-2 families. *Journal of Carcinogenesis*, 10, 24.
- Elmore, S. J. T. p. 2007. Apoptosis: a review of programmed cell death. 35, 495-516.
- Elwood, P. C., Morgan, G., Pickering, J. E., Galante, J., Weightman, A. L., Morris, D., Kelson, M. & Dolwani, S. 2016. Aspirin in the Treatment of Cancer: Reductions in Metastatic Spread and in Mortality: A Systematic Review and Meta-Analyses of Published Studies. *PloS one*, 11, e0152402-e0152402.
- Elwood, P. C., Pickering, J. E., Morgan, G., Galante, J., Weightman, A. L., Morris, D., Longley, M., Mason, M., Adams, R., Dolwani, S., Chia W K, J. & Lanasa, A. 2018. Systematic review update of observational studies further supports aspirin role in cancer treatment: Time to share evidence and decision-making with patients? *PloS one*, 13, e0203957-e0203957.
- Epstein, J. I., Egevad, L., Amin, M. B., Delahunt, B., Srigley, J. R. & Humphrey, P. A. J. T. A. j. o. s. p. 2016. The 2014 International Society of Urological Pathology (ISUP) consensus conference on Gleason grading of prostatic carcinoma. 40, 244-252.
- Escarcega, R., Fuentes-Alexandro, S., Garcia-Carrasco, M., Gatica, A. & Zamora, A. 2007. The transcription factor nuclear factor-kappa B and cancer. *Clinical Oncology*, 19, 154-161.
- Eskicorapci, S. Y., Baydar, D. E., Akbal, C., Sofikerim, M., Günay, M., Ekici, S. & Ozen, H. 2004. An extended 10-core transrectal ultrasonography guided prostate biopsy protocol improves the detection of prostate cancer. *European urology*, 45, 444-449.
- Eskicorapci, S. Y., Guliyev, F., Akdogan, B., Dogan, H. S., Ergen, A. & Ozen, H. 2005. Individualization of the biopsy protocol according to the prostate gland volume for prostate cancer detection. *The Journal of urology*, 173, 1536-1540.
- Fang, F.-M., Wang, Y.-M., Wang, C.-J., Huang, H.-Y. & Chiang, P.-H. 2008. Comparison of the outcome and morbidity for localized or locally advanced prostate cancer treated by high-dose-rate brachytherapy plus external beam radiotherapy (EBRT) versus EBRT alone. *Japanese journal of clinical oncology*, 38, 474-479.

- Fatehullah, A., Appleton, P. L. & Näthke, I. S. 2013. Cell and tissue polarity in the intestinal tract during tumorigenesis: cells still know the right way up, but tissue organization is lost. *Phil. Trans. R. Soc. B*, 368, 20130014.
- Fenech, M., Chang, W. P., Kirsch-Volders, M., Holland, N., Bonassi, S., Zeiger, E. J. M. R. G. T. & Mutagenesis, E. 2003. HUMN project: detailed description of the scoring criteria for the cytokinesis-block micronucleus assay using isolated human lymphocyte cultures. 534, 65-75.
- Fenech, M., Kirsch-Volders, M., Natarajan, A. T., Surralles, J., Crott, J. W., Parry, J., Norppa, H., Eastmond, D. A. & Tucker, J. D. 2011. Molecular mechanisms of micronucleus, nucleoplasmic bridge and nuclear bud formation in mammalian and human cells. *Mutagenesis*, 26, 125-132.
- Feng, J., Huang, C., Wren, J. D., Wang, D.-W., Yan, J., Zhang, J., Sun, Y., Han, X. & Zhang, X. A. 2015. Tetraspanin CD82: a suppressor of solid tumors and a modulator of membrane heterogeneity. *Cancer and Metastasis Reviews*, 34, 619-633.
- Fennema, E., Rivron, N., Rouwkema, J., van Blitterswijk, C. & de Boer, J. 2013. Spheroid culture as a tool for creating 3D complex tissues. *Trends in biotechnology*, 31, 108-115.
- Fernández-Martínez, A. B., Collado, B., Bajo, A. M., Sánchez-Chapado, M., Prieto, J. C. & Carmena, M. J. 2007a. Vasoactive intestinal peptide induces cyclooxygenase-2 expression through nuclear factor- κ B in human prostate cell lines: Differential time-dependent responses in cancer progression. *Molecular and cellular endocrinology*, 270, 8-16.
- Fernández-Martínez, A. B., Collado, B., Bajo, A. M., Sánchez-Chapado, M., Prieto, J. C., Carmena, M. J. J. M. & endocrinology, c. 2007b. Vasoactive intestinal peptide induces cyclooxygenase-2 expression through nuclear factor- κ B in human prostate cell lines: Differential time-dependent responses in cancer progression. 270, 8-16.
- Ferrandez, A., Prescott, S. & Burt, R. 2003. COX-2 and colorectal cancer. *Current pharmaceutical design*, 9, 2229-2251.
- Finetti, F., Solito, R., Morbidelli, L., Giachetti, A., Ziche, M., Donnini, S. & Donnini, S. 2008. Prostaglandin E 2 regulates angiogenesis via activation of fibroblast growth factor receptor-1. *Journal of Biological Chemistry*, 283, 2139-2146
- Fitzgerald, K. A., Guo, J., Tierney, E. G., Curtin, C. M., Malhotra, M., Darcy, R., O'Brien, F. J. & O'Driscoll, C. M. 2015. The use of collagen-based scaffolds to simulate prostate cancer bone metastases with potential for evaluating delivery of nanoparticulate gene therapeutics. *Biomaterials*, 66, 53-66.
- Fitzwalter, B. E. & Thorburn, A. J. N. c. b. 2017. A caspase-independent way to kill cancer cells. 19, 1014.
- Foekens, J., Diamandis, E., Yu, H., Look, M., Meijer-van Gelder, M. & Klijn, J. 1999. Expression of prostate-specific antigen (PSA) correlates with poor response to tamoxifen therapy in recurrent breast cancer. *British journal of cancer*, 79, 888.
- Foley, K. E. 2017. Organoids: a better in vitro model. Nature Publishing Group.
- Fosslien, E. J. A. o. C. & Science, L. 2000. Molecular pathology of cyclooxygenase-2 in neoplasia. 30, 3-21.

- Foty, R. 2011. A Simple Hanging Drop Cell Culture Protocol for Generation of 3D Spheroids. *Journal of Visualized Experiments : JoVE*, 2720.
- Fowler, P., Homan, A., Atkins, D., Whitwell, J., Lloyd, M., Bradford, R. J. M. R. G. T. & Mutagenesis, E. 2016. The utility of the in vitro micronucleus test for evaluating the genotoxicity of natural and manmade nano-scale fibres. 809, 33-42.
- Fujita, H., Koshida, K., Keller, E. T., Takahashi, Y., Yoshimoto, T., Namiki, M. & Mizokami, A. J. T. P. 2002. Cyclooxygenase-2 promotes prostate cancer progression. 53, 232-240.
- Gamble, C., McIntosh, K., Scott, R., Ho, K. H., Plevin, R. & Paul, A. 2012. Inhibitory kappa B kinases as targets for pharmacological regulation. *British Journal of Pharmacology*, 165, 802-819.
- Gan, L., Qiu, Z., Huang, J., Li, Y., Huang, H., Xiang, T., Wan, J., Hui, T., Lin, Y., Li, H. & Ren, G. 2016. Cyclooxygenase-2 in tumor-associated macrophages promotes metastatic potential of breast cancer cells through Akt pathway. *International Journal of Biological Sciences*, 12, 1533-1543.
- Gandhi, J., Khera, L., Gaur, N., Paul, C. & Kaul, R. 2017. Role of Modulator of Inflammation Cyclooxygenase-2 in Gammaherpesvirus Mediated Tumorigenesis. *Frontiers in Microbiology*, 8, 538.
- Gao, L. & Williams, J. L. 2012. Nitric oxide-donating aspirin induces G2/M phase cell cycle arrest in human cancer cells by regulating phase transition proteins. *International journal of oncology*, 41, 325-330.
- García-González, M., Abdulkader, I., Boquete, A. V., Neo, X. M. L., Forteza, J. & Cameselle-Teijeiro, J. 2005. Cyclooxygenase-2 in normal, hyperplastic and neoplastic follicular cells of the human thyroid gland. *Virchows Archiv*, 447, 12-17.
- Garg, R., Blando, J., Perez, C. J., Wang, H., Benavides, F. J. & Kazanietz, M. G. 2012. Activation of Nuclear Factor κ B (NF- κ B) in Prostate Cancer Is Mediated by Protein Kinase C ϵ (PKC ϵ). *The Journal of Biological Chemistry*, 287, 37570-37582.
- Garg, R., Blando, J. M., Perez, C. J., Lal, P., Feldman, M. D., Smyth, E. M., Ricciotti, E., Grosser, T., Benavides, F. & Kazanietz, M. G. 2018. COX-2 mediates pro-tumorigenic effects of PKC ϵ in prostate cancer. *Oncogene*, 1.
- Geiger, T. R. & Peeper, D. S. 2009. Metastasis mechanisms. *Biochimica et Biophysica Acta (BBA)-Reviews on Cancer*, 1796, 293-308.
- Ghosh, N., Chaki, R., Mandal, V. & Mandal, S. C. 2010. COX-2 as a target for cancer chemotherapy. *Pharmacological reports*, 62, 233-244.
- Ghosh, S., May, M. J. & Kopp, E. B. J. A. r. o. i. 1998. NF- κ B and Rel proteins: evolutionarily conserved mediators of immune responses. 16, 225-260.
- Gleason, D. 1977. Histologic grading and clinical staging of prostate carcinoma. *Urologic Pathology: The Prostate*. . Philadelphia: Lea and Febiger.
- Glinsky, V. V., Huflejt, M. E., Glinsky, G. V., Deutscher, S. L. & Quinn, T. P. 2000. Effects of Thomsen-Friedenreich antigen-specific peptide P-30 on β -galactoside-mediated homotypic aggregation and adhesion to the endothelium of MDA-MB-435 human breast carcinoma cells. *Cancer research*, 60, 2584-2588.
- Gomella, L. G. 2009. Effective testosterone suppression for prostate cancer: is there a best castration therapy?

Reviews in urology, 11, 52-60.

- Gómez, J., García-Domingo, D., Martínez-A, C. & Rebollo, A. 1997. Role of NF-KB in the control of apoptotic and proliferative responses in IL-2-responsive T cells. *Frontiers in Bioscience*, 2, d49-60.
- Gong, X., Lin, C., Cheng, J., Su, J., Zhao, H., Liu, T., Wen, X. & Zhao, P. 2015. Generation of Multicellular Tumor Spheroids with Microwell-Based Agarose Scaffolds for Drug Testing. *PLoS ONE*, 10, e0130348.
- Goonewardene, S. S., Phull, J. S., Bahl, A. & Persad, R. A. 2014. Interpretation of PSA levels after radical therapy for prostate cancer. *Trends in Urology & Men's Health*, 5, 30-34.
- Gorin, M. A., Chalfin, H. J., Epstein, J. I., Feng, Z., Partin, A. W. & Trock, B. J. 2014. Predicting the Risk of Non-organ-confined Prostate Cancer When Perineural Invasion Is Found on Biopsy. *Urology*, 83, 1117-1121.
- Griffin, R. M. 2018. *Hormone Treatment Fights Prostate Cancer* [Online]. Webmd. Available: <https://www.webmd.com/prostate-cancer/features/hormone-therapy-for-prostate-cancer#1> [Accessed 19 Dec 2018].
- Gu, X., Gao, X., Cui, M., Xie, M., Ma, M., Qin, S., Li, X., Qi, X., Bai, Y. & Wang, D. 2018. Survival outcomes of radical prostatectomy and external beam radiotherapy in clinically localized high-risk prostate cancer: a population-based, propensity score matched study. *Cancer management and research*, 10, 1061-1067.
- Guo, C. C., Zuo, G., Cao, D., Troncoso, P. & Czerniak, B. A. J. M. P. 2009. Prostate cancer of transition zone origin lacks TMPRSS2-ERG gene fusion. 22, 866.
- Guo, G., Xu, Y. & Zhang, X. 2017. TRUS-guided transperineal prostate 12+X core biopsy with template for the diagnosis of prostate cancer. *Oncology Letters*, 13, 4863-4867.
- Gupta, S. C., Sung, B., Prasad, S., Webb, L. J. & Aggarwal, B. B. 2013. Cancer drug discovery by repurposing: teaching new tricks to old dogs. *Trends in pharmacological sciences*, 34, 508-517.
- Haile, R. W., Yochim, J. M., Cortessis, V. K., Lin, J., Levine, A. J., Diep, A., Danenberg, K. & Danenberg, P. 2005. A molecular/epidemiologic analysis of expression of cyclooxygenases 1 and 2, use of nonsteroidal antiinflammatory drugs, and risk of colorectal adenoma. *Clinical colorectal cancer*, 4, 390-395.
- Hamilton, G. 1998. Multicellular spheroids as an in vitro tumor model. *Cancer letters*, 131, 29-34.
- Han, X., Li, H., Su, L., Zhu, W., Xu, W., Li, K., Zhao, Q., Yang, H. & Liu, H. 2014. Effect of celecoxib plus standard chemotherapy on serum levels of vascular endothelial growth factor and cyclooxygenase-2 in patients with gastric cancer. *Biomedical reports*, 2, 183-187.
- Hao, W., Shen, Y., Feng, M., Wang, H., Lin, M., Fang, Y. & Tan, L. 2018. Aspirin acts in esophageal cancer: a brief review. *Journal of thoracic disease*, 10, 2490-2497.
- Härmä, V., Haavikko, R., Virtanen, J., Ahonen, I., Schukov, H.-P., Alakurtti, S., Purev, E., Rischer, H., Yli-Kauhala, J. & Moreira, V. M. 2015. Optimization of invasion-specific effects of betulin derivatives on prostate cancer cells through lead development. *PLoS one*, 10, e0126111.
- Harrison, R. G. 1908. Embryonic transplantation and development of the nervous system. *The Anatomical Record*, 2(9), 385-410.
- Hashemipour, M. A., Mehrabizadeh Honarmand, H., Falsafi, F., Tahmasebi Arashlo, M., Rajabalian, S. &

- Gandjalikhan Nassab, S. A. H. 2016. In Vitro Cytotoxic Effects of Celecoxib, Mefenamic Acid, Aspirin and Indometacin on Several Cells Lines. *Journal of Dentistry*, 17, 219-225.
- He, B., Lu, N. & Zhou, Z. J. C. o. i. c. b. 2009. Cellular and nuclear degradation during apoptosis. 21, 900-912.
- He, Y., Huang, H., Farischon, C., Li, D., Du, Z., Zhang, K., Zheng, X. & Goodin, S. 2017. Combined effects of atorvastatin and aspirin on growth and apoptosis in human prostate cancer cells. *Oncology reports*, 37, 953-960.
- Heams, T. 2012. Selection within organisms in the nineteenth century: Wilhelm Roux's complex legacy. *Progress in Biophysics and Molecular Biology*, 110(1), 24-33.
- Heidenreich, A., Bastian, P. J., Bellmunt, J., Bolla, M., Joniau, S., van der Kwast, T., Mason, M., Matveev, V., Wiegel, T. & Zattoni, F. 2014. EAU guidelines on prostate cancer. Part II: treatment of advanced, relapsing, and castration-resistant prostate cancer. *European urology*, 65, 467-479.
- Helmy, I. M. & Abdel Azim, A. M. 2012. Efficacy of ImageJ in the assessment of apoptosis. *Diagnostic Pathology*, 7, 15-15.
- Hensley, P. J. & Kyprianou, N. 2012. Modeling Prostate Cancer in Mice: Limitations and Opportunities. *Journal of andrology*, 33, 133-144.
- Herrmann, D., Conway, J. R., Vennin, C., Magenau, A., Hughes, W. G. & Timpson, P. 2014. Three-dimensional cancer models mimic cell-matrix interactions in the tumour microenvironment. *Carcinogenesis*, bgu108.
- Hinev, A. I., Anakievski, D. & Hadjiev, V. I. 2012. Radical prostatectomy as a first-line treatment in patients with initial PSA > 20 ng/mL. *International journal of surgical oncology*, 2012.
- Hodge, K., McNeal, J. & Stamey, T. 1989. Ultrasound guided transrectal core biopsies of the palpably abnormal prostate. *The Journal of urology*, 142, 66-70.
- Holton, S. E., Bergamaschi, A., Katzenellenbogen, B. S. & Bhargava, R. 2014. Integration of molecular profiling and chemical imaging to elucidate fibroblast-microenvironment impact on cancer cell phenotype and endocrine resistance in breast cancer. *PLoS One*, 9, e96878.
- Hossain, M. A., Kim, D. H., Jang, J. Y., Kang, Y. J., Yoon, J.-H., Moon, J.-O., Chung, H. Y., Kim, G.-Y., Choi, Y. H. & Copple, B. L. 2012. Aspirin induces apoptosis in vitro and inhibits tumor growth of human hepatocellular carcinoma cells in a nude mouse xenograft model. *International journal of oncology*, 40, 1298-1304.
- Hosseinkhani, H. J. C. d. s. 2012. 3D in vitro technology for drug discovery. 7, 37-43.
- Hsu, Y., Hou, M., Kuo, P., Huang, Y. & Tsai, E. 2013. Breast tumor-associated osteoblast-derived CXCL5 increases cancer progression by ERK/MSK1/Elk-1/snail signaling pathway. *Oncogene*, 32, 4436.
- Hua, H., Zhang, H., Kong, Q., Wang, J. & Jiang, Y. 2018. Complex roles of the old drug aspirin in cancer chemoprevention and therapy. *Medicinal research reviews*.
- Huang, H., Chen, F. J. N. A. J. o. M. & Science 2012. Prostatic Ductal Adenocarcinoma Ex-hibits More Advanced Histopathological Features than Acinar Adenocarcinoma. 5, 208-11.
- Huang, S. H., Xu, W., Waldron, J., Siu, L., Shen, X., Tong, L., Ringash, J., Bayley, A., Kim, J. & Hope, A. 2015. Refining American Joint Committee on Cancer/Union for International Cancer Control TNM stage and prognostic

- groups for human papillomavirus–related oropharyngeal carcinomas. *Journal of clinical oncology*, 33, 836-845.
- Huang, X., Ding, L., Bennewith, K. L., Tong, R. T., Welford, S. M., Ang, K. K., Story, M., Le, Q.-T. & Giaccia, A. J. 2009. Hypoxia-inducible *miR-210* regulates normoxic gene expression involved in tumor initiation. *Molecular cell*, 35, 856-867.
- Huang, X., Le, Q.-T. & Giaccia, A. J. 2010. *MiR-210*–micromanager of the hypoxia pathway. *Trends in molecular medicine*, 16, 230-237.
- Huch, M. & Koo, B.-K. 2015. Modeling mouse and human development using organoid cultures. *Development*, 142, 3113-3125.
- Hudson, B. D., Kulp, K. S. & Loots, G. G. 2013. Prostate cancer invasion and metastasis: insights from mining genomic data. *Briefings in Functional Genomics*, 12, 397-410.
- Huggins, C. 1978. Endocrine-induced regression of cancers. *The American Journal of Surgery*, 136, 233-238.
- Hugo, H. J., Saunders, C., Ramsay, R. G. & Thompson, E. W. 2015. New Insights on COX-2 in Chronic Inflammation Driving Breast Cancer Growth and Metastasis. *Journal of Mammary Gland Biology and Neoplasia*, 20, 109-119.
- Huo, X., Zhang, X., Yu, C., Cheng, E., Zhang, Q. D., Dunbar, K. B., Pham, T., Lynch, J. P., Wang, D. H. & Bresalier, R. S. 2017. Aspirin Prevents NF-κB Activation and CDX2 Expression Induced by Acid and Bile Salts in Esophageal Squamous Cells of Patients with Barrett’s Esophagus. *Gastroenterology*, 152, S233.
- Hurwitz, A. A., Foster, B. A., Allison, J. P., Greenberg, N. M. & Kwon, E. D. 2001. The TRAMP mouse as a model for prostate cancer. *Current protocols in immunology*, 45, 20.5. 1-20.5. 23.
- Hutmacher, D. W., Sittinger, M. & Risbud, M. V. 2004. Scaffold-based tissue engineering: rationale for computer-aided design and solid free-form fabrication systems. *Trends in Biotechnology*, 22(7), 354-362.
- Hwang, Y. W., Kim, S. Y., Jee, S. H., Kim, Y. N. & Nam, C. M. 2009. Soy food consumption and risk of prostate cancer: a meta-analysis of observational studies. *Nutrition and cancer*, 61, 598-606.
- Iglesias-Guimaraes, V., Gil-Guiñón, E., Gabernet, G., García-Belinchón, M., Sánchez-Osuna, M., Casanelles, E., Comella, J. X. & Yuste, V. J. 2012. Apoptotic DNA degradation into oligonucleosomal fragments, but not apoptotic nuclear morphology, relies on a cytosolic pool of DFF40/CAD endonuclease. *The Journal of biological chemistry*, 287, 7766-7779.
- Imamura, Y., Mukohara, T., Shimono, Y., Funakoshi, Y., Chayahara, N., Toyoda, M., Kiyota, N., Takao, S., Kono, S. & Nakatsura, T. 2015. Comparison of 2D-and 3D-culture models as drug-testing platforms in breast cancer. *Oncology reports*, 33, 1837-1843.
- Imperiale, T. F. 2013. Aspirin and the prevention of colorectal cancer. *New England Journal of Medicine*, 348, 879-880.
- Ishikawa, H., Mutoh, M., Suzuki, S., Tokudome, S., Saida, Y., Abe, T., Okamura, S., Tajika, M., Joh, T. & Tanaka, S. 2014. The preventive effects of low-dose enteric-coated aspirin tablets on the development of colorectal tumours in Asian patients: a randomised trial. *Gut*, 63, 1755-1759.

- Ishiyama, D., Vujaklija, D. & Davies, J. 2004. Novel pathway of salicylate degradation by *Streptomyces* sp. strain WA46. *Applied and environmental microbiology*, 70, 1297-1306.
- Ito, K. 2014. Prostate cancer in Asian men. *Nature Reviews Urology*, 11, 197-212.
- Jabbour, H., Kelly, R., Boddy, S. J. P., leukotrienes & acids, e. f. 2002. Autocrine/paracrine regulation of apoptosis in epithelial cells by prostaglandin E2. 67, 357-363.
- Jacobi, N., Seeboeck, R., Hofmann, E., Schweiger, H., Smolinska, V., Mohr, T., Boyer, A., Sommergruber, W., Lechner, P., Pichler-Huebschmann, C., Önder, K., Hundsberger, H., Wiesner, C. & Eger, A. 2017. Organotypic three-dimensional cancer cell cultures mirror drug responses in vivo: lessons learned from the inhibition of EGFR signaling. *Oncotarget*, 8, 107423-107440.
- Jamieson, T., Clarke, M., Steele, C. W., Samuel, M. S., Neumann, J., Jung, A., Huels, D., Olson, M. F., Das, S. & Nibbs, R. J. 2012. Inhibition of CXCR2 profoundly suppresses inflammation-driven and spontaneous tumorigenesis. *The Journal of clinical investigation*, 122, 3127-3144.
- Jani, A., Su, A., Correa, D. & Gratzle, J. 2007. Comparison of late gastrointestinal and genitourinary toxicity of prostate cancer patients undergoing intensity-modulated versus conventional radiotherapy using localized fields. *Prostate cancer and prostatic diseases*, 10, 82-86.
- Jaradat, M. S., Wongsud, B., Phornchirasilp, S., Rangwala, S. M., Shams, G., Sutton, M., Romstedt, K. J., Noonan, D. J. & Feller, D. R. 2001. Activation of peroxisome proliferator-activated receptor isoforms and inhibition of prostaglandin H 2 synthases by ibuprofen, naproxen, and indomethacin. *Biochemical pharmacology*, 62, 1587-1595.
- Jemal, A., Bray, F., Center, M. M., Ferlay, J., Ward, E. & Forman, D. 2011. Global cancer statistics. *CA: a cancer journal for clinicians*, 61, 69-90.
- Jeon, Y.-J., Athukorala, Y. & Lee, J.-H. J. A. 2005. Characterization of agarose product from agar using DMSO. 20, 61-67.
- Jiang, W. G., Sanders, A. J., Katoh, M., Ungefroren, H., Gieseler, F., Prince, M., Thompson, S., Zollo, M., Spano, D. & Dhawan, P. Tissue invasion and metastasis: Molecular, biological and clinical perspectives. *Seminars in cancer biology*, 2015. Elsevier, S244-S275.
- Joan, C. 2003. Cyclooxygenase-2 Biology. *Current Pharmaceutical Design*, 9, 2177-2190.
- Jones, C. U., Hunt, D., McGowan, D. G., Amin, M. B., Chetner, M. P., Bruner, D. W., Leibenhaut, M. H., Husain, S. M., Rotman, M. & Souhami, L. 2011. Radiotherapy and short-term androgen deprivation for localized prostate cancer. *New England Journal of Medicine*, 365, 107-118.
- Kaisani, A., Delgado, O., Fasciani, G., Kim, S. B., Wright, W. E., Minna, J. D. & Shay, J. W. 2014. Branching morphogenesis of immortalized human bronchial epithelial cells in three-dimensional culture. *Differentiation*, 87, 119-126.
- Kalle, A. M. & Rizvi, A. 2011. Inhibition of bacterial multidrug resistance by celecoxib, a cyclooxygenase-2 inhibitor. *Antimicrobial agents and chemotherapy*, 55, 439-442.
- Kalogeris, T., Baines, C. P., Krenz, M. & Korthuis, R. J. 2012. Cell Biology of Ischemia/Reperfusion Injury.

International review of cell and molecular biology, 298, 229-317.

- Kamble, P., Litvinov, D., Aluganti Narasimhulu, C., Jiang, X. & Parthasarathy, S. 2015. Aspirin may influence cellular energy status. *European journal of pharmacology*, 749, 12-19.
- Kanao, K., Komori, O., Nakashima, J., Ohigashi, T., Kikuchi, E., Miyajima, A., Nakagawa, K., Eguchi, S. & Oya, M. 2014. Individualized prostate-specific antigen threshold values to avoid overdiagnosis of prostate cancer and reduce unnecessary biopsy in elderly men. *Japanese journal of clinical oncology*, 44, 852-859.
- Kapałczyńska, M., Kolenda, T., Przybyła, W., Zajączkowska, M., Teresiak, A., Filas, V., Ibbs, M., Bliźniak, R., Łuczewski, Ł. & Lamperska, K. 2018. 2D and 3D cell cultures - a comparison of different types of cancer cell cultures. *Archives of medical science : AMS*, 14, 910-919.
- Karin, M. 2006. Nuclear factor- κ B in cancer development and progression. *Nature*, 441, 431.
- Kashiwagi, E., Shiota, M., Yokomizo, A., Itsumi, M., Inokuchi, J., Uchiumi, T. & Naito, S. 2013. Prostaglandin receptor EP3 mediates growth inhibitory effect of aspirin through androgen receptor and contributes to castration resistance in prostate cancer cells. *Endocrine-related cancer*, 20, 431-441.
- Kawamura, M., Toiyama, Y., Tanaka, K., Saigusa, S., Okugawa, Y., Hiro, J., Uchida, K., Mohri, Y., Inoue, Y. & Kusunoki, M. 2012. CXCL5, a promoter of cell proliferation, migration and invasion, is a novel serum prognostic marker in patients with colorectal cancer. *European journal of cancer*, 48, 2244-2251.
- Kay, J. G. & Grinstein, S. 2011. Sensing phosphatidylserine in cellular membranes. *Sensors (Basel, Switzerland)*, 11, 1744-1755.
- Khosravi, A., Nemati, E., Soleimani, M., Raesi, N. & Abbaszadeh, S. 2016. Association between prostate specific antigen levels and coronary artery angioplasty. *Journal of renal injury prevention*, 6, 132-136.
- Kim, B. H., Kim, C. I., Chang, H. S., Choe, M. S., Jung, H. R., Kim, D. Y. & Park, C. H. 2011. Cyclooxygenase-2 overexpression in chronic inflammation associated with benign prostatic hyperplasia: is it related to apoptosis and angiogenesis of prostate cancer? *Korean journal of urology*, 52, 253-259.
- Kim, D. H., Chung, J. H., Yoon, J. S., Ha, Y. M., Bae, S., Lee, E. K., Jung, K. J., Kim, M. S., Kim, Y. J. & Kim, M. K. 2013. Ginsenoside Rd inhibits the expressions of iNOS and COX-2 by suppressing NF- κ B in LPS-stimulated RAW264. 7 cells and mouse liver. *Journal of Ginseng Research*, 37, 54.
- Kim, E. H., Larson, J. A. & Andriole, G. L. 2016. Management of Benign Prostatic Hyperplasia. *Annual Review of Medicine*, 67, 137-151.
- Kim, J. B. Three-dimensional tissue culture models in cancer biology. *Seminars in cancer biology*, 2005. Elsevier, 365-377.
- Kimura, T. 2012. East meets West: ethnic differences in prostate cancer epidemiology between East Asians and Caucasians. *Chinese journal of cancer*, 31, 421.
- Knudsen, E. S. & Witkiewicz, A. K. J. O. 2016. Defining the transcriptional and biological response to CDK4/6 inhibition in relation to ER+/HER2-breast cancer. 7, 69111.
- Ko, C. J., Lan, S. W., Lu, Y. C., Cheng, T. S., Lai, P. F., Tsai, C. H., Hsu, T. W., Lin, H. Y., Shyu, H. Y., Wu, S. R., Lin, H. H., Hsiao, P. W., Chen, C. H., Huang, H. P. & Lee, M. S. 2017. Inhibition of cyclooxygenase-2-mediated

- matriptase activation contributes to the suppression of prostate cancer cell motility and metastasis. *Oncogene*, 36, 4597.
- Kopp, E. & Ghosh, S. 1994. Inhibition of NF-kappa B by sodium salicylate and aspirin. *Science*, 265, 956-959.
- Korfage, I. J., De Koning, H. J., Habbema, J. D. F., Schröder, F. H. & Essink-Bot, M. L. 2007. Side-effects of treatment for localized prostate cancer: are they valued differently by patients and healthy controls? *BJU international*, 99, 801-806.
- Kraus, S., Naumov, I. & Arber, N. 2013. COX-2 active agents in the chemoprevention of colorectal cancer. *Prospects for Chemoprevention of Colorectal Neoplasia*. Springer.
- Krawczyk-Rusiecka, K., Wojciechowska-Durczynska, K., Cyniak-Magierska, A., Zygmunt, A. & Lewinski, A. 2014. Assessment of cyclooxygenase-1 and 2 gene expression levels in chronic autoimmune thyroiditis, papillary thyroid carcinoma and nontoxic nodular goitre. *Thyroid research*, 7, 10.
- Kroemer, G. & Martin, S. J. J. N. m. 2005. Caspase-independent cell death. 11, 725.
- Kulshreshtha, R., Ferracin, M., Wojcik, S. E., Garzon, R., Alder, H., Agosto-Perez, F. J., Davuluri, R., Liu, C.-G., Croce, C. M. & Negrini, M. 2007. A microRNA signature of hypoxia. *Molecular and cellular biology*, 27, 1859-1867.
- Kumar, B. P., Rajput, S., Dey, K. K., Parekh, A., Das, S., Mazumdar, A. & Mandal, M. 2013. Celecoxib alleviates tamoxifen-instigated angiogenic effects by ROS-dependent VEGF/VEGFR2 autocrine signaling. *BMC cancer*, 13, 273.
- Kumari, K. & Durga, R. B. 2014. Transrectal Ultrasound Guided Needle Core Biopsy of Prostatic Lesions. *International Journal of Health Sciences and Research (IJHSR)*, 4, 142-148.
- Kurahashi, N., Iwasaki, M., Sasazuki, S., Otani, T., Inoue, M. & Tsugane, S. 2007. Soy product and isoflavone consumption in relation to prostate cancer in Japanese men. *Cancer Epidemiology and Prevention Biomarkers*, 16, 538-545.
- Kutuk, O. & Basaga, H. 2004. Aspirin inhibits TNF α -and IL-1-induced NF- κ B activation and sensitizes HeLa cells to apoptosis. *Cytokine*, 25, 229-237.
- Kuwano, T., Nakao, S., Yamamoto, H., Tsuneyoshi, M., Yamamoto, T., Kuwano, M. & Ono, M. 2004. Cyclooxygenase 2 is a key enzyme for inflammatory cytokine-induced angiogenesis. *The FASEB Journal*, 18, 300-310.
- Kyriakopoulos, A. M., Nagl, M., Baliou, S. & Zoumpourlis, V. 2017. Alleviating Promotion of Inflammation and Cancer Induced by Nonsteroidal Anti-Inflammatory Drugs. *International Journal of Inflammation*, 2017, 9632018.
- Laaksonen, R., Katajamaa, M., Päivä, H., Sysi-Aho, M., Saarinen, L., Junni, P., Lütjohann, D., Smet, J., Van Coster, R. & Seppänen-Laakso, T. J. P. o. 2006. A systems biology strategy reveals biological pathways and plasma biomarker candidates for potentially toxic statin-induced changes in muscle. 1, e97.
- Lai, T. S., Davies, C. & Greenberg, C. S. 2010. Human tissue transglutaminase is inhibited by pharmacologic and chemical acetylation. *Protein Science*, 19, 229-235.
- Lalier, L., Pedelaborde, F., Braud, C., Menanteau, J., Vallette, F. M. & Olivier, C. 2011. Increase in intracellular PGE2

- induces apoptosis in Bax-expressing colon cancer cell. *BMC cancer*, 11, 153-153.
- Lam, R., Han, W. & Yu, K. 2015. Unirradiated cells rescue cells exposed to ionizing radiation: Activation of NF- κ B pathway in irradiated cells. *Mutation Research/Fundamental and Molecular Mechanisms of Mutagenesis*, 782, 23-33.
- Langley, R. E. 2013. Clinical evidence for the use of aspirin in the treatment of cancer. *ecancermedicalscience*, 7, 297.
- Langley, R. E., Burdett, S., Tierney, J. F., Cafferty, F., Parmar, M. K. B. & Venning, G. 2011. Aspirin and cancer: has aspirin been overlooked as an adjuvant therapy? *British journal of cancer*, 105, 1107-1113.
- Lant, B. & Derry, W. B. J. M. 2013. Methods for detection and analysis of apoptosis signaling in the *C. elegans* germline. 61, 174-182.
- Lapi, F., Levi, M., Simonetti, M., Cancian, M., Parretti, D., Cricelli, I., Sobrero, A. & Cricelli, C. 2016. Risk of prostate cancer in low-dose aspirin users: A retrospective cohort study. *International journal of cancer*, 139, 205-211.
- Lau, W.-H., Pandey, V., Kong, X., Wang, X.-N., Wu, Z., Zhu, T. & Lobie, P. E. 2015. Trefoil factor-3 (TFF3) stimulates de novo angiogenesis in mammary carcinoma both directly and indirectly via IL-8/CXCR2. *PloS one*, 10, e0141947.
- Laube, M., Kniess, T. & Pietzsch, J. 2016. Development of Antioxidant COX-2 Inhibitors as Radioprotective Agents for Radiation Therapy-A Hypothesis-Driven Review. *Antioxidants (Basel, Switzerland)*, 5, 14.
- Lee, C. T. & Oesterling, J. E. Diagnostic markers of prostate cancer: Utility of prostate-specific antigen in diagnosis and staging. *Seminars in surgical oncology*, 1995. Wiley Online Library, 23-35.
- Lee, E. Y., Kang, J. Y. & Kim, K.-W. 2015. Expression of cyclooxygenase-2, peroxiredoxin I, peroxiredoxin 6 and nuclear factor- κ B in oral squamous cell carcinoma. *Oncology Letters*, 10, 3129-3136.
- Lee, J. M., Mhawech-Fauceglia, P., Lee, N., Parsanian, L. C., Lin, Y. G., Gayther, S. A. & Lawrenson, K. 2013. A three-dimensional microenvironment alters protein expression and chemosensitivity of epithelial ovarian cancer cells in vitro. *Laboratory investigation*, 93, 528.
- Lee, S. K., Park, M. S. & Nam, M. J. 2008. Aspirin has antitumor effects via expression of calpain gene in cervical cancer cells. *Journal of oncology*, 2008.
- Leslie, K., Gao, S. P., Berishaj, M., Podsypanina, K., Ho, H., Ivashkiv, L. & Bromberg, J. 2010. Differential interleukin-6/Stat3 signaling as a function of cellular context mediates Ras-induced transformation. *Breast Cancer Research : BCR*, 12(5), R80-R80.
- Li, D., Wang, P., Yu, Y., Huang, B., Zhang, X., Xu, C., Zhao, X., Yin, Z., He, Z., Jin, M. & Liu, C. 2018. Tumor-preventing activity of aspirin in multiple cancers based on bioinformatic analyses. *PeerJ*, 6, e5667-e5667.
- Li, J. & Wang, Z. J. C. J. o. C. R. 2016. The pathology of unusual subtypes of prostate cancer. 28, 130.
- Li, Y., Wu, L., Li, K., Liu, Y., Xiang, R., Zhang, S., Zhu, L. & Zhang, L. 2011. Involvement of nuclear factor κ B (NF- κ B) in the downregulation of cyclo-oxygenase-2 (COX-2) by genistein in gastric cancer cells. *Journal of International Medical Research*, 39, 2141-2150.

- Liao, D., Zhong, L., Duan, T., Zhang, R.-H., Wang, X., Wang, G., Hu, K., Lv, X. & Kang, T. 2015. Aspirin suppresses the growth and metastasis of osteosarcoma through the NF- κ B pathway. *Clinical cancer research*, 21, 5349-5359.
- Liberman, D., Jarosek, S., Virnig, B. A., Chu, H. & Elliott, S. P. 2016. The patient burden of bladder outlet obstruction after prostate cancer treatment. *The Journal of urology*, 195, 1459-1463.
- Lichtenstein, P., Holm, N. V., Verkasalo, P. K., Iliadou, A., Kaprio, J., Koskenvuo, M., Pukkala, E., Skytthe, A. & Hemminki, K. 2000. Environmental and heritable factors in the causation of cancer—analyses of cohorts of twins from Sweden, Denmark, and Finland. *New England journal of medicine*, 343, 78-85.
- Lickteig, A. J., Slitt, A. L., Arkan, M. C., Karin, M., Cherrington, N. J. J. D. m. & disposition 2007. Differential regulation of hepatic transporters in the absence of tumor necrosis factor- α , interleukin-1 β , interleukin-6, and nuclear factor- κ B in two models of cholestasis. 35, 402-409.
- Lin, P.-H., Aronson, W. & Freedland, S. J. 2015. Nutrition, dietary interventions and prostate cancer: the latest evidence. *BMC medicine*, 13, 3.
- Lin, R. Z. & Chang, H. Y. 2010. Recent advances in three-dimensional multicellular spheroid culture for biomedical research. *Biotechnology journal*, 3, 1172-1184.
- Liu, B., Han, M. & Wen, J.-K. 2008. Acetylbritannilactone inhibits neointimal hyperplasia after balloon injury of rat artery by suppressing nuclear factor- κ B activation. *Journal of Pharmacology and Experimental Therapeutics*, 324, 292-298.
- Liu, B. & Pan, T.-j. 2014. Role of PSA-related variables in improving positive ratio of biopsy of prostate cancer within serum PSA gray zone. *Urologia*, 81.
- Liu, B., Qu, L. & Yan, S. 2015a. Cyclooxygenase-2 promotes tumor growth and suppresses tumor immunity. *Cancer cell international*, 15, 106-106.
- Liu, C., Liu, Y., Xie, H. g., Zhao, S., Xu, X. x., Fan, L. x., Guo, X., Lu, T., Sun, G. W. & Ma, X. j. 2015b. Role of three-dimensional matrix stiffness in regulating the chemoresistance of hepatocellular carcinoma cells. *Biotechnology and applied biochemistry*, 62, 556-562.
- Liu, L.-T., Chang, H.-C., Chiang, L.-C. & Hung, W.-C. 2012. Induction of RECK by nonsteroidal anti-inflammatory drugs in lung cancer cells. *Oncogene*, 21, 8347.
- Liu, T., Zhang, L., Joo, D. & Sun, S.-C. 2017. NF- κ B signaling in inflammation. *Signal transduction and targeted therapy*, 2, 17023.
- Llorens, E., Calderón, S., Del Valle, L. J. & Puiggali, J. 2015. Polybiguanide (PHMB) loaded in PLA scaffolds displaying high hydrophobic, biocompatibility and antibacterial properties. *Materials Science & Engineering C*, 50, 74-84.
- Lloyd, F. P., Slivova, V., Valachovicova, T. & Sliva, D. 2003. Aspirin inhibits highly invasive prostate cancer cells. *International journal of oncology*, 23, 1277-1283.
- Lotrionte, M., Biasucci, L. M., Peruzzi, M., Frati, G., Giordano, A. & Biondi-Zoccai, G. 2016. Which aspirin dose and preparation is best for the long-term prevention of cardiovascular disease and cancer? Evidence from a

- systematic review and network meta-analysis. *Progress in cardiovascular diseases*, 58, 495-504.
- Lu, L., Sun, H.-C., Zhang, W., Chai, Z.-T., Zhu, X.-D., Kong, L.-Q., Wang, W.-Q., Zhang, K.-Z., Zhang, Y.-Y. & Zhang, Q.-B. 2013. Aspirin minimized the pro-metastasis effect of Sorafenib and improved survival by up-regulating HTATIP2 in hepatocellular carcinoma.
- Luciani, L. G., De Giorgi, G., Valotto, C., Zanin, M., Bierti, S. & Zattoni, F. 2006. Role of transperineal six-core prostate biopsy in patients with prostate-specific antigen level greater than 10 ng/mL and abnormal digital rectal examination findings. *Urology*, 67, 555-558.
- Luciani, M. G., Campregher, C. & Gasche, C. 2007. Aspirin blocks proliferation in colon cells by inducing a G 1 arrest and apoptosis through activation of the checkpoint kinase ATM. *Carcinogenesis*, 28, 2207-2217.
- Lucido, M. J., Orlando, B. J., Vecchio, A. J. & Malkowski, M. G. 2016. Crystal Structure of Aspirin-Acetylated Human Cyclooxygenase-2: Insight into the Formation of Products with Reversed Stereochemistry. *Biochemistry*, 55, 1226-1238.
- Lv, D., Hu, Z., Lu, L., Lu, H. & Xu, X. 2017. Three-dimensional cell culture: A powerful tool in tumor research and drug discovery. *Oncology letters*, 14, 6999-7010.
- Ma, H.-l., Jiang, Q., Han, S., Wu, Y., Tomshine, J. C., Wang, D., Gan, Y., Zou, G. & Liang, X.-J. 2012. Multicellular tumor spheroids as an in vivo-like tumor model for three-dimensional imaging of chemotherapeutic and nano material cellular penetration. *Molecular imaging*, 11, 7290.2012. 00012.
- Ma, N., Yang, G.-Z., Liu, X.-W., Yang, Y.-J., Mohamed, I., Liu, G.-R. & Li, J.-Y. 2017. Impact of Aspirin Eugenol Ester on Cyclooxygenase-1, Cyclooxygenase-2, C-Reactive Protein, Prothrombin and Arachidonate 5-Lipoxygenase in Healthy Rats. *Iranian Journal of Pharmaceutical Research : IJPR*, 16, 1443-1451.
- Machida, M. & Takemasa, T. 2010. Ibuprofen administration during endurance training cancels running-distance-dependent adaptations of skeletal muscle in mice. *Journal of Physiology and Pharmacology*, 61, 559.
- Maishi, N. & Hida, K. 2017. Tumor endothelial cells accelerate tumor metastasis. *Cancer Science*, 108, 1921-1926.
- Malik, F. A., Sanders, A. J. & Jiang, W. G. 2009. KAI-1/CD82, the molecule and clinical implication in cancer and cancer metastasis. *Histology and histopathology*, 24, 519-530.
- MALIK, R. D., DAKWAR, G., HARDEE, M. E., SANFILIPPO, N. J., ROSENKRANTZ, A. B. & TANEJA, S. S. 2011. Squamous Cell Carcinoma of the Prostate. *Reviews in Urology*, 13, 56-60.
- Maloney, J. P. & Gao, L. 2015. Proinflammatory Cytokines Increase Vascular Endothelial Growth Factor Expression in Alveolar Epithelial Cells. *Mediators of inflammation*, 2015, 387842-387842.
- Manu, K. A., Shanmugam, M. K., Li, F., Chen, L., Siveen, K. S., Ahn, K. S., Kumar, A. P. & Sethi, G. 2014. Simvastatin sensitizes human gastric cancer xenograft in nude mice to capecitabine by suppressing nuclear factor-kappa B-regulated gene products. *Journal of Molecular Medicine*, 92, 267-276.
- Marimuthu, S., Chivukula, R. S., Alfonso, L. F., Moridani, M., Hagen, F. K. & Bhat, G. J. 2011. Aspirin acetylates multiple cellular proteins in HCT-116 colon cancer cells: Identification of novel targets. *International journal of oncology*, 39, 1273-1283.
- Martin, F., Fletcher, D., Chauvin, M. & Bouhassira, D. 2007. Constitutive cyclooxygenase-2 is involved in central

- nociceptive processes in humans. *Anesthesiology*, 106, 1013-1018.
- Martin, T. A., Ye, L., Sanders, A. J., Lane, J. & Jiang, W. G. 2013. *Cancer Invasion and Metastasis: Molecular and Cellular Perspective*. [Online]. Available: www.ncbi.nlm.nih.gov/books/NBK164700/ 2018].
- Mattei, C., Alshawaf, A., D'Abaco, G., Nayagam, B. & Dottori, M. 2018. Generation of neural organoids from human embryonic stem cells using the rotary cell culture system: effects of microgravity on neural progenitor cell fate. *Stem cells and development*, 27, 848-857.
- Mazhar, D., Ang, R. & Waxman, J. 2006. COX inhibitors and breast cancer. *British journal of cancer*, 94, 346.
- Mc Menamin, Ú. C., Cardwell, C. R., Hughes, C. M. & Murray, L. M. 2015. Low-dose aspirin and survival from lung cancer: a population-based cohort study. *BMC cancer*, 15, 911.
- Mccormack, P. L. 2011. Celecoxib: a review of its use for symptomatic relief in the treatment of osteoarthritis, rheumatoid arthritis and ankylosing spondylitis.(Adis Drug Evaluation)(Report). *Drugs*, 71, 2457.
- Mcneal, J., Kindrachuk, R., Freiha, F., Bostwick, D., Redwine, E. & Stamey, T. 1986. Patterns of progression in prostate cancer. *The Lancet*, 327, 60-63.
- McNeal, J. E., Redwine, E. A., Freiha, F. S. & Stamey, T. A. J. T. A. j. o. s. p. 1988. Zonal distribution of prostatic adenocarcinoma. Correlation with histologic pattern and direction of spread. 12, 897-906.
- Mehner, C., Hockla, A., Miller, E., Ran, S., Radisky, D. C. & Radisky, E. S. 2014. Tumor cell-produced matrix metalloproteinase 9 (MMP-9) drives malignant progression and metastasis of basal-like triple negative breast cancer. *Oncotarget*, 5, 2736-2749.
- Merseburger, A. S., Hammerer, P., Rozet, F., Roumeguère, T., Caffo, O., Da Silva, F. C. & Alcaraz, A. 2015. Androgen deprivation therapy in castrate-resistant prostate cancer: how important is GnRH agonist backbone therapy? *World journal of urology*, 33, 1079-1085.
- Miller, B., Patel, V. A. & Sorokin, A. 2006. Cyclooxygenase-2 rescues rat mesangial cells from apoptosis induced by adriamycin via upregulation of multidrug resistance protein 1 (P-glycoprotein). *Journal of the American Society of Nephrology*, 17, 977-985.
- Mitrugno, A., Pang, J., Williams, C., Sears, R. & Mccarty, O. J. 2016. Aspirin inhibits colon cancer cell proliferation through synergistic suppression of Nf-kb and c-myc oncoproteins. *Journal of Thrombosis and Haemostasis*, 14, 75.
- Mitsiades, C., Sourla, A., Doillon, C., Lembessis, P. & Koutsilieris, M. 2000. Three-dimensional type I collagen co-culture systems for the study of cell-cell interactions and treatment response in bone metastases. *Journal of musculoskeletal & neuronal interactions*, 1(2), 153-5.
- Mitteregger, R., Vogt, G., Rossmanith, E. & Falkenhagen, D. 1999. Rotary cell culture system (RCCS): a new method for cultivating hepatocytes on microcarriers. *The International journal of artificial organs*, 22, 816-822.
- Miyashita, M., Makino, H., Katsuta, M., Nomura, T., Shinji, S., Kashiwabara, M., Takahashi, K., Kudo, M., Ishiwata, T. & Naito, Z. 2006. Cyclo-oxygenase-2 over-expression is associated with human esophageal squamous cell carcinoma. *Journal of Nippon Medical School*, 73, 308-313.
- Montanez-Sauri, S. I., Beebe, D. J. & Sung, K. E. 2015. Microscale screening systems for 3D cellular

- microenvironments: platforms, advances, and challenges. *Cellular and molecular life sciences*, 72, 237-249.
- Mossanen, M., Nepple, K. G., Grubb, R. L., 3rd, Androile, G. L., Kallogjeri, D., Klein, E. A., Stephenson, A. J. & Kibel, A. S. 2018. Heterogeneity in Definitions of High-risk Prostate Cancer and Varying Impact on Mortality Rates after Radical Prostatectomy. *European Urology Oncology*, 1, 143-148.
- Mundy, G. R. 2002. Metastasis: Metastasis to bone: causes, consequences and therapeutic opportunities. *Nature Reviews Cancer*, 2, 584.
- Munoz, F., Franco, P., Ciammella, P., Clerico, M., Giudici, M., Filippi, A. R. & Ricardi, U. J. R. O. 2007. Squamous cell carcinoma of the prostate: long-term survival after combined chemo-radiation. 2, 15.
- Mutoh, H., Hayakawa, H., Sakamoto, H. & Sugano, K. 2007. Homeobox protein CDX2 reduces Cox-2 transcription by inactivating the DNA-binding capacity of nuclear factor- κ B. *Journal of gastroenterology*, 42, 719-729.
- Mutter, R., Lu, B., Carbone, D. P., Csiki, I., Moretti, L., Johnson, D. H., Morrow, J. D., Sandler, A. B., Shyr, Y. & Ye, F. 2009. A phase II study of celecoxib in combination with paclitaxel, carboplatin, and radiotherapy for patients with inoperable stage IIIA/B non-small cell lung cancer. *Clinical Cancer Research*, 15, 2158-2165.
- Nagahara, T., Okano, J.-i. & Murawaki, Y. 2007. Mechanisms of anti-proliferative effect of JTE-522, a selective cyclooxygenase-2 inhibitor, on human liver cancer cells. *Oncology reports*, 18, 1281-1290.
- Nakanishi, M. & Rosenberg, D. W. 2013. Multifaceted roles of PGE2 in inflammation and cancer. *Seminars in immunopathology*, 35, 123-137.
- Nash, A. & Melezinek, I. 2000. The role of prostate specific antigen measurement in the detection and management of prostate cancer. *Endocrine-related cancer*, 7, 37-51.
- Nath, S. & Devi, G. R. 2016. Three-Dimensional Culture Systems in Cancer Research: Focus on Tumor Spheroid Model. *Pharmacology & therapeutics*, 163, 94-108.
- Nelson, W. G., Sfanos, K. G., DeMarzo, A. M. & Yegnasubramanian, S. 2012. Prostate Inflammation and Prostate Cancer. In: KLEIN, E. A. & JONES, J. S. (eds.) *Management of Prostate Cancer*. Humana Press.
- Ng, K., Meyerhardt, J. A., Chan, A. T., Sato, K., Chan, J. A., Niedzwiecki, D., Saltz, L. B., Mayer, R. J., Benson, A. B. & Schaefer, P. L. 2015. Aspirin and COX-2 inhibitor use in patients with stage III colon cancer. *Journal of the National Cancer Institute*, 107, dju345.
- NHS. 2015. *Prostate cancer* [Online]. NHS: NHS. Available: <http://www.nhs.uk/conditions/Cancer-of-the-prostate/Pages/Introduction.aspx> [Accessed 1 Jan 2019].
- NHS. 2018. *Treatment - Prostate cancer* [Online]. Available: <https://www.nhs.uk/conditions/prostate-cancer/treatment/> [Accessed 19 Dec 2018].
- Nickerson, M. & List, J. A. 2007. Does price matter in charitable giving? Evidence from a large-scale natural field experiment. *The American economic review*, 97, 1774-1793.
- Nissen, S. E., Yeomans, N. D., Solomon, D. H., Lüscher, T. F., Libby, P., Husni, M. E., Graham, D. Y., Borer, J. S., Wisniewski, L. M. & Wolski, K. E. 2016. Cardiovascular safety of celecoxib, naproxen, or ibuprofen for arthritis. *New England Journal of Medicine*, 375, 2519-2529.

- Nordin, B. E. C. 2013. The Source of Intracellular Calcium for Cell Activation. *In: NORDIN, B. E. C. (ed.) Calcium in Human Biology*. Springer London.
- Norouzi, S., Norouzi, M., Amini, M., Amanzadeh, A., Nabiuni, M., Irian, S. & Salimi, M. 2016. Two COX-2 inhibitors induce apoptosis in human erythroleukemia K562 cells by modulating NF- κ B and FHC pathways. *DARU Journal of Pharmaceutical Sciences*, 24, 1.
- Nørregaard, R., Kwon, T.-H. & Frøkiær, J. 2015. Physiology and pathophysiology of cyclooxygenase-2 and prostaglandin E2 in the kidney. *Kidney Research and Clinical Practice*, 34, 194-200.
- Núñez, L., Valero, R. A., Senovilla, L., Sanz-Blasco, S., García-Sancho, J. & Villalobos, C. 2006. Cell proliferation depends on mitochondrial Ca²⁺ uptake: inhibition by salicylate. *The Journal of physiology*, 571, 57-73.
- Oates, J., Massion, P., Knollmann, B., Smith, J., Haddad, E., Lammers, P., Oram, D., Amin, T., Harris, B. & Hoeksema, M. 2015. Abstract PR05: Low dose aspirin that reduces mortality from lung adenocarcinoma inhibits both platelet COX-1 and the biosynthesis of PGE2. AACR.
- Oeckinghaus, A. & Ghosh, S. 2009. The NF- κ B Family of Transcription Factors and Its Regulation. *Cold Spring Harbor Perspectives in Biology*, 1, a000034.
- Ong, C. K. S., Lirk, P., Tan, C. H. & Seymour, R. A. 2007. An evidence-based update on nonsteroidal anti-inflammatory drugs. *Clinical medicine & research*, 5, 19-34.
- Osterhoudt, K. C. & Penning, T. M. 2011. Drug toxicity and poisoning. McGraw-Hill, NY, USA.
- Ostrowski, J., Wocial, T., Skurzak, H. & Bartnik, W. 2003. Do altering in ornithine decarboxylase activity and gene expression contribute to antiproliferative properties of COX inhibitors? *British Journal of Cancer*, 88, 1143
- Page, H., Flood, P. & Reynaud, E. G. 2013. Three-dimensional tissue cultures: current trends and beyond. *Cell and tissue research*, 352, 123-131.
- Pahl, H. L. J. O. 1999. Activators and target genes of Rel/NF- κ B transcription factors. 18, 6853.
- Pajak, B. & Orzechowski, A. 2006. Overview how adenocarcinoma cancer cells avoid immune- and chemotherapy-induced apoptosis. *Adv Med Sci*, 51, 39-45.
- Palmer, N., Shanmugam, M. K., Sethi, G. & Kaldis, P. 2017. NF- κ B as a Potential Molecular Target for Therapy of Gastrointestinal Cancers. *Therapeutic Targets For Inflammation And Cancer: Novel Therapies For Digestive Diseases*. World Scientific.
- Pandeya, N., Webb, P. M., Sadeghi, S., Green, A. C. & Whiteman, D. C. 2010. Gastro-oesophageal reflux symptoms and the risks of oesophageal cancer: are the effects modified by smoking, NSAIDs or acid suppressants? *Gut*, 59, 31-38.
- Pang, L. Y., Hurst, E. A. & Argyle, D. J. 2016. Cyclooxygenase-2: a role in cancer stem cell survival and repopulation of cancer cells during therapy. *Stem cells international*, 2016.
- Papadimitropoulos, A., Piccinini, E., Brachat, S., Braccini, A., Wendt, D., Barbero, A., Jacobi, C. & Martin, I. 2014. Expansion of human mesenchymal stromal cells from fresh bone marrow in a 3D scaffold-based system under direct perfusion. *PLoS one*, 9, e102359.

- Park, J.-Y., Chung, T.-W., Jeong, Y.-J., Kwak, C.-H., Ha, S.-H., Kwon, K.-M., Abekura, F., Cho, S.-H., Lee, Y.-C. & Ha, K.-T. 2017. Ascofuranone inhibits lipopolysaccharide-induced inflammatory response via NF-kappaB and AP-1, p-ERK, TNF- α , IL-6 and IL-1 β in RAW 264.7 macrophages. *PLoS one*, 12, e0171322.
- Parks, S. K., Cormerais, Y. & Pouysségur, J. 2017. Hypoxia and cellular metabolism in tumour pathophysiology. *The Journal of Physiology*, 595, 2439-2450.
- Pathak, R. A., Broderick, G. A., Igel, T. C., Petrou, S. P., Young, P. R., Wehle, M. J., Heckman, M. G., Diehl, N. N., Vargas, E. R. & Shah, K. 2017. Impact of Minimally Invasive Benign Prostatic Hyperplasia Therapies on 30-and 90-Day Postoperative Office Encounters. *Urology*, 99, 186-191.
- Pathak, R. K., Marrache, S., Choi, J. H., Berding, T. B. & Dhar, S. 2014. The Prodrug Platin-A: Simultaneous Release of Cisplatin and Aspirin. *Angewandte Chemie*, 126, 1994-1998.
- Pathi, S., Jutooru, I., Chadalapaka, G., Nair, V., Lee, S.-O. & Safe, S. 2012. Aspirin inhibits colon cancer cell and tumor growth and downregulates specificity protein (Sp) transcription factors. *PLoS one*, 7, e48208.
- Patrignani, P. & Patrono, C. 2015. Cyclooxygenase inhibitors: from pharmacology to clinical read-outs. *Biochimica et Biophysica Acta (BBA)-Molecular and Cell Biology of Lipids*, 1851, 422-432.
- Patrignani, P., Patrono, C. J. B. e. B. A.-M. & Lipids, C. B. o. 2015. Cyclooxygenase inhibitors: from pharmacology to clinical read-outs. 1851, 422-432.
- Perlman, R. L. 2016. Mouse models of human disease: An evolutionary perspective. *Evolution, Medicine, and Public Health*, 2016, 170-176.
- Phillips, D. H. & Arlt, V. M. 2009. Genotoxicity: damage to DNA and its consequences. *Molecular, Clinical and Environmental Toxicology*. Springer.
- Piazuelo, E., Esquivias, P., De Martino, A., Cebrián, C., Conde, B., Santander, S., Emperador, S., García-González, M. A., Carrera-Lasfuentes, P. & Lanas, A. 2016. Acetylsalicylic acid exhibits antitumor effects in esophageal adenocarcinoma cells in vitro and in vivo. *Digestive diseases and sciences*, 61, 2896-2907.
- Pieters, B. R., van de Kamer, J. B., van Hertem, Y. R., van Wieringen, N., D'Olieslager, G. M., van der Heide, U. A. & Koning, C. C. 2008. Comparison of biologically equivalent dose-volume parameters for the treatment of prostate cancer with concomitant boost IMRT versus IMRT combined with brachytherapy. *Radiotherapy and Oncology*, 88, 46-52.
- Pikarsky, E., Porat, R. M., Stein, I., Abramovitch, R., Amit, S., Kasem, S., Galkovitch, E., Urieli-Shoval, S., Galun, E. & Ben-Neriah, Y. 2004. NF- κ B functions as a tumour promoter in inflammation-associated cancer. *Nature*, 431, 461.
- Pires, B. R. B., Mencialha, A. L., Ferreira, G. M., de Souza, W. F., Morgado-Díaz, J. A., Maia, A. M., Corrêa, S. & Abdelhay, E. S. F. W. 2017. NF-kappaB Is Involved in the Regulation of EMT Genes in Breast Cancer Cells. *PLoS one*, 12, e0169622-e0169622.
- Poeck, H., Bscheider, M., Gross, O., Finger, K., Roth, S., Rebsamen, M., Hanneschläger, N., Schlee, M., Rothenfusser, S. & Barchet, W. 2010. Recognition of RNA virus by RIG-I results in activation of CARD9 and inflammasome signaling for interleukin 1 β production. *Nature immunology*, 11, 63.

- Polascik, T. J., Oesterling, J. E. & Partin, A. W. 1999. Prostate specific antigen: a decade of discovery-what we have learned and where we are going. *The Journal of urology*, 162, 293-306.
- Pomerantz, M. M. & Freedman, M. L. 2010. Genetics of prostate cancer risk. *Mount Sinai Journal of Medicine: A Journal of Translational and Personalized Medicine*, 77, 643-654.
- Poorani, R., Bhatt, A. N., Dwarakanath, B. & Das, U. N. 2016. COX-2, aspirin and metabolism of arachidonic, eicosapentaenoic and docosahexaenoic acids and their physiological and clinical significance. *European journal of pharmacology*, 785, 116-132.
- Porcaro, A. B., Petrozziello, A., Brunelli, M., Migliorini, F., Cacciamani, G., De Marchi, D., Luyk, N. d., Tamanini, I., Caruso, B. & Cerruto, M. A. 2016. Prostate cancer volume associates with preoperative plasma levels of testosterone that independently predicts high grade tumours which show low densities (quotient testosterone/tumour volume). *Asian Journal of Urology*, 3, 26-32.
- Pozdeyev, N., Berlinberg, A., Zhou, Q., Wuensch, K., Shibata, H., Wood, W. M. & Haugen, B. R. 2015. Targeting the NF- κ B Pathway as a Combination Therapy for Advanced Thyroid Cancer. *PLOS ONE*, 10, e0134901.
- Prostate Cancer UK. 2018. *External beam radiotherapy* [Online]. Available: <https://prostatecanceruk.org/prostate-information/treatments/external-beam-radiotherapy> [Accessed 19 Dec 2019].
- Rainsford, K., Schweitzer, A. & Brdne, K. 1983. Distribution of the acetyl compared with the salicyl moiety of acetylsalicylic acid: Acetylation of macromolecules in organs wherein side-effects are manifest. *Biochemical pharmacology*, 32, 1301-1308.
- Rajab, R., Fisher, G., Kattan, M. W., Foster, C. S., Møller, H., Oliver, T., Reuter, V., Scardino, P. T., Cuzick, J. & Berney, D. M. 2011. An improved prognostic model for stage T1a and T1b prostate cancer by assessments of cancer extent. *Modern pathology : an official journal of the United States and Canadian Academy of Pathology, Inc*, 24, 10.1038/modpathol.2010.182.
- Rajabi, M. & Mousa, S. A. 2017. The Role of Angiogenesis in Cancer Treatment. *Biomedicines*, 5, 34.
- Rakoff-Nahoum, S. 2006. Why Cancer and Inflammation? *The Yale Journal of Biology and Medicine*, 79, 123-130.
- Ratajczak, M. Z. & Kim, C. 2012. The use of chemokine receptor agonists in stem cell mobilization. *Expert opinion on biological therapy*, 12, 287-297.
- Rayet, B. & Gelinas, C. J. O. 1999. Aberrant rel/nfkb genes and activity in human cancer. 18, 6938.
- Ren, K. & Torres, R. 2009. Role of interleukin-1 β during pain and inflammation. *Brain research reviews*, 60, 57-64.
- Ricciotti, E. & FitzGerald, G. A. 2011. Prostaglandins and Inflammation. *Arteriosclerosis, thrombosis, and vascular biology*, 31, 986-1000.
- Rice, P. L., Washington, M., Schleman, S., Beard, K. S., Driggers, L. J. & Ahnen, D. J. 2013. Sulindac sulfide inhibits epidermal growth factor-induced phosphorylation of extracellular-regulated kinase 1/2 and Bad in human colon cancer cells. *Cancer research*, 63, 616-620.
- Rifkin, M. D. 1998. Prostate cancer: the diagnostic dilemma and the place of imaging in detection and staging. *World journal of urology*, 16, 76-80.

- Rizzo, M. T. 2011. Cyclooxygenase-2 in oncogenesis. *Clinica Chimica Acta*, 412, 671-687.
- Roach III, M., Bae, K., Speight, J., Wolkov, H. B., Rubin, P., Lee, R. J., Lawton, C., Valicenti, R., Grignon, D. & Pilepich, M. V. 2008. Short-term neoadjuvant androgen deprivation therapy and external-beam radiotherapy for locally advanced prostate cancer: long-term results of RTOG 8610. *Journal of Clinical Oncology*, 26, 585-591.
- Robertson, D. 2013. Uses, interactions and side effects of aspirin in older people. *Nursing & Residential Care*, 15, 263-266.
- Robich, M. P., Chu, L. M., Feng, J., Burgess, T. A., Laham, R. J., Bianchi, C. & Sellke, F. W. 2010. Effects of selective cyclooxygenase-2 and non-selective COX inhibition on ischemic myocardium. *The Journal of thoracic and cardiovascular surgery*, 140, 1143-1152.
- Rodday, B., Hirschhaeuser, F., Walenta, S. & Mueller-Klieser, W. 2011. Semiautomatic growth analysis of multicellular tumor spheroids. *Journal of biomolecular screening*, 16, 1119-1124.
- Rodrigues, M. M., Di Santis, G. W., De Moura, V. M. & Amorim, R. L. 2017. COX-2 and TGF- β expression in proliferative disorders of canine prostate. *Brazilian Journal of Veterinary Pathology*, 3, 31-36.
- Rosenberg, L., Palmer, J. R., Rao, R. S., Coogan, P. F., Strom, B. L., Zauber, A. G., Stolley, P. D. & Shapiro, S. 2009. A case-control study of analgesic use and ovarian cancer. *Cancer Epidemiology and Prevention Biomarkers*, 9, 933-937.
- Roth, G. J., Stanford, N. & Majerus, P. W. 1975. Acetylation of prostaglandin synthase by aspirin. *Proceedings of the National Academy of Sciences*, 72, 3073-3076.
- Rothwell, P. M., Wilson, M., Price, J. F., Belch, J. F., Meade, T. W. & Mehta, Z. 2012. Effect of daily aspirin on risk of cancer metastasis: a study of incident cancers during randomised controlled trials. *The Lancet*, 379, 1591-1601.
- Ruan, D. & So, S.-P. J. L. s. 2014. Prostaglandin E2 produced by inducible COX-2 and mPGES-1 promoting cancer cell proliferation in vitro and in vivo. 116, 43-50.
- Sahin, I. H., Hassan, M. M. & Garrett, C. R. 2014. Impact of non-steroidal anti-inflammatory drugs on gastrointestinal cancers: current state-of-the science. *Cancer letters*, 345, 249-257.
- Sakai, S., Inamoto, K., Liu, Y., Tanaka, S., Arai, S. & Taya, M. 2012. Multicellular tumor spheroid formation in duplex microcapsules for analysis of chemosensitivity. *Cancer science*, 103, 549-554.
- Salinas, C. A., Kwon, E. M., FitzGerald, L. M., Feng, Z., Nelson, P. S., Ostrander, E. A., Peters, U. & Stanford, J. L. 2010. Use of aspirin and other nonsteroidal antiinflammatory medications in relation to prostate cancer risk. *American journal of epidemiology*, 172, 578-590.
- Samanta, S. & Dey, P. 2012. Micronucleus and its applications. *Diagnostic cytopathology*, 40, 84-90.
- Santoni, M., Scarpelli, M., Mazzucchelli, R., Lopez-Beltran, A., Cheng, L., Epstein, J. I., Cascinu, S., Briganti, A., Catto, J. W. & Montorsi, F. 2016. Current histopathologic and molecular characterisations of prostate cancer: towards individualised prognosis and therapies. Elsevier.
- Sato, T. & Clevers, H. 2013. Growing self-organizing mini-guts from a single intestinal stem cell: mechanism and

- applications. *Science*, 340, 1190-1194.
- Scarpino, S., Duranti, E., Giglio, S., Di Napoli, A., Galafate, D., Del Bufalo, D., Desideri, M., Socciarelli, F., Stoppacciaro, A. & Ruco, L. 2013. Papillary carcinoma of the thyroid: high expression of COX-2 and low expression of KAI-1/CD82 are associated with increased tumor invasiveness. *Thyroid*, 23, 1127-1137.
- Schweighofer, B., Testori, J., Sturtzel, C., Sattler, S., Mayer, H., Wagner, O., Bilban, M. & Hofer, E. 2009. The VEGF-induced transcriptional response comprises gene clusters at the crossroad of angiogenesis and inflammation. *Thrombosis and haemostasis*, 102, 544.
- Sen, R. 2004. NF-kappaB and the immunoglobulin kappa gene enhancer. *The Journal of experimental medicine*, 200, 1099-1102.
- Sha, W., Olesch, C., Hanaka, H., Rådmark, O., Weigert, A. & Brüne, B. 2013. Necrosis in DU145 prostate cancer spheroids induces COX-2/mPGES-1-derived PGE2 to promote tumor growth and to inhibit T cell activation. *International Journal of Cancer*, 133, 1578-1588.
- Shaikhibrahim, Z., Lindstrot, A., Ellinger, J., Rogenhofer, S., Buettner, R., Perner, S. & Wernert, N. J. M. r. 2012. The peripheral zone of the prostate is more prone to tumor development than the transitional zone: is the ETS family the key? 5, 313-316.
- Shan, Y., Zhang, L., Bao, Y., Li, B., He, C., Gao, M., Feng, X., Xu, W., Zhang, X. & Wang, S. 2013. Epithelial-mesenchymal transition, a novel target of sulforaphane via COX-2/MMP2, 9/Snail, ZEB1 and miR-200c/ZEB1 pathways in human bladder cancer cells. *The Journal of nutritional biochemistry*, 24, 1062-1069.
- Shao, N., Feng, N., Wang, Y., Mi, Y., Li, T. & Hua, L. 2012. Systematic review and meta-analysis of COX-2 expression and polymorphisms in prostate cancer. *Molecular biology reports*, 39, 10997-11004.
- Sharma, B., Varney, M. L., Saxena, S., Wu, L. & Singh, R. K. 2016. Induction of CXCR2 ligands, stem cell-like phenotype, and metastasis in chemotherapy-resistant breast cancer cells. *Cancer letters*, 372, 192-200.
- Sharma, S. & Sharma, S. 1997. An update on eicosanoids and inhibitors of cyclooxygenase enzyme systems. *Indian journal of experimental biology*, 35, 1025-1031.
- Shebl, F. M., Hsing, A. W., Park, Y., Hollenbeck, A. R., Chu, L. W., Meyer, T. E. & Koshiol, J. 2014. Non-Steroidal Anti-Inflammatory Drugs Use Is Associated with Reduced Risk of Inflammation-Associated Cancers: NIH-AARP Study. *PLoS ONE*, 9, e114633.
- Shen, K.-H., Hung, S.-H., Yin, L.-T., Huang, C.-S., Chao, C.-H., Liu, C.-L. & Shih, Y.-W. 2010. Acacetin, a flavonoid, inhibits the invasion and migration of human prostate cancer DU145 cells via inactivation of the p38 MAPK signaling pathway. *Molecular and cellular biochemistry*, 333, 279-291.
- Shi, C., Zhang, N., Feng, Y., Cao, J., Chen, X. & Liu, B. 2017. Aspirin Inhibits IKK- β -mediated Prostate Cancer Cell Invasion by Targeting Matrix Metalloproteinase-9 and Urokinase-Type Plasminogen Activator. *Cellular Physiology and Biochemistry*, 41, 1313-1324.
- Shi, G., Li, D., Fu, J., Sun, Y., Li, Y., Qu, R., Jin, X. & Li, D. 2015. Upregulation of cyclooxygenase-2 is associated with activation of the alternative nuclear factor kappa B signaling pathway in colonic adenocarcinoma.

- American journal of translational research*, 7, 1612-1620.
- Shiao, J., Thomas, K., Rahimi, A., Rao, R., Yan, J., Xie, X.-J., DaSilva, M., Spangler, A., Leitch, M. & Wooldridge, R. 2017. Aspirin/antiplatelet agent use improves disease-free survival and reduces the risk of distant metastases in Stage II and III triple-negative breast cancer patients. *Breast cancer research and treatment*, 161, 463-471.
- Shin, C. S., Kwak, B., Han, B. & Park, K. 2013. Development of an in vitro 3D tumor model to study therapeutic efficiency of an anticancer drug. *Molecular pharmaceutics*, 10(6), 2167-75.
- Shiple, W. U., Seiferheld, W., Lukka, H. R., Major, P. P., Heney, N. M., Grignon, D. J., Sartor, O., Patel, M. P., Bahary, J.-P. & Zietman, A. L. 2017. Radiation with or without antiandrogen therapy in recurrent prostate cancer. *New England Journal of Medicine*, 376, 417-428.
- Shirakawa, T., Hamada, K., Zhang, Z., Okada, H., Tagawa, M., Kamidono, S., Kawabata, M. & Gotoh, A. 2004. A cox-2 promoter-based replication-selective adenoviral vector to target the cox-2-expressing human bladder cancer cells. *Clinical cancer research : an official journal of the American Association for Cancer Research*, 10(13), 4342-8.
- Shrihari, T. G. 2017. Dual role of inflammatory mediators in cancer. *ecancermedicalscience*, 11, 721.
- Sim, J. 2014. Examination of Human Embryonic Kidney cells and Cardiomyocytes using Glass Microcarrier Beads and Scanning Electron Microscopy.
- Singh, M., Mukundan, S., Jaramillo, M., Oesterreich, S. & Sant, S. 2016. Three-dimensional breast cancer models mimic hallmarks of size-induced tumor progression. *Cancer research*.
- Slaninová, J., Mlsová, V., Kroupová, H., Alán, L., Tůmová, T., Monincová, L., Borovičková, L., Fučík, V. & Čeřovský, V. 2012. Toxicity study of antimicrobial peptides from wild bee venom and their analogs toward mammalian normal and cancer cells. *Peptides*, 33, 18-26.
- Small, E. J. & Roach, M. Prostate-specific antigen in prostate cancer: a case study in the development of a tumor marker to monitor recurrence and assess response. *Seminars in oncology*, 2002. Elsevier, 264-273.
- Sobolewski, C., Cerella, C., Dicato, M., Ghibelli, L. & Diederich, M. 2010. The role of cyclooxygenase-2 in cell proliferation and cell death in human malignancies. *International journal of cell biology*, 2010.
- Sokołowski, G., Bałdys-Waligórska, A., Trofimiuk, M., Adamek, D., Hubalewska-Dydejczyk, A. & Gołkowski, F. 2012. Expression of cyclooxygenase-2 (COX-2) in pituitary tumours. *Medical science monitor: international medical journal of experimental and clinical research*, 18, CR252.
- Song, F., He, M., Li, H., Qian, B., Wei, Q., Zhang, W., Chen, K. & Hao, X. 2008. A cancer incidence survey in Tianjin: the third largest city in China—between 1981 and 2000. *Cancer Causes & Control*, 19, 443.
- Sostres, C., Gargallo, C. J. & Lanás, A. 2014. Aspirin, cyclooxygenase inhibition and colorectal cancer. *World Journal of Gastrointestinal Pharmacology and Therapeutics*, 5, 40-49.
- Soumarová, R., Homola, L., Perková, H. & Stursa, M. 2007. Three-dimensional conformal external beam radiotherapy versus the combination of external radiotherapy with high-dose rate brachytherapy in localized carcinoma of the prostate: comparison of acute toxicity. *Tumori*, 93, 37.

- Sreeramkumar, V., Fresno, M. & Cuesta, N. 2011. Prostaglandin E2 and T cells: friends or foes? *Immunology And Cell Biology*, 90, 579.
- Stangelberger, A., Waldert, M. & Djavan, B. 2008. Prostate cancer in elderly men. *Reviews in urology*, 10, 111-119.
- Stark, T., Livas, L. & Kyprianou, N. 2015. Inflammation in prostate cancer progression and therapeutic targeting. *Translational Andrology and Urology*, 4, 455-463.
- Steele, C. W., Karim, S. A., Leach, J. D., Bailey, P., Upstill-Goddard, R., Rishi, L., Foth, M., Bryson, S., McDaid, K. & Wilson, Z. 2016. CXCR2 inhibition profoundly suppresses metastases and augments immunotherapy in pancreatic ductal adenocarcinoma. *Cancer cell*, 29, 832-845.
- Stevens, W., Buchheit, K. & Cahill, K. N. 2015. Aspirin-exacerbated diseases: advances in asthma with nasal polyposis, urticaria, angioedema, and anaphylaxis. *Current allergy and asthma reports*, 15, 69.
- Strobel, H. A., Calamari, E. L., Alphonse, B., Hookway, T. A. & Rolle, M. W. 2018. Fabrication of Custom Agarose Wells for Cell Seeding and Tissue Ring Self-assembly Using 3D-Printed Molds. *Journal of visualized experiments : JoVE*, 56618.
- Struss, W. & Black, P. 2017. Radiation With or Without Antiandrogen Therapy in Recurrent Prostate Cancer. *Urology*.
- Sui, H., Zhou, S., Wang, Y., Liu, X., Zhou, L., Yin, P., Fan, Z. & Li, Q. 2011. COX-2 contributes to P-glycoprotein-mediated multidrug resistance via phosphorylation of c-Jun at Ser63/73 in colorectal cancer. *Carcinogenesis*, 32, 667-675.
- Sun, L., Yang, C., Ge, Y., Yu, M., Chen, G., Guo, W. & Tian, W. 2014. In vitro three-dimensional development of mouse molar tooth germs in a rotary cell culture system. *International Journal of Paediatric Dentistry*, 24, 175-183.
- Sun, M., Liu, C., Nadiminty, N., Lou, W., Zhu, Y., Yang, J., Evans, C. P., Zhou, Q. & Gao, A. C. 2012. Inhibition of Stat3 activation by sanguinarine suppresses prostate cancer cell growth and invasion. *The Prostate*, 72, 82-89.
- Sun, S.-C. 2011. Non-canonical NF- κ B signaling pathway. *Cell research*, 21, 71-85.
- Sutherland, R. M., Inch, W. R., McCredie, J. A. & Kruuv, J. 1970. A multi-component radiation survival curve using an in vitro tumour model. *International Journal of Radiation Biology and Related Studies in Physics. Chemistry and Medicine*, 18(5), 491-4.
- Suva, L. J., Washam, C., Nicholas, R. W. & Griffin, R. J. 2011. Bone metastasis: mechanisms and therapeutic opportunities. *Nature Reviews Endocrinology*, 7, 208.
- Taddei, M. L., Giannoni, E., Comito, G. & Chiarugi, P. 2013. Microenvironment and tumor cell plasticity: an easy way out. *Cancer letters*, 341, 80-96.
- Tait, S. W. G. & Green, D. R. 2013. Mitochondrial regulation of cell death. *Cold Spring Harbor perspectives in biology*, 5, a008706.
- Tak, P. P. & Firestein, G. S. 2001. NF- κ B: a key role in inflammatory diseases. *Journal of clinical investigation*, 107, 7.
- Takada, Y., Bhardwaj, A., Potdar, P. & Aggarwal, B. B. 2004. Nonsteroidal anti-inflammatory agents differ in their

- ability to suppress NF- κ B activation, inhibition of expression of cyclooxygenase-2 and cyclin D1, and abrogation of tumor cell proliferation. *Oncogene*, 23, 9247.
- Tan, H., Chen, W., Liu, Q., Yang, G. & Li, K. 2018. Pectin Oligosaccharides (POS) Ameliorate Colon Cancer by Regulating Oxidative Stress-and Inflammation-Activated Signaling Pathways. *Frontiers in Immunology*, 9, 1504.
- Tan, P. H., Aung, K., Toh, S., Goh, J. C. & Nathan, S. 2011. Three-dimensional porous silk tumor constructs in the approximation of in vivo osteosarcoma physiology. *Biomaterials*, 32, 6131-6137.
- Tanaka, T., Narazaki, M. & Kishimoto, T. 2014. IL-6 in inflammation, immunity, and disease. *Cold Spring Harbor perspectives in biology*, 6, a016295-a016295.
- Tang, L., Hu, H., Liu, H., Jian, C., Wang, H. & Huang, J. 2016. Association of nonsteroidal anti-inflammatory drugs and aspirin use and the risk of head and neck cancers: a meta-analysis of observational studies. *Oncotarget*, 7, 65196-65207.
- Tarin, D. 2012. Clinical and Biological Implications of the Tumor Microenvironment. *Cancer Microenvironment*, 5, 95-112.
- Tazi, H., Manunta, A., Rodriguez, A., Patard, J. J., Lobel, B. & Guill e, F. 2003. Spinal Cord Compression in Metastatic Prostate Cancer. *European Urology*, 44, 527-532.
- The National Comprehensive Cancer Network 2010. NCCN clinical practice guidelines in oncology: prostate cancer. Available at: www.nccn.org/professionals/physician_gls/pdf/prostate.pdf.
- The World Bank. 2016. GDP [Online]. <http://data.worldbank.org>: <http://data.worldbank.org>. Available: <http://data.worldbank.org/indicator/NY.GDP.MKTP.CD> [Accessed 24th March 2017].
- Thoma, C. R., Zimmermann, M., Agarkova, I., Kelm, J. M. & Krek, W. 2014. 3D cell culture systems modeling tumor growth determinants in cancer target discovery. *Advanced Drug Delivery Reviews*, 69-70, 29-41.
- Thrasher, J. B. 2006. Refining prostate biopsy strategies. Elsevier.
- Tit-Oon, P., Chokchaichamnankit, D., Khongmanee, A., Sawangareetrakul, P., Svasti, J. & Srisomsap, C. 2014. Comparative Secretome analysis of cholangiocarcinoma cell line in three dimensional culture. *Int J Oncol*, 45(5), 2108-16.
- Tobias, J. S., Hochhauser, D. & Tobias, J. 2014. *Cancer and its management*, John Wiley & Sons.
- Tombal, B. & Berges, R. 2005. How Good do Current LHRH Agonists Control Testosterone? Can this be Improved with Eligard^{®}? *European Urology Supplements*, 4, 30-36.
- Topaz, M., Lai, K., Dhopeswarkar, N., Seger, D. L., Sa'adon, R., Goss, F., Rozenblum, R. & Zhou, L. 2016. Clinicians' reports in electronic health records versus patients' concerns in social media: a pilot study of adverse drug reactions of aspirin and atorvastatin. *Drug safety*, 39, 241-250.
- Torre, L. A., Bray, F., Siegel, R. L., Ferlay, J., Lortet-Tieulent, J. & Jemal, A. J. C. a. c. j. f. c. 2015. Global cancer statistics, 2012. 65, 87-108.
- Tree, A. & Khoo, V. 2009. Treatment of early prostate cancer: radiotherapy, including brachytherapy. *Trends in Urology, Gynaecology & Sexual Health*, 14, 18-23.

- Tsai, C.-S. S., Luo, S.-F., Ning, C.-C., Lin, C.-L., Jiang, M.-C. & Liao, C.-F. 2009. Acetylsalicylic acid regulates MMP-2 activity and inhibits colorectal invasion of murine B16F0 melanoma cells in C57BL/6J mice: effects of prostaglandin F2 α . *Biomedicine & Pharmacotherapy*, 63, 522-527.
- Tsai, S.-T., Tsou, C.-C., Mao, W.-Y., Chang, W.-C., Han, H.-Y., Hsu, W.-L., Li, C.-L., Shen, C.-N. & Chen, C.-H. 2012. Label-free quantitative proteomics of CD133-positive liver cancer stem cells. *Proteome science*, 10, 69.
- Tsubouchi, Y., Mukai, S., Kawahito, Y., Yamada, R., Kohno, M., Inoue, K. & Sano, H. J. A. r. 2000. Meloxicam inhibits the growth of non-small cell lung cancer. 20, 2867-2872.
- Ukimura, O., Hung, A. J. & Gill, I. S. 2011. Innovations in prostate biopsy strategies for active surveillance and focal therapy. *Current opinion in urology*, 21, 115-120.
- van Zijl, F. & Mikulits, W. 2010. Hepatospheres: Three dimensional cell cultures resemble physiological conditions of the liver. *World journal of hepatology*, 2, 1.
- Vane, J. R. 1971. Inhibition of prostaglandin synthesis as a mechanism of action for aspirin-like drugs. *Nature new biology*, 231, 232.
- Vane, J. R. J. A. i. t. B. 2014. Inhibition of prostaglandin biosynthesis as the mechanism of action of aspirin-like drugs. 9, 395-411.
- VanWormer, J. J., Greenlee, R. T., McBride, P. E., Peppard, P. E., Malecki, K. C., Che, J. & Nieto, F. J. 2012. Aspirin for primary prevention of CVD: are the right people using it? *The Journal of family practice*, 61, 525-532.
- Verloes, R. & Kanarek, L. 1976 Tumour microenvironment studies open new perspectives for immunotherapy. *Arch Int Physiol Biochim*, 84(2), 420-2.
- Voronov, E., Carmi, Y. & Apte, R. N. 2014. The role IL-1 in tumor-mediated angiogenesis. *Frontiers in Physiology*, 5, 114.
- Wang, D. & DuBois, R. N. 2010. The role of COX-2 in intestinal inflammation and colorectal cancer. *Oncogene*, 29, 781.
- Wang, L., Chen, W., Xie, X., He, Y. & Bai, X. 2008. Celecoxib inhibits tumor growth and angiogenesis in an orthotopic implantation tumor model of human colon cancer. *Experimental Oncology*, 30, 42.
- Wang, Z.-l., Fan, Z.-q., Jiang, H.-d. & Qu, J.-m. 2012. Selective Cox-2 inhibitor celecoxib induces epithelial-mesenchymal transition in human lung cancer cells via activating MEK-ERK signaling. *Carcinogenesis*, 34, 638-646.
- Wang, Z., Chen, J.-q. & Liu, J.-l. 2014. COX-2 Inhibitors and Gastric Cancer. *Gastroenterology Research and Practice*, 2014, 132320.
- Wänman, J., Grabowski, P., Nyström, H., Gustafsson, P., Bergh, A., Widmark, A. & Crnalic, S. 2017. Metastatic spinal cord compression as the first sign of malignancy. *Acta orthopaedica*, 88, 457-462.
- Waseem, M., Aslam, M. & Gernsheimer, J. R. 2017. *Salicylate Toxicity Workup* [Online]. WebMD LLC. . Available: <https://emedicine.medscape.com/article/1009987-workup> [Accessed 5th June 2018].
- Wei, D., Wang, L., He, Y., Xiong, H. Q., Abbruzzese, J. L. & Xie, K. 2004. Celecoxib inhibits vascular endothelial growth factor expression in and reduces angiogenesis and metastasis of human pancreatic cancer via

- suppression of Sp1 transcription factor activity. *Cancer research*, 64, 2030-2038.
- Weiswald, L.-B., Bellet, D. & Dangles-Marie, V. 2015. Spherical cancer models in tumor biology. *Neoplasia*, 17, 1-15.
- Weltin, A., Hammer, S., Noor, F., Kaminski, Y., Kieninger, J. & Urban, G. A. 2017. Accessing 3D microtissue metabolism: Lactate and oxygen monitoring in hepatocyte spheroids. *Biosensors and Bioelectronics*, 87, 941-948.
- WERNERT, N., GOEBBELS, R., BONKHOF, H. & DHOM, G., 17, . 1990. Squamous cell carcinoma of the prostate. *Histopathology*, 339-344.
- White, W. B., Faich, G., Whelton, A., Maurath, C., Ridge, N. J., Verburg, K. M., Geis, G. S. & Lefkowitz, J. B. J. T. A. j. o. c. 2002. Comparison of thromboembolic events in patients treated with celecoxib, a cyclooxygenase-2 specific inhibitor, versus ibuprofen or diclofenac. 89, 425-430.
- Wlodkowic, D., Skommer, J. & Darzynkiewicz, Z. 2009. Flow cytometry-based apoptosis detection. *Methods in molecular biology (Clifton, N.J.)*, 559, 19-32.
- Wlodkowic, D., Telford, W., Skommer, J. & Darzynkiewicz, Z. 2011. Apoptosis and beyond: cytometry in studies of programmed cell death. *Methods in cell biology*. Elsevier.
- Wodarz, D., Goel, A., Boland, C. R. & Komarova, N. L. 2017. Effect of aspirin on tumour cell colony formation and evolution. *Journal of The Royal Society Interface*, 14, 20170374.
- Wood, L. V., Fojo, A., Roberson, B. D., Hughes, M. S., Dahut, W., Gulley, J. L., Madan, R. A., Arlen, P. M., Sabatino, M. & Stronck, D. F. 2016. TARP Vaccination is associated with slowing in PSA velocity and decreasing tumor growth rates in patients with Stage D0 prostate cancer. *Oncoimmunology*, 5, e1197459.
- Wu, I. C., Hsieh, H. M., Yu, F. J., Wu, M. C., Wu, T. S. & Wu, M. T. 2016. A long-term risk-benefit analysis of low-dose aspirin in primary prevention. *European journal of clinical investigation*, 46, 130-140.
- Wynne, S. & Djakiew, D. 2010. NSAID inhibition of prostate cancer cell migration is mediated by Nag-1 induction via the p38 MAPK-p75NTR pathway. *Molecular Cancer Research*, 8, 1656-1664.
- Xia, Y., Shen, S. & Verma, I. M. 2014. NF- κ B, an active player in human cancers. *Cancer immunology research*, 2, 823-830.
- Xie, H., Gao, L., Chai, N., Song, J., Wang, J., Song, Z., Chen, C., Pan, Y., Zhao, L. & Sun, S. 2009. Potent cell growth inhibitory effects in hepatitis B virus X protein positive hepatocellular carcinoma cells by the selective cyclooxygenase-2 inhibitor celecoxib. *Molecular carcinogenesis*, 48, 56-65.
- Xu, D., McKee, C. M., Cao, Y., Ding, Y., Kessler, B. M. & Muschel, R. J. 2010. Matrix metalloproteinase-9 regulates tumor cell invasion through cleavage of protease nexin-1. *Cancer research*, 70, 6988-6998.
- Xu, H., Lin, F., Wang, Z., Meng, J., Sun, H., Qi, Z., Wang, Y., Ou, Z., Shao, Z. & Di, G. 2013a. CXCR2 controls breast cancer metastasis and chemoresistance through PI3K/AKT and COX-2 signalings. AACR.
- Xu, L. & Croix, B. S. 2014. Improving VEGF-targeted therapies through inhibition of COX-2/PGE(2) signaling. *Molecular & Cellular Oncology*, 1, e969154.
- Xu, L., Stevens, J., Hilton, M., Seaman, S. & Conrads, T. V., TD ; Logsdon, D ; Morris H ; Swing DA ; Patel NL ; Kalen

- J ; Haines DC ; Zudaire E ; St Croix B ; 2014a. COX-2 Inhibition Potentiates Antiangiogenic Cancer Therapy and Prevents Metastasis in Preclinical Models.
- Xu, P., Cai, F., Liu, X. & Guo, L. J. O. r. 2015. Sesamin inhibits lipopolysaccharide-induced proliferation and invasion through the p38-MAPK and NF- κ B signaling pathways in prostate cancer cells. *33*, 3117-3123.
- Xu, W., Li, Y., Liu, C. & Zhao, S. 2014b. Protein lysine acetylation guards metabolic homeostasis to fight against cancer. *Oncogene*, *33*, 2279.
- Xu, X., Farach-Carson, M. C. & Jia, X. 2014c. Three-dimensional in vitro tumor models for cancer research and drug evaluation. *Biotechnology advances*, *32*, 1256-1268.
- Xu, Z., Gao, Y., Hao, Y., Li, E., Wang, Y., Zhang, J., Wang, W., Gao, Z. & Wang, Q. 2013b. Application of a microfluidic chip-based 3D co-culture to test drug sensitivity for individualized treatment of lung cancer. *Biomaterials*, *34*, 4109-4117.
- Xylinas, E., Durand, X., Ploussard, G., Campeggi, A., Allory, Y., Vordos, D., Hoznek, A., Abbou, C. C., de la Taille, A. & Salomon, L. Evaluation of combined oncologic and functional outcomes after robotic-assisted laparoscopic extraperitoneal radical prostatectomy: trifecta rate of achieving continence, potency and cancer control. *Urologic Oncology: Seminars and Original Investigations*, 2013. Elsevier, 99-103.
- Yan, F., He, Q., Hu, X., Li, W., Wei, K., Li, L., Zhong, Y., Ding, X., Xiang, S. & Zhang, J. 2013. Direct regulation of caspase-3 by the transcription factor AP-2 α is involved in aspirin-induced apoptosis in MDA-MB-453 breast cancer cells. *Molecular medicine reports*, *7*, 909-914.
- Yan, L. & Spitznagel, E. L. 2009. Soy consumption and prostate cancer risk in men: a revisit of a meta-analysis. *The American journal of clinical nutrition*, *89*, 1155-1163.
- Yang, L., Chen, Y., Tang, Z., Xue, W., Qiu, S., Tan, P. & Wei, Q. 2016. Aspirin and levofloxacin for the prevention of the occurrence of prostate cancer or transformation to castration-resistant prostate cancer: a two-part, open-label, randomised, controlled study. *The Lancet*, *388*, S85.
- Yasugi, E., Uemura, I., Kumagai, T., Nishikawa, Y., Yasugi, S. & Yuo, A. J. Z. s. 2002. Disruption of mitochondria is an early event during dolichyl monophosphate-induced apoptosis in U937 cells. *19*, 7-13.
- Yeatts, A. B., Geibel, E. M., Fears, F. F. & Fisher, J. P. 2012 Human mesenchymal stem cell position within scaffolds influences cell fate during dynamic culture. *Biotechnol Bioeng*, *109*(9), 2381-91.
- Yin, M.-J., Yamamoto, Y. & Gaynor, R. B. 1998. The anti-inflammatory agents aspirin and salicylate inhibit the activity of I κ B kinase- β . *Nature*, *396*, 77.
- Yoshimura, R., Sano, H., Masuda, C., Kawamura, M., Tsubouchi, Y., Chargui, J., Yoshimura, N., Hla, T. & Wada, S. 2000. Expression of cyclooxygenase-2 in prostate carcinoma. *Cancer*, *89*, 589-596.
- Youle, R. J. & Strasser, A. 2008. The BCL-2 protein family: opposing activities that mediate cell death. *Nature Reviews Molecular Cell Biology*, *9*, 47.
- Yu, M., Bardia, A., Aceto, N., Bersani, F., Madden, M. W., Donaldson, M. C., Desai, R., Zhu, H., Comaills, V. & Zheng, Z. 2014. Ex vivo culture of circulating breast tumor cells for individualized testing of drug susceptibility. *Science*, *345*, 216-220.

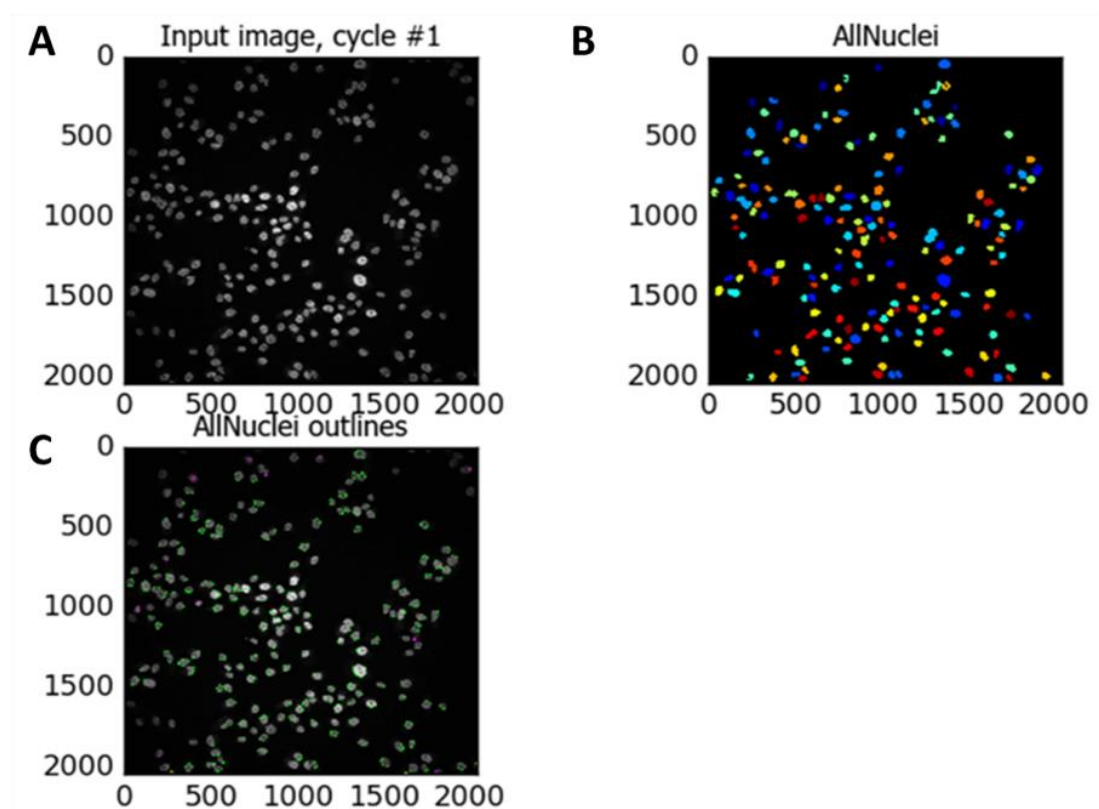
- Yu, P., Huang, Y., Han, Y., Lin, L., Sun, W., Rabson, A., Wang, Y. & Shi, Y. 2017. TNF α -activated mesenchymal stromal cells promote breast cancer metastasis by recruiting CXCR2+ neutrophils. *Oncogene*, 36, 482.
- Yuan, J., Yang, M., Threapleton, D., Qi, X., Ye, D., Mao, C., Tang, J. & Higgins, J. 2016. Systematic review with meta-analysis: the gastrointestinal benefits of COX-2 selective inhibitors with concomitant use of low-dose aspirin. *Alimentary pharmacology & therapeutics*, 44, 785-795.
- Yuan, X., Cai, C., Chen, S., Chen, S., Yu, Z. & Balk, S. 2014. Androgen receptor functions in castration-resistant prostate cancer and mechanisms of resistance to new agents targeting the androgen axis. *Oncogene*, 33, 2815.
- Yuhas, J. M., Li, A. P., Martinez, A. O. & Ladman, A. J. 1977. A simplified method for production and growth of multicellular tumor spheroids. *Cancer research*, 37, 3639-3643.
- Zapata, L. M., Bock, B. C., Orozco, L. Y., Palacio, J. A. J. E. & safety, e. 2016. Application of the micronucleus test and comet assay in *Trachemys callirostris* erythrocytes as a model for in situ genotoxic monitoring. 127, 108-116.
- Zelevsky, M. J., Levin, E. J., Hunt, M., Yamada, Y., Shippy, A. M., Jackson, A. & Amols, H. I. 2008. Incidence of late rectal and urinary toxicities after three-dimensional conformal radiotherapy and intensity-modulated radiotherapy for localized prostate cancer. *International Journal of Radiation Oncology* Biology* Physics*, 70, 1124-1129.
- Zhan, P., Qian, Q. & Yu, L.-K. 2013. Prognostic value of COX-2 expression in patients with non-small cell lung cancer: a systematic review and meta-analysis. *Journal of thoracic disease*, 40-7, 5(1).
- Zhang, J.-l., Wang, Z., Zhuang, B.-b. & Zhou, H.-J. 2009. Action mechanism of dihydroartemisinin combined with COX-2 inhibitor in S180 carcinoma [J]. *Chinese Pharmacological Bulletin*, 3, 011.
- Zhang, L., Valencia, C. A., Dong, B., Chen, M., Guan, P.-J. & Pan, L. 2015a. Transfer of microRNAs by extracellular membrane microvesicles: a nascent crosstalk model in tumor pathogenesis, especially tumor cell-microenvironment interactions. *Journal of hematology & oncology*, 8, 14.
- Zhang, W., Zhuang, A., Gu, P., Zhou, H. & Fan, X. 2016. A review of the three-dimensional cell culture technique: Approaches, advantages and applications. *Current stem cell research & therapy*, 11, 370-380.
- Zhang, X.-w., Bu, P., Liu, L., Zhang, X.-z. & Li, J. 2015b. Overexpression of long non-coding RNA PVT1 in gastric cancer cells promotes the development of multidrug resistance. *Biochemical and biophysical research communications*, 462, 227-232.
- Zhang, Y.-P., Wan, Y.-D., Sun, Y.-L., Li, J. & Zhu, R.-T. 2015c. Aspirin might reduce the incidence of pancreatic cancer: A meta-analysis of observational studies. *Scientific reports*, 5, 15460-15460.
- Zhang, Y. & Daaka, Y. 2011. PGE2 promotes angiogenesis through EP4 and PKA γ pathway. *Blood*, 118, 5355-5364.
- Zhang, Y., Fei, M., Xue, G., Zhou, Q., Jia, Y., Li, L., Xin, H. & Sun, S. 2012. Elevated levels of hypoxia-inducible microRNA-210 in pre-eclampsia: new insights into molecular mechanisms for the disease. *Journal of cellular and molecular medicine*, 16, 249-259.

- Zhao, S., Xu, W., Jiang, W., Yu, W., Lin, Y., Zhang, T., Yao, J., Zhou, L., Zeng, Y. & Li, H. 2010. Regulation of cellular metabolism by protein lysine acetylation. *Science*, 327, 1000-1004.
- Zhi, H., Yang, X., Kuhnmuensch, J., Berg, T., Thill, R., Yang, H., See, W., Becker, C., Williams, C. & Li, R. 2009. SmgGDS is up-regulated in prostate carcinoma and promotes tumour phenotypes in prostate cancer cells. *The Journal of Pathology: A Journal of the Pathological Society of Great Britain and Ireland*, 217, 389-397.
- Zhou, Y., Ran, J., Tang, C., Wu, J., Honghua, L., Xingwen, L., Chen, N. & Qiao, L. 2007. Effect of celecoxib on E-cadherin, VEGF, Microvessel density and apoptosis in gastric cancer. *Cancer biology & therapy*, 6, 269-275.
- Zlotta, A. & Debruyne, F. M. 2005. Expert opinion on optimal testosterone control in prostate cancer. *European Urology Supplements*, 4, 37-41.
- Zong, M., Fan, D.-D., Lin, S., Song, Y.-P., Wang, Z.-Y., Ma, X.-L., Qiu, W.-H., Bai, Y.-H., Li, L. & Li, S. 2016. Anti-cancer activity and potential mechanism of a novel aspirin derivative. *European journal of pharmacology*, 791, 137-146.

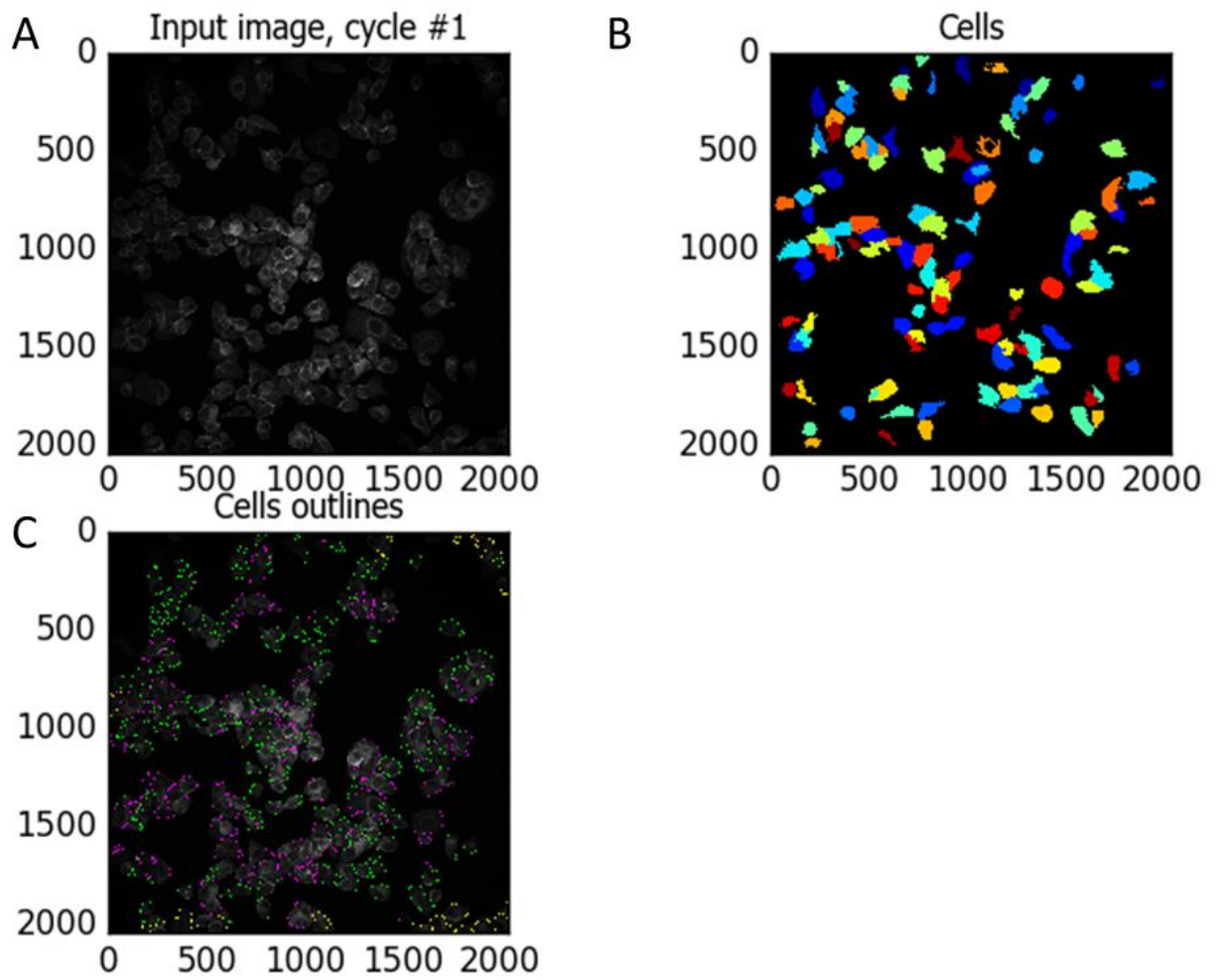
Appendix 1- IN Cell Analyser 2000 analysis pipeline for micronucleus identification

The pipeline for micronuclei detection using the INCell Analyser 2000 is located in the CD-ROM submitted with the thesis. The following images demonstrate the process of this identification (A1-1 to A1-5).

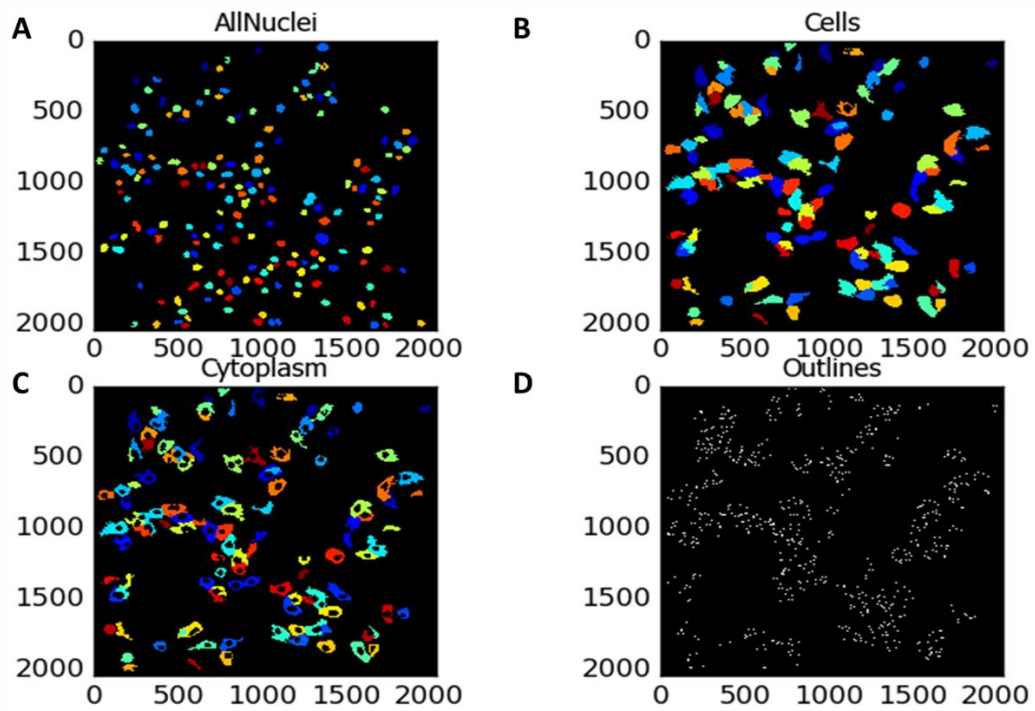
Each sample was prepared in triplicate. Within each replicate 2000 cells were analysed for the presence of MN; thus, in total 6000 cells were evaluated for MN per dose.



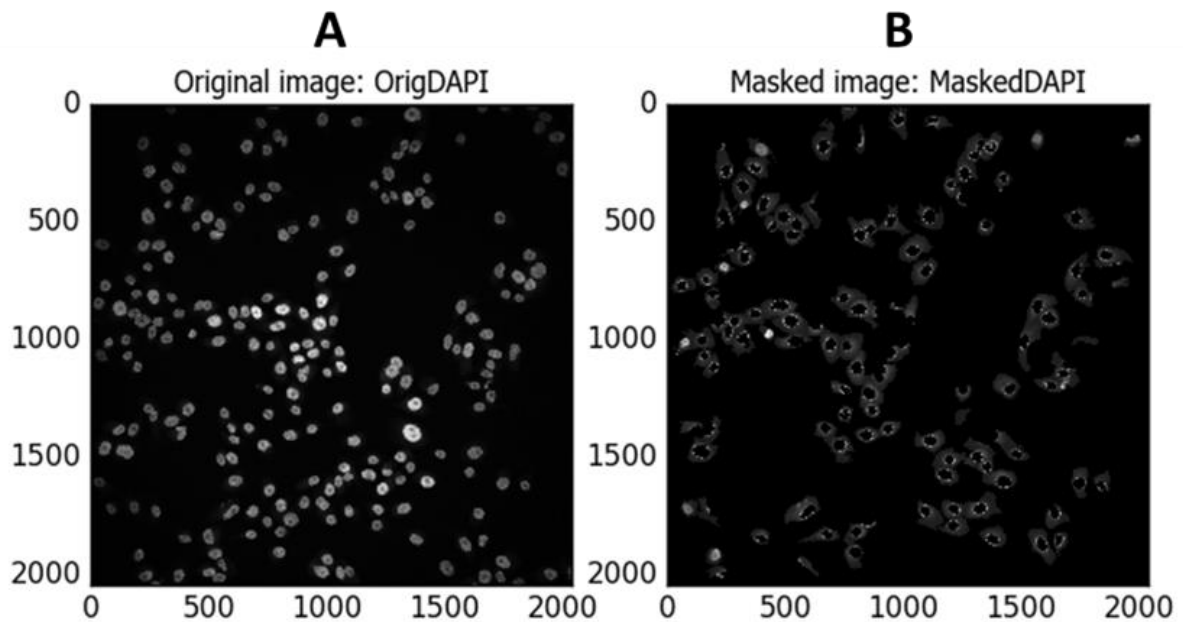
A1-1. The pipeline identified nuclei from the DAPI image. A was the original image of nuclei as an input. B represents the software identification of nuclei (the different colours in B were applied by the software to distinguish nuclei). C represents the outline of the identified nuclei.



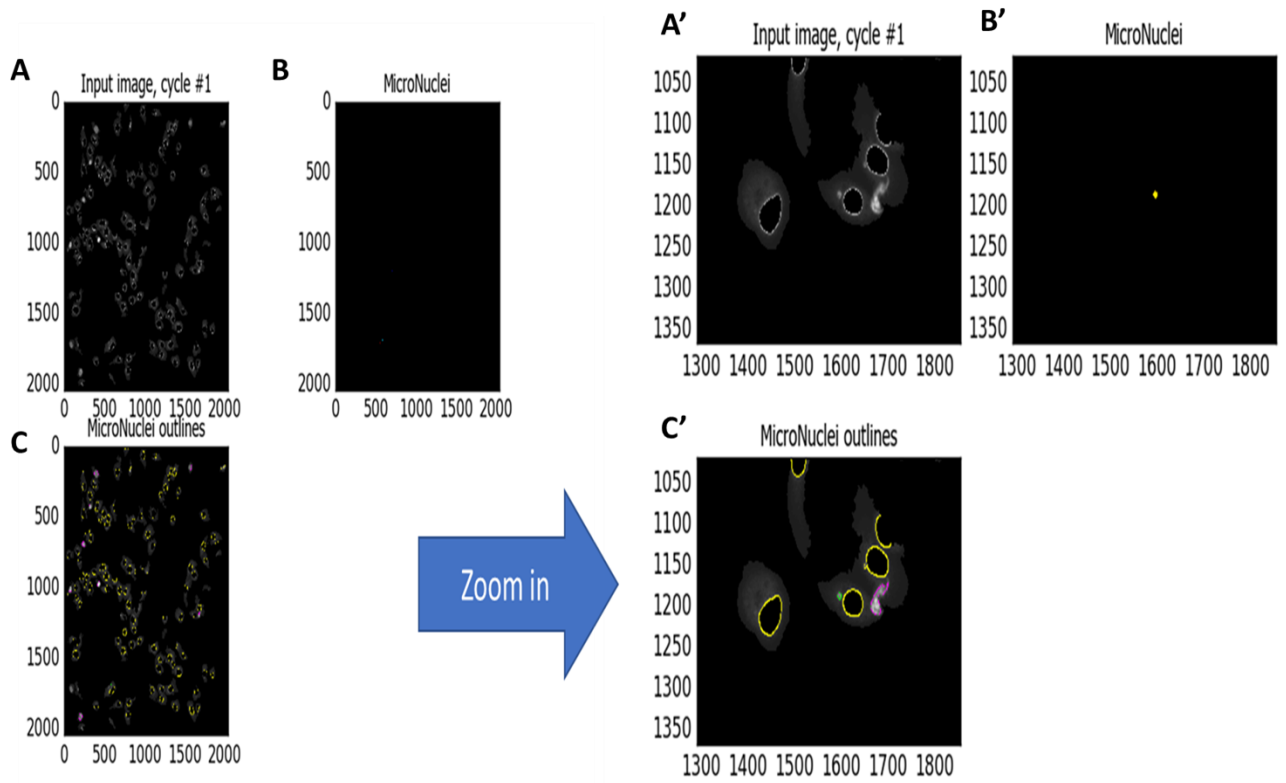
A1-2. The pipeline identified cells from the FITC image. A was the original image of cells as an input. B represents the software identification of cells (the different colours in B were applied by the software to distinguish cells). C represents the outline of the identified cells.



A1-3. A subtraction was used for the identified nuclei from the associated cell to pin-point the cytoplasm. A was the nuclei identified in A1-1. B is the results of identification of cells in A1-2. C (cytoplasm) and D (outline) were the result of subtraction (data generated in image B minus image A).



A1-4. A "Masking" was then used to block out the nuclei, avoiding the incorrect identification of MN within the nucleus. A was the original image of nuclei as an input and with outlined nuclei. B is the resulting image following masking of nuclei identified in image A.



A1-5. Final identification of the MN. A', B' and C' are the same as A, B and C but zoomed in. A' was the input images after process mentioned above (subtraction and masking). B' was the results of the identification of MN, which was labelled in yellow. In C', MN was outlined in green and nuclei were outlined in yellow. Note: the pink outlines the outliers (such as extremely small or large nuclei or non-round shape).

Appendix 2-Representative images of DU145 nuclei following 24-h NaS treatment

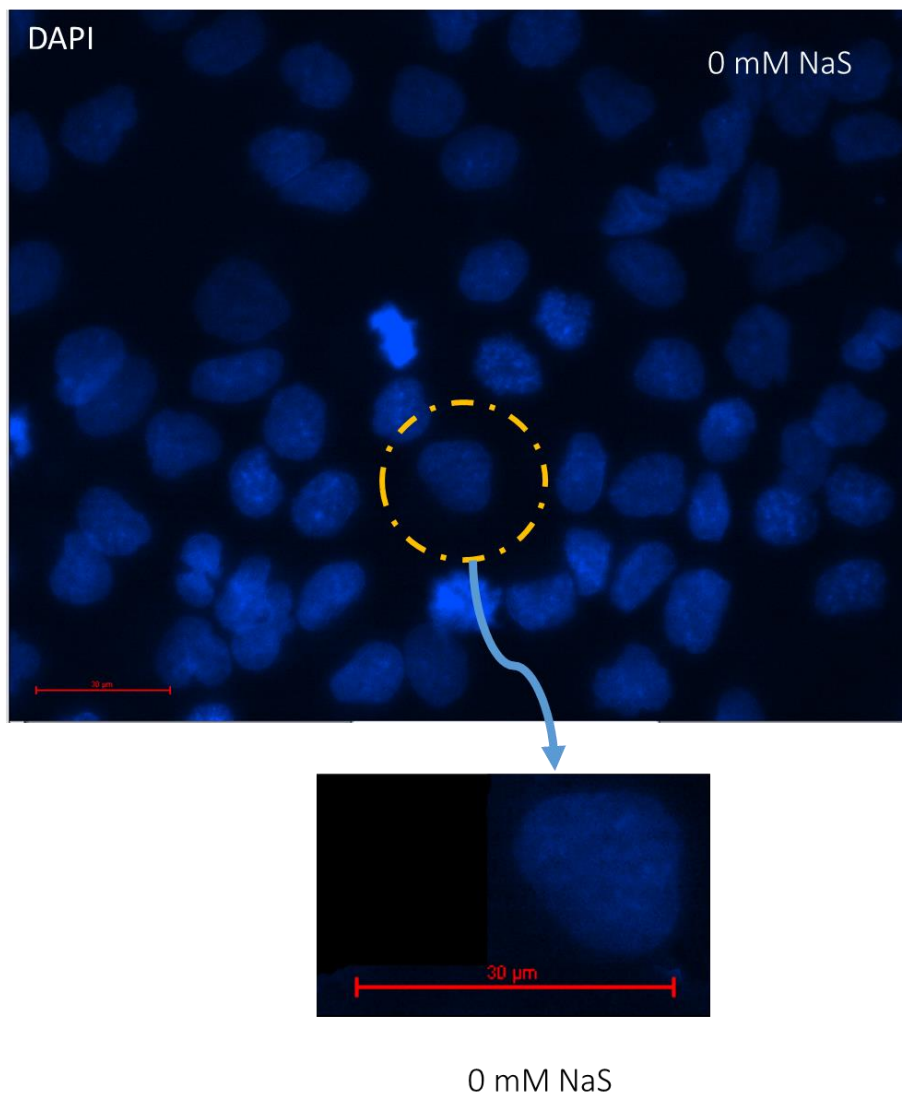
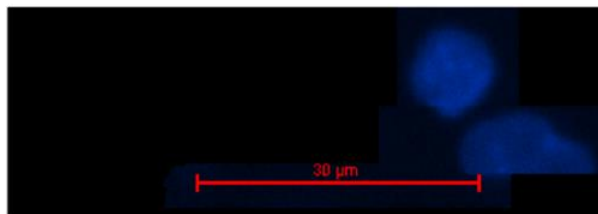
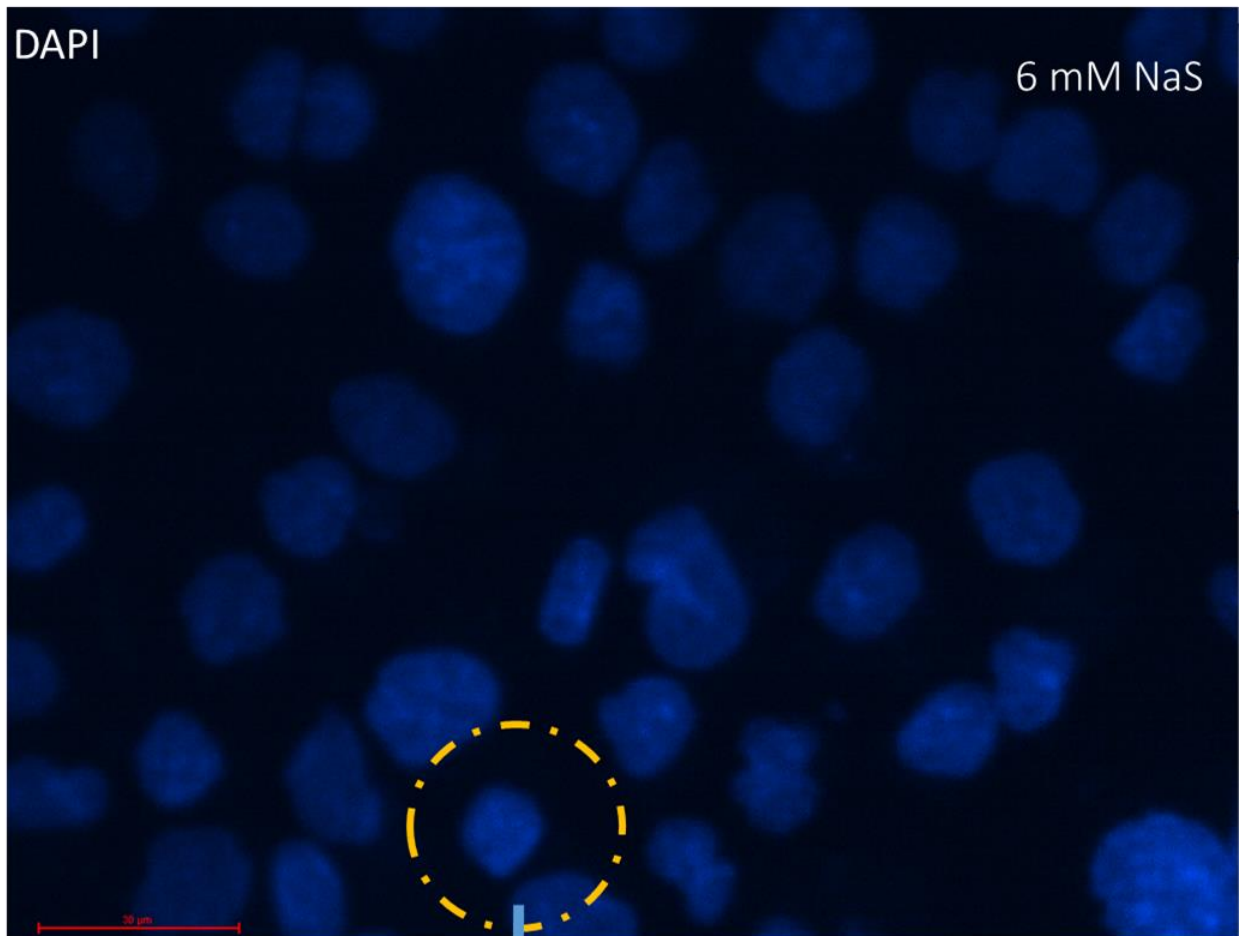


Figure A2-1: Representative images of large DU145 nuclei following 24-hour treatment with NaS. The lower row images were taken from the corresponding upper row images utilising an IN Cell Analyzer 2000. Size was determined by the INCell Analyser Workstation. Objective: 40x. Scale bar: 30 µm.



8 mM NaS

Figure A2-2: Representative images of the small DU145 cells nuclei following treatment with NaS. The lower row images were taken from the corresponding upper row images. Size was determined by In Cell Analyser Workstation. Objective: 40x. Scale bar: 30 μm .

Appendix 3-PCR array raw results for Chapter 3

The genes involved in PCR array are as follows and their layout are demonstrated in Table A3-1:

- Cell Adhesion Molecules

Cell Adhesion Molecules: APC, *CD44*, CDH1 (E-Cadherin), CDH11, CDH6, FAT1, FXYD5, ITGA7, PNN, SYK, VEGFA.

Transmembrane Receptors: *CD44*, ITGA7, *ITGB3*, RPSA.

Other Cell Adhesion Molecules: CTNNA1, FN1, MCAM, MGAT5, MTSS1.

- Extracellular Matrix (ECM) Molecules

Extracellular Matrix (ECM) Proteases: MMP10, MMP11, MMP13, MMP2, MMP3, MMP7, MMP9.

Extracellular Matrix (ECM) Protease Inhibitors: TIMP2, TIMP3, TIMP4.

Other Extracellular Matrix (ECM) Molecules: COL4A2, HPSE, SERPINE1 (PAI-1).

- Cell Cycle

Regulation of the Cell Cycle: APC, BRMS1, CDKN2A (p16INK4a), HRAS, IL1B, KRAS, MTSS1, NF2, NME1 (NM23), PTEN, RB1, TGFB1, TP53 (p53), VEGFA.

Cell Cycle Arrest & Checkpoints: CDKN2A (p16INK4a), MYC, RB1, TP53 (p53).

- Cell Growth & Proliferation

Negative Regulation of Cell Proliferation: CDKN2A (p16INK4a), CTBP1, GNRH1, IL1B, MDM2, NF2, NME1 (NM23), SSTR2.

Positive Regulation of Cell Proliferation: IGF1, IL18, TSHR, VEGFA.

Growth Factors & Hormones: GNRH1, HGF, IGF1, TGFB1, VEGFA.

Cytokines: CCL7 (MCP-3), CXCL12 (SDF1), IL18, IL1B, TNFSF10 (TRAIL).

Cell Surface Receptors: *CXCR2* (IL8RB), *CXCR4*, EPHB2, FGFR4, FLT4 (VEGFR2), KISS1R, MET, *NR4A3* (NOR1), PLAUR (UPAR), RORB, SSTR2, TSHR.

Other Cell Growth Genes: DENR, EWSR1, HRAS, MYC, SET, SRC, SYK, TRPM1.

- Apoptosis

CXCR4, HTATIP2, IL1B, IL18, TGFB1, TIMP3, TNFSF10 (TRAIL), TP53 (p53).

- Transcription Factors & Regulators

CHD4, ETV4, EWSR1, HTATIP2, MTA1, MYC, MYCL, *NR4A3* (NOR1), RB1, RORB, SMAD2 (MADH2), SMAD4 (MADH4), TCF20, TP53 (p53).

- Other Tumour Metastasis Genes

CST7, CTSK, CTSL, *CD82* (KAI1), KISS1, METAP2, NME4.

Table A3-1. Gene Resource List (plate payout)

	1	2	3	4	5	6	7	8	9	10	11	12
A	APC	BRMS1	CCL7	CD44	CD82	CDH1	CDH11	CDH6	CDKN2A	CHD4	COL4A2	CST7
B	CTBP1	CTNNA1	CTSK	CTSL1	CXCL12	CXCR2	CXCR4	DENR	EPHB2	ETV4	EWSR1	FAT1
C	FGFR4	FLT4	FN1	FXYS5	GNRH1	HGF	HPSE	HRAS	HTATIP2	IGF1	IL18	IL1B
D	ITGA7	ITGB3	KISS1	KISS1R	KRAS	MCAM	MDM2	MET	METAP2	MGAT5	MMP10	MMP11
E	MMP13	MMP2	MMP3	MMP7	MMP9	MTA1	MTSS1	MYC	MYCL1	NF2	NME1	NME4
F	NR4A3	PLAUR	PNN	PTEN	RB1	RORB	RPSA	SERPINE1	SET	SMAD2	SMAD4	SRC
G	SSTR2	SYK	TCF20	TGFB1	TIMP2	TIMP3	TIMP4	TNFSF10	TP53	TRPM1	TSHR	VEGFA
H	ACTB	B2M	GAPDH	HPRT1	RPLP0	HGDC	RTC	RTC	RTC	PPC	PPC	PPC

Table A3-2 and A3-3 are the PCR array results from PC3 and DU145 cells respectively.

Table A3-2. PCR array results in PC3 cells following 4 mM NaS treatment vs. the control.

Position	Control Group	4 mM
A01	29.18	30.90
A02	26.09	27.49
A03	34.53	35.44
A04	22.91	24.93
A05	30.96	28.11
A06	26.06	25.02
A07	22.89	Undetermined
A08	32.55	Undetermined
A09	25.29	24.04
A10	24.31	25.13
A11	27.10	27.09
A12	31.38	33.13
B01	25.49	25.26
B02	33.17	24.02
B03	28.94	27.14
B04	24.53	22.23
B05	35.21	39.55
B06	29.19	30.78

B07	33.75	28.63
B08	23.75	25.59
B09	28.43	31.10
B10	28.02	31.59
B11	24.17	24.87
B12	25.93	28.60
C01	30.63	30.90
C02	34.89	28.86
C03	25.05	27.56
C04	23.83	25.48
C05	29.57	29.45
C06	35.20	38.23
C07	27.12	27.05
C08	25.13	27.02
C09	25.16	24.36
C10	36.84	34.95
C11	24.15	26.36
C12	25.98	36.08
D01	30.68	32.09
D02	30.07	28.28
D03	30.38	30.07
D04	33.11	32.90
D05	26.53	24.90
D06	25.53	29.40
D07	25.67	26.21
D08	22.28	26.67
D09	24.07	24.53
D10	26.45	27.09
D11	31.27	33.43
D12	33.06	30.10
E01	29.60	34.20
E02	36.09	37.49
E03	34.08	36.14
E04	34.11	37.11
E05	30.14	31.96

E06	24.08	25.10
E07	28.86	30.88
E08	23.32	24.52
E09	31.60	31.25
E10	23.82	26.28
E11	22.03	24.51
E12	24.27	24.72
F01	31.43	29.53
F02	24.76	27.64
F03	23.60	24.92
F04	38.32	25.77
F05	25.95	26.76
F06	38.49	Undetermined
F07	19.85	22.34
F08	25.85	33.61
F09	21.33	22.06
F10	25.05	24.15
F11	26.03	26.81
F12	26.00	28.09
G01	32.49	34.25
G02	30.46	29.79
G03	25.87	26.98
G04	24.60	25.34
G05	22.75	23.70
G06		36.99
G07	33.29	36.41
G08	31.44	25.48
G09	29.46	23.84
G10	37.87	Undetermined
G11	35.04	35.26
G12	25.06	23.52
H01	17.86	19.53
H02	21.27	21.75
H03	19.49	20.56
H04	24.13	26.72

H05	17.43	19.48
H06	38.42	36.06
H07	22.77	23.69
H08	22.85	23.82
H09	22.85	23.62
H10	21.10	21.27
H11	20.94	21.25
H12	21.17	21.45

Table A3-3. PCR array results in DU145 cells following 4 mM NaS treatment vs. the control

Position	Control Group	4 mM
A01	30.90	29.06
A02	27.49	26.47
A03	35.44	33.42
A04	24.93	22.65
A05	28.11	27.38
A06	25.02	24.52
A07/A08	Undetermined	Undetermined
A09	24.04	22.67
A10	25.13	24.80
A11	27.09	26.49
A12	33.13	32.94
B01	25.26	24.38
B02	24.02	23.19
B03	27.14	25.14
B04	22.23	19.48
B05	39.55	38.07
B06	30.78	29.57
B07	28.63	27.11
B08	25.59	24.21
B09	31.10	30.33
B10	31.59	30.16
B11	24.87	24.83
B12	28.60	27.48
C01	30.90	30.02
C02	28.86	28.15

C03	27.56	26.67
C04	25.48	23.51
C05	29.45	27.69
C06	38.23	37.11
C07	27.05	25.61
C08	27.02	26.06
C09	24.36	22.96
C10	34.95	34.64
C11	26.36	24.67
C12	36.08	34.57
D01	32.09	31.20
D02	28.28	25.85
D03	30.07	28.78
D04	32.90	32.10
D05	24.90	23.50
D06	29.40	28.18
D07	26.21	25.44
D08	26.67	25.02
D09	24.53	23.70
D10	27.09	26.24
D11	33.43	31.57
D12	30.10	29.27
E01	34.20	33.45
E02	37.49	36.13
E03	36.14	34.49
E04	37.11	35.25
E05	31.96	30.03
E06	25.10	23.82
E07	30.88	29.17
E08	24.52	23.15
E09	31.25	31.33
E10	26.28	25.20
E11	24.51	23.25
E12	24.72	23.66
F01	29.53	28.72

F02	27.64	25.57
F03	24.92	23.12
F04	25.77	24.26
F05	26.76	25.12
F06	Undetermined	38.72
F07	22.34	20.53
F08	33.61	32.30
F09	22.06	21.31
F10	24.15	22.89
F11	26.81	25.42
F12	28.09	27.98
G01	34.25	32.38
G02	29.79	28.48
G03	26.98	25.67
G04	25.34	23.90
G05	23.70	22.27
G06	36.99	35.20
G07	36.41	34.55
G08	25.48	25.55
G09	23.84	23.19
G10	Undetermined	Undetermined
G11	35.26	33.05
G12	23.52	21.74
H01	19.53	18.16
H02	21.75	20.07
H03	20.56	19.30
H04	26.72	25.00
H05	19.48	17.17
H06	36.06	36.66
H07	23.69	23.51
H08	23.82	23.56
H09	23.62	23.62
H10	21.27	20.97
H11	21.25	20.99
H12	21.45	21.22

Appendix 4-Western blots underlying densitometry data in Ch

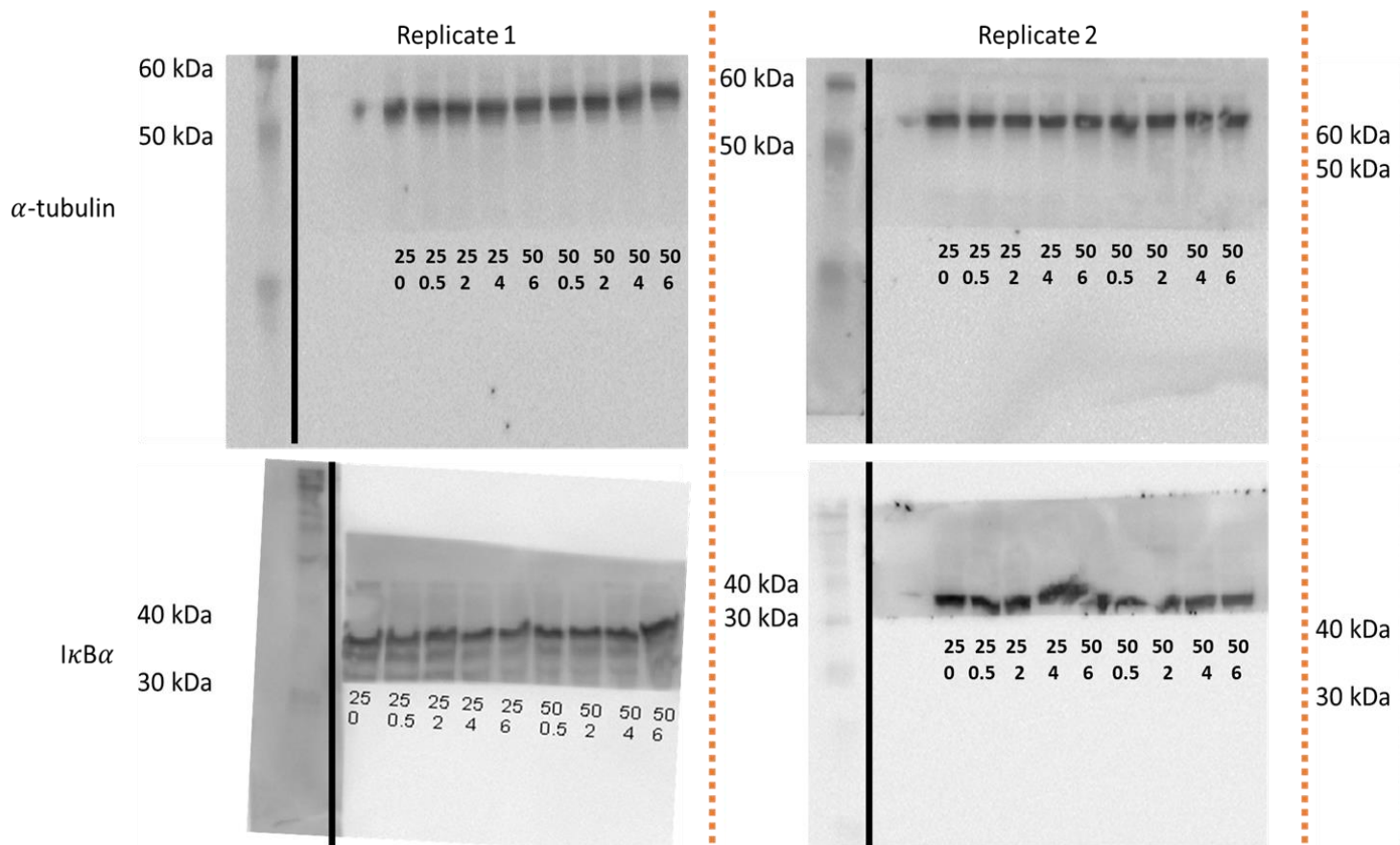


Figure A4-1. Individual Western blots supporting the data shown in Figure 4.3, I κ B α protein expression levels after TNF- α treatment exposure time (h). 25 and 50, TNF- α dose (ng/mL). The black lines are to distinguish the ladder and the proteins sections; and the orange

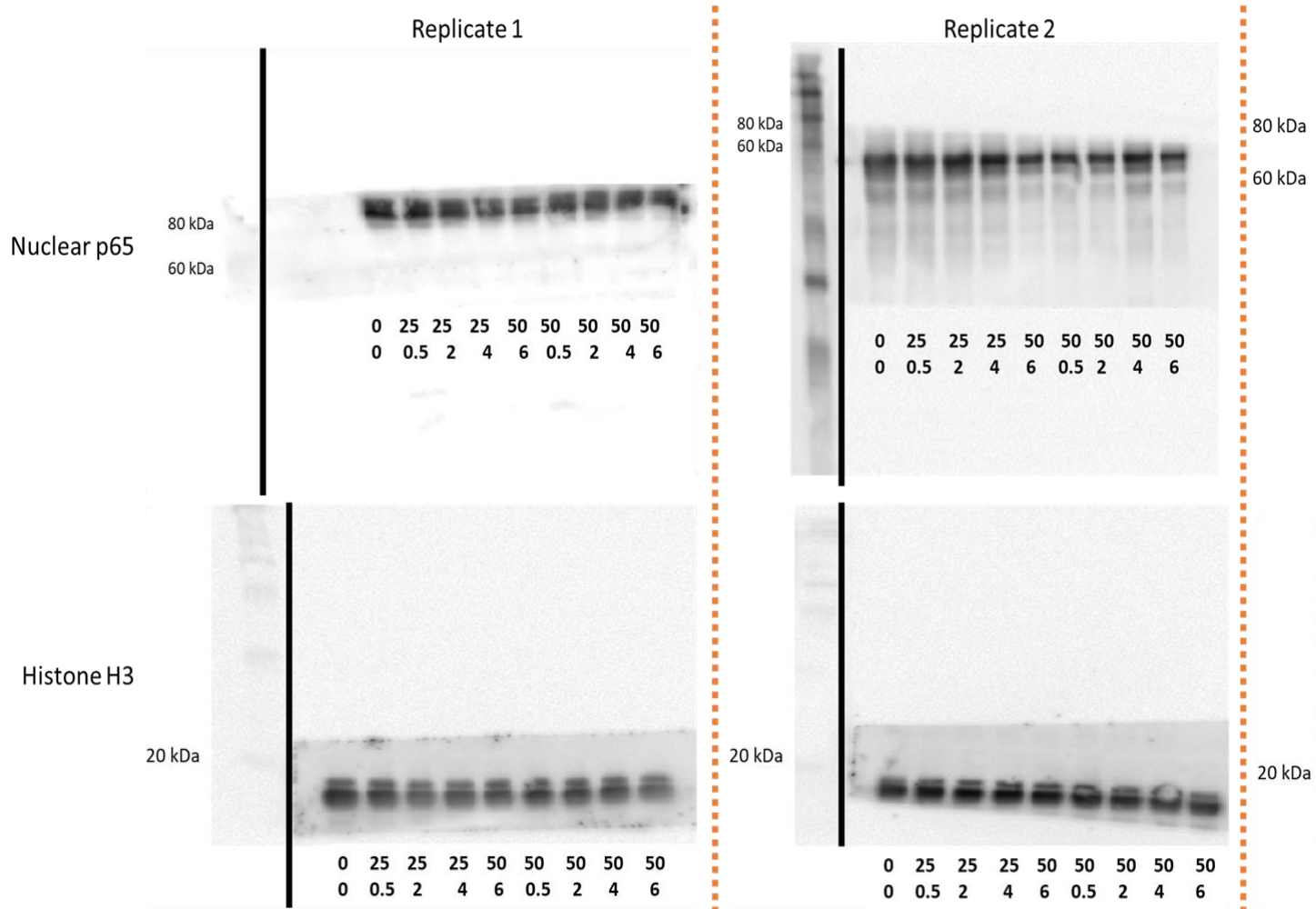


Figure A4-2. Individual Western blots supporting the data shown in Figure 4.3 nuclear p65 protein expression levels after TNF- α treatment. The blots show p65 protein levels (80 kDa and 60 kDa) and Histone H3 (20 kDa) as a loading control. The blots are organized by replicate (Replicate 1 and Replicate 2) and protein type (Nuclear p65 and Histone H3). The lanes represent different TNF- α doses (0, 25, 50 ng/mL) and exposure times (0, 0.5, 2, 4, 6 h). The black lines are to distinguish the ladder and the proteins sections; and the orange dashed lines separate the replicates.

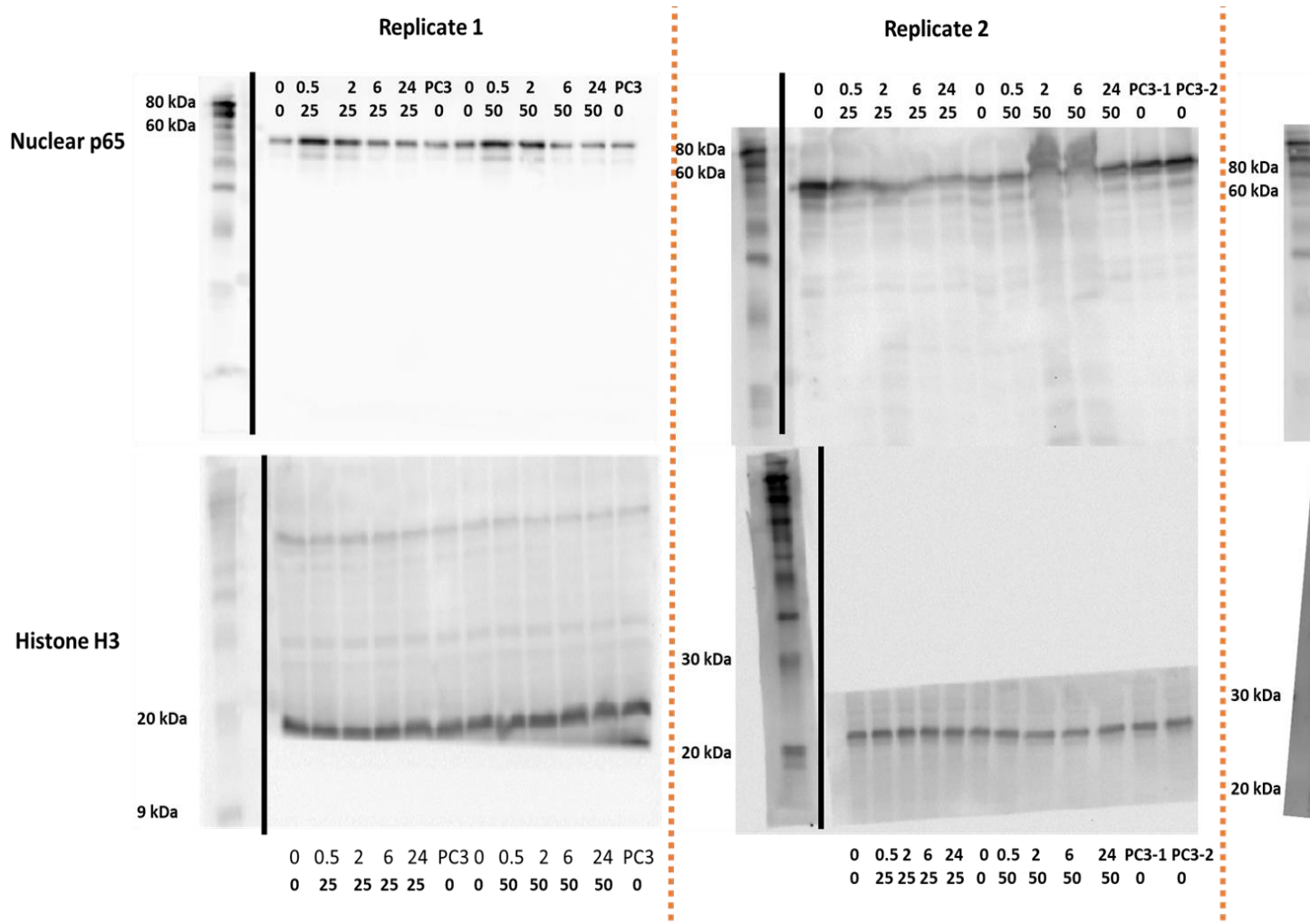


Figure A4-3. Western blots derived in Figure 4.4 that is the profile of nuclear p65 protein levels after TNF- α treatment in PNT2 cells at different time (h). 25 and 50, TNF- α dose (ng/mL). PC3, the PCE3 cells without TNF- α . The black lines are to distinguish the ladder and the protein bands. The dotted lines are to distinguish the replicates.

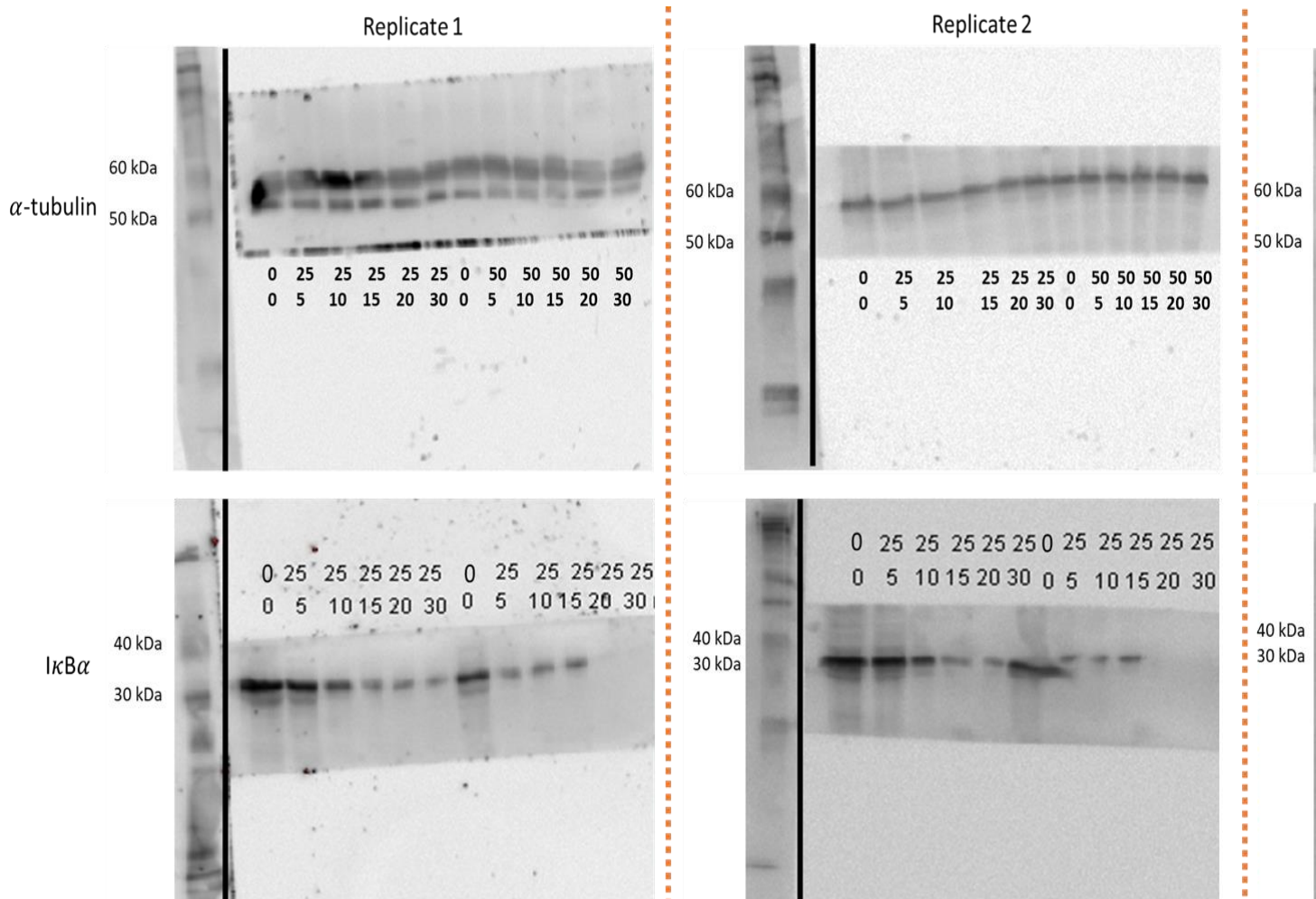


Figure A4-4. Western blots derived in Figure 4.5 that is the profile of I κ B α protein levels after TNF- α treatment in PNT2 cells over the (h). 25 and 50, TNF- α dose (ng/mL). The black lines are to distinguish the ladder and the proteins sections; and the orange dotted lines

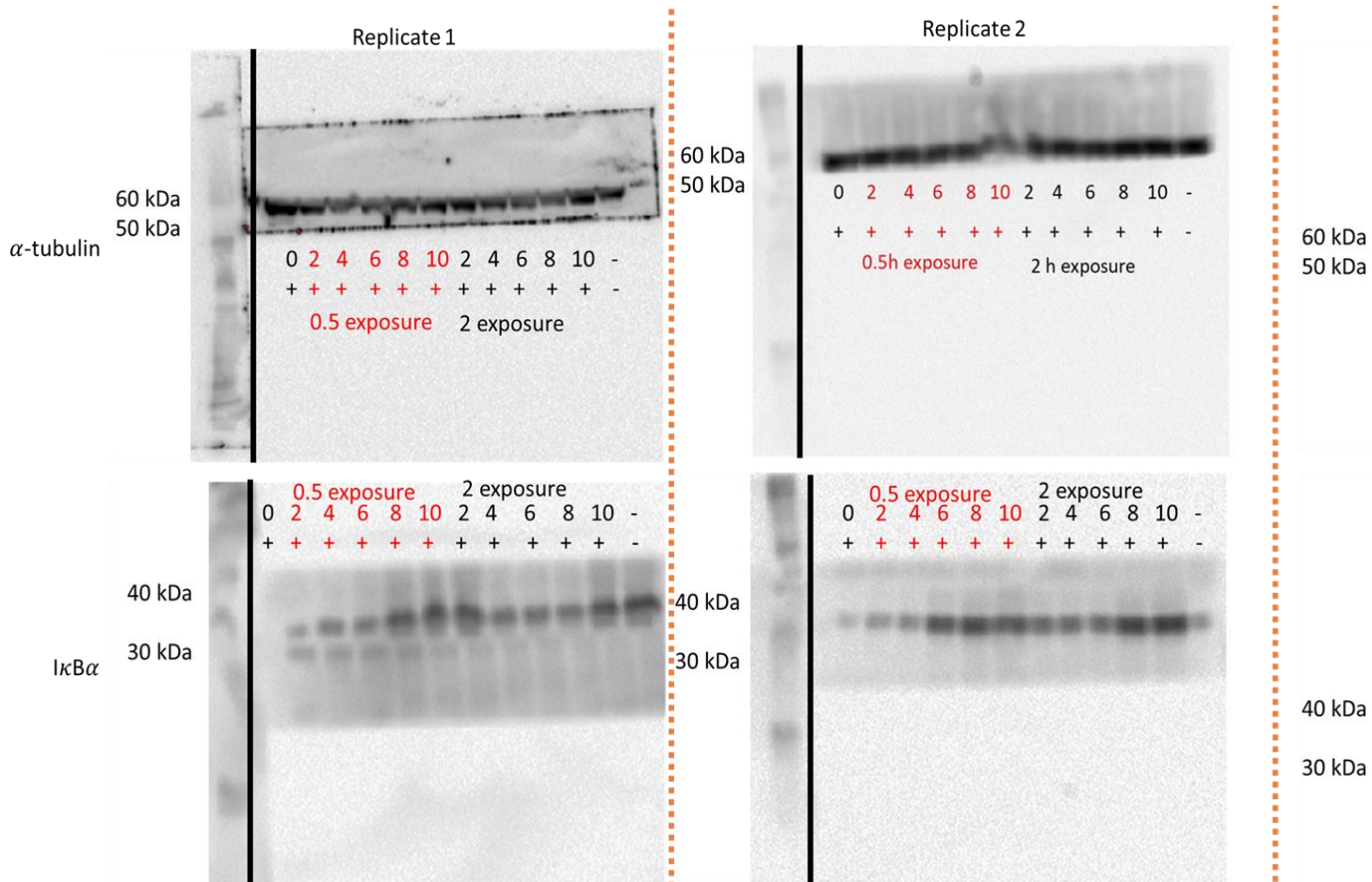


Figure A4-5. Individual Western blots supporting the data shown in Figure 4.7 IκBα protein expression levels after NaS treatment in T8, and 10, NaS dose (mM). +, and -, TNF-α (25ng/mL, 30min) treatment. The black lines are to distinguish the ladder and the protein bands. The dashed orange lines distinguish the replicates.

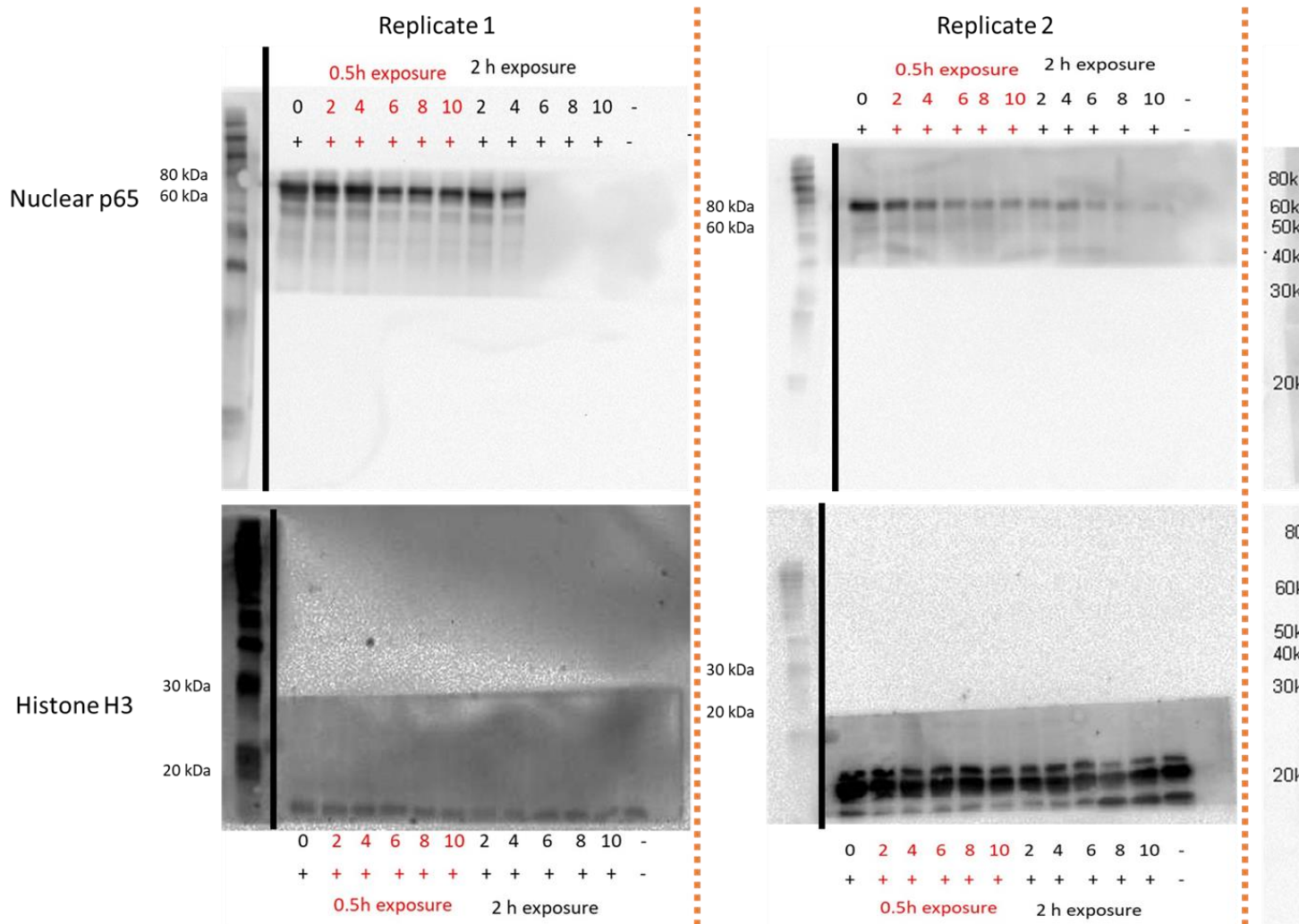


Figure A4-6. Individual Western blots supporting the data shown in Figure 4.7 nuclear p65 protein expression levels after NaS treatment 2, 4, 6, 8, and 10, NaS dose (mM). +, and -, TNF- α (25ng/mL, 30min) treatment. The black lines are to distinguish the ladder and the protein bands. The orange dashed lines distinguish the replicates.

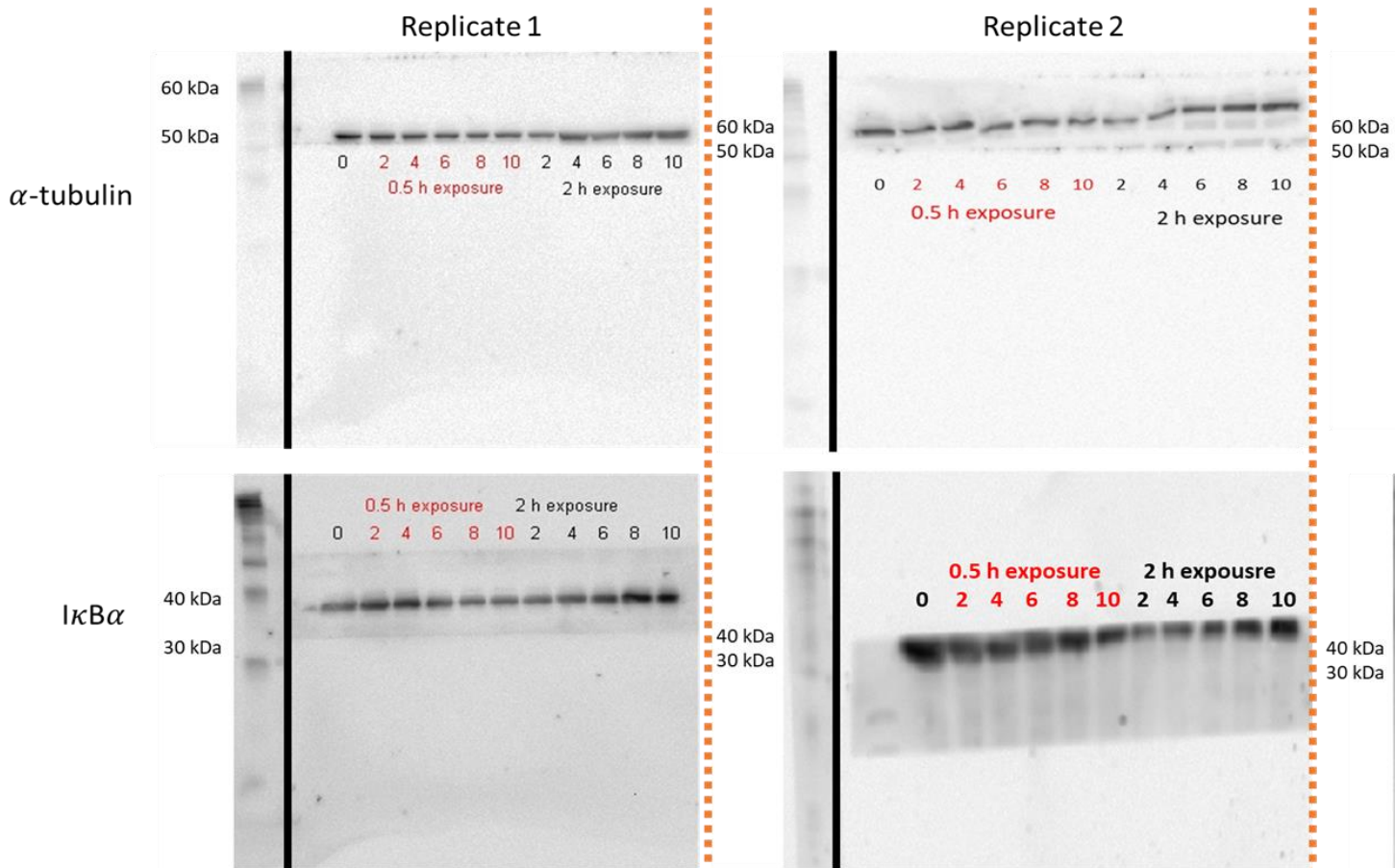


Figure A4-7. Western blots derived in the Figure 4.9 that is NaS role in PC3 cells with constitutive activation of NF- κ B pathway present NaS dose (mM). The black lines are to distinguish the ladder and the proteins sections; and the orange dotted lines are to distinguish the

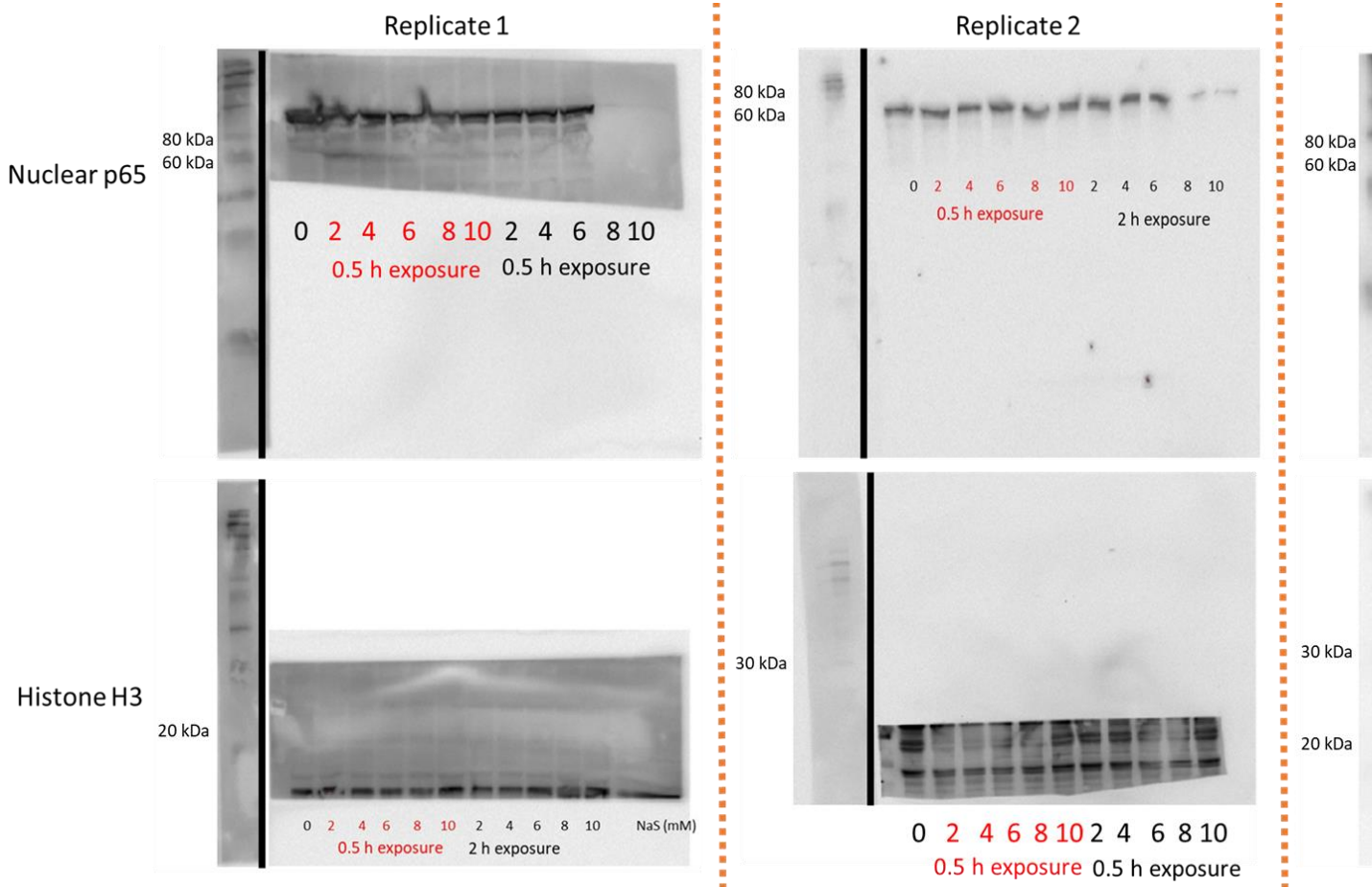


Figure A4-8. Western blots derived in the Figure 4.9 that is NaS role in PC3 cells with constitutive activation of NF- κ B pathway present 10, NaS dose (mM). The black lines are to distinguish the ladder and the proteins sections; and the orange dotted lines are to distinguish

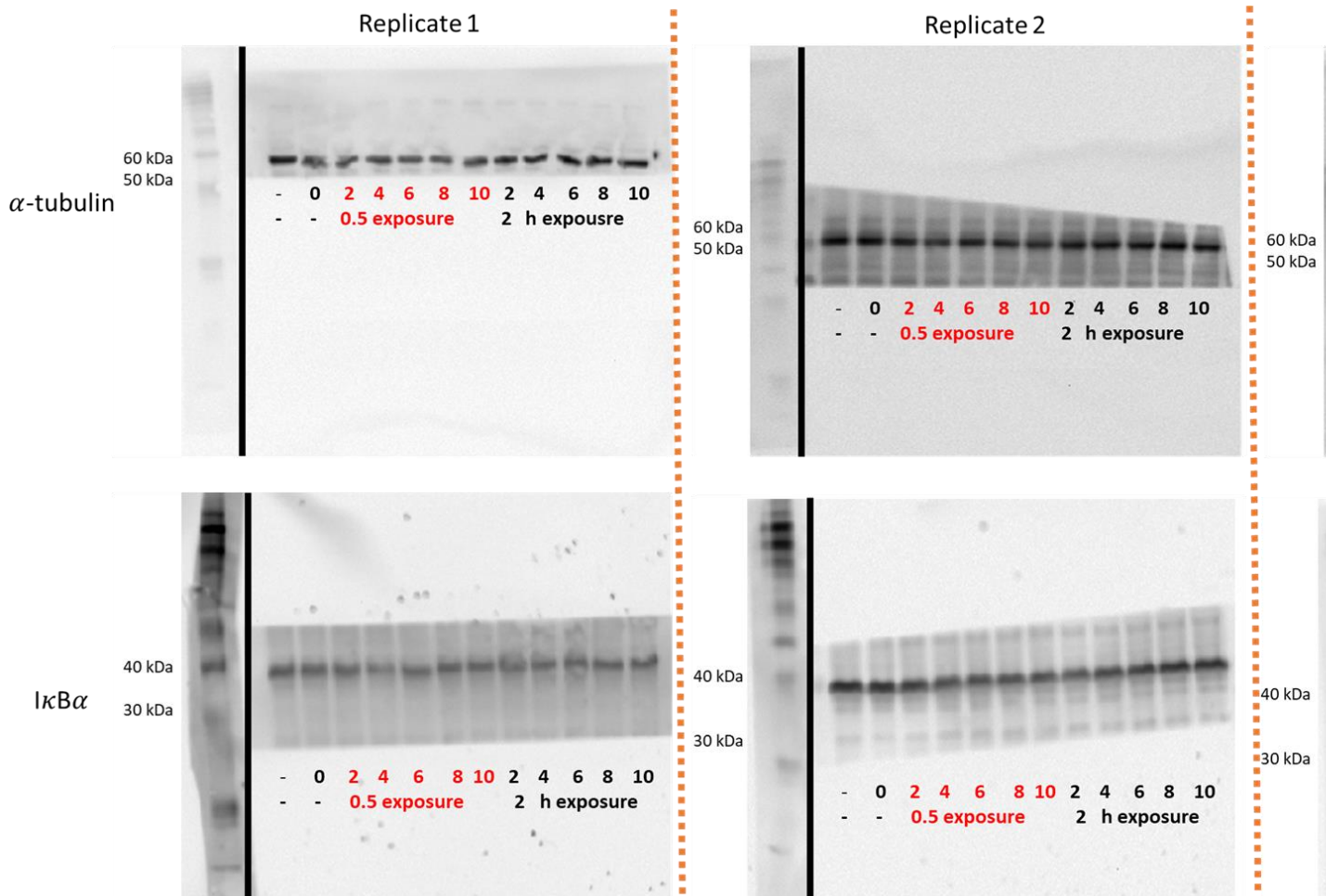


Figure A4-9. Western blots derived in the Figure 5.10 that is NaS role in PC3 spheroids presenting profile of $I\kappa B\alpha$. 0, 2, 4, 6, 8, and 10, the ladder and the proteins sections; and the orange dotted lines are to distinguish the replicates.

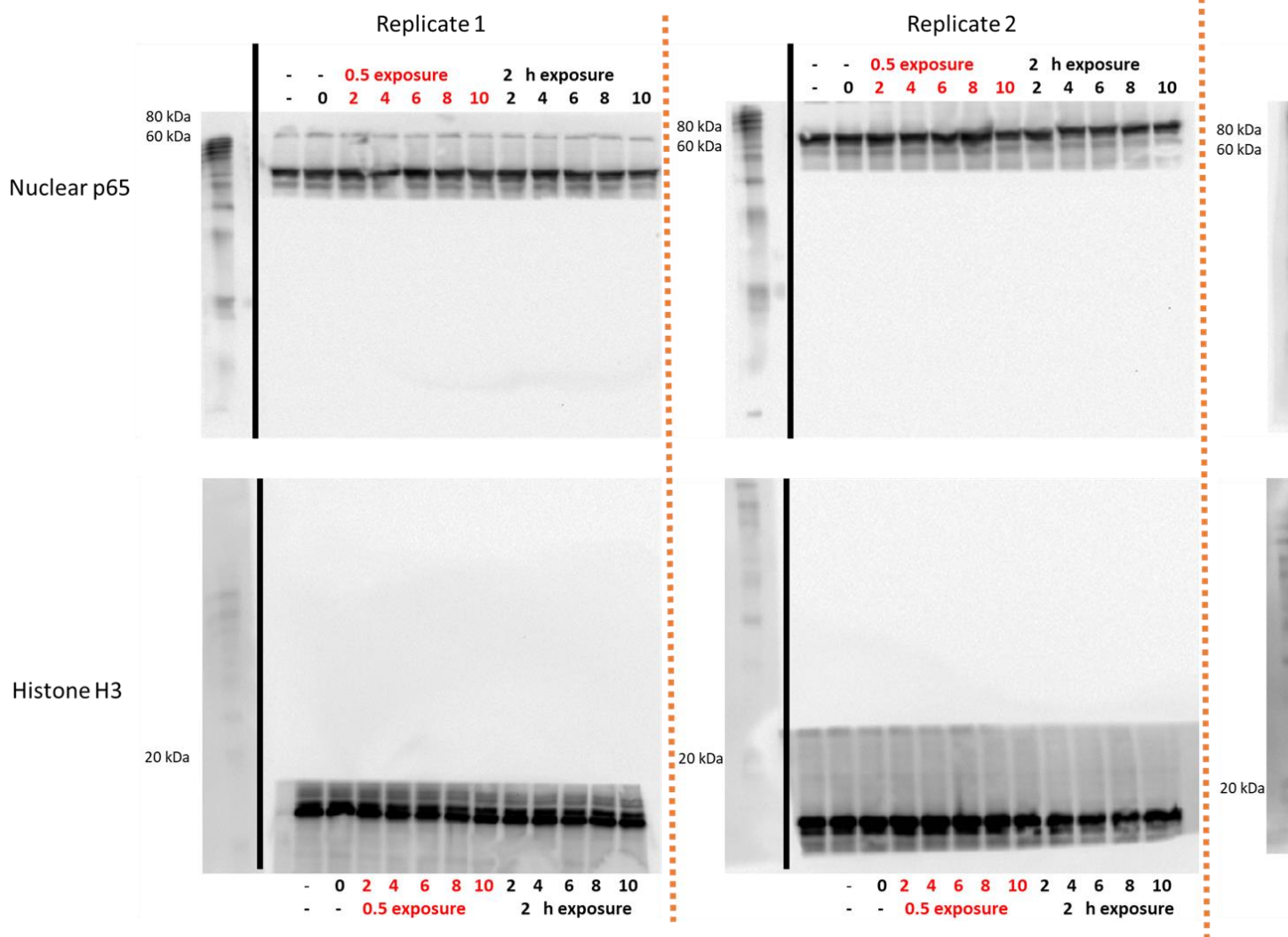
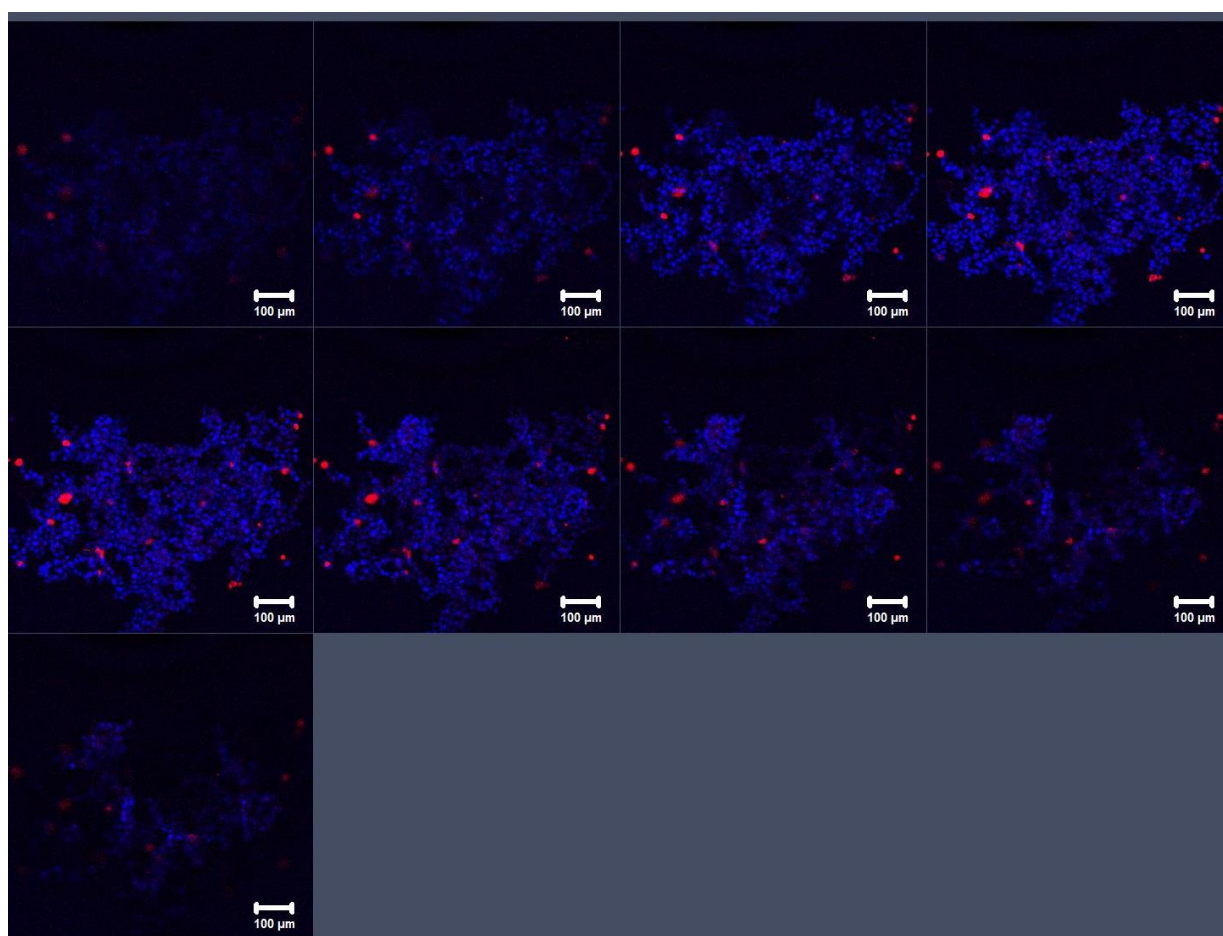


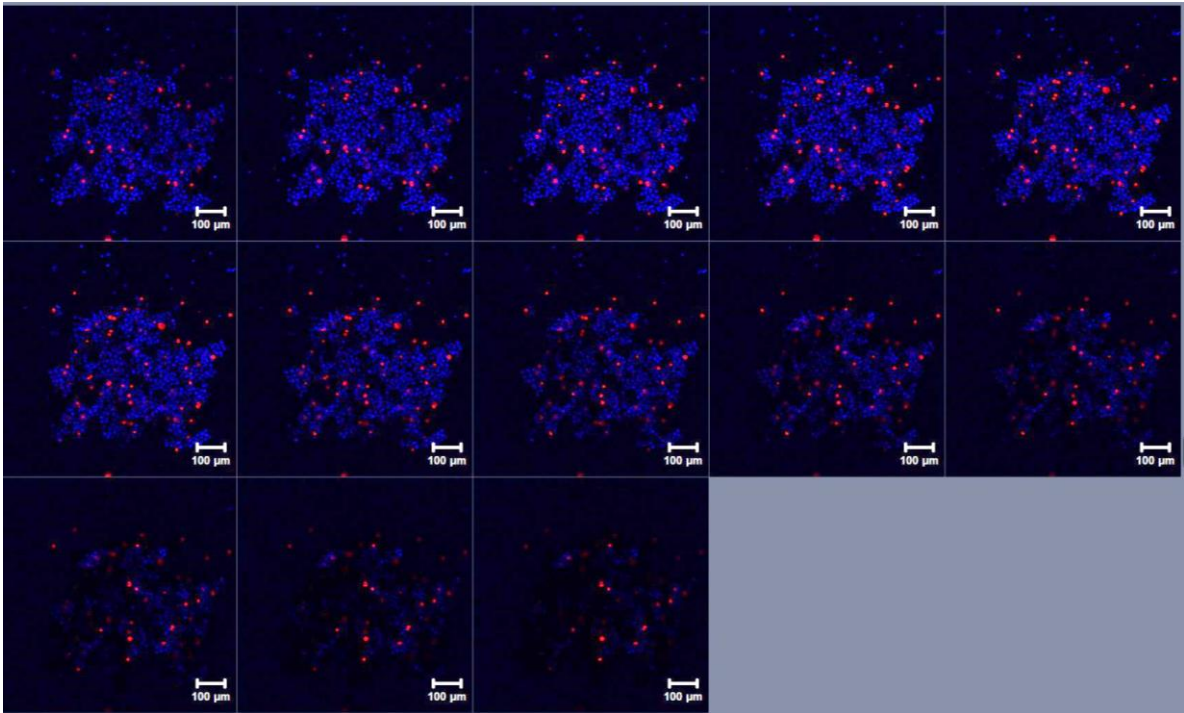
Figure A4-10. Western blots derived in the Figure 5.10 that is NaS role in PC3 spheroids presenting profile of the nuclear p65. 0, 2, 4, to distinguish the ladder and the proteins sections; and the orange dotted lines are to distinguish the replicates.

Appendix 5-Confocal microscopy generated Z-stack images supporting data in Chapter 5

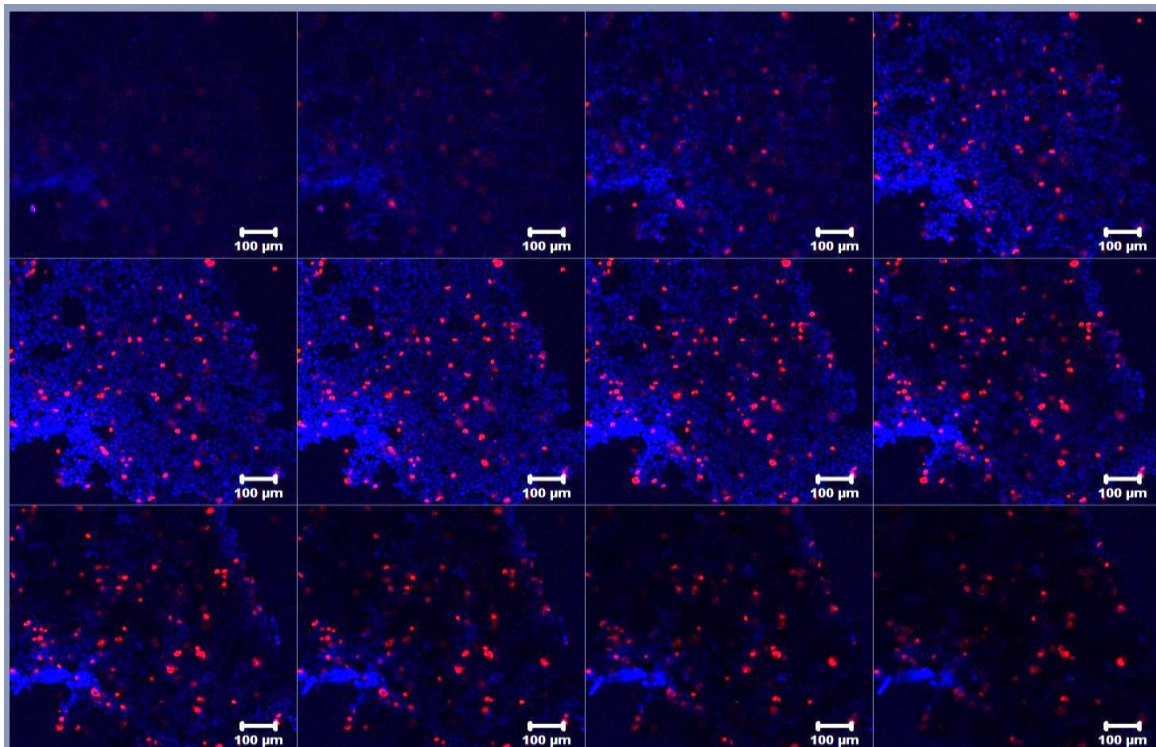
This appendix includes a series of Z-stack serial images generated by incrementally stepping through each 3D PC3 spheroid sample, generated by confocal microscopy. The following figures are representative examples of Z-stack galleries produced to support the data analysis in Chapter 5, Section 5.3.1.3 and Section 5.3.2.1. Figure A5-1 to A5-9 are the galleries for monitoring necrosis in spheroids, converted from Z-stack videos. Figure A5-10 to A5-12 are the galleries for monitoring O₂ availability in spheroids, converted from Z-stack videos.



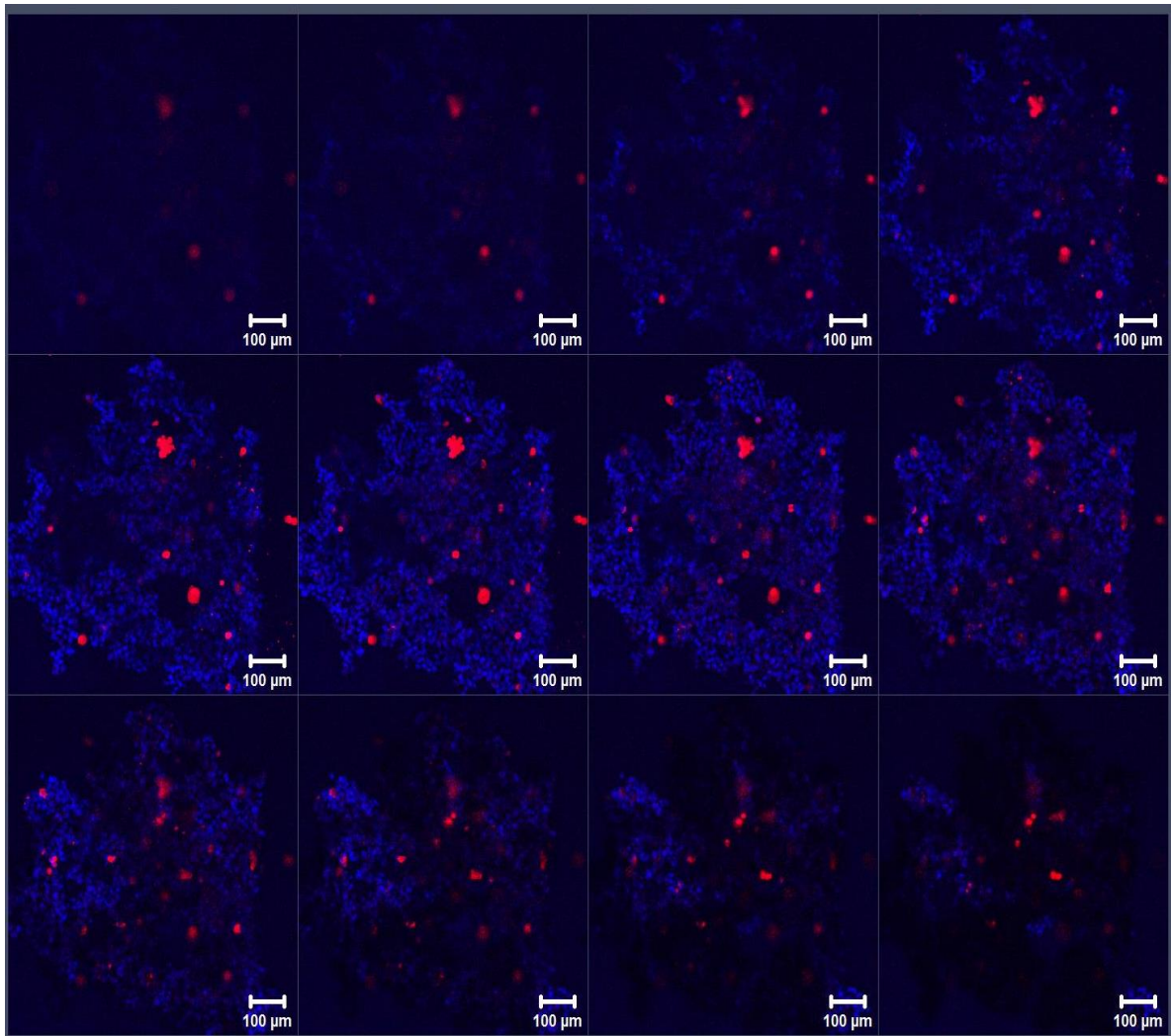
A5-1. Gallery demonstrating necrosis in PC3 spheroids seeded at 1000 cells / well after 1 day of culture. The spheroid was stained with Hoechst (blue, representing cell nuclei) and PI (red, representing dead cells). The gallery displays the sections of the spheroids from bottom to the top. Scale bar: 100 μm . Note: due to the number of the images, scale bars might be not clearly readable.



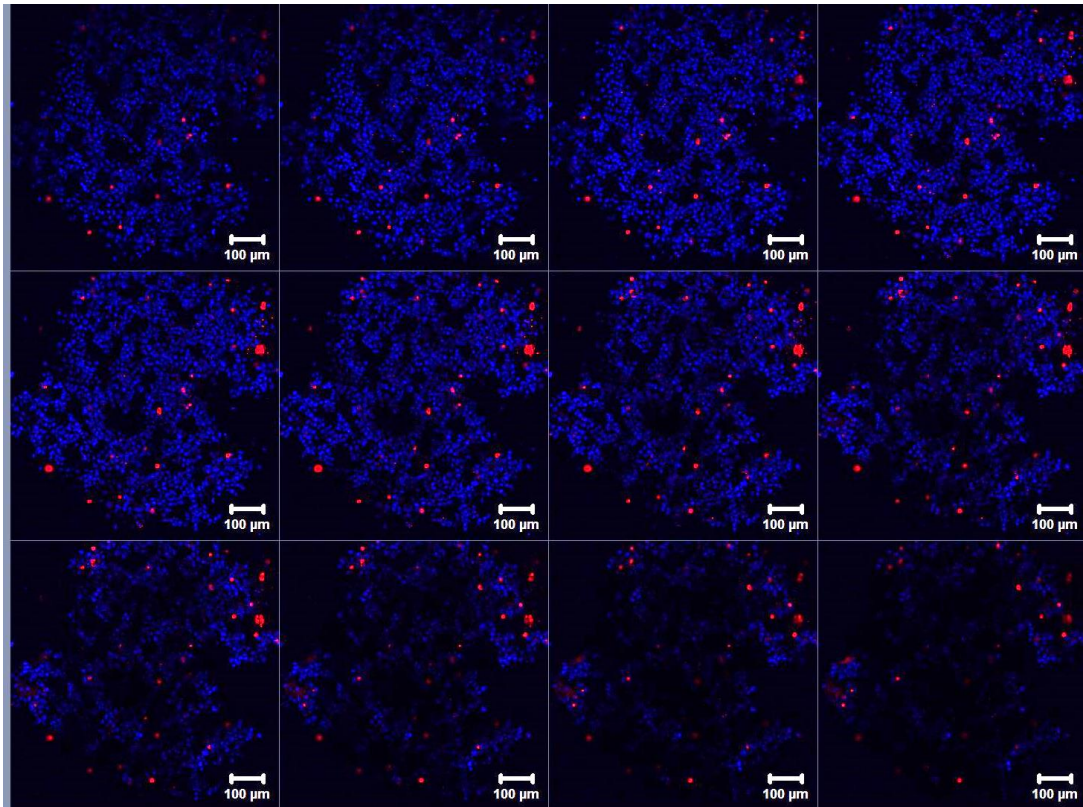
A5-2. Gallery demonstrating necrosis in PC3 spheroids seeded at 2000 cells / well after 1 day of culture. The spheroid was stained with Hoechst (blue, representing live cells) and PI (red, representing dead cells). The gallery displays the sections of the spheroids from bottom to the top. Scale bar: 100 μm . Note: due to the number of the images, scale bars might be not clearly readable.



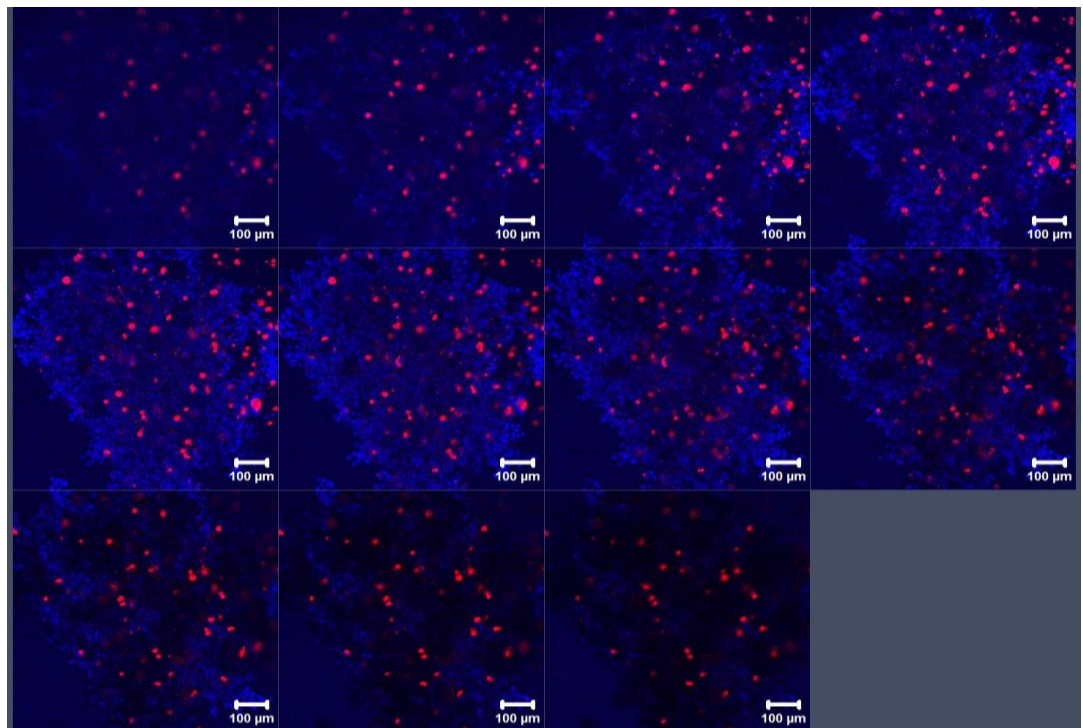
A5-3. Gallery demonstrating necrosis in PC3 spheroids seeded at 5000 cells / well after 1 day of culture. The spheroids were stained with Hoechst (blue, representing live cells) and PI (red, representing dead cells). The gallery displays the sections of the spheroids from bottom to the top. Scale bar: 100 μm . Note: due to the number of the images, scale bars might be not clearly readable.



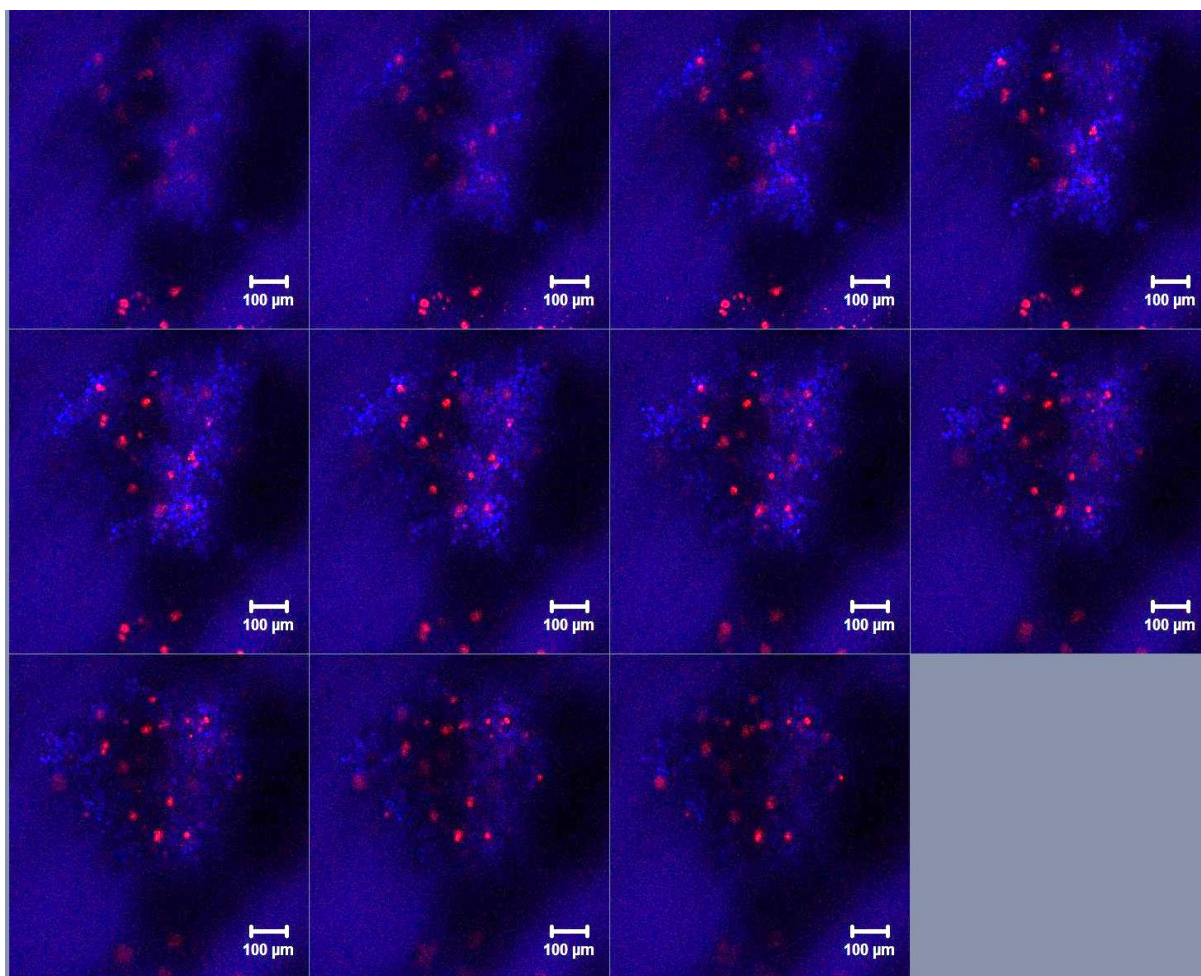
A5-4. Gallery demonstrating necrosis in PC3 spheroids seeded at 1000 cells / well after 3 days of culture. The spheroid was stained with Hoechst (blue, representing live cells) and PI (red, representing dead cells). The gallery displays the sections of the spheroids from bottom to the top. Scale bar: 100 μm . Note: due to the number of the images, scale bars might be not clearly readable.



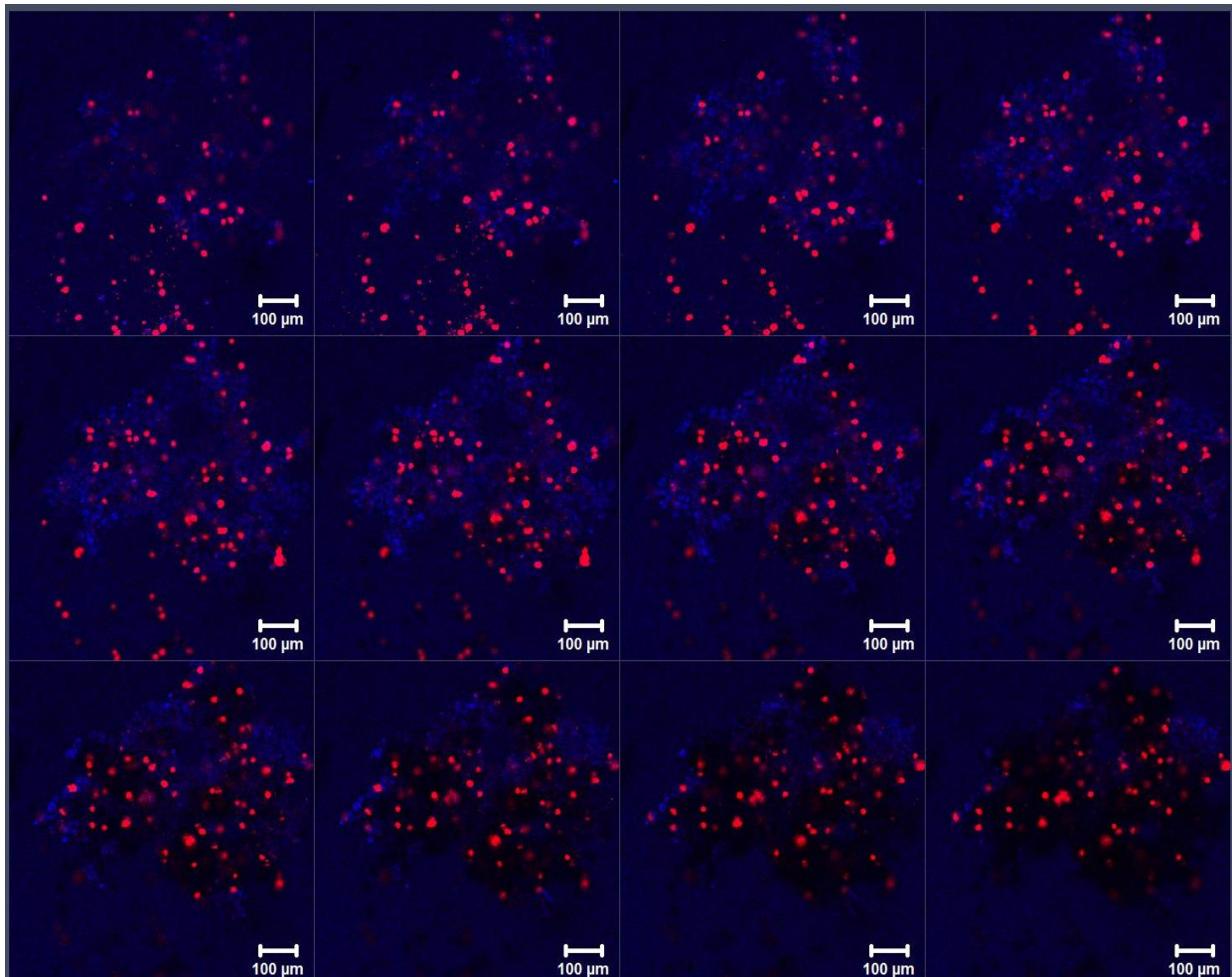
A5-5. Gallery demonstrating necrosis in PC3 spheroids seeded at 2000 cells / well after 3 days of culture. The spheroid was stained with Hoechst (blue, representing live cells) and PI (red, representing dead cells). The gallery displays the sections of the spheroids from bottom to the top. Scale bar: 100 μm. Note: due to the number of the images, scale bars might be not clearly readable.



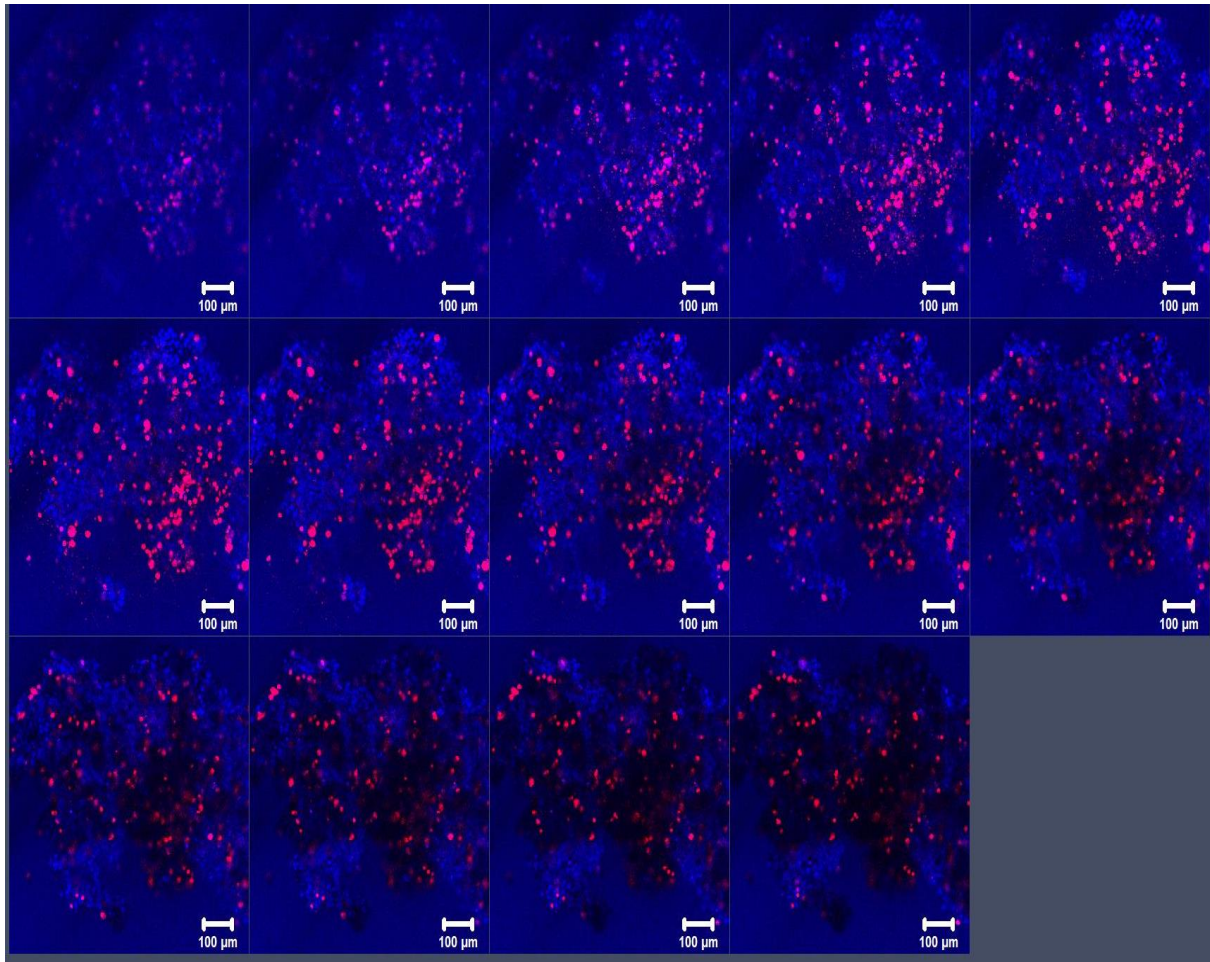
A5-6. Gallery demonstrating necrosis in PC3 spheroids seeded at 5000 cells / well after 3 days of culture. The spheroid was stained with Hoechst (blue, representing live cells) and PI (red, representing dead cells). The gallery displays the sections of the spheroids from bottom to the top. Scale bar: 100 μm. Note: due to the number of the images, scale bars might be not clearly readable.



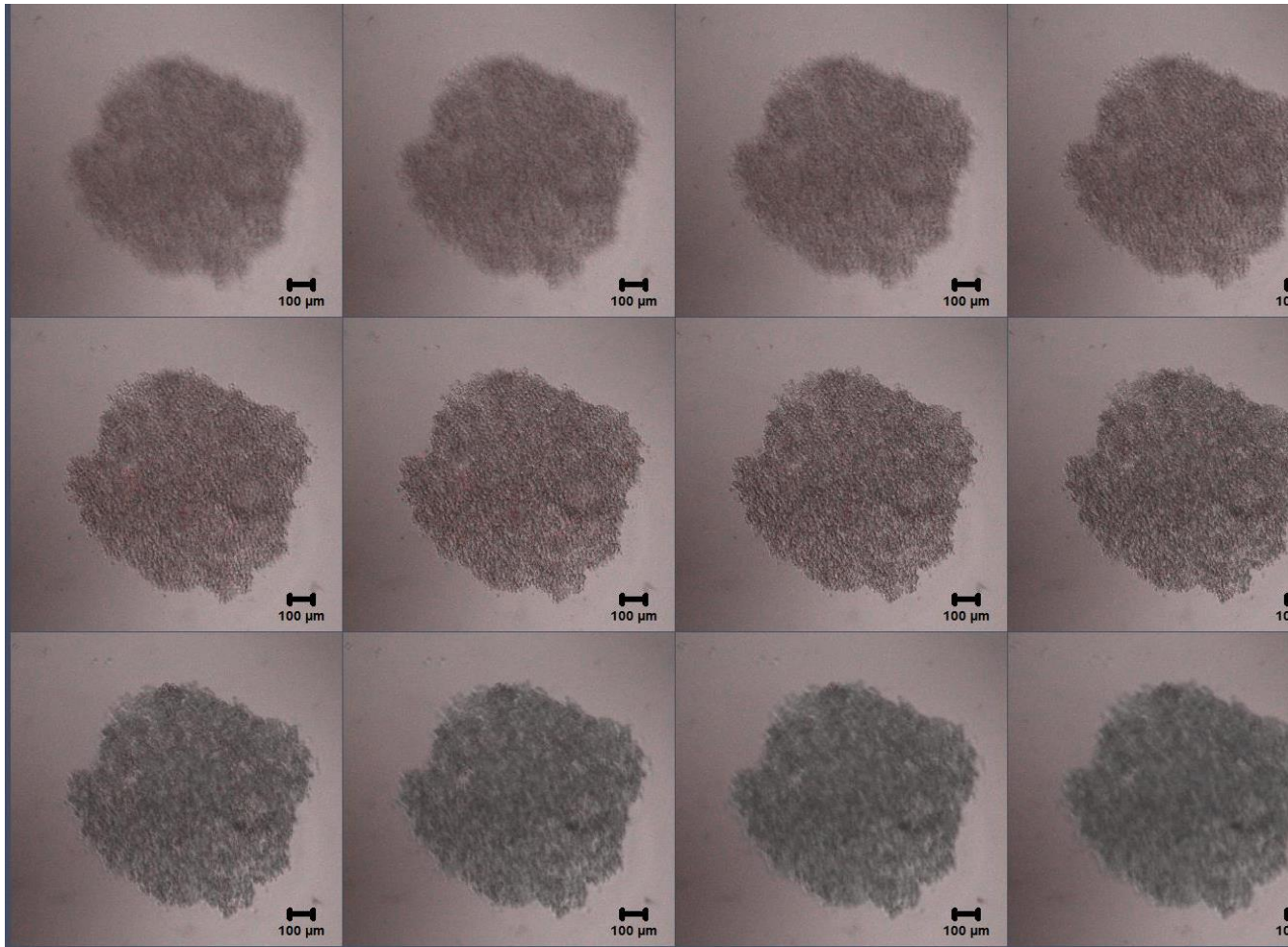
A5-7. Gallery demonstrating necrosis in PC3 spheroids seeded at 1000 cells / well after 7 day of culture. The spheroid was stained with Hoechst (blue, representing live cells) and PI (red, representing dead cells). The gallery displays the sections of the spheroids from bottom to the top. Scale bar: 100 μm . Note: due to the number of the images, scale bars might be not clearly readable.



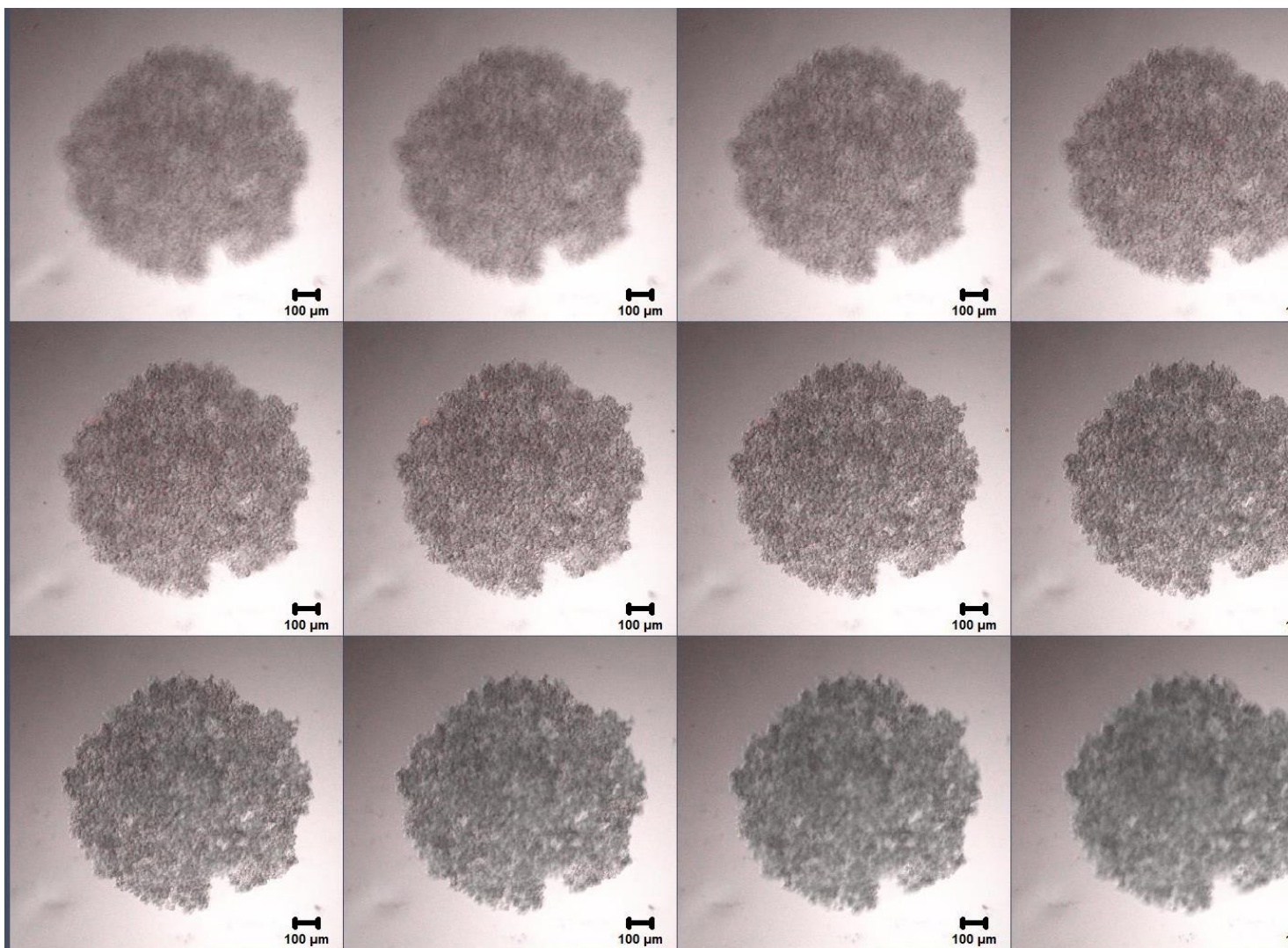
A5-8. Gallery demonstrating necrosis in PC3 spheroids seeded at 2000 cells / well after 7 day of culture. The spheroid was stained with Hoechst (blue, representing live cells) and PI (red, representing dead cells). The gallery displays the sections of the spheroids from bottom to the top. Scale bar: 100 μm. Note: due to the number of the images, scale bars might be not clearly readable.



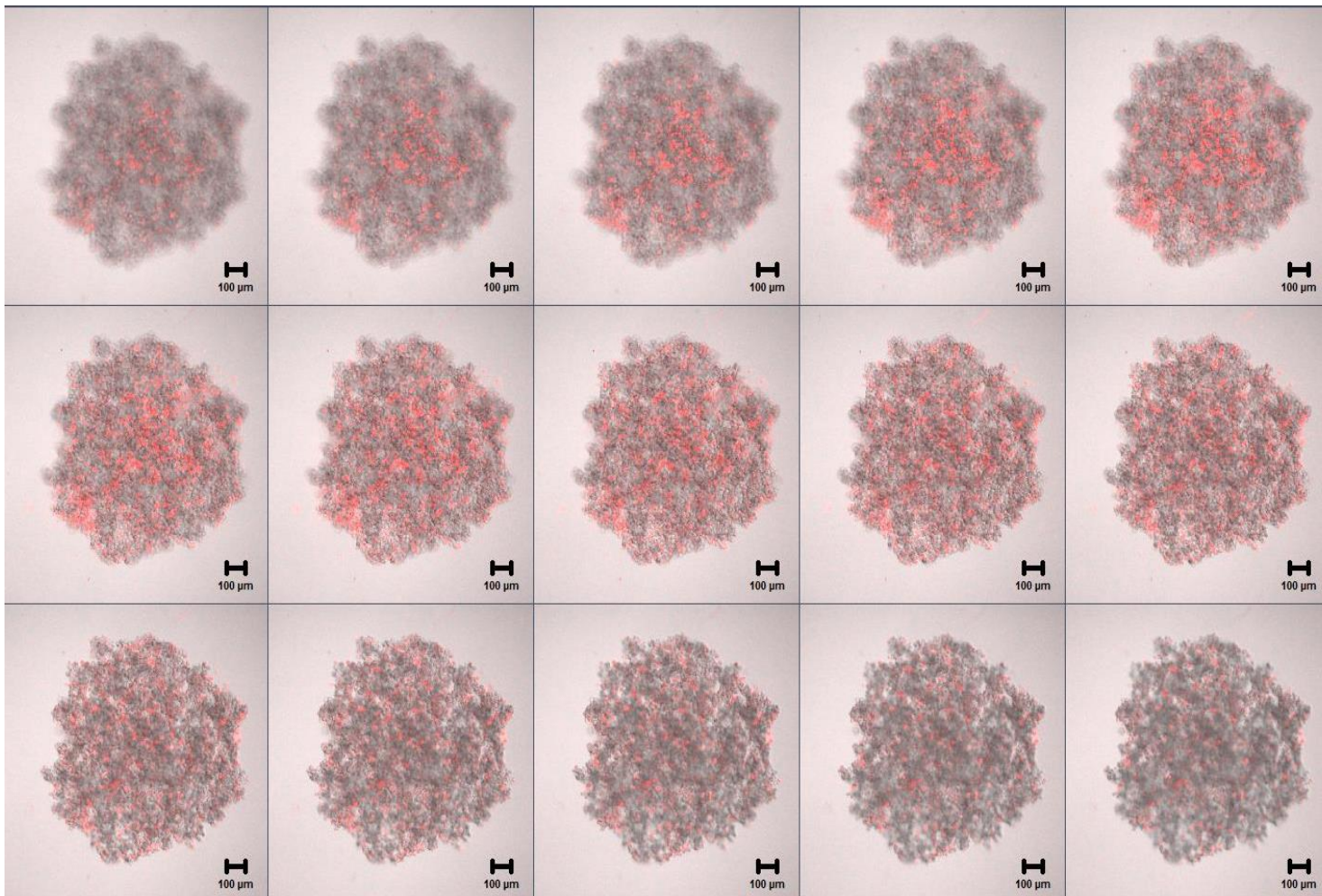
A5-9. Gallery demonstrating necrosis in PC3 spheroids seeded at 5000 cells / well after 7 day of culture. The spheroid was stained with Hoechst (blue, representing live cells) and PI (red, representing dead cells). The gallery displays the sections of the spheroids from bottom to the top. Scale bar: 100 μm . Note: due to the number of the images, scale bars might be not clearly readable.



A5-10. Gallery demonstrating O_2 availability in PC3 spheroids seeded at 5000 cells / well after 1 day of culture. The spheroid was stained with
The gallery displays the sections of the spheroids from bottom to the top. Scale bar: 100 μ m. Note: due to the number of the images, sca



A5-11. Gallery demonstrating O_2 availability in PC3 spheroids seeded at 5000 cells / well after 3 days of culture. The spheroid was stained with DAPI. The gallery displays the sections of the spheroids from bottom to the top. Scale bar: 100 μ m. Note: due to the number of the images, scale bar is not visible in all images.



A5-12. Gallery demonstrating O₂ availability in PC3 spheroids seeded at 5000 cells / well after 7 days of culture. The spheroid was stained with... The gallery displays the sections of the spheroids from bottom to the top. Scale bar: 100 µm. Note: due to the number of the images, scale...